
Eburnian, Kibaran and Pan-African metamorphic events in the Ubendian belt of Tanzania: Petrology, zircon and monazite geochronology

Dissertation
zur Erlangung des Doktorgrades
an der Mathematisch–Naturwissenschaftlichen Fakultät
der Christian–Albrechts–Universität
zu Kiel

vorgelegt von

Nelson Boniface



Kiel 2009

Eburnian, Kibaran and Pan-African metamorphic events in the Ubendian belt of Tanzania: Petrology, zircon and monazite geochronology

Dissertation
zur Erlangung des Doktorgrades
an der Mathematisch–Naturwissenschaftlichen Fakultät
der Christian–Albrechts–Universität
zu Kiel

vorgelegt von

Nelson Boniface



Kiel 2009

Gedruckt mit Unterstützung des Deutschen Akademischen Austauschdienstes

Referent: *Prof. Dr. Volker Schenk*

Korreferentin: *Prof. Dr. Astrid Holzheid*

Tag der mündlichen Prüfung: *29. Januar 2009*

Zum Druck genehmigt:

Der Dekan

Erklärung

Hiermit erkläre ich, Nelson Boniface, dass die vorgelegte Abhandlung, abgesehen von der Beratung durch meinen akademischen Lehrer Professor Dr. Volker Schenk, nach Inhalt und Form meine Arbeit ist und ausschließlich unter Verwendung der angegebenen Hilfsmittel entstanden ist.

Des Weiteren erkläre ich, dass ich weder diese noch eine ähnliche Arbeit an dieser oder einer anderen Hochschule im Rahmen eines Prüfungsverfahrens vorgelegt oder veröffentlicht habe.

Kiel, den

.....

Acknowledgment

I am greatly indebted to my academic advisor Prof. Dr. Volker Schenk who planned this project. His supervision, advices, guidances and constructive criticism are lifeblood of my achievement. Our relationship was not strictly academic, he always treated me as a good friend, I immensely value this!

It was a great honor to get the financial support for the project from DAAD (Deutscher Akademischer Austausch Dienst) and the DFG (Deutsche Forschungsgemeinschaft). The permits to research in the Ubendian belt, issued by the Mpanda district commissioner (2004) and by the director for Tanzania geological survey, Dodoma (2006) are appreciated.

Many thanks to Prof. Dr. Astrid Holzheid for her enthusiastic participations in seminars and for always giving positive recommendations and constructive comments.

A lot of thanks to Prof. Abdul Mruma of the geological survey of Tanzania for the guidance in the field during a second field trip in 2006. It was much easier with him to locate useful outcrops.

Special thanks go to my lovely wife Flora Stephano and to our wonderful kids, Kennedy and Elizabeth, for patience and prayers. The kids missed very much the paternal care as most of the time I was away.

I highly appreciate the contributions of Dr. Peter Appel in dating monazite, discussing the results and the guides on how to use Electron Probe Microanalyser (EPMA). Thanks to Dr. Timm John for his guides in handling samples with acids in a clean geochemical laboratory. A lot of thanks to Dr. Peter Raase as he was available whenever I need help to read thin sections. Dr. Sönke Brandt is appreciated for reading chapter four and giving constructive comments.

My colleagues, Dr. Niels Jöns, Dr. Denny Loose, Dr. François van der Straaten and Dr. Christoph Beier who pursued doctoral degrees during my stay in Kiel were academically co-operative and not to mention the social activities we did together. By sharing with me whatever they knew facilitated my world of using many computer programs like L^AT_EX and others.

The contributions of the technical stuffs of the Petrology division were of significant importance. Mrs. Barbara Mader apart from being helpful in the EPMA laboratory always provided social help at any time of need. Mr. Andreas Fehler prepared all the thin sections I needed on time. Mrs. Astrid Weinkauff helped me a lot in preparing glass disks for XRF and ICP-MS.

I wish to thank the ICP-MS laboratory team at the University of Kiel. Dr. Dieter Garbe-Schönberg made useful comments whenever I approached him, Mrs. Petra Fiedler and

Mrs. Ulrike Westernströer were always available to help me to use the ICP-MS laboratories in a proper way.

Many thanks to a team of technical staffs of the SHRIMP laboratory in St. Petersburg, Russia. Just to name few of them; A. Larionov, I. Paderin, S. Presniakov and N. Rodionov were very kind and co-operative.

Other members in our institute of geosciences provided me with academic or social support in one way or another. Dr. Ralf Halama, Dr. Petra Herms, Dr. Wolf-Achim Kahl, Dr. Philip Kegler, Mrs. Maike Zakrotzky and Ms. Katja Beier.

Last but not least thanks to Mr. Nambunga, now a retired driver from the University of Dar es Salaam, for driving our car during a field trip in the Ubendian belt in 2004.

Contents

Declaration	v
Acknowledgment	vi
Einführung und Zusammenfassung	xvii
Introduction and outline of the thesis	xix
1 Paleoproterozoic and Neoproterozoic sutures in the Ubendian belt	1
Abstract	1
1.1 Introduction	2
1.2 Geological settings	2
1.3 Analytical techniques	4
1.4 Metamorphic events	4
1.4.1 Ubende terrane	4
1.4.2 Ufipa terrane	5
1.4.3 Wakole and Katuma terranes	6
1.4.4 Mbozi terrane	6
1.5 Discussion and conclusions	9
1.6 Acknowledgment	10
References	10
2 Paleoproterozoic eclogites of the Ubendian belt	13
Abstract	13
2.1 Introduction	13
2.2 Geological settings	15
2.3 Analytical techniques	17
2.4 Petrology, geochemistry and geochronology of eclogites	19
2.4.1 Petrography and mineral chemistry	19
2.4.2 <i>P-T</i> conditions	22
2.4.3 Geochemistry	25
2.4.4 U-Pb SHRIMP zircon ages	29
2.5 Geochronology of metapelites and mafic granulites	32
2.5.1 Sample localities	33

2.5.2	U-Pb SHRIMP zircon ages	34
2.5.3	Th-U-total Pb CHIME monazite ages	37
2.6	Conclusions	45
2.6.1	Paleoproterozoic subduction of oceanic crust	45
2.6.2	Relationships between subduction and regional metamorphism . . .	45
2.6.3	Kibaran and Pan-African orogenic impacts in the Ubendian belt . .	46
2.7	Acknowledgment	46
	References	46
3	Kibaran age metamorphism in NW Ubendian belt of Tanzania	53
	Abstract	53
3.1	Introduction	53
3.2	Geological settings	54
3.3	Analytical techniques	56
3.4	Petrography and mineral chemistry	57
3.4.1	Wakole terrane	57
3.4.2	Ubende terrane	58
3.5	Mineral reactions	59
3.6	Geothermobarometry	62
3.7	U-Pb SHRIMP zircon dating	64
3.7.1	Zircon textures and U-Th contents	64
3.7.2	Zircon ages	64
3.8	Th-U-total Pb monazite dating	66
3.8.1	Monazite composition and textures	66
3.8.2	Monazite isochron ages	68
3.9	Discussion and conclusions	71
3.10	Acknowledgment	72
	References	72
4	Neoproterozoic eclogites in the Ubendian belt	77
	Abstract	77
4.1	Introduction	78
4.2	Analytical techniques	79
4.3	Geological setting	79
4.4	Petrography and mineral chemistry	83
4.4.1	Kyanite-free eclogites	83
4.4.2	Kyanite-bearing eclogites	83
4.5	Mineral reaction history	86
4.5.1	Kyanite-free eclogites	86
4.5.2	Kyanite-bearing eclogites	86
4.6	Geothermobarometry	93
4.7	Geochemistry of kyanite-free eclogites	96
4.8	Geochronology	100

4.8.1	Textures and U-Th-Pb compositions of zircons	100
4.8.2	Results of the U-Pb dating	101
4.9	Discussion	103
4.9.1	Geochronological and geochemical results	103
4.9.2	Neoproterozoic eclogite formation in the Ubendian belt and geodynamic consequences	103
4.10	Conclusions	105
4.11	Acknowledgment	106
	References	106
	Curriculum vitae	111

List of Figures

1.1	Locations of Kibaran orogenic system in southern Africa	3
1.2	REE patterns of the Eclogites	5
1.3	Monazite BSE images for the Ubendian belt metapelites	7
1.4	Simplified geological map of central Gondwana with Pan-African sutures and eclogites	10
2.1	The 2.1-1.8 Ga collisional orogens of the World	14
2.2	Location of the Ubendian belt	15
2.3	Textures of mylonitic eclogites of the Ubende terrane	19
2.4	Grt and Cpx composition of the Ubende terrane eclogites.	20
2.5	BSE image of rutile and calculated temperatures	22
2.6	P - T conditions in mylonitic eclogites	24
2.7	Classification of mylonitic eclogites on magma discrimination diagrams	25
2.8	REE and trace element patterns of the Ubende terrane eclogites	26
2.9	Plot of Nb/La vs $(La/Sm)_N$ for Ubende terrane eclogites	26
2.10	Zircon textures, Ubende terrane eclogites	29
2.11	Concordia diagrams with U-Pb zircon ages of eclogites	30
2.12	Map of the Ubendian belt showing ages distribution	32
2.13	Textures of zircon of metapelites and mafic granulites	35
2.14	Concordia diagrams with U-Pb zircon ages of metapelites and mafic granulite	36
2.15	Textures in monazite showing ages in cores and rims	38
2.16	Monazite composition, Ufipa terrane	39
2.17	Monazite isochron ages	40
2.18	Textures in monazite showing ages in cores and rims	41
2.19	Monazite composition sample T21-1-04	42
2.20	Monazite isochron ages, Mbozi terrane	43
3.1	Geological map of southern Africa depicting Kibaran orogens	54
3.2	Kibaran metamorphic events in the NW Ubendian belt	55
3.3	Textures of Grt-Bt-Ky-bearing metapelites	59
3.4	Mineral compositions: Grt-Bt-Ms-Pl-St	60
3.5	P - T conditions and path	63
3.6	Textures of zircon and monazite	65
3.7	U-Pb SHRIMP zircon ages from samples T107-3-04 and T45-3-04	66

3.8	Monazite REE composition	67
3.9	U-Pb monazite ages from the Wakole terrane	69
4.1	Pan-African sutures in the central part of Gondwana	78
4.2	Location of the Ubendian belt	80
4.3	Field photos of the eclogites in the Ufipa terrane	81
4.4	Location of Pan-African eclogites in the Ubendian belt	82
4.5	Microphotographs showing reaction textures in eclogites of the Ufipa terrane	84
4.6	Mineral chemistry of eclogites of the Ufipa terrane	85
4.7	The P - T conditions in the eclogites of the Ufipa terrane	95
4.8	BSE image of rutile and calculated temperatures	96
4.9	Classification of porphyroblastic eclogites on magma discrimination diagrams	97
4.10	REE patterns of the ufipa terrane eclogites	98
4.11	Discrimination diagrams of basalts	98
4.12	Texture and U/Th ratios of zircons of eclogites of the Ufipa terrane	100
4.13	SHRIMP-II U-Pb zircon ages of eclogitic zircons	101
4.14	Pan-African subduction zones around the margins of Bangweulu block . . .	104

List of Tables

1.1	Zircon composition for the Ubendian belt eclogites and metapelites	8
1.2	Th-U-Pb monazite composition for the Ubendian belt metapelites	8
2.1	Representative Grt, Pl and Cpx compositions of the Ubende terrane eclogites	21
2.2	Summary of <i>P-T</i> conditions of the Ubende terrane eclogites	23
2.3	Geochemical composition of the Ubende terrane eclogites	28
2.4	U-Th-Pb composition of zircon of Ubende terrane eclogites	31
2.5	Zircon and monazite age of the metapelites and mafic granulites	33
2.6	SHRIMP U-Pb Zircon composition of Ubendian belt rocks	37
2.7	Representative monazite compositions of the Ubendian belt metapelites . .	44
3.1	Metamorphic mineral assemblages of the Wakole terrane metapelites	58
3.2	Representative Grt and Pl compositions of the Wakole and Ubende terranes metapelites	61
3.3	Representative Bt, Ms and St compositions of the Wakole and Ubende ter- ranes metapelites	62
3.4	Summary of <i>P-T</i> conditions of the Wakole terrane metapelites	63
3.5	SHRIMP U-Th-Pb composition of zircon of the Wakole terrane metapelite	68
3.6	Representative monazite compositions of the Wakole terrane	70
4.1	Representative composition of Grt of the kyanite-free eclogites	87
4.2	Representative composition of Cpx of the kyanite-free eclogites	88
4.3	Representative composition of Pl and Hbl of the kyanite-free eclogites . . .	89
4.4	Representative composition of Grt and Cpx of the Ky-bearing eclogites . .	90
4.5	Representative composition of St, Spl, Zo and Hbl of Ky-bearing eclogite .	91
4.6	Representative Pl composition of Ky-bearing eclogites	92
4.7	Summary of <i>P-T</i> conditions of kyanite-bearing and kyanite-free eclogites .	94
4.8	Trace element composition of the kyanite-free eclogites	99
4.9	SHRIMP U-Th-Pb zircon composition of the Ufipa terrane eclogites	102

Einführung und Zusammenfassung

Unter Geowissenschaftlern ist es weithin akzeptiert, dass die Subduktion von ozeanischer Lithosphäre eine der wichtigsten Antriebskräfte für Plattenbewegungen ist. Bei der Subduktion von ozeanischer Lithosphäre werden Ozeanbodenbasalte und –gabbros in Blauschiefer und Eklogite umgewandelt. Aus diesem Grund stellen Vorkommen von Eklogiten mit dem Chemismus von Ozeanbodenbasalten, die in Orogenen auftreten, einen Beweis für plattentektonische Bewegungen in der geologischen Vergangenheit dar. Ebenfalls durch Plattenbewegungen kommt es zum Zusammenfügen von kontinentalen Blöcken und zu Superkontinenten. Die Bildung von Super-kontinenten wiederum führt zum Wachstum kontinentaler Kruste durch Akkretion juveniler Inselbögen, zum Recycling von ozeanischer Kruste in den Erdmantel und zu Vulkanismus und Entgasungen in Subduktionszonen. Auf lange Sicht kann dies zu globalen Klimaveränderungen führen. In wirtschaftlicher Hinsicht bedeutend kann die Entstehung von Orogenen sein, in denen sich Metallagerstätten für Gold, porphyrisches Kupfer und Kupfer-Zink-Sulfid-Lagerstätten bilden können.

Im Ubendian Orogengürtel treten paleoproterozoische Eklogite mit Ozeanbodenbasalt-Chemismus und neoproterozoische Eklogite mit einer chemischen Signatur auf, die der von Inselbogen und Back-Arc-Becken-Laven entspricht. Diese Eklogitvorkommen manifestieren wiederholte Schließungen von Ozeanbecken am südlichen Rand des archaischen Tansania-Kratons. Paleoproterozoische Eklogite mit Ozeanbodenbasalt-Chemismus treten auch im Usagaran Orogen, am Ostrand des Tansania-Kratons gelegen, und an der Nordostgrenze des Kongo-Kratons in Kamerun auf und belegen somit plattentektonische Prozesse am Rande des Kongo-Kratons in paleoproterozoischer Zeit. Dennoch kommen präkambrische Eklogite insgesamt relativ selten auf der Erde vor. Ihr Auffinden stellt deshalb einen wichtigen Beweis für plattentektonische Bewegungen im Präkambrium dar, die dem heutigen plattentektonischen System ähneln. Außerdem markieren Eklogite auch ehemalige Suturzonen und sind aus diesem Grund wichtig für die Rekonstruktion von früheren Konfigurationen der Kontinente.

Die vorliegende Arbeit befasst sich schwerpunktmäßig mit der metamorphen Entwicklung des paleoproterozoischen Ubendian Gürtels. Geochronologische und phasenpetrologische Daten wurden dabei sowohl von Eklogiten als auch von umgebenden Metapeliten und mafischen Granuliten gewonnen. Zusätzlich wurden die Eklogite und die mafischen Granulite geochemisch untersucht. Durch diese Daten wurde erstmalig erkannt, dass das Ubendian Gebirge zwischen dem archaischen Tansania-Kraton im Nordosten und dem paleoproterozoischen Bangweulu Block im Südwesten gelegen, zwei mal im Präkambrium als Sutur zone diente: Einmal bei der Bildung des hypothetischen Superkontinents Columbia

(2.1-1.8 Ga), das zweite Mal bei der Bildung des Superkontinents Gondwana (650-500 Ma). Eine neue Erkenntnis ist zudem die mesoproterozoische Überprägung im Nordwest-Teil des Gebirges, bei der Bildung des Superkontinents Rodinia (1.1 Ga). Die gewonnenen Daten werden in vier Kapiteln, die im Folgenden kurz beschrieben werden, dargestellt:

Kapitel 1 gibt einen allgemeinen Überblick über die regionale Verteilung von metamorphen Ereignissen im Ubendian Gürtel, die Lage der Suturezonen, die räumlichen Beziehungen des Ubendian Gürtels mit den benachbarten präkambrischen Kratonen und die post-Ubendian orogenen Ereignisse. Die internen Texturen von Monazit- und Zirkon-Körnern werden kurz vorgestellt und scheinbare Alter, die mehrfache Metamorphosen andeuten, werden präsentiert. Auf diese Weise wird in Kapitel 1 die polyorogene Entwicklung des Ubendian Gürtels zusammengefasst, die nicht nur paleoproterozoische (Eburnisch) Ozeanbodensubduktion und Kollisionsereignisse umfasst, sondern auch mesoproterozoische (Kibaran) Krustenverdickung und granulitfazielle, mylonitische Aufarbeitung der paleoproterozoischen Gesteine. Zusätzlich tritt eine neoproterozoische (Panafrikanisch) eklogitfazielle Metamorphose, sowie ein granulitfazielles (hochgradiges) Wiederaufarbeiten der paleoproterozoischen Ausgangsgesteine auf.

In **Kapitel 2** werden geochronologische, petrographische und geochemische Daten der paleoproterozoischen Eklogite des Ubendian Gürtels mit Ozeanbodenbasalt-Chemismus sowie der assoziierten Metapelite und granulitfaziellen Metabasiten präsentiert. Sowohl SHRIMP U-Pb Zirkonalter als auch CHIME Monazitalter werden für das eburnische Gebirgsbildungereignis und die darauf folgenden meso- und neoproterozoischen Überprägungen dargelegt. Um die P-T-Bedingungen des paleoproterozoischen Ubendian Ozeans zu ermitteln, wurden phasenpetrologische Untersuchungen an den Eklogiten durchgeführt.

Kapitel 3 beschreibt das metamorphe Kibaran Ereignis im NW des Ubendian Gürtels. Die Metamorphose der Metapelite des Wakole- und des Ubende Terranes wurden auf 1170-1010 Ma zur Zeit des Kibaran datiert (U-Pb, Zirkon und CHIME, Monazit). Die Alter der Metapelite des Wakole Terranes gehen einher mit den metamorphen Altern der Krustenverdickung im Kibaran und im Irumiden Gürtel und zeigen daher eindeutig auf das Kibaran Ereignis hin. Dahingegen zeigen die auf das Eburnian datierten Kerne der Zirkone und der Monazite in den Metapeliten des Ubende Terranes, eine mylonitische Überprägung während des Kibarans.

In **Kapitel 4** wird die Petrogenese der panafrikanischen Eklogite des Ufipa Terranes im Ubendian Gürtel bezüglich ihres Chemismus diskutiert. Diese Eklogite weisen Ähnlichkeiten mit Laven von Inselbögen und Back-Arc-Becken auf. U-Pb Zirkondatierungen mittels der SHRIMP wurden durchgeführt, um das Alter der panafrikanischen Subduktion zu bestimmen. Spurenelement-Zusammensetzungen werden benutzt, um das tektonische Milieu und den Ursprung der Vorgängergesteine der Eklogite einzugrenzen. Abschließend werden metamorphe P-T-Bedingungen und der Subduktionspfad mit Hilfe von Mineralzusammensetzungen und Reaktionstexturen bestimmt.

Introduction and outline of the thesis

Oceanic lithosphere subduction is widely accepted among geoscientists as the major driving force of plate motions on Earth. Ocean floor basalts and gabbros are converted into blueschists and eclogites in the process of oceanic lithosphere subduction. Therefore, outcrops of MORB-like chemistry eclogites in orogenic belts manifest the operation of plate tectonics. The assembly of continental blocks to form supercontinents is derived by plate motions, which result into continental crustal growth by accretions of juvenile volcanic arcs, recycling of oceanic crust into the mantle, volcanism and degassing at subduction zones. This might result in a long term global climate change and, more of economic importance, the creation of orogenic settings, which are important sites for metal deposits such as gold, porphyry copper and the volcanogenic massive sulfide copper-zinc ores.

The Ubendian orogenic belt hosts Paleoproterozoic eclogites with MORB-like chemistry and Neoproterozoic eclogites with geochemical signatures like volcanic island-arc and back-arc lavas, which manifest the repeated ocean basin closures at the southern margin of the Archean Tanzania craton. Paleoproterozoic MORB-like chemistry eclogites are also known to crop out in the Usagaran belt, at the eastern margin of the Tanzania craton and at the north-eastern border of the Congo Craton in Cameroon. However, Precambrian eclogites are rarely outcropping on planet Earth, therefore their recognition provides evidence for the operation of plate tectonics in Precambrian time similar to those in modern plate tectonic regimes. Eclogite occurrences also mark the sites of suture zones; consequently, they are important for the reconstruction of former continental configurations.

This work focuses on the metamorphic evolution of the Paleoproterozoic Ubendian belt. Geochronological and phase petrological data were acquired from eclogites, metapelites and mafic granulites. In addition, eclogites were geochemically investigated and the obtained data are presented in four chapters, which are briefly described below:

Chapter 1 gives a general overview on the distribution of metamorphic events in the Ubendian belt, the location of sutures and the spatial relationship of the Ubendian belt and the adjoining Precambrian cratons as well as the post-Ubendian orogenic events. Internal textures of monazite and zircon grains are briefly described and apparent ages, which indicate multiple metamorphism, are presented. In this way chapter 1 summarizes the polyorogenic evolution of the Ubendian belt, which comprises not only Paleoproterozoic (Eburnian) ocean floor subduction and collisional events, but also Mesoproterozoic (Kibaran) crustal thickening and granulite-facies mylonitic reworking of the Paleoproterozoic rocks, in addition to Neoproterozoic (Pan-African) eclogite-facies metamorphism and high-grade up to granulite-facies reworking of Paleoproterozoic precursors.

Chapter 2 provides geochronological, petrographical and geochemical data about the Paleoproterozoic MORB-like chemistry eclogites of the Ubendian belt and the associated metapelites and granulite-facies metabasites. SHRIMP U-Pb zircon ages and CHIME monazite ages are presented for the Eburnian orogenic event and the subsequent orogenic overprints of Mesoproterozoic and Neoproterozoic age. The phase petrology of eclogites was studied to decipher the subduction path and peak P - T conditions during the subduction of the Paleoproterozoic Ubendian ocean floor.

Chapter 3 is about Kibaran metamorphic events in the NW Ubendian belt, metapelites of the terranes of Wakole and Ubende recorded Kibaran ages at 1170-1010 Ma (U-Pb zircon and CHIME monazite ages). Metapelites of the Wakole terrane give pure Kibaran ages, which are equivalent to the crustal thickening metamorphic age of the Kibaran and Irumide belts, whereas the metapelites of the Ubende terrane show Kibaran mylonitic overprint on the Eburnian zircon and monazite cores.

Chapter 4 discusses the petrogenesis of the Pan-African eclogites of the Ufipa terrane in the Ubendian belt, with a chemistry of lavas erupting in back-arc and island-arc settings. U-Pb zircon SHRIMP dating was performed to obtain the ages of the Pan-African subduction metamorphism. Tectonic settings and the magmatic origin of the eclogite precursors were constrained by using trace element compositions. Finally, the metamorphic P - T conditions and the subduction path were constrained by using mineral compositions and reaction textures.

Chapter 1

A Paleoproterozoic and a Neoproterozoic suture zone in the Ubendian belt of Tanzania: evidence from eclogites and the regional distribution of metamorphic zircon and monazite ages

Abstract

The Ubendian belt situated between the Archean Tanzania craton and the Paleoproterozoic Bangweulu block is regarded as a rare example of a Paleoproterozoic linear belt containing eclogites. These features suggest that modern-style plate tectonic processes may have operated already in Paleoproterozoic time. However, geochemical studies combined with zircon and monazite geochronology and petrology of eclogites and their country rocks revealed that the eclogites of different lithotectonic terranes within this belt formed during two different orogenic cycles, the Paleoproterozoic Ubendian orogeny and the Neoproterozoic Pan-African orogeny. In addition, the Paleoproterozoic metamorphic basement of the belt has been affected by amphibolite- to granulite-facies reworking during the Pan-African orogenic cycle. In contrast, a (so far unknown) Mesoproterozoic reworking during the Kibaran orogeny is restricted to the northwestern terranes of the belt. The southern boundary of this Kibaran reworking is located where the Neoproterozoic eclogites are outcropping. This suggests the existence of a Neoproterozoic convergent plate boundary between the Tanzania craton and the Bangweulu block. The linear zone of Neoproterozoic high-grade reworking associated with eclogite formation between Lake Tanganyika and Lake Malawi is interpreted as the result of the collision (at ca. 560 Ma) between the Bangweulu block and the Tanzania craton (we suggest the name “Tanganyika orogeny” for this event). The occurrences of Neoproterozoic eclogites to the north (Tanganyika orogenic belt), the east (Malawi) and the south (Zambezi belt) of the Bangweulu block suggest that this continental block formed a microplate during the Neoproterozoic Era, which has to be considered in future models of Gondwana formation.

1.1 Introduction

The ages of orogens at the margins of the Archean-Paleoproterozoic cratons in central and southern Africa cluster at 2.05-1.8 Ga, 1.35-1.0 Ga and 650-500 Ma (Cahen *et al.*, 1984; Hanson, 2003), and are attributed to the Eburnian, Kibaran and Pan-African orogenic cycles, respectively. The corresponding orogenic belts are thought to represent sutures along which continental blocks fused to form hypothetical supercontinents. Columbia is one of the names given to a proposed Paleoproterozoic supercontinent with Eburnian sutures (Rogers & Santosh, 2002; Zhao *et al.*, 2002), Rodinia contains Mesoproterozoic and Gondwana Neoproterozoic suture zones. The Ubendian-Usagaran orogenic belt of Tanzania (Fig. 1.1) is regarded as an example of a linear Paleoproterozoic orogen, for which it was assumed, in analogy to eclogites in the nearby Usagaran belt (Fig. 1; Möller *et al.*, 1995), that rare Eburnian eclogites are preserved (e.g. Sklyarov *et al.*, 1998). During the course of studying the origin of the eclogites and the nature of the subduction zone metamorphism in the Ubendian belt, we discovered relics of two suture zones: Eburnian eclogites with a chemical affinity to mid-ocean ridge basalts and Pan-African eclogites with geochemical characteristics similar to that of back-arc and to that of volcanic-arc lavas. In this paper we propose a Pan-African suture in the Ubendian belt, which was not known before. The interpretation is based on the occurrence of eclogites and the distribution of zircon and monazite ages related to Eburnian, Kibaran and Pan-African orogenic events in the different tectonic terranes of the Ubendian belt.

1.2 Geological settings

The Ubendian belt extends for more than 500 km between the Tanzania craton and the Bangweulu block. It has been divided into eight NW-SE oriented lithotectonic terranes (Fig. 1.1), which are internally deformed and are separated by extensive tracts of mylonitic and ultra-mylonitic gneisses (Daly *et al.*, 1985). These terranes (dominant lithologies in brackets) are: Ubende (hornblende gneisses), Wakole (alumino-silicate schists), Katuma (migmatitic biotite gneisses), Ufipa (granitic gneisses), Mbozi (metabasites), Lupa (meta-volcanics), Upangwa (meta-anorthosite), Nyika (cordierite gneisses).

Eburnian and Pan-African metamorphic and magmatic events have been dated from the Ubendian belt in Tanzania and Malawi. In Tanzania, Lenoir *et al.* (1994) associated the U-Pb zircon ages of granitoids at 2084 ± 86 Ma and 2026 ± 8 Ma to the formation of high-pressure granulites in the Mbozi and Ubende terranes. In Malawi (Nyika terrane), ages of low-pressure cordierite gneisses and high-pressure orthopyroxene-clinopyroxene enderbitic gneisses between 2093 ± 0.6 Ma and 1988 ± 0.6 were reported by Dodson *et al.* (1975) and Ring *et al.* (1997). These ages are equivalent to the 2.0 Ga age of eclogites of the Usagaran belt (Möller *et al.*, 1995) and were interpreted by Ring *et al.* (1997) as the possible relict of an Ubendian-Usagaran paired metamorphic belt of Paleoproterozoic age. A second phase of amphibolite-facies metamorphism and granitoid intrusion at ca.1860 Ma in the northern Ubendian belt (the terranes of Katuma, Ufipa, Lupa and Ubende),

is thought to have produced the NW-SE striking structures of the Ubendian belt (Lenoir *et al.*, 1994). However, Theunissen *et al.* (1992) proposed that the NW-SE structure of the Ubendian belt was imposed during Pan-African time because they dated a sheared gneiss (U-Pb zircon) at 814 ± 120 Ma (lower intercept) and another gneiss with a Rb-Sr whole rock isochron at 724 ± 6 Ma.

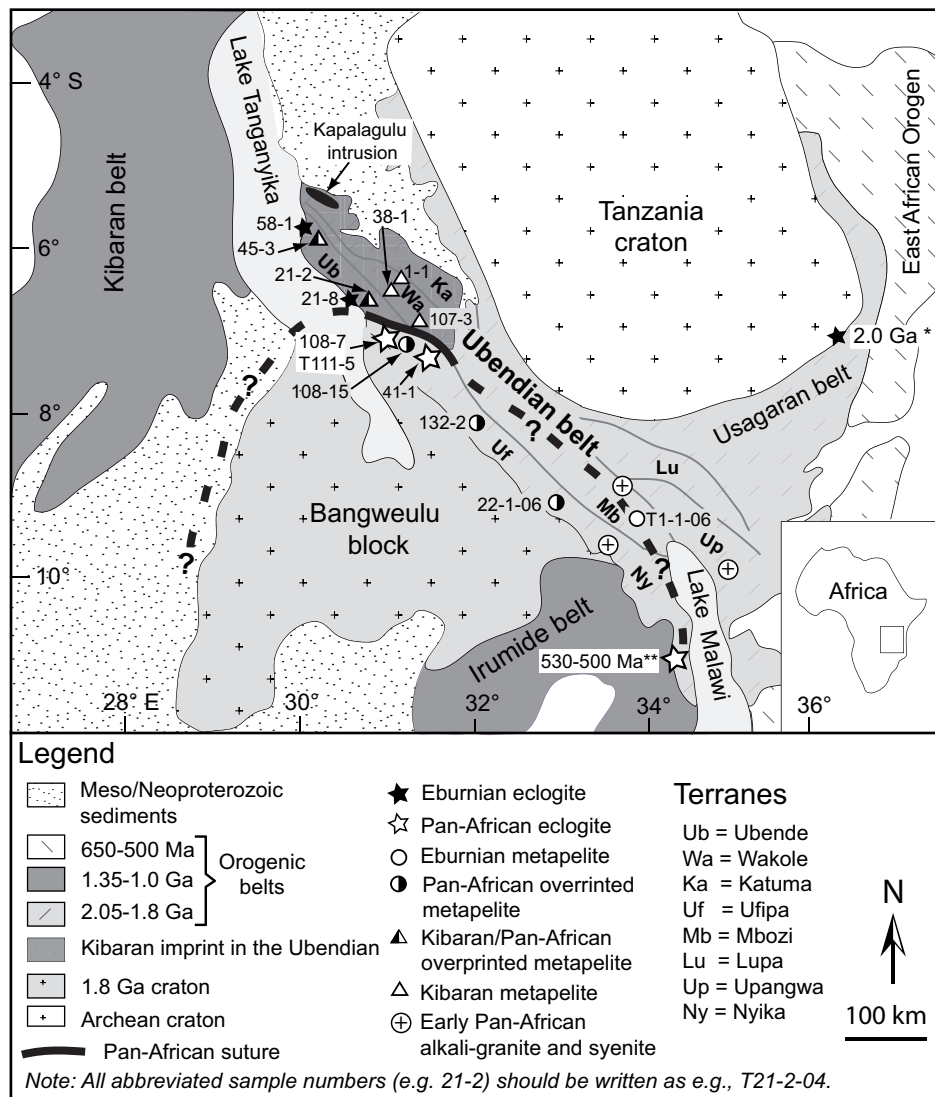


Figure 1.1: Geological map of south-eastern Africa indicating the location of the Ubendian belt, eclogite occurrences, the regional distribution of zircon and monazite ages and the position of the proposed Pan-African suture. Ages of eclogites: this paper in the Ubendian belt, * Möller *et al.* (1995) in the Usagaran belt and ** Ring *et al.* (2002) in Malawi. Map modified after Hanson (2003).

The available geochronological data in the Ubendian belt suggest that the Eburnian geologic events spanned a period between 2100 and 1800 Ma. Kibaran metamorphic events have not yet been reported from the Ubendian belt. Only the intrusion of the Kapalagulu

ultramafic-mafic igneous complex at 1392 ± 26 Ma (Maier *et al.*, 2007), which occurs at the NW margin of the Katuma terrane, can be attributed to an early Kibaran stage. The early Pan-African orogenic event was associated with alkali-granitoid intrusions dated at 842 ± 80 Ma (Lenoir *et al.*, 1994) and at 724 ± 6 Ma (Theunissen *et al.*, 1992) in the Upangwa terrane, and with syenites from the Mbozi terrane dated at 743 ± 30 (Brock, 1963) and 685 ± 62 Ma (Ray, 1974). These early Pan-African ages may reflect a time of extension preceding the subduction and collision event.

1.3 Analytical techniques

In-situ U-Th-total Pb dating of monazite was performed by using an electron microprobe 'JEOL Superprobe JXA-8900R' at the University of Kiel, Germany. Backscattered electron images coupled with X-ray maps of Th, U, Pb, Si and Y were produced. Th, U and Pb concentrations were eventually used to produce maps of apparent ages in single monazite grains. Isotopic *U-Pb* dating of zircon was done with a SHRIMP-II at the Center of Isotopic Research of VSEGEI in Saint Petersburg, Russia. Cathodoluminescence (CL) images of zircons were produced to reveal internal textures of zircons. Trace element data of eclogites were acquired by using an ICP-MS instrument 'Agilent 75000C' at the University of Kiel. Sample preparation procedure was as described by Gabe-Schönberg (1993) and John *et al.* (2008). Precision and accuracy of data were ensured by using international reference standards, blanks and sample duplicates.

1.4 Metamorphic events

1.4.1 Ubende terrane

The Ubende terrane of the Ubendian belt (Fig. 1.1) is dominated by amphibolites and amphibole gneisses (McConnell, 1950; Sutton *et al.*, 1954; Nanyaro *et al.*, 1983; Sklyarov *et al.*, 1998), which host lenses of mylonitic eclogites and mylonitic garnet-kyanite metapelites. Most eclogites have MORB-like REE patterns, characterized by depletion of the LREE (Fig. 1.2A), and are interpreted as remnants of an oceanic crust. Zircons of these eclogites are either unzoned or show domainal zonation but lack concentric magmatic zonation and overgrown metamorphic rims (Fig. 1.2B). We interpret the uniform Eburnian ages at around 1860 to 1890 Ma (Fig. 1.2B, Tab. 1.1) to reflect the metamorphic growth during subduction of oceanic crust.

The mylonitic garnet-kyanite gneisses of the Ubende terrane that are associated with eclogites (T21-2-04 and T45-3-04 in Fig. 1.1) contain zircons and monazites that have been affected by multiple metamorphic events. Zircons have Paleoproterozoic cores reflecting the Eburnian event and are overgrown by Kibaran rims; no Pan-African event was detected in these zircons (Fig. 1.2C, Tab. 1.1). In contradistinction to zircon, monazite grains that occur in the matrix of a metapelitic sample (T21-2-04) have cores that are overgrown by two consecutive rims (Fig. 1.3A). The age map of one of these monazite grains reveals a

Paleoproterozoic core overgrown by a Mesoproterozoic inner rim and a Pan-African outer rim (Fig. 1.3A, Tab. 1.2). In contrast, monazite grains occurring as inclusions in garnet have only Mesoproterozoic rims overgrowing Paleoproterozoic cores (Fig. 1.3B). Since Pan-African rims are missing, garnet growth in these mylonitic metapelites occurred most likely during the Kibaran overprint and prohibited Pan-African monazite regrowth.

In summary, the Ubende terrane of the Ubendian belt hosting mylonitic eclogites and associated mylonitic garnet-kyanite gneisses experienced three metamorphic events, attributed to the Eburnian, the Kibaran and the Pan-African orogenic cycles. Eclogite-facies metamorphism is of Eburnian age. Garnet growth in the metapelitic mylonites is most likely of Kibaran age: Pan-African reworking is reflected in rims of monazites occurring in the matrix of mylonitic metapelites, but not in monazites included in garnet.

1.4.2 Ufipa terrane

The Ufipa terrane bordering the Ubende terrane to the southeast (Fig. 1.1) is mainly composed of granitic biotite gneiss and minor amphibolite, hornblende gneiss and garnet-kyanite gneiss (McConnell, 1950; Sutton *et al.*, 1954). The biotite gneisses and garnet-kyanite metapelites in the NW part of the Ufipa terrane (Fig. 1.1) host lenses (10 - 100 m scale) of kyanite-free and kyanite-bearing eclogites. Texturally, the Ufipa terrane eclogites are massive and coarse grained and thus contrast to the mylonitic Paleoproterozoic eclogites of the Ubende terrane. The zircons show concentric magmatic growth zoning in the core and may be overgrown by a metamorphic rim (Fig. 1.2D). However, core and rim ages are indistinguishable, both pointing to a Pan-African formation (ca. 560 Ma; Fig. 1.2D). Geochemically, some of these eclogites resemble basalts of back-arc basins (Fig. 1.2A, Tab. 4.8) others of volcanic arcs (not shown).

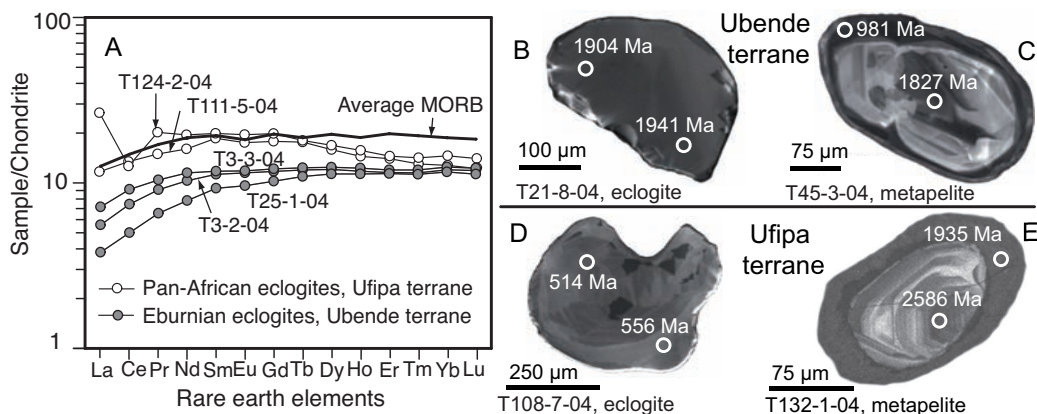


Figure 1.2: A: REE patterns of the Ubendian belt eclogites of Eburnian and Pan-African age; the chondrite normalizing values are from Boynton (1984). B, C, D & E: Zircon CL images for eclogites and metapelites displaying Eburnian, Kibaran and Pan-African $^{207}\text{Pb}/^{206}\text{Pb}$ apparent ages.

The host rocks of these eclogites preserved a more complex metamorphic history that could be resolved by the combination of microprobe monazite dating with SHRIMP U-

Pb zircon dating. High-pressure garnet-kyanite-biotite-muscovite metapelites crop out in the northern part of the Ufipa terrane whereas low-pressure garnet-cordierite-sillimanite-bearing metapelites crop out in the south, pointing to different metamorphic histories and conditions in the different parts of the Ufipa terrane. The high-pressure metapelites in the north hosting the Pan-African eclogites contain zircons that do not show overgrown rims of Pan-African age; their metamorphic rims yield only Paleoproterozoic ages (ca. 1900 Ma) reflecting high-grade Eburnian metamorphism (Fig. 1.2E). In contrast to zircons, age maps of single monazite grains from metapelites reveal a two-stage evolution with similar ages of metamorphic events in the entire Ufipa terrane: Paleoproterozoic monazite cores (ca. 1860 Ma) are overgrown by Pan-African rims (ca. 560 Ma; Fig. 1.3C). In the southern part of the Ufipa terrane (T22-1-06) the Pan-African reworking is so intense (garnet-cordierite-sillimanite-grade) that hardly any relicts of Paleoproterozoic monazite ages could be found. The Kibaran metamorphic event is neither recorded in zircons nor in monazites of the Ufipa terrane. This is in contradistinction to the metamorphic ages found in the Ubende terrane.

1.4.3 Wakole and Katuma terranes

Metapelites are the most common rock type of the Wakole terrane. These rocks preserved peak-metamorphic conditions that are variable, ranging from about 9 kbar/670 °C found in garnet-biotite-muscovite schists (with or without staurolite) to ca. 9.5 kbar/750 °C found in garnet-biotite-kyanite-K-feldspar gneisses. Monazite shows a concentric to patchy zonation in BSE images (Fig. 1.3D). However, the ages are uniform at about 1000 Ma and do not present any evidence for other than Kibaran orogenic events. Metapelitic zircon also gives (not presented here) solely concordant Kibaran ages at 1166 ± 14 Ma and $1007 \pm$ Ma.

The Katuma terrane bordering the Wakole terrane the northwest contains mafic and felsic granulites besides the dominating migmatitic biotite gneisses. Zircons of one mafic granulite sample exhibit magmatic cores and metamorphically overgrown rims of Paleoproterozoic age. However, the discordance of the isotopic U-Pb apparent ages point to a severe disturbance during the Kibaran orogeny.

1.4.4 Mbozi terrane

The most common rock types of the Mbozi terrane are mafic granulites. The apparent monazite ages of the associated garnet-biotite-sillimanite gneisses reveal only an Eburnian metamorphic event without a younger Kibaran or Pan-African overprint (Fig. 1.3E). However, an early Pan-African event in this terrane is documented in the solitary alkali-granites and syenites outcropping in the Mbozi terrane, as discussed before. This magmatic event may be attributed to early extensional tectonics. There are no geochronological data on the mafic granulites that dominate in the Mbozi terrane.

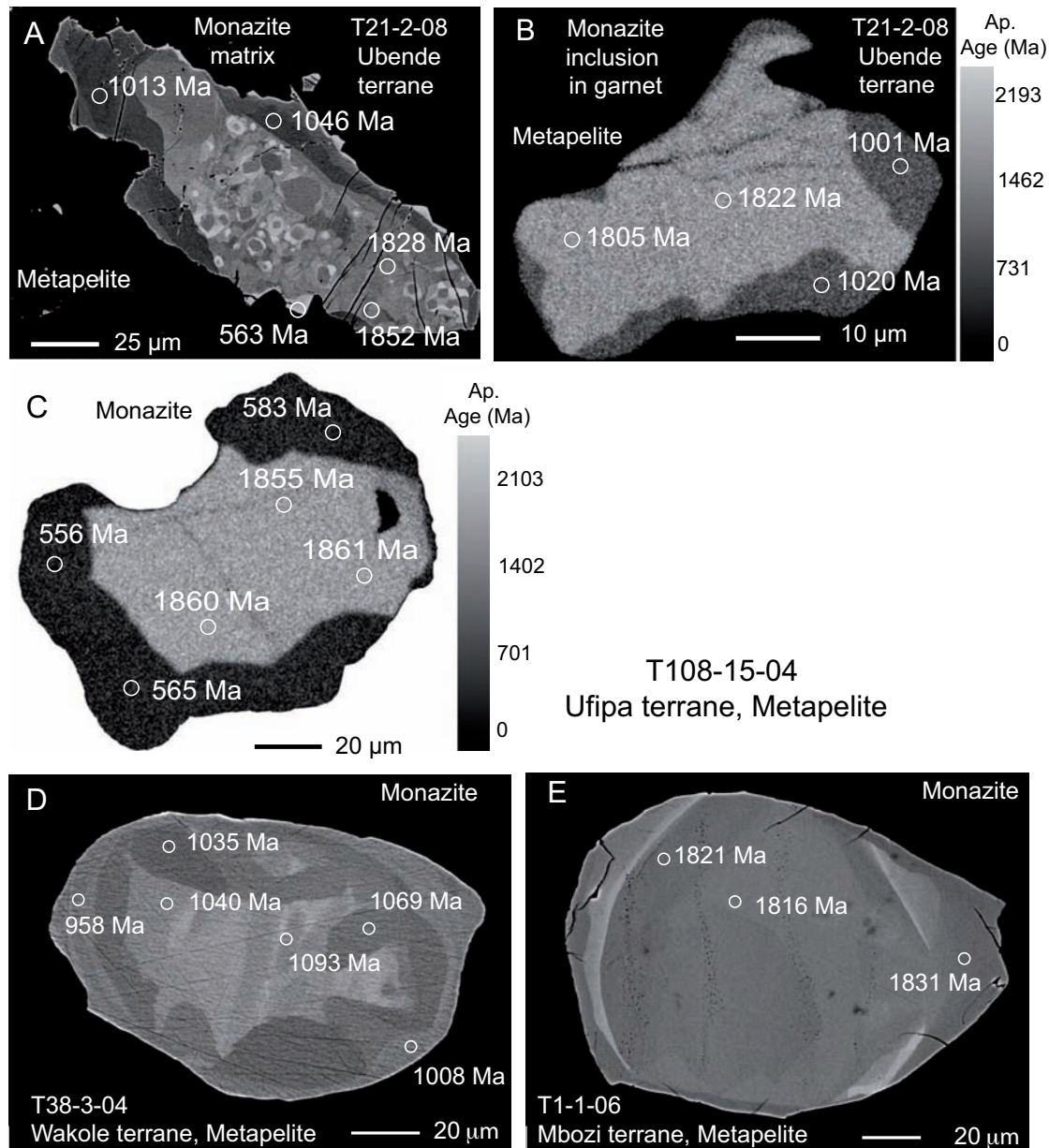


Figure 1.3: BSE image (A, D and E) and maps of apparent ages (B and C) of monazite of the Ubendian belt, demonstrating the different metamorphic overprints of different terranes within the belt. A: Matrix monazite of mylonitic metapelite (T21-2-04) from the Ubende terrane displays three metamorphic ages: Eburnian, Kibaran and Pan-African. B: Monazite inclusion in garnet of the same sample as in A shows only the Eburnian and Kibaran ages, but no Pan-African. C: Monazite from a garnet-kyanite gneiss (T108-15-04) of the Ufipa terrane showing Eburnian and Pan-African ages but no Kibaran. D: Monazite from a metapelite of the Wakole terrane (T38-3-04) with Kibaran apparent ages in all growth zones. E: Monazite of a garnet-kyanite-sillimanite mylonite (T1-1-06) of the Mbozi terrane with Eburnian apparent ages in core and rim.

Table 1.1: U-Pb isotopic composition and apparent ages of zircon from eclogites and metapelites of the Ufipa and Ubende terranes.

No.	U (ppm)	Th (ppm)	$\frac{^{232}\text{Th}}{^{238}\text{U}}$	^{206}Pb (%) comm.	Apparent age (Ma) $\frac{^{207}\text{Pb}}{^{206}\text{Pb}}$ $\frac{^{206}\text{Pb}}{^{238}\text{U}}$		$\frac{^{207}\text{Pb}}{^{206}\text{Pb}}$ *	error (%)	$\frac{^{206}\text{Pb}}{^{238}\text{U}}$ *	error (%)	$\frac{^{207}\text{Pb}}{^{235}\text{U}}$ *	error (%)	disc. (%)
T21-8-04													
7.1	140	142	1.05	—	1904 ± 22	1891 ± 58	0.116	1.2	5.48	3.7	0.34	3.5	1
9.1	27	10	0.39	0.21	1941 ± 55	1872 ± 61	0.119	3.1	5.53	4.9	0.33	3.8	4
T108-7-04													
1.1	78	22	0.29	0.93	514 ± 210	570 ± 20	0.058	9.4	0.73	10	0.092	3.7	-10
1.2	75	22	0.30	0.54	556 ± 150	586 ± 21	0.059	7	0.77	7.9	0.095	3.7	-5
T45-3-04													
2.1	281	253	0.93	—	1827±14	1790±55	0.112	0.76	0.32	3.5	4.93	3.6	2
2.2	505	17	0.03	0.11	981±29	945±31	0.072	1.4	0.1579	3.5	1.563	3.8	4
T132-1-04													
5.1	421	13	0.03	0.18	1935±12	1868±76	0.119	0.64	0.335	4.7	5.49	4.7	4
13.1	369	189	0.53	0.01	2586±7.7	2665±110	0.173	0.46	0.512	4.7	12.21	4.7	-3

*common Pb corrected by using measured ^{204}Pb **Table 1.2:** Th-U-Pb composition of monazite with relative errors; the calculated apparent ages with absolute errors

No.	ThO ₂ (wt-%)	±2σ	UO ₂ (wt-%)	±2σ	PbO (wt-%)	±2σ	Apparent age (Ma)	±2σ
T21-2-04								
10	4.960	0.9	0.428	4.8	0.525	3.7	1822	72
11	6.707	0.8	0.022	13.8	0.538	3.3	1805	61
12	6.703	0.8	0.048	11.0	0.296	5.1	1001	52
23	10.354	0.6	0.013	8.4	0.249	4.4	563	25
128	6.393	0.8	0.074	8.8	0.292	3.9	1020	40
139	5.049	0.9	0.065	9.0	0.425	3.3	1828	63
141	5.249	1.0	0.038	11.2	0.439	3.7	1852	71
146	5.098	0.9	0.391	3.9	0.281	4.0	1013	42
152	4.871	0.9	0.362	4.1	0.276	4.1	1046	44
T108-15-04								
70	5.302	0.8	0.294	4.7	0.151	6.8	565	39
72	6.795	0.7	0.134	6.6	0.597	2.2	1860	44
74	7.458	0.7	0.172	5.6	0.663	2.0	1861	40
75	7.585	0.7	0.112	6.8	0.653	2.1	1855	41
77	5.175	0.8	0.271	4.8	0.151	6.6	583	39
79	5.559	0.8	0.211	5.6	0.148	6.9	556	39
T38-3-04								
162	4.614	0.9	0.521	3.2	0.278	3.9	1008	41
165	4.500	0.9	0.806	2.4	0.336	3.4	1069	38
168	4.006	0.9	0.551	3.1	0.279	3.9	1093	45
174	4.601	0.9	0.285	4.8	0.249	4.3	1035	46
175	4.590	0.9	0.835	2.4	0.335	3.4	1040	37
178	4.681	0.9	0.532	3.2	0.268	4.1	958	41
T1-1-06								
105	5.321	0.8	0.008	15.4	0.428	2.8	1821	53
109	6.270	0.8	0.013	12.8	0.504	2.5	1816	48
112	3.027	1.1	0.015	22.7	0.248	4.4	1831	83

1.5 Discussion and conclusions

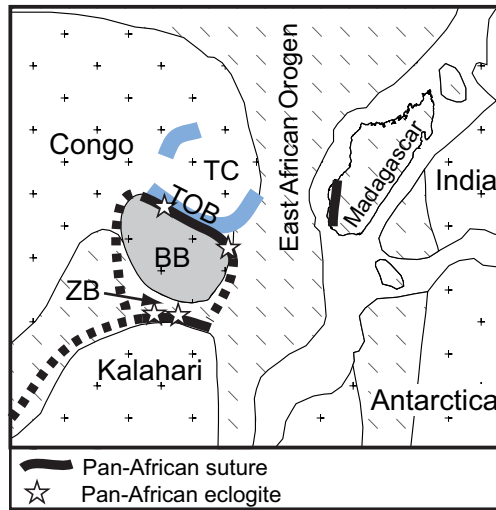
U-Pb zircon and U-Th-total Pb monazite ages of amphibolite- to granulite-facies rocks and of mylonitic eclogites revealed that the terranes of the northwestern Ubendian belt experienced both Paleoproterozoic and Neoproterozoic metamorphic events. Only monazite and zircon of metapelites of the Wakole terrane are missing both metamorphic events, but point to a mono-orogenic overprint during the Mesoproterozoic Kibaran event. The Kibaran metamorphic and orogenic events affected also the polymetamorphic Ubende and Katuma terranes adjoining the Wakole terrane to the southwest and northeast. The Ubende, Katuma and Wakole terranes should therefore be regarded as part of the Kibaran belt that stretches N-S to the west of lake Tanganyika (Fig. 1.1). The 1.39 Ga (Maier *et al.*, 2007) Kapalagulu layered mafic-ultramafic intrusion, which occurs near the northwestern end of the Wakole terrane, underlines the Kibaran connection of the Wakole terrane. As no evidence of a Kibaran imprint was found in the Ufipa terrane bordering the Ubende and Wakole terranes in the southeast, we conclude that the Mesoproterozoic Kibaran terranes and the Ufipa terrane came into contact in the Neoproterozoic, but were in separate positions during the Kibaran orogenic event.

The mylonitic eclogites of the Ubende terrane are relicts of a Paleoproterozoic oceanic crust. The timing of mylonitization is not yet clear. It might be of Kibaran and/or of Pan-African age. During both events monazite growth is recorded by U-Th-total Pb ages. As only the Kibaran monazite occurs as inclusion in garnet and is depleted in Y-HREE, it seems that the Kibaran overprint was of high metamorphic grade.

The geochemistry and zircon ages of the massive coarse-grained eclogites along the northern border of the Ufipa terrane (Fig. 1.1) indicate that they are remnants of a Pan-African suture whose island-arc and back-arc basins separated the Ufipa terrane from the Ubende and Wakole terranes to the north. A southwestward dipping subduction zone would be in accordance with the presence of Pan-African garnet-cordierite-sillimanite gneisses in the southeastern part of the Ufipa terrane that may have formed the upper hot plate above the subduction.

The metamorphic age distribution in the Ubendian belt suggests that the current configuration of terranes was acquired in Pan-African time, during which a suture between the Ubende and Ufipa terranes was formed and the Paleoproterozoic rocks were intensively overprinted. Therefore the dominant NW-SE striking Ubendian structures presumably have been imposed during Pan-African time when all the Ubendian terranes attained their present positions. The proposed Pan-African suture at the northern border of the Ufipa terrane may find its continuation in northern Malawi where another occurrence of Neoproterozoic eclogites has been described (Fig. 1.1; Ring *et al.*, 2002). Very little is known about the western continuation of the proposed suture. It seems not to crosscut the N-S striking Mesoproterozoic Kibaran belt (Fig. 1.1). We speculate that it follows the western margins of the Bangweulu block and may meet the Zambezi belt suture bordering the Bangweulu block to the south. In this case the Bangweulu block may be surrounded by Pan-African sutures and may have formed a microplate during Neoproterozoic times (Fig. 1.4).

Figure 1.4: Simplified geological map of central Gondwana showing eclogites occurrences and Pan-African sutures around the Bangweulu block (BB) and the newly proposed Tanganyika orogenic belt (TOB). Other abbreviations: ZB = Zambezi belt and TC = Tanzania craton. Map modified after Kusky *et al.* (2003).



The Neoproterozoic orogenic belt running NW-SE between lake Tanganyika and lake Malawi is characterized by high-grade (up to garnet-cordierite-sillimanite grade) reworking of Paleoproterozoic crust of the Ufipa terrane and by the occurrence of eclogites formed during the subduction of back-arc and island arc basalts. We propose to call this newly discovered Neoproterozoic orogen “Tanganyika orogenic belt”.

Former simplifying models of Gondwana formation had assumed that west Gondwana (Congo-Kalahari-Southern America) formed one continental block when Indo-Antarctica and later Antarctica-Australia (East Gondwana) amalgamated (Boger & Miller, 2004) or that the Congo-Tanzania-Bangweulu block formed one continental block throughout the Neoproterozoic (Collins & Pisarevsky, 2005). In this paper we demonstrate that the Bangweulu block was separated by a Neoproterozoic suture from the Tanzania craton in the north and that it formed most likely a microplate, as also at its southern border the eclogites of the Zambezi belt were formed from a subducted oceanic floor (John *et al.*, 2003).

1.6 Acknowledgment

This research has been funded by DAAD and DFG (Sche 265/10). We highly value the support provided by D. Garbe-Schönberg and T. John in acquiring geochemical data. The support of A. Mruma in the field is greatly appreciated. We thank B. Mader for assistance with microprobe analyses and A. Fehler for producing thin sections.

References

- Boger, S. D. & Miller, J. M., 2004. Terminal suturing of Gondwana and the onset of the Ross-Delamerian Orogeny: the cause and effect of an Early Cambrian reconfiguration of plate motions. *Earth and Planetary Science Letters*, **219**, 35–48.

- Boynnton, W. V., 1984. Cosmochemistry of the rare earth elements: meteorite studies. In: *Rare earth element geochemistry*, Elsevier Sci. Publ. 63–114.
- Brock, P. W. G., 1963. *The Mbozi syenite-gabbro complex*. Unpublished Ph.D. thesis, University of Leeds.
- Cahen, L., Snelling, N. J., Delhal, J. & Vail, J., 1984. *The geochronology and evolution of Africa*. Clarendon Press, Oxford.
- Collins, A. S. & Pisarevsky, S. A., 2005. Amalgamating eastern Gondwana: the evolution of the circum-Indian orogens. *Earth-Science Reviews*, **71**, 229–270.
- Daly, M. C., Klerkx, J. & Nanyaro, J. T., 1985. Early Proterozoic terranes and strike-slip accretion in the Ubendian belt of southwest Tanzania. *Terra Cognita (Abstract)*, **5**, 257.
- Dodson, M. H., Cavanagh, B. J., Thatcher, E. C. & Aftalion, M., 1975. Age limits for the Ubendian metamorphic episode in northern Malawi. *Geological Magazine*, **112**, 403–410.
- Gabe-Schönberg, C. D., 1993. Simultaneous determination of thirty seven trace elements in twenty-eight international rock standards by ICP-MS. *Geostandards Newsletter*, **17**, 81–97.
- Hanson, R. E., 2003. Proterozoic geochronology and tectonic evolution of southern Africa. In: *Proterozoic East Gondwana: supercontinent assembly and breakup*, Geological Society of London. Special volume, 427–463.
- John, T., Klemd, R., Gao, J. & Garbe-Schoenberg, D., 2008. Trace element mobilization in slabs due to non steady fluid-rock interaction: Constraints from an eclogite-facies transport vein in blueschist (Tianshang, China). *Lithos*, **103**, 1–24.
- John, T., Schenk, V., Haase, K., Scherer, E. & Tembo, F., 2003. Evidence for a Neoproterozoic ocean in south-central Africa from mid-oceanic-ridge-type geochemical signatures and pressure-temperature estimates of Zambian eclogites. *Geology*, **31**, 243–246.
- Kusky, T. M., Abdelsalam, M., Tucker, R. D. & Stern, R. J., 2003. Evolution of the East African and related orogens, and the assembly of Gondwana. *Precambrian Research*, **123**, 81–85.
- Lenoir, J. L., Liegeois, J. P., Theunissen, K. & Klerkx, J., 1994. The Palaeoproterozoic Ubendian shear belt in Tanzania: geochronology and structure. *Journal of African Earth Sciences*, **19**, 169–184.
- Maier, W. D., Peltonen, P. & Livesey, T., 2007. The ages of the Kabanga north and Kapalagulu intrusions, western Tanzania: A reconnaissance study. *Economic Geology*, **102**, 147–154.

- McConnell, R., 1950. Outline of the Geology of Ufipa and Ubende. Bulletin 19, Geological Survey of Tanganyika.
- Möller, A., Appel, P., Mezger, K. & Schenk, V., 1995. Evidence for a 2 Ga subduction zone: eclogites in the Usagaran Belt of Tanzania. *Geology*, **23**, 1067–1070.
- Nanyaro, J. T., Basu, N. K., Muhongo, S. M., Mruma, A. H., Djare, S. A., Mduma, I., Mudiguza, K. M., Van, S. P. & Klerkx, J., 1983. Structural evolution of the Ubendian Belt: preliminary results of a traverse between Karema and Mpanda (Tanzania). *Rapport Annuel - Musee Royal de l'Afrique Centrale*.
- Ray, G. E., 1974. The structural and metamorphic geology of northern Malawi. *Journal of Geological Society of London*, **130**, 427–440.
- Ring, U., Kroener, A., Buchwaldt, R., Toulkeridis, T. & Layer, P. W., 2002. Shear-zone patterns and eclogite-facies metamorphism in the Mozambique Belt of northern Malawi, east-central Africa: implications for the assembly of Gondwana. *Precambrian Research*, **116**, 19–56.
- Ring, U., Kroener, A. & Toulkeridis, T., 1997. Palaeoproterozoic granulite-facies metamorphism and granitoid intrusions in the Ubendian-Usagaran Orogen of northern Malawi, east-central Africa. *Precambrian Research*, **85**, 27–51.
- Rogers, J. J. W. & Santosh, M., 2002. Configuration of Columbia, a Mesoproterozoic supercontinent. In: *Mesoproterozoic supercontinent*, International Association for Gondwana Research, Osaka, Japan. 5–22.
- Sklyarov, E. V., Theunissen, K., Melnikov, A. I., Klerkx, J., Gladkochub, D. P. & Mruma, A., 1998. Paleoproterozoic eclogites and garnet pyroxenites of the Ubende Belt (Tanzania). *Schweiz. Mineral. Petrogr. Mitt.*, **78**, 257–271.
- Sutton, J., Watson, J. & James, T., 1954. A Study of the Metamorphic Rocks of Karema and Kungwe Bay, Western Tanganyika. Bulletin 22, Geological Survey of Tanganyika.
- Theunissen, K., Lenoir, J. L., Liegeois, J. P., Delvaux, D. & Mruma, A., 1992. Major Pan-African imprint in the Ubendian belt of SW Tanzania: U-Pb zircon geochronology and structural context. *C. R. Acad. Sci. Paris*, **314**, 1355–1362.
- Zhao, G., Cawood, P. A., Wilde, S. A. & Sun, M., 2002. Review of global 2.1–1.8 Ga orogens: implications for a pre-Rodinia supercontinent. *Earth-Science Reviews*, **59**, 125–162.

Chapter 2

Paleoproterozoic eclogites of MORB-type chemistry in the Ubendian belt of Tanzania: Evidence for subduction of oceanic lithosphere in a Paleoproterozoic orogenic belt

Abstract

Major and trace element concentrations of eclogites of the Ubende terrane in the Ubendian belt of Tanzania point to a formation of the magmatic precursors of the eclogites in a MOR-type setting. The LREE are depleted with low $(La/Sm)_N$ ratios <1 at variable Nb/La, and the HREE are 10-14 times chondritic values. The chondrite normalized REE patterns resemble that of N-MORB and E-MORB. U-Pb SHRIMP dating of the zircons revealed a metamorphic age of 1886 ± 16 and 1866 ± 14 Ma for the Ubende terrane eclogites. These data indicate that the eclogites may represent a former ocean floor, which became metamorphosed during a Paleoproterozoic subduction.

Mylonitic textures characterize all the eclogites of the Ubende terrane, and have been attained under high-pressure amphibolite- to granulite-facies conditions at $680\text{-}750^\circ\text{C}/10\text{-}11$ kbar during Kibaran and/or Pan-African orogenic events. Omphacitic clinopyroxene (Jd_{17}), matrix plagioclase (Ab_{72}) and garnet core give a minimum peak pressure of 15 kbar at 700°C , which suggests a geothermal gradient lower than $13^\circ\text{C}/\text{km}$.

U-Pb SHRIMP zircon dating of the eclogites and CHIME monazite dating of their country rocks turned out that the Ubende terrane was affected by three orogenic cycles. Metapelites and mafic granulites give Paleoproterozoic metamorphic ages between 1977 ± 40 and 1900 ± 10 Ma. Intensive metamorphic reworking of the Ubendian belt rocks occurred in specific terranes during the Mesoproterozoic Era (1180-1000 Ma) and in the Neoproterozoic Era (620-540 Ma).

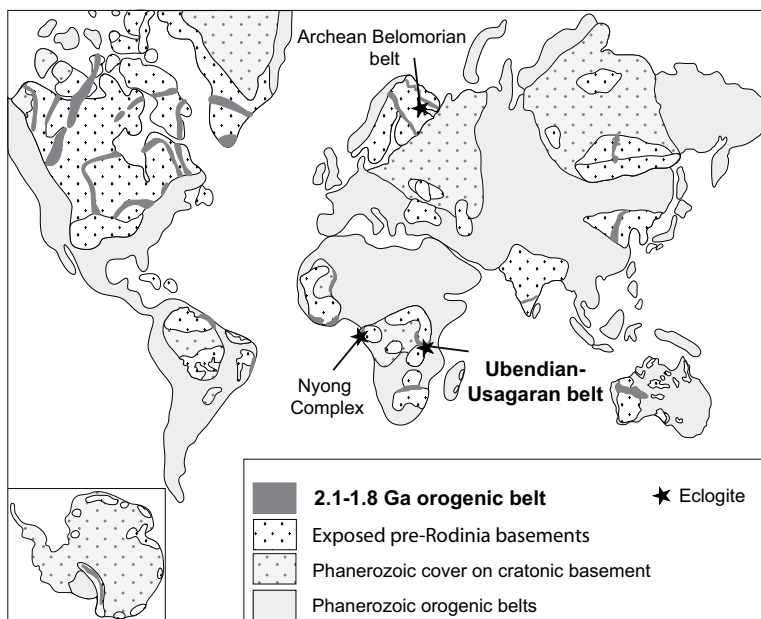
2.1 Introduction

The Ubendian-Usagaran belt of Tanzania is one of the few Paleoproterozoic orogenic belts on Earth that hosts eclogites (Fig. 2.1; Möller *et al.*, 1995; Sklyarov *et al.*, 1998; Smirnov

et al., 1973). According to the theory of plate tectonics, eclogites form at convergent plate margins by subduction processes, therefore are marking the sites of ancient plate collisions and might represent relics of a subducted oceanic lithosphere. The 2.09 Ga eclogites of the Nyong complex of Cameroon and the 2.0 Ga eclogites of the Usagaran belt of Tanzania (Möller *et al.*, 1995; Collins *et al.*, 2004; Loose, 2007) have geochemically an oceanic crust affinity and are interpreted to represent the relics of a Paleoproterozoic oceanic crust at the margins of the Congo craton. The oldest subduction zone rocks exposed in an orogenic belt are recorded in the Belomorian belt in Russia, whose Archean eclogites are dated at 2.7 Ga (Fig. 2.1; Volodichev *et al.*, 2004). The above described eclogite records point to the operation of plate tectonics and subduction processes of oceanic lithosphere in the Archean and Paleoproterozoic Earth, the Earth's modus operandi that is doubted to occur in the Precambrian due to the lack of evidences (e.g. Goodwin, 1996; Hamilton, 1998). However, whether plume tectonics dominated over plate tectonics in Precambrian time is debatable (Windley, 1998; Cawood *et al.*, 2006).

During the course of our study it turned out that the eclogites of the Ubendian belt are not all Paleoproterozoic in age but have been formed during two different orogenic cycles. In this paper we concentrate on the Paleoproterozoic eclogites, the occurrence of which is restricted to the Ubende terrane in the NW part of the Ubendian belt (Fig. 2.2A).

Figure 2.1: The world geological map illustrating the distribution of the 2.1-1.8 Ga orogens and the locations of the Archean and the Paleoproterozoic eclogites of MORB-like chemistry. Map modified after Zhao *et al.* (2002).



The first aim of this paper is to demonstrate that the eclogites of the Ubendian belt represent the remains of a Paleoproterozoic ocean and subduction zone by dating zircons and by studying trace element contents of the eclogites. The reconstruction of the subduction P - T path will contribute in finding out the thermal conditions and tectonic processes taking place in a Paleoproterozoic subduction zone. Secondly, this paper aims to establish the relationship between the subduction zone metamorphism and the regional metamorphism affecting the Paleoproterozoic crustal rocks in the Ubendian belt.

2.2 Geological settings

The linear NW-SE oriented Ubendian belt separates the Archean Tanzania craton from the Paleoproterozoic Bangweulu block. It has been divided into eight litho-tectonic terranes by Daly *et al.* (1985) and Daly (1988): Ubende, Wakole, Katuma, Ufipa, Mbozi, Lupa, Upangwa and Nyika (Fig.2.2). The NW oriented multiphase strike-slip mylonite zones of different ages (see below) mark the terrane boundaries (Theunissen *et al.*, 1996; Boven *et al.*, 1999).

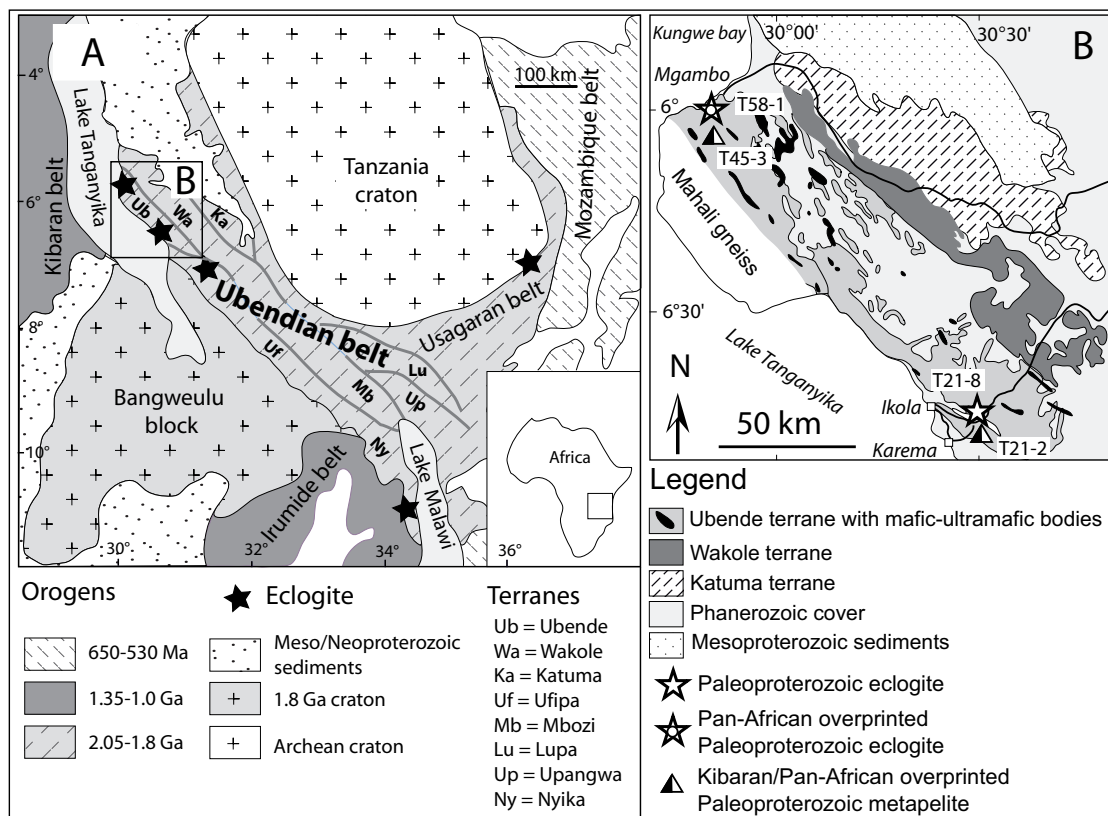


Figure 2.2: A: Geological map of central east Africa with the location of the Ubendian belt; map modified after Hanson (2003). Ubendian belt terranes and dominant lithologies by Daly *et al.* (1985) and Daly (1988): Ubende (metabasites), Wakole (aluminosilicate schists), Katuma (Bt gneisses), Ufipa (gneissic granite), Mbozi (metabasic granulites, quartzites), Lupa (metavolcanics), Upangwa (meta-anorthosite) and Nyika (Crd gneisses). B: Geological map of Ubendian belt depicting the location of eclogites and the associated metapelites and granulites. Map modified after Smirnov *et al.* (1973).

The Ubendian eclogites are known to crop out in the terranes of Ubende and Ufipa Smirnov *et al.* (Fig.2.2A; 1973). The hornblende-rich mafic gneisses that dominate in the Ubende terrane host mylonitic eclogites at Ikola-Karema and Mgambo villages (Fig.2.2B). The lenses (10-100 m scale) of mylonitic eclogites, mylonitic garnet-kyanite gneisses, mylonitic felsic gneisses and the high-pressure mafic granulites are included in the Ubende metabasite complex. The detailed geology of the Ubende terrane has been described by

McConnell (1950), Smirnov *et al.* (1973), Sutton *et al.* (1954) and Nanyaro *et al.* (1983). The structural analyses of the gneissic fabric and mineral lineations are given by Theunissen *et al.* (1996) and Boven *et al.* (1999).

The Ufipa terrane is dominated by granitic biotite gneisses and consisting also garnet-kyanite gneisses (Sutton *et al.*, 1954). Eclogites outcropping in the northern part of the terrane (Smirnov *et al.*, 1973; Sklyarov *et al.*, 1998) are not mylonitic but coarse grained granoblastic and are thus distinct from the eclogites of the Ubende terrane. In the course of this study, it turned out that the Ufipa terrane eclogites are Neoproterozoic in age. They will be discussed in separate paper. Other rock types like hornblende gneiss and garnet amphibolite, micaceous quartzite and albite gneiss are also present in the Ufipa terrane. The Ufipa terrane is separated from the other terranes (Ubende, Mbozi and Kate sheared granites to the southwest) by the NW oriented greenschist to amphibolite-facies sinistral strike-slip planar mylonites, which are attributed to Mesoproterozoic or Neoproterozoic Ubendian belt reactivation events (Theunissen *et al.*, 1996).

Sklyarov *et al.* (1998) did petrological studies and determined a P - T evolution for the eclogites of the Ubendian belt. However, in the absence of geochronological data these authors did not realize that there are eclogites of two orogenic cycles and mixed together petrological data from Paleoproterozoic and Pan-African eclogites to deduce one P - T evolution for these Ubendian rocks. They assumed that the eclogites are Paleoproterozoic in age, in analogy to the 2.0 Ga old eclogites found in the Usagaran belt at the SE side of the Tanzania craton (Fig.2.2A; Möller *et al.*, 1995). Most of the available geochronological data from the Ubendian belt were acquired from granitoids and a few from metamorphic lithologies. The Rb-Sr whole rock ages at 2084 ± 86 Ma and 2026 ± 8 Ma from the Upangwa terrane orthogneisses and granites, respectively, were attributed to the formation of the EW trending granulitic structure in the Mbozi and Ubende terranes (Lenoir *et al.*, 1994). Ages between 2002 ± 0.2 Ma and 1988 ± 0.6 Ma were obtained from the high-pressure and the low-pressure granulites of the Nyika terrane enderbite gneisses and the Crd gneisses (Ring *et al.* (1997); $^{207}\text{Pb}/^{206}\text{Pb}$ zircon evaporation method). These data were used to propose a 2 Ga collisional orogeny in the Ubendian belt which is concurrent to the subduction zone metamorphism in the Usagaran belt at 2.0 Ga (Möller *et al.*, 1995). U-Pb zircon and Rb-Sr whole-rock ages between 1950 and 1850 Ma were interpreted as the onset of an amphibolite-facies ductile dextral strike-slip deformation responsible for the creation of the eight crustal blocks and the prominent NW-SE striking Ubendian belt structure (Lenoir *et al.*, 1994; Theunissen *et al.*, 1996; Boven *et al.*, 1999). Mesoproterozoic and Neoproterozoic greenschist- to amphibolite-facies sinistral strike-slip mylonites were proposed to be formed due to reactivation of the NW-SE striking structure of the Ubendian belt (Theunissen *et al.*, 1996). The later reactivations were so severe in their extent that some authors have interpreted the major NW Ubendian structure to be as young as Kibaran (Ring, 1993) or Pan-African (Theunissen *et al.*, 1992).

The Pan-African orogenic cycle was preceded by alkali-granitoid intrusions, dated at 842 ± 80 Ma (Lenoir *et al.*, 1994) and at 724 ± 6 Ma (Theunissen *et al.*, 1992) in the Upangwa terrane. In addition, syenites from Mbozi terrane were dated at 743 ± 30 (Brock,

1963) and 685 ± 62 Ma (Ray, 1974). These early Pan-African ages may reflect a time of extension preceding the collision event.

2.3 Analytical techniques

Minerals were analysed by using a "JEOL Superprobe JXA-8900R" electron microprobe at the University of Kiel. The acceleration potential used for analyses was 15 to 20 kV for a beam current of 20 nA. The raw data were corrected by using the CITZAF method (Armstrong, 1995).

Major and trace element concentrations of whole rocks were analyzed at the University of Kiel. The Philips PW 1400 X-ray fluorescence analyzer was used to acquire the major element data. The elements were determined on fused glass discs, which were prepared by mixing in a platinum crucible 0.6g of sample powder with 3.6g of $\text{Li}_2\text{B}_4\text{O}_7$, and then the mixture was subjected to the OXIFLUX 5-stage burner. Trace elements were measured by using the Agilent 75000C ICP-MS machine, the sample preparation procedure was that as described by Gabe-Schönberg (1993) and John *et al.* (2008). The data quality, precision and accuracy were ensured by using international reference standards, blanks and some sample duplicates.

Zircons were separated from the crashed rocks by using the conventional magnetic and heavy liquid methods at the University of Kiel. Isotopic *U-Pb* dating of zircon was done on a SHRIMP-II at the Center of Isotopic Research of VSEGEI in St. Petersburg, Russia. Handpicked round and prismatic zircons were mounted on epoxy resin discs and polished to expose their cores, whose transmitted light and cathodoluminescence (CL) images were prepared. The diameter of the analyzing ion beam was approximately 20 μm and the primary beam intensity was about 4 nA. Data reduction was done in the manner described by Williams (1998), using the SQUID Excel Makro by Ludwig (2001). The Pb/U ratios have been normalized relative to a value of 0.0668 for the $^{206}\text{Pb}/^{238}\text{U}$ ratio of the TEMORA-1 internal standard reference zircon, equivalent to an age of 416.75 Ma (Black *et al.*, 2003).

In-situ monazite analyses on Pb-free polished thin sections were performed by using the "JEOL Superprobe JXA-8900R" at the University of Kiel. The Jeol H-Type spectrometer with reduced Rowland circle for high count rates was used for measurements of lead, thorium and uranium. Background offsets were selected after long time fine WD scans of natural monazite. The interference of Th $M\gamma$ on U $M\beta$ was corrected with an experimentally determined correction factor.

As standard materials synthetic REE orthophosphates (Jarosewich & Boatner, 1991) were used for P, REE and Y, synthetic U-bearing glass for U, natural wollastonite for Ca and Si, natural thorianite for Th, crocoite for Pb and corundum for Al. Matrix correction for the analyses was performed by the JEOL ZAF program. Counting times for Pb and U were adapted to net intensities to achieve the desired objective of a low error for counting statistics at reasonable counting times. To control the quality of the data an internal laboratory standard from SE Madagascar (kindly provided by Michael Raith,

Bonn), was repetitively analysed during the measurements. This monazite is homogeneous in composition and was dated with the U-Pb method of cogenetic zircon and by a Sm-Nd monazite-biotite-garnet-zircon isochron at 545 ± 2 and 542 ± 11 Ma, respectively (Paquette *et al.*, 1994), and recently by A. Möller (pers. comm.) with TIMS at an age of 560 ± 1 Ma. Data with significant Al contents were rejected to eliminate analyses with secondary fluorescence artefacts that may occur if analytical points are close to grain boundaries.

Two methods were used to calculate ages for a set of data: (1) the widely used chemical isochron method (Suzuki & Adachi, 1991) and (2) the calculation of a weighted average, which is frequently used in more recent studies on chemical dating of monazite (e.g. Pyle *et al.*, 2005). Isochron calculations were performed with the CHIME-program of (Kato *et al.*, 1999). The isochron plot has the advantage that it easily enables the identification of data sets with distinct ages and provides information about the chemical variation of the analysed monazite in terms of ThO_2^* and PbO. Also, the intercept of the isochron with the axis yields information about the quality of the analytical data. A drawback of this method is that it can suffer from high errors. This may especially occur when the variation of ThO_2^* is small, thus leading to a poorly defined regression line. In contrast to this, the error of the weighted mean does not depend on the chemical variation of the data. Errors that are calculated for the weighted mean tend to decrease with the number of points and typically are significantly lower than the error calculated from the isochrone method.

Age maps were calculated from raw elemental x-ray maps of U, Th and Pb. X-ray maps were measured with 12 kV accelerating potential and a probe current of 200 or 250 nA. Counting times per pixel vary between 0,5 and 0.8 s. The Jeol H-Type spectrometer with reduced Rowland circle was used for Pb. The conversion from count rate maps to concentration maps was performed with the in-house-written software MacAgeMap¹. This software applies a simple calibration line method using monazite as standard material (ZAF=1) to perform a background correction and then convert net intensities to concentration data. Afterwards the program converts each image pixel to an apparent age by solving the age equation iteratively for each pixel and archives the data to an image file.

¹Software available from PA on request

2.4 Petrology, geochemistry and geochronology of Paleoproterozoic eclogites

2.4.1 Petrography and mineral chemistry

The occurrence of Paleoproterozoic eclogites is restricted to the Ubende terrane, cropping out at the villages of Mgambo (Kungwe bay) and Ikola-Karema (Fig. 2.2B). They form lenses (100 m scale) or small bands (dm scale) in the matrix of garnet-clinopyroxene gneisses and hornblende-rich mafic gneisses (Fig. 2.3A). Outcrops of orthopyroxene-clinopyroxene-garnet and garnet-clinopyroxene-biotite gneisses are abundant in the field and in a few outcrops mylonitic garnet-kyanite metapelites are interlayered with the eclogites.

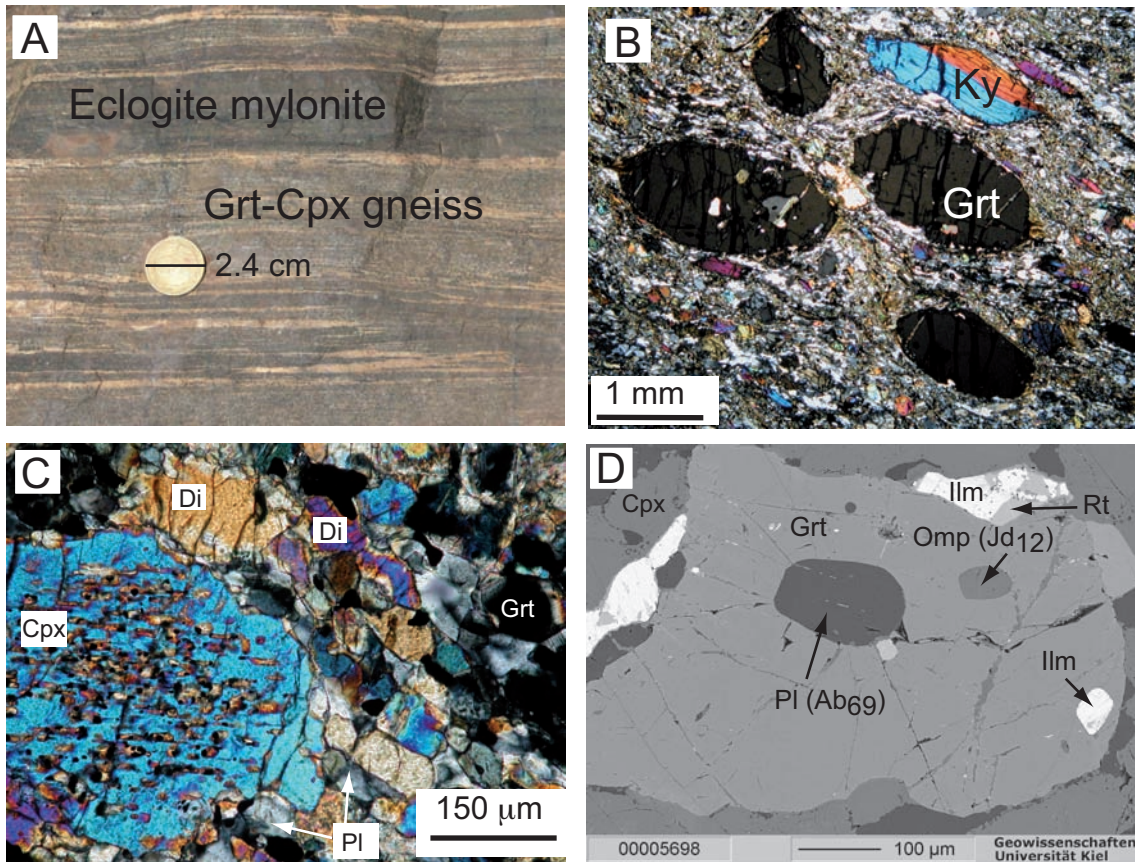


Figure 2.3: A: Bands of eclogite (dark) in a mylonitic garnet-clinopyroxene gneiss from Ikola-Karema village. B: Mylonitic garnet-kyanite metapelite from Ikola-Karema village (T21-2-04) interlayered with eclogites. C: Omphacitic Cpx with Qtz lamellae in the core. The rim is recrystallized into Di and Pl; T24-3-04 from Ikola-Karema villages. D: BSE image of Grt porphyroblast with inclusions of Cpx (Jd = 12 mol%) and Pl ($X_{Ab}=0.69$) from Mgambo village (T41-3-04). Mineral abbreviation after Kretz (1983).

Penetrative mylonitization features all the eclogites and associated garnet-pyroxene gneisses and garnet-kyanite metapelites at Ikola-Karema and Mgambo villages (Fig. 2.3-A&B). However, few porphyroclasts of garnet and omphacitic clinopyroxene are preserved.

The margins of omphacitic clinopyroxene porphyroclasts are recrystallized and transformed into diopside and plagioclase and the cores contain lamellae of quartz (Fig. 2.3C). Garnet porphyroclasts rarely preserve prograde inclusions of omphacite, plagioclase, rutile and quartz (Fig. 2.3D). The characteristic mineral assemblage in the mylonitic and retrogressed eclogites of the Ubende terrane is garnet-clinopyroxene-rutile-quartz-plagioclase-hornblende-ilmenite-zircon. This assemblage has been formed during the granulite-facies mylonitic overprint and can not be used to determine P - T during the eclogite-facies stage (cf. Muhongo *et al.*, 2002).

Garnet porphyroclasts have X_{Mg} ratios between 0.33 and 0.41 with a representative core composition of $X_{Alm} = 0.44$, $X_{Prp} = 0.30$, $X_{Grs} = 0.25$ and $X_{Sps} = 0.01$ (Tab. 2.1; T40-1-04). Chemical profiles display garnet cores that are slightly richer in grossular than the rim. X_{Prp} slightly increases from the core towards the rim and drops at the outermost rim (Fig. 2.4A).

The cores of the clinopyroxene porphyroclasts are Na-richer than the rims and the recrystallized clinopyroxene grains of the matrix. Jadeite contents in the core may reach up to 18 mol% and drop to about 11 mol% in the rims (Fig. 2.4B). The inclusions in garnet have between 8.5 and 14 mol% jadeite and the recrystallized clinopyroxene in the matrix has low contents of jadeite between 8 and 9 mol% (Tab. 2.1).

Plagioclase in the matrix is Na rich with X_{Ab} between 0.72 and 0.71, which is similar to the plagioclase inclusion in garnet with $X_{Ab} = 0.69$ (Fig. 2.3D).

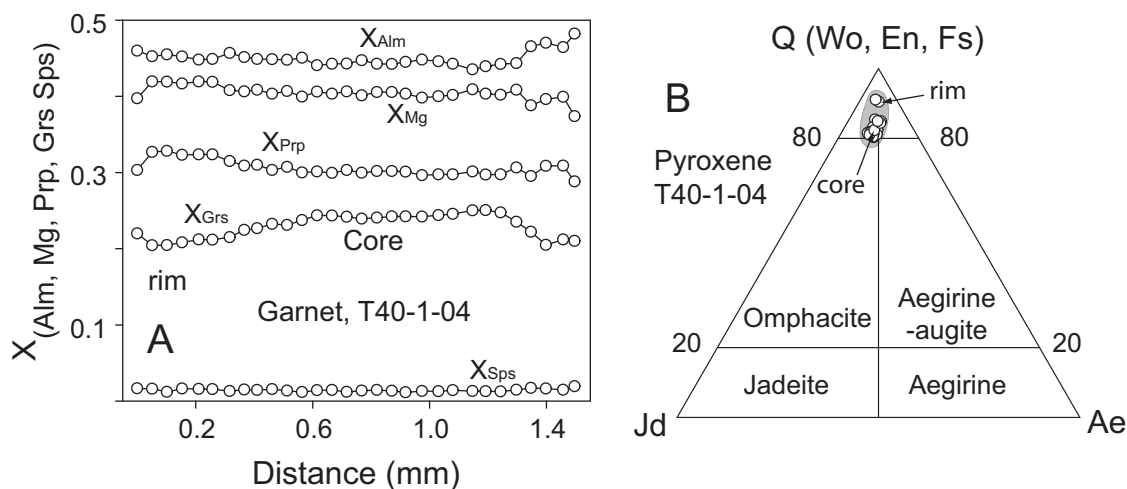


Figure 2.4: A: Zoning profile through a porphyroclastic garnet of eclogite T40-1-04. B: Composition of omphacitic porphyroclasts (T40-1-04); pyroxene classification according to Morimoto *et al.* (1988).

Table 2.1: Representative electron microprobe analyses of garnet, plagioclase and clinopyroxene of the Ubende terrane eclogites

Sample No.	Grt						Pl						Cpx								
	T25-1 118 ^{core}	T40-1 17 ^{core}	T41-3 215 ^{core}	T60-1 287 ^{core}	T40-1 38 ^{rim}	T40-1 39.33	T25-1 58.20	T25-1b 127 ^{core}	T25-1 41 ^{incl.}	T40-1 69 ^{core}	T41-3 208 ^{incl.}	T60-1 280 ^{core}	T43-1 210 ^{incl.}	T25-1b 176 ^{core}	T25-1 60 ^{incl.}	T40-1 51 ^{core}	T40-1 54 ^{core}	T40-1 55 ^{core}	T41-3 204 ^{incl.}	T41-3 191 ^{incl.}	T60-1 27 ^{incl.}
SiO ₂	39.24	39.02	39.55	38.88	38.77	39.33	58.20	57.55	60.58	59.88	62.62	59.69	50.58	50.51	50.55	50.62	50.36	50.24	50.88	52.43	
Al ₂ O ₃	21.39	21.33	22.22	21.53	21.74	22.04	26.25	26.53	24.85	24.92	23.30	25.27	0.19	0.26	0.48	0.38	0.42	0.60	0.40	0.29	
FeO	21.62	22.92	21.58	22.51	25.63	22.98	0.19	0.08	0.10	0.79	0.39	0.92	5.31	4.96	6.71	7.01	6.95	5.95	5.50	4.37	
MgO	6.92	6.23	8.36	6.93	6.74	7.70	8.27	8.13	5.95	6.48	4.13	6.35	5.32	3.68	5.66	4.78	5.33	3.74	3.92	6.81	
MnO	0.88	1.15	0.68	0.59	0.66	0.92	6.90	6.80	8.40	8.03	9.15	7.98	4.10	4.66	3.45	4.64	3.93	4.42	4.03	1.62	
CaO	9.95	9.42	8.51	9.58	6.93	7.81	0.04	0.09	0.09	0.03	0.12	0.00	11.61	12.23	10.42	10.44	10.32	11.64	12.01	11.45	
Total	100.00	100.07	100.90	100.02	100.47	100.78	99.86	99.78	99.97	100.12	99.71	100.21	0.14	0.02	0.10	0.09	0.00	0.00	0.00	0.08	0.05
Si	3.01	3.01	2.99	2.99	2.99	3.00	2.61	2.58	2.70	2.67	2.78	2.66	1.87	1.87	1.88	1.86	1.87	1.86	1.88	1.95	
Al	1.94	1.94	1.98	1.95	1.98	1.98	1.39	1.41	1.30	1.31	1.22	1.33	0.01	0.01	0.01	0.01	0.01	0.02	0.01	0.01	
Fe	1.39	1.48	1.37	1.45	1.65	1.46	0.01	0.02	0.00	0.03	0.01	0.03	0.23	0.22	0.29	0.30	0.30	0.26	0.24	0.19	
Mg	0.79	0.72	0.94	0.80	0.78	0.87	0.40	0.39	0.28	0.31	0.20	0.30	0.16	0.11	0.18	0.15	0.17	0.12	0.12	0.21	
Mn	0.06	0.08	0.04	0.04	0.04	0.06	0.60	0.59	0.72	0.69	0.79	0.69	0.11	0.13	0.10	0.13	0.11	0.12	0.11	0.05	
Ca	0.82	0.78	0.69	0.79	0.57	0.64	0.00	0.01	0.01	0.00	0.01	0.00	0.64	0.68	0.58	0.57	0.57	0.64	0.66	0.64	
Total	8.00	8.01	8.02	8.02	8.01	8.01	5.00	5.00	5.02	5.01	5.00	5.01	0.00	0.00	0.00	0.00	0.00	0.00	0.00	0.00	
X _{Mg}	0.36	0.33	0.41	0.35	0.32	0.37	0.60	0.60	0.72	0.69	0.79	0.69	0.86	0.88	0.78	0.79	0.79	0.84	0.85	0.80	
X _{Alm}	0.45	0.49	0.45	0.47	0.54	0.48	0.40	0.40	0.28	0.31	0.20	0.31	0.10	0.10	0.18	0.18	0.18	0.14	0.13	0.16	
X _{Prp}	0.26	0.24	0.31	0.26	0.25	0.29	0.00	0.01	0.01	0.00	0.01	0.00	0.00	0.00	0.00	0.00	0.00	0.00	0.00	0.00	
X _{Grs}	0.27	0.26	0.23	0.26	0.19	0.21	0.00	0.00	0.00	0.00	0.00	0.00	0.00	0.00	0.00	0.00	0.00	0.00	0.00	0.00	
X _{Sps}	0.02	0.03	0.01	0.01	0.01	0.02	0.00	0.00	0.00	0.00	0.00	0.00	4.00	4.00	4.00	4.00	4.00	4.00	4.00	4.00	
X _{Mg}	0.80	0.86	0.77	0.80	0.78	0.85	0.80	0.86	0.77	0.80	0.78	0.85	0.80	0.86	0.77	0.80	0.78	0.85	0.85	0.75	
Jd%	10.30	8.67	17.27	16.82	17.51	11.90	10.30	8.67	17.27	16.82	17.51	11.90	10.30	8.67	17.27	16.82	17.51	11.90	11.49	14.17	

Cations calculated on the basis of 12 oxygens for Grt, 8 oxygens for Pl and 6 oxygens for Cpx; incl. = inclusions in Grt

2.4.2 P - T conditions

Mylonitic overprinting, mineral recrystallization and exsolution exclude the estimate of peak-metamorphic pressures of the Ubende terrane eclogites. However, a minimum peak pressure can be estimated (garnet core of porphyroclasts, exsolved clinopyroxene porphyroclast with $Jd = 17$ mol% and a matrix plagioclase of $X_{Ab} = 0.72$). The equilibrium garnet-plagioclase-clinopyroxene-quartz has been used as geobarometer (Powell & Holland, 1988), which results in an estimate of the minimum pressure of about 15 kbar at temperatures of 700-750 °C (Tab. 2.2).

Zr-in-rutile thermometry was applied (Fig. 2.5 and Tab. 2.2) on the well preserved rutile grains that coexist with zircon and quartz. This thermometer seems to be more reliable than the garnet-clinopyroxene thermometers in estimating the temperatures of eclogites and blueschists (Spear *et al.*, 2006). Four rutile grains (3 from matrix and 1 included in garnet) were analyzed from two eclogites T40-3-04 and T60-1-04 and the results are listed in Tab. 2.2. Rutile thermometers calibrated by Watson *et al.* (2006), Tomkins *et al.* (2007) and Ferry & Watson (2007) give average temperatures between 603 ± 21 and 647 ± 32 °C for the matrix grains, whereas relatively higher average temperatures between 707 ± 12 and 742 ± 13 °C were calculated with the three calibrations from rutile included in garnet. The temperature distribution in single rutile grains of the analyzed samples fall into narrow ranges. For example in grain 1 of sample T40-3-04 there is a temperature difference of 61 °C between maximum and minimum values (632-571 °C; Fig. 2.5).

The lower Zr contents in matrix rutile grains than in rutile inclusions in garnet can be explained by reequilibration of the matrix grains during the late-stage mylonitization that affected the eclogites. We assume that Zr-in-rutile temperatures obtained from inclusions in garnet are closer to the peak metamorphic temperatures than those obtained from matrix grains.

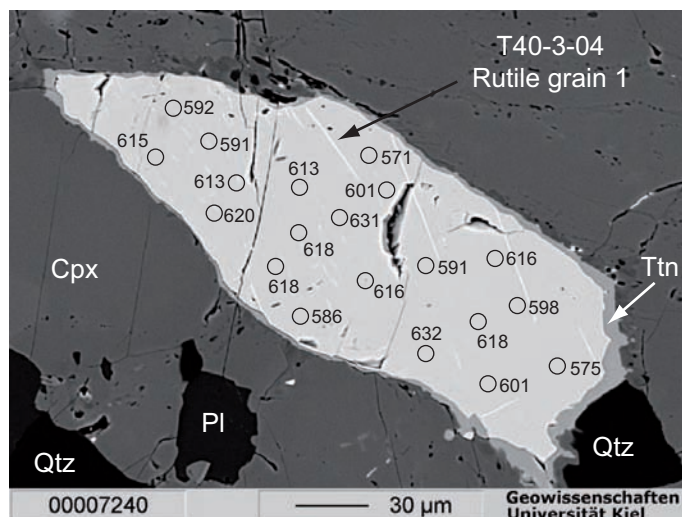


Figure 2.5: Backscattered electron image of a rutile matrix crystal from sample T40-3-04. Circles show location of analysis points. Numbers are temperatures in °C calculated from the rutile thermometer calibration of Ferry & Watson (2007).

The P - T conditions during the prograde subduction have been constrained by using the preserved compositions of the inclusions of clinopyroxene, plagioclase and rutile in

garnet. The temperatures were estimated by using the Fe-Mg exchange equilibria between garnet and clinopyroxene as calibrated by Ellis & Green (1979) and Powell (1985), whereas the corresponding pressure values of 11 and 12.2 kbar were calculated by using the clinopyroxene-plagioclase-garnet-quartz equilibrium (Tab. 2.2; Powell & Holland, 1988). The clinopyroxene inclusions with jadeite contents of 9 and 12 mol% from different garnet grains give a narrow range in temperature between 630 °C and 650 °C (Fig. 2.6; Tab. 2.2). The sets of P - T values that were obtained give a possible P - T trajectory during subduction (Fig. 2.6).

Table 2.2: Results of the pressure and temperature estimates of the Ubende terrane eclogites.

Sample No.	Mineral & analysis No.	T (°C)	Thermometer	P (kbar)	Barometer	Remarks
Grt-Cpx: Fe-Mg exchange thermometers and Grt-Pl-Cpx-Qtz barometers						
Thermometers: Grt-Cpx: Fe-Mg exchange; EG = Ellis & Green (1979) and P= Powell (1985),						
Geobarometers: H = Holland (1980), NP = Newton & Perkins (1982) and PH = Powell & Holland (1988)						
T25-1-04 Cpx (Jd=9%)	Grt ₂₇ -Cpx ₆₀ -Pl ₄₁	630 620	EG P	11.0	PH	Cpx-Pl inclusion in Grt
T41-1-04 Cpx (Jd=12%)	Grt ₂₁₅ -Cpx ₂₀₄ -Pl ₂₀₈	650 640	EG P	12.2	PH	Cpx-Pl inclusion in Grt
T40-1-04 Cpx (Jd=17%)	Grt ₁₇ -Cpx ₅₁ -Pl ₆₉	700		15.0**	PH	Grt-Cpx porphyroclasts
T25-1b-04	Grt ₁₁₈ -Cpx ₁₇₆ -Pl ₁₂₇	750 740	EG P	11.0 10.2	NP H	Cpx-Grt-Pl in matrix
T60-1-04 Cpx (Jd=14%)	Grt ₂₈₇ -Cpx ₂₇ -Pl ₂₈₀	700 680	EG P	10.9 10.2	NP H	Cpx-Grt-Pl in matrix

** Pressure calculated at a reference temperature of 700 °C (Zr-in-rutile thermometry)

Zr-in-rutile thermometry

Thermometers: W=Watson *et al.* (2006), T= Tomkins *et al.* (2007) and FW = Ferry & Watson (2007)

Sample	Grain	No. of spots	Mean Zr (ppm) error at 1 σ	Mean T (°C), error at 1 σ		
				W	T	FW
T40-3-04	Rt-1 in matrix	21	202±43	610±17	638±17*	606±16
	Rt-2 in matrix	19	195±43	606±21	635±21*	603±21
T60-1-04	Rt-1 in matrix	8	237±90	619±31	647±32*	615±30
	Rt-2 inclusion in Grt	6	676±91	713±13	742±13*	707±12

* Temperature calculated at a reference minimum peak pressure of 15 kbar

The late-stage mylonitic overprint that affected all the eclogites of the Ubende terrane most likely was not related to the uplift after subduction but is attributed to later orogenic events (Mesoproterozoic and Neoproterozoic). This is indicated by zircon and monazite ages of associated metapelites and some rare zircon rim ages of eclogites (chapter 1 & 3). A pressure of about 10-11 kbar and a temperature of approximately 680-750 °C are obtained

from the recrystallized minerals of the matrix. Therefore, the mylonitization stage was in the high-pressure amphibolite- to granulite-facies (Fig. 2.6). The pressure was estimated by using the garnet-plagioclase-clinopyroxene-quartz geobarometer calibrated by Newton & Perkins (1982) and Powell & Holland (1988); the temperature estimate is based on the Fe-Mg exchange reaction between garnet and clinopyroxene using the calibrations of Ellis & Green (1979) and Powell (1985).

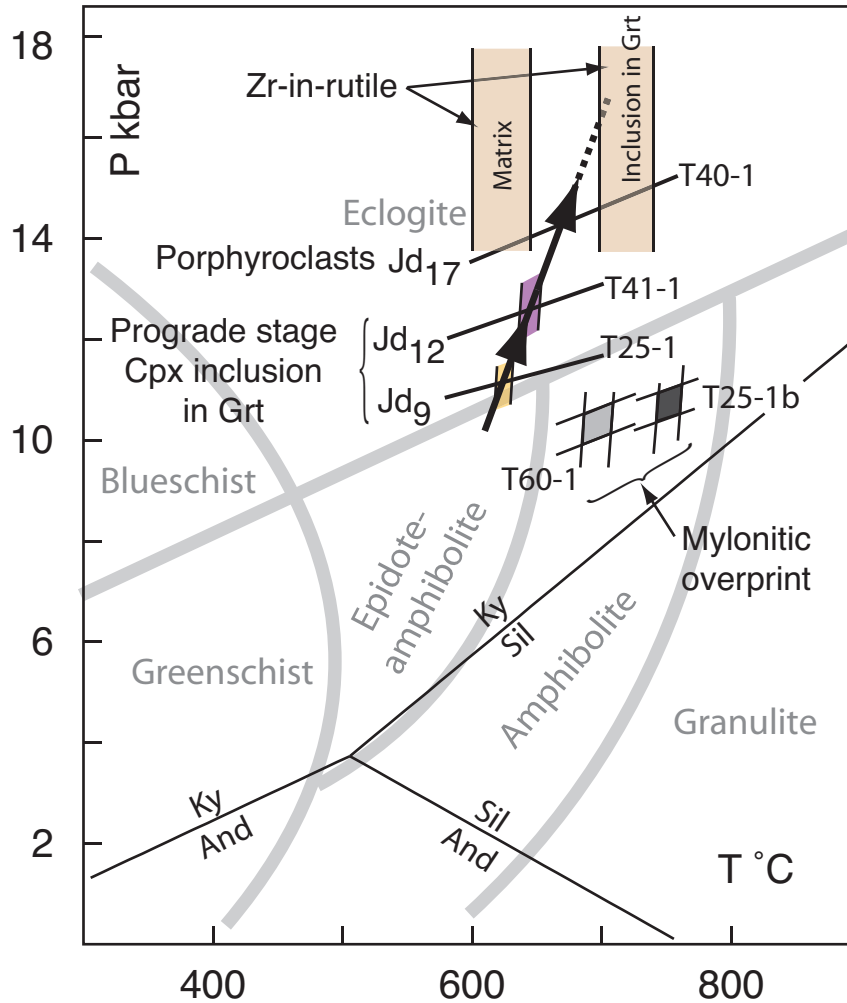


Figure 2.6: *P-T* conditions at different stages of metamorphism of the Ubende terrane eclogites: Minimum *P* conditions during peak are obtained from the porphyroclast of Cpx (Jd₁₇) and Grt core composition. The peak-temperature range was estimated by using the Zr-in-rutile thermometry (Ferry & Watson, 2007). The prograde *P-T* conditions were estimated by using the compositions of the inclusions of Cpx (Jd₉ and Jd₁₂) and Pl in Grt (Powell & Holland, 1988). The *P-T* values for the mylonitic overprint during a later orogenic event were obtained with recrystallized Cpx-Pl-Grt-Qtz of the matrix; geothermometers of Ellis & Green (1979) and Powell (1985); geobarometer after Powell & Holland (1988).

2.4.3 Geochemistry

A total of 20 eclogite samples from Ikola-Karema and Mgambo villages in the Ubende terrane were analyzed for major and trace elements, the analyses are given in Tab. 2.3. All the analyzed eclogites are basaltic in composition (SiO_2 , 45.3-49.2%) and they plot in the basalt field in the Zr/Ti vs Nb/Y diagram of Pearce (1996) (Fig. 2.7A); they also follow a tholeiitic magma trend in the triangular AFM plot $[(\text{Na}_2\text{O}+\text{K}_2\text{O})-(\text{FeO}+\text{TiO}_2)]-(\text{MgO})$ (Fig. 2.7B). However, the plotting position in the AFM diagram might have changed during metamorphism because of the high mobility of Na_2O and K_2O (e.g. Tatsumi *et al.*, 1986), but still data are consistent with their origin as tholeiite basalts.

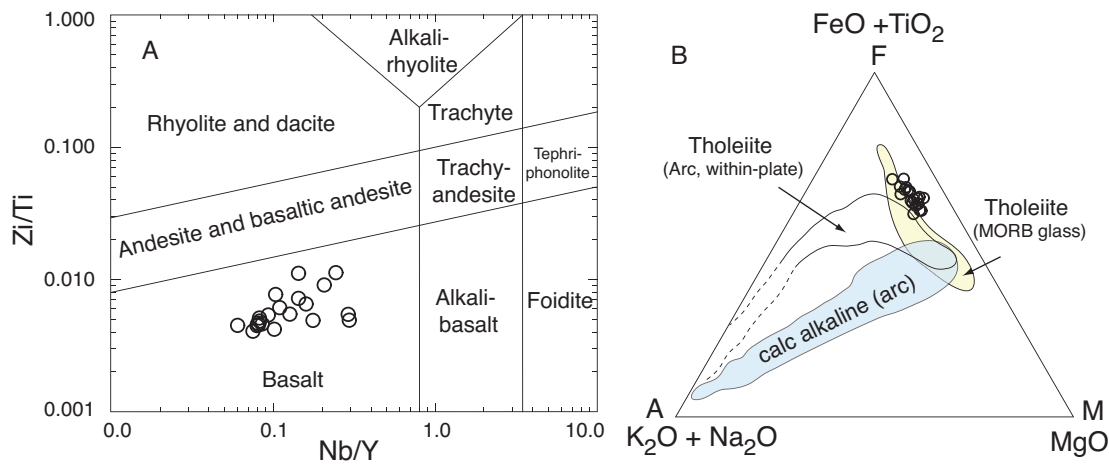


Figure 2.7: Plots of the Ubende terrane eclogites in magma discrimination diagrams. A: The analyses fall into the basaltic magma field in the Zr/Ti vs Nb/Y diagram of Pearce (1996). B: The analyses follow the tholeiitic magma trend in the AFM diagram.

Tholeiite basalts are known to be generated by decompressional partial melting of upper mantle peridotite at plate margins at mid oceanic ridges (MOR) or at island arcs and within plates at oceanic islands and in continental rifts. However, the tholeiite basalts from these tectonic settings can be distinguished by systematic observation of their rare earth and other trace element concentrations and ratios, e.g. Pearce & Cann (1973) and John *et al.* (2003).

The eclogites of tholeiitic composition in the Ubende terrane are subdivided into two groups on the basis of chondrite normalized REE (rare earth element) patterns, labeled group I and group II eclogites (Fig. 2.8A&B). The REE patterns of group I eclogites lie below the average MORB values and are depleted in the LREE (light rare earth element), which range between 4 to 14 times chondritic values. The concentrations of the HREE (heavy rare earth element) are fairly constant with values about 10 times chondritic. The REE pattern is strikingly similar to that of basaltic magmas that erupt at the spreading axes of mid oceanic ridges (N-MORB; Schilling *et al.*, 1983).

The REE patterns of group II eclogites are similar to those of group I but are relatively enriched in LREE (ranging between 10 to 18 times the chondritic values) when compared

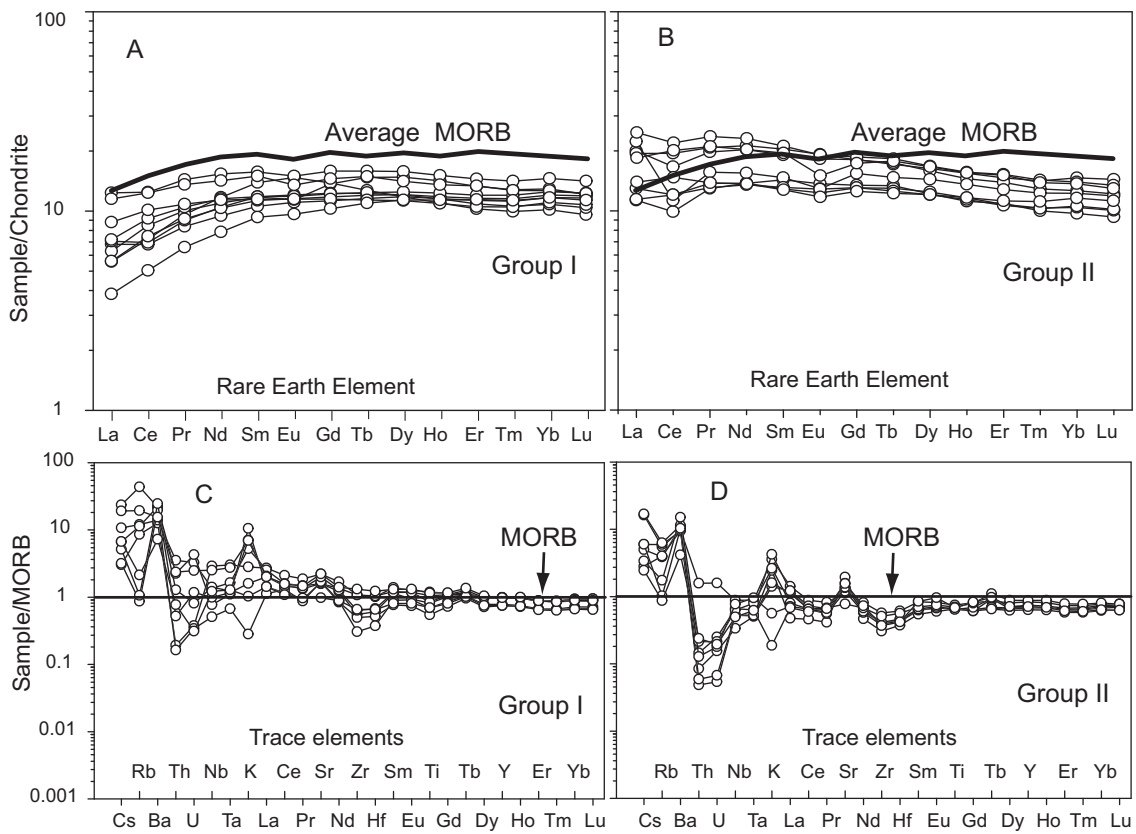


Figure 2.8: LREE depleted (Group I) and LREE enriched (Group II) eclogites of the Ubende terrane. A&B: Sample/chondrite normalized REE, the normalization values are from Boynton (1984). C&D: Sample/MORB normalized trace element patterns; normalizing values after Hofmann (1988).

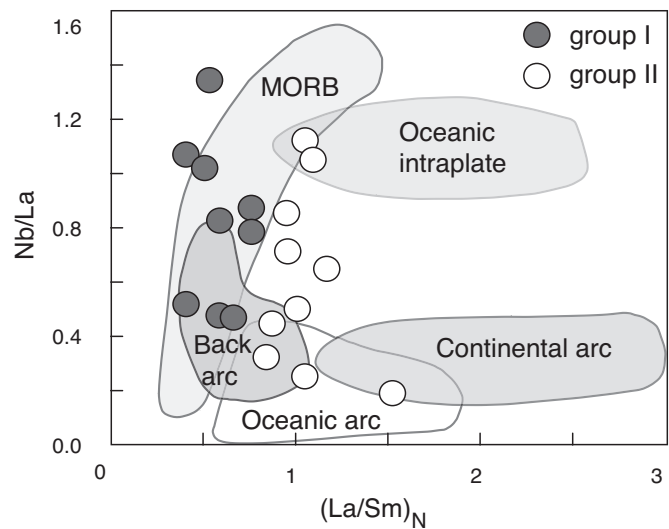


Figure 2.9: Nb/La vs $(La/Sm)_N$ diagram after John *et al.* (2003) showing the tectonic setting of the precursor melts of the mylonitic eclogites of the Ubende terrane (group I and group II; cf. Fig. 2.8). The $(La/Sm)_N$ ratio is low in group I and somewhat higher in group II eclogites.

to group I eclogites. The REE patterns are almost flat and look very similar to the enriched MORBs known as E-MORB (Schilling *et al.*, 1983). Both eclogite groups lack an Eu anomaly, which implies that the mantle derived eclogite precursor magmas were not contaminated by the continental crust and originated from greater depths, outside the stability of plagioclase. A high degree of partial melting is implied in both groups of eclogites due to lower concentrations of REE than the average MORB.

The sample/MORB normalized trace element patterns of group I (Fig. 2.8C) are flat, giving ratios of about one. However, positive anomalies of Cs, Rb, Ba and K might originate from secondary processes due to high fluid mobility of these elements. These features are as well observed in group II eclogites (Fig. 2.8D).

Trace element ratios of group I eclogites are similar to those of basalts that erupt at mid oceanic ridges or in back-arc environments in small ocean basins (Fig. 2.9). The ratios of Nb/La have a wide range between 0.4 and 1.4 and that of $(La/Sm)_N$ is < 1 , whereas group II eclogite has $(La/Sm)_N$ ratios that range between 0.9 and 1.5 and Nb/La ratios that lie between 0.2 and 1.2. These trace element ratios are within the range of the composition of basalts that erupt at mid oceanic ridge or back-arc settings.

The information obtained from the trace element patterns and the trace element ratios show that the Ubende terrane eclogites have a chemical affinity to N-MORB others to oceanic arc and/or back-arc systems. In all diagrams, the group I eclogites are clearly fitting to the N-MORB composition. Group II eclogites, which scatter between E-MORB, oceanic arc basalt and back-arc basalt geochemistry, may be attributed to a marginal ocean basin. It has been described that N-MORB erupts in well developed back-arc basins and E-MORB during the early stages of the evolution of an arc system (Hawkins & Melchior, 1985; Gill, 1987). However, in large ocean basins like in the Atlantic the N-MORB and E-MORB may be associated if plumes are close to the MOR (e.g. Schilling *et al.*, 1983). Therefore the eclogite association of the Ubende terrane seem to have been derived from a marginal ocean basin in a back arc environment or from an ocean basin in which a plume was close to the MOR.

Table 2.3: Geochemical composition of the Ubende terrane eclogites

Sample	T3-1	T3-3	T17-1	T18-2	T21-4	T25-1	T40-2	T41-3	T58-2	T60-2	T3-1	T19-2	T21-8	T24-3	T40-1	T43-1	T43-2	T53-1	T58-1	T60-1	
Group I eclogites											Group II eclogites										
SiO ₂	47.59	48.04	45.27	47.09	47.15	46.36	47.82	47.76	48.24	47.19	47.50	48.93	46.91	46.29	47.89	47.57	46.13	49.21	48.28	47.44	
TiO ₂	1.08	1.06	1.34	1.21	1.06	1.06	1.13	1.10	1.04	1.16	1.92	1.71	1.32	0.88	1.12	1.06	1.36	1.13	1.12	1.86	
Al ₂ O ₃	13.75	13.50	12.61	12.89	13.85	12.80	13.95	13.83	13.38	13.58	13.59	13.31	13.31	13.02	13.52	13.44	13.88	13.56	13.92	12.41	
FeO	14.88	14.70	16.91	15.72	14.76	15.87	15.41	14.51	15.14	15.92	16.43	15.14	16.50	13.27	14.78	15.51	16.04	14.56	13.93	17.92	
MnO	0.25	0.25	0.26	0.21	0.23	0.27	0.24	0.23	0.24	0.23	0.32	0.23	0.25	0.24	0.21	0.29	0.22	0.37	0.22	0.28	
MgO	7.72	7.71	6.83	6.28	7.02	6.80	7.61	7.17	7.87	7.88	6.07	6.35	6.94	7.30	7.29	8.01	6.02	7.07	8.04	5.76	
CaO	11.98	12.17	12.31	13.62	12.95	14.42	12.46	14.02	11.77	11.89	10.83	10.66	11.38	15.02	12.57	12.38	12.74	11.47	11.78	9.83	
Na ₂ O	1.94	1.88	1.67	1.83	1.94	1.91	1.89	1.82	2.09	1.73	1.85	2.33	1.61	1.46	2.37	1.38	2.47	2.00	1.87	2.42	
K ₂ O	0.15	0.17	0.93	0.38	0.45	0.26	0.06	0.02	0.28	0.08	0.30	0.56	0.75	1.12	0.03	0.14	0.17	0.11	0.21	0.74	
P ₂ O ₅	0.07	0.07	0.12	0.10	0.08	0.08	0.10	0.09	0.08	0.08	0.24	0.16	0.12	0.13	0.10	0.09	0.13	0.08	0.09	0.17	
LOI	0.08	0.26	1.06	0.74	0.00	0.45	0.00	0.00	0.00	0.00	0.77	0.16	0.62	1.24	0.02	0.04	0.58	0.00	0.00	1.01	
Total	99.49	99.81	99.31	100.07	99.49	100.28	100.78	100.65	100.13	99.87	99.05	99.54	99.71	99.97	99.90	99.91	99.74	99.56	99.57	99.84	
Trace elements in ppm																					
Zr	51	57	102	62	55	49	56	52	51	52	127	114	65	60	43	52	70	69	61	126	
Li	11.3	10.5	6.7	18.8	10.9	17.0	18.7	19.8	15.1	18.9	10.6	9.7	7.5	17.4	21.1	19.0	14.5	20.1	13.6	9.3	
Sc	56.9	59.7	55.9	57.0	51.6	58.4	60.1	52.2	56.4	55.4	50.7	53.4	60.9	54.2	56.7	55.0	51.2	53.2	52.6	45.8	
V	373	368	390	407	347	333	383	366	339	377	372	391	397	311	385	367	382	377	365	421	
Co	57.2	56.1	63.7	59.6	56.6	60.3	61.4	55.7	57.1	61.6	54.8	56.3	64.3	53.9	60.3	60.8	58.1	57.3	54.1	62.2	
Ni	95.0	93.4	82.9	84.7	97.9	66.2	114	113	94.4	106	59.6	58.0	97.6	77.2	119	124	80.3	120	122	61.3	
Cu	98	153	156	16	116	15	426	98	131	83	385	41	50	8	114	35	216	66	158	152	
Zn	122	114	117	117	111	98	125	102	109	129	133	122	134	92	121	150	102	108	112	126	
Ga	15.5	15.2	15.7	17.6	15.7	13.2	16.5	15.7	14.4	15.6	16.4	19.7	19.3	14.6	18.0	15.7	15.8	16.4	15.4	20.5	
Rb	3.18	3.40	25.37	6.67	6.86	6.02	0.55	0.46	1.42	0.67	5.13	14.5	14.4	47.0	0.49	1.83	0.86	2.06	2.37	22.7	
Sr	122	138	167	128	161	190	74	144	127	178	238	182	179	154	174	116	195	95	158	227	
Y	21.8	22.4	27.0	29.2	20.6	20.5	25.5	20.3	20.5	20.8	31.3	33.9	33.3	21.6	24.4	26.8	28.1	21.6	21.2	30.3	
Zr	29.0	29.7	49.2	56.1	26.7	28.6	33.2	26.8	31.9	32.1	62.8	114	57.1	48.1	30.5	30.8	43.9	44.4	36.8	126	
Nb	1.76	1.83	3.01	3.07	2.12	1.25	4.56	1.54	1.71	1.81	9.23	4.94	4.86	4.54	2.02	2.24	2.67	3.50	2.73	7.49	
Cs	0.070	0.040	0.074	0.229	0.238	0.084	0.084	0.035	0.048	0.066	0.043	0.151	0.094	0.332	0.045	0.074	0.072	0.094	0.067	0.269	
Ba	154	141	632	142	162	118	136	55	186	115	175	200	308	291	220	146	314	87	136	199	
La	1.73	2.21	3.80	3.54	2.71	1.18	1.93	1.71	2.09	2.17	8.28	7.66	5.72	4.33	3.50	6.92	6.20	4.02	3.55	6.02	
Ce	6.0	7.4	10.0	9.9	8.1	4.0	6.8	5.8	5.5	5.6	24.0	17.8	16.3	11.9	8.0	9.1	13.4	9.7	9.7	15.7	
Pr	1.11	1.27	1.74	1.65	1.31	0.80	1.22	1.16	1.01	1.09	3.73	2.88	2.57	1.69	1.58	1.91	2.41	1.68	1.60	2.53	
Nd	6.18	6.87	9.15	8.46	6.77	4.67	6.53	6.97	5.63	6.23	18.1	13.8	12.2	8.19	8.25	9.30	12.2	8.25	8.10	12.8	
Sm	2.19	2.29	3.04	2.90	2.22	1.80	2.27	2.69	2.05	2.28	4.96	4.12	3.81	2.49	2.79	2.86	3.72	2.51	2.56	3.98	
Eu	0.84	0.87	1.09	0.99	0.84	0.70	0.83	1.07	0.81	0.88	1.59	1.40	1.10	0.86	1.01	0.95	1.34	0.91	0.95	1.41	
Gd	3.02	3.14	4.08	3.74	2.95	2.64	3.52	3.55	2.89	3.16	5.66	4.83	4.50	3.25	3.49	3.99	4.69	3.38	3.39	4.66	
Tb	0.566	0.582	0.748	0.701	0.535	0.517	0.694	0.597	0.545	0.576	0.966	0.867	0.843	0.581	0.635	0.699	0.813	0.616	0.596	0.825	
Dy	3.86	3.99	5.04	4.51	3.61	3.63	4.73	3.76	3.77	3.85	6.13	5.40	5.36	3.89	3.92	4.64	5.26	4.01	3.88	5.11	
Ho	0.84	0.88	1.08	0.97	0.78	0.81	1.01	0.78	0.82	0.82	1.27	1.12	1.12	0.84	0.80	0.98	1.11	0.83	0.82	1.04	
Er	2.42	2.50	3.02	2.79	2.19	2.38	2.78	2.14	2.36	2.26	3.56	3.20	3.17	2.36	2.29	2.69	3.07	2.27	2.24	2.92	
Tm	0.371	0.387	0.455	0.408	0.337	0.364	0.411	0.320	0.360	0.340	0.533	0.463	0.449	0.361	0.324	0.399	0.458	0.335	0.333	0.418	
Yb	2.50	2.59	3.02	2.63	2.29	2.42	2.68	2.11	2.42	2.24	3.56	2.92	2.86	2.42	2.03	2.56	3.07	2.18	2.21	2.64	
Lu	0.381	0.393	0.452	0.392	0.343	0.362	0.387	0.306	0.371	0.332	0.536	0.434	0.417	0.362	0.300	0.383	0.463	0.324	0.328	0.391	
Hf	1.07	1.11	1.70	1.56	1.01	1.08	1.23	0.99	1.11	1.14	1.99	2.86	1.57	1.48	0.97	1.14	1.47	1.38	1.26	2.96	
Ta	0.096	0.097	0.185	0.160	0.117	0.070	2.502	0.081	0.103	0.088	0.539	0.282	0.211	2.168	0.100	0.124	0.162	0.179	0.151	0.405	
Pb	10.6	7.22	7.44	3.04	3.82	10.5	3.89	2.75	11.19	4.62	9.18	11.40	4.41	7.30	4.44	10.7	2.53	2.75	9.79	3.50	
Th	0.008	0.011	0.093	0.292	0.027	0.007	0.015	0.032	0.027	0.131	0.036	0.644	0.231	0.379	0.021	0.093	0.092	0.131	0.054	0.372	
U	0.003	0.003	0.060	0.110	0.014	0.010	0.010	0.010	0.012	0.035	0.023	0.233	0.056	0.277	0.023	0.021	0.085	0.018	0.015	0.160	

2.4.4 U-Pb SHRIMP zircon ages

Zircons were separated from three eclogite samples with MORB-like chemistry: T21-8-04 and T25-1-04 (from Ikola-Karema village) and sample T58-1-04 (from Mgambo village; Fig. 2.2B). Zircons of T21-8-04 and T25-1-04 are irregular in shape with resorbed margins. The CL images display domain zones or a uniform composition. The grains are not overgrown by rims (Fig. 2.10A&B). Zircons of sample T58-1-04 are rounded to subrounded with dark luminescent cores, which are surrounded by light luminescent rims (Fig. 2.10C).

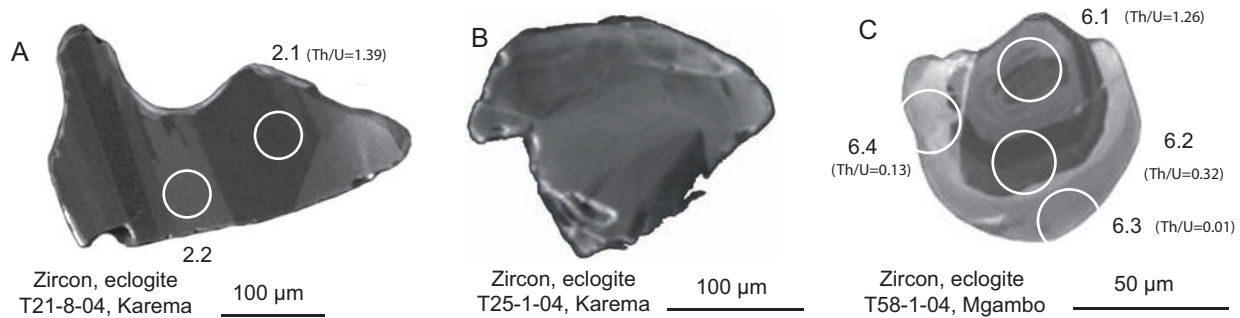


Figure 2.10: CL images of eclogite zircons A&B: Zircons without overgrown rims from two mylonitic eclogites (T21-8-04, T25-1-04) of Ikola-Karema village, dark and light grey domains of zircon A yield the same Paleoproterozoic age, zircon B has low U contents. C: Zoned zircon from an eclogite of Mgambo village; the young Pan-African rim overgrowing the old Paleoproterozoic core is interpreted to be formed during mylonitization.

The domains of zircons in sample T21-8-04 have U contents (12-172 ppm) and Th contents (2-189 ppm), which give Th/U ratios that range between 0.17 and 1.34 (Tab. 2.4). Zircons of sample T25-1-04 have very low U contents, therefore this sample was not suitable for dating. Zircons of sample T58-1-04 have cores with U contents (42-496 ppm) and Th contents (2.5-1016 ppm), which give Th/U ratios that range between 0.06 and 2.05. Their rims have U contents (5-43 ppm) and Th contents (0.05-8 ppm) giving very low Th/U ratios between 0.01 and 0.50 (Tab. 2.4). Th/U ratios in zircons were proposed by Rubatto (2002) to be useful to distinguish metamorphic (low ratios) from magmatic zircons (high ratios). However, Harley *et al.* (2007) argued that a low Th/U ratio is not a good criterion for metamorphic zircons by referring to the studies of Carson *et al.* (2002), Möller *et al.* (2003) and Kelly & Harley (2005) in which high U/Th ratios (>0.15 and up to 3.2) were recorded from metamorphic zircons. Nonetheless, generally metamorphic zircons have low Th/U ratios (Harley *et al.*, 2007), supporting the interpretation that the zircons of the Ubende terrane eclogites are metamorphic in origin. This is in accordance with the absence of a magmatic growth zoning in most samples (e.g., Corfu *et al.*, 2003). Whereas zircons from two samples (T21-8-04 and T25-1-04) have no rim overgrowths, zircons of sample T58-1-04 from Kungwe bay have a pronounced rim (Fig. 2.10C). This metamorphic rim is attributed to the late stage amphibolite- to granulite-facies mylonitisation that affected the mylonitic and retrogressed eclogites after the subduction, during a later orogenic event (see below).

Six points from different zircon grains which were analyzed from eclogite T21-8-04, plot very near to the concordia (Fig. 2.11A) and give a concordant age of 1866 ± 14 Ma. This age is interpreted as the age of the subduction zone metamorphism in the Ubende terrane.

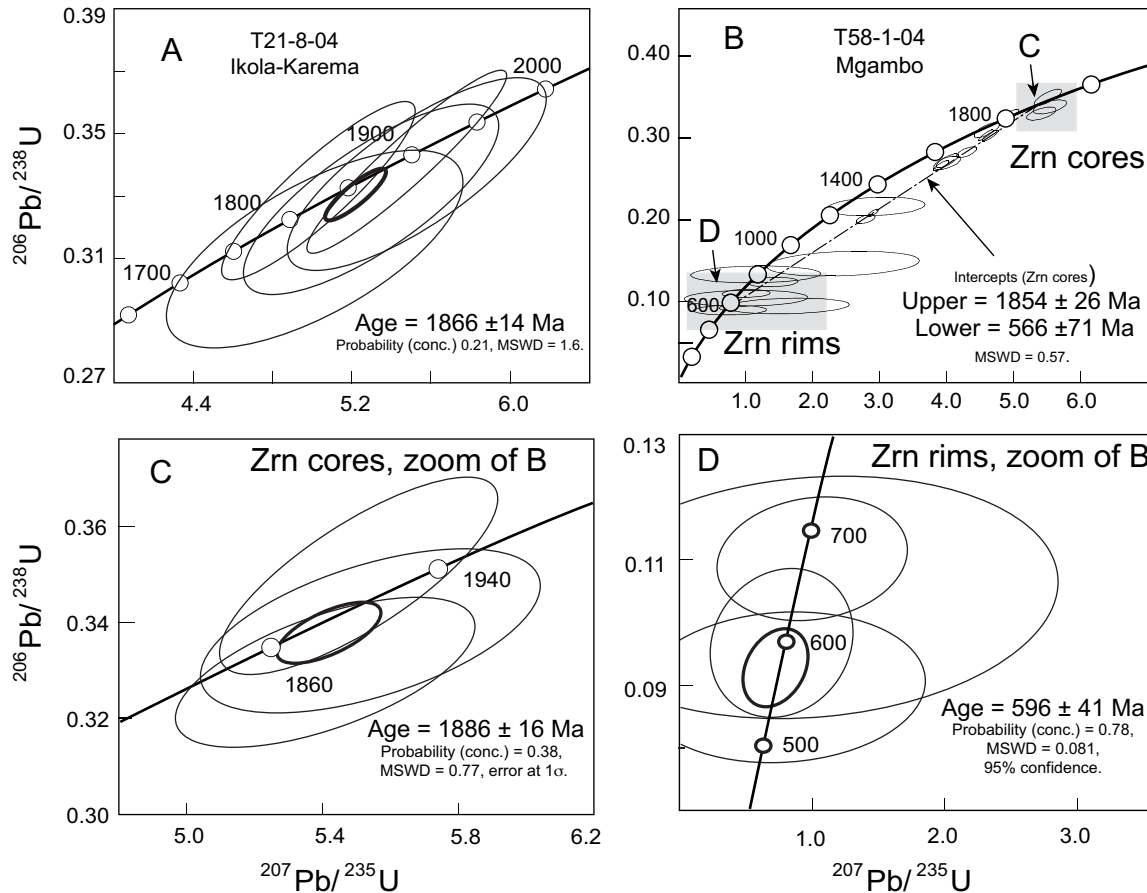


Figure 2.11: Concordia diagrams with U-Pb SHRIMP analyses of zircons from group I eclogites of MORB geochemistry. A: A concordant age of eclogite T21-8-04 from Ikola-Karema village. B: Discordant and concordant ages of sample T58-1-04 from Mgambo village. C: A zoom of the concordant core age from B. D: A zoom of the concordant rim age from B.

A total of 18 points (11 cores, 7 rims) were analyzed from zircon grains of sample T58-1-04 (Tab. 2.4 and Fig. 2.11B). The core analyses vary from concordance to discordance. The discordant analyses plot linearly, cutting the concordia at 1854 ± 26 Ma (upper intercept) and at 566 ± 71 Ma (lower intercept). These intercept ages are similar to those of the concordant core points at 1886 ± 16 Ma and the concordant rims at 596 ± 41 Ma (Fig. 2.11B). The ages at 1886 ± 16 Ma and 1854 ± 26 Ma are considered to reflect the eclogite metamorphism and are similar to that of sample T21-8-04 discussed above. The younger metamorphic ages (596 ± 41 Ma and 566 ± 71 Ma) are considered to reflect the mylonitic overprint during Pan-African time, an age that has also been found in overgrown rims in monazites of associated mylonitic metapelites (chapter 1).

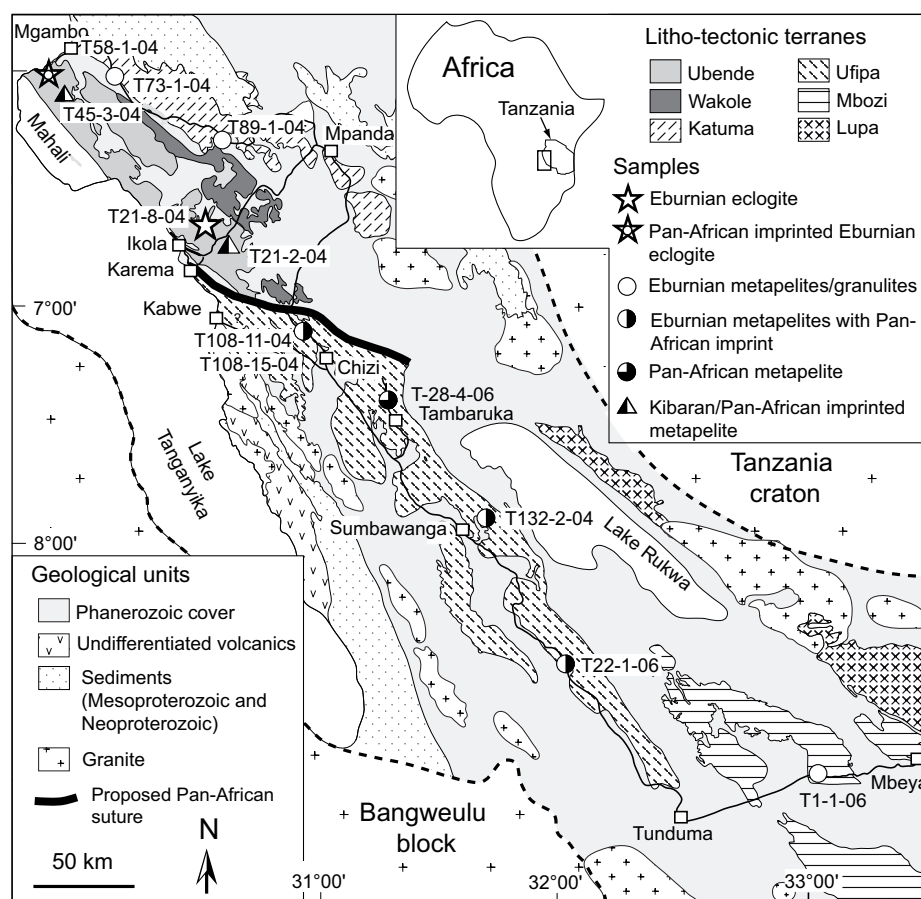
Table 2.4: SHRIMP U-Pb zircon composition of Ubende terrane eclogites.

No.	U (ppm)	Th (ppm)	$\frac{\text{Th}}{\text{U}}$	$\frac{^{232}\text{Th}}{^{238}\text{U}}$	^{206}Pb (%) comm.	Apparent age (Ma) $\frac{^{207}\text{Pb}}{^{206}\text{Pb}}$ $\frac{^{206}\text{Pb}}{^{238}\text{U}}$	$\frac{^{207}\text{Pb}^*}{^{206}\text{Pb}}$ (%) error	$\frac{^{206}\text{Pb}^*}{^{238}\text{U}}$ (%) error	$\frac{^{207}\text{Pb}^*}{^{235}\text{U}}$ (%) error	disc. (%)
T21-8-04										
1.1	30	12	0.40	0.41	1.16	1710 ± 160	0.105	4.75	0.33	-7
2.1	141	189	1.34	1.39	0.40	1799 ± 33	0.110	5.03	0.33	-3
3.1	172	109	0.63	0.65	0.06	1712 ± 22	0.105	4.07	0.28	7
4.1	103	64	0.63	0.65	—	1337 ± 110	0.086	2.12	0.18	26
5.1	128	65	0.51	0.52	0.21	1568 ± 32	0.097	3.50	0.26	5
6.1	23	7	0.30	0.30	0.20	1908 ± 56	0.117	5.30	0.33	4
7.1	140	142	1.01	1.05	—	1904 ± 22	0.116	5.48	0.34	1
7.1	88	47	0.53	0.56	—	1736 ± 39	0.106	4.00	0.27	12
8.1	12	2	0.17	0.18	0.24	1898 ± 81	0.116	5.01	0.31	8
9.1	27	10	0.37	0.39	0.21	1941 ± 55	0.119	5.53	0.33	4
T58-1-04										
1.1 core	129	100.83	0.78	0.81	0.30	1745 ± 40	0.107	4.01	0.27	12
1.2 core	66	78.40	1.19	1.22	0.47	1637 ± 65	0.101	2.79	0.20	39
1.3 rim	5	1.15	0.23	0.26	9.47	1977 ± 660	0.121	2.45	0.15	124
1.4 rim	17	8.44	0.50	0.51	3.78	1600 ± 370	0.099	2.94	0.22	27
2.1 core	77	102.11	1.33	1.36	0.24	1941 ± 47	0.119	5.41	0.33	6
3.1 core	51	29.19	0.57	0.59	1.08	1760 ± 60	0.108	3.3	0.27	14
3.2 rim	12	0.18	0.02	0.02	5.56	670 ± 1200	0.062	0.76	0.09	20
4.1 core	42	2.55	0.06	0.06	0.25	1938 ± 54	0.119	5.54	0.34	3
5.1 core	120	90.83	0.76	0.78	0.18	1802 ± 39	0.110	4.29	0.28	12
5.2 rim	5	0.05	0.01	0.01	6.29	2028 ± 800	0.125	1.63	0.09	248
6.1 core	136	165.59	1.22	1.26	0.24	1786 ± 26	0.109	4.93	0.33	-2
6.2 core	318	99.26	0.31	0.32	0.07	1639 ± 25	0.101	2.90	0.23	34
6.3 rim	43	0.5	0.01	0.01	1.55	481 ± 280	0.057	0.73	0.09	-16
6.4 rim	15	1.83	0.12	0.13	4.43	1254 ± 420	0.082	1.41	0.12	66
7.1 core	496	1016.53	2.05	2.12	0.16	1790 ± 14	0.109	4.58	0.30	5
7.2 core	168	153.50	0.91	0.95	0.12	1744 ± 26	0.107	3.92	0.27	15
7.3 core	323	97.28	0.30	0.31	0.08	1820 ± 20	0.111	4.65	0.30	7
7.4 rim	26	0.44	0.02	0.02	6.01	920 ± 1500	0.070	1	0.10	44

*common Pb corrected by using measured ^{204}Pb

2.5 Geochronology of metapelites and mafic granulites

Zircon from five metasediment samples of the Ubendian belt was dated to get information about the age of regional metamorphism in the Ubendian belt. The dated samples were taken from the Ubende, Katuma, Ufipa and Wakole terranes to prove whether these terranes might have different geological histories (Tab. 2.5 and Fig. 2.12). In addition, zircon of one mafic granulite of the Katuma terrane was dated to get information about the relationship between magmatism and metamorphism during the Paleoproterozoic crustal evolution.



As it turned out that the Ubendian rocks were affected by up to three orogenic cycles, it seemed necessary to expand the data set of radiometric ages and to cover regionally a large part of the Ubendian belt between Mgamba in the NW and Mbeya in the SE (Fig. 2.12). The Th-U-total Pb method of *in-situ* chemical dating of monazite was chosen as monazite is more sensitive than zircon to recrystallization and resetting during later orogenic events affecting already high-grade metamorphic rocks.

The samples of the Wakole terrane turned out not to be affected by a Paleoproterozoic metamorphic event. These samples will not be discussed here but in a separate paper on the Kibaran imprint in the Ubendian belt.

2.5.1 Sample localities

All dated zircons and monazite samples (together 10) and their mineral assemblages are listed in Tab. 2.5.

Table 2.5: Mineral assemblages of metapelites and mafic granulites from different terranes of the Ubendian belt, from which zircon and monazite ages have been determined.

Sample	Mineral assemblage	Rock type
Metapelites		
Ufipa Terrane T22-1-06	Grt-Sil-Bt-Pl-Kfs-Qtz-Crd	Medium grained gneiss, Crd occurs in matrix and forms coronas around Grt
T28-4-06	Grt-Ky-Bt-Ms-Pl-Qtz	Medium grained mica schist
T108-11-04	Grt-Ky-Bt-Ms-Pl-Qtz	Medium grained gneiss with Grt porphyroblasts
T108-15-04	Grt-Ky-Bt-Ms-Pl-Qtz	Medium grained gneiss with Grt porphyroblasts
T132-1-04	Grt-(Ky)-Sil-Bt-Pl-Kfs-Qtz	Medium grained gneiss; Ky is included in Grt Sil occur in the matrix
Ubende Terrane		
T21-2-04	Grt-Ky-Bt-Pl-Qtz-[Ms]	Mylonite with Grt and Ky porphyroclasts in a fine grained matrix of Pl-Qtz-Bt and late-stage Ms
T45-3-04	Grt-Ky-Bt-Pl-Qtz-Hbl-Scp	Mylonite with Grt and Ky porphyroclasts in a fine matrix of Pl-Qtz-Bt-Hbl-Scp
Mbozi Terrane		
T1-1-06	Grt-(Ky)-Sil-Bt-Pl-Kfs-Qtz	Mylonite with Grt porphyroclasts; Ky is included in Grt Sil occurs in the matrix
Katuma Terrane		
T89-1-04	Grt-Bt-Pl-Ms-Qtz	Mica schist with Grt porphyroblasts
Mafic granulite		
Katuma Terrane T73-1-04	Cpx-Pl-Grt-Qtz-Hbl-Ilm	Fine grained mafic granulite, massive texture

(Ky)= early-stage mineral, [Ms]=late-stage mineral

In the Ubende terrane, metapelites are very rare. At both sample localities (T21-2-04, river section near Karema and T45-3-04 near Mgambo; Fig. 2.12) the metapelites display a mylonitic texture (Fig. 2.3B), indicating a late-stage overprint pointing to a possible poly-metamorphic evolution. Sample T45-3-04 (Mgambo) is hornblende-kyanite-garnet bearing and lacks monazite. Metapelites form mappable lenses (10 to 100 m) within felsic gneisses and eclogites (Sutton *et al.*, 1954). At Karema the metapelites form meter-scale layers between mylonitic eclogites and garnet-clinopyroxene gneisses.

In the Ufipa terrane, metapelites are much more common. In the northern part of the terrane (near Chizi and Tambaruka; Fig. 2.12), where they occur in association with eclogite lenses, they contain kyanite-muscovite-garnet (T28-4, T108-11, T108-15-04; Tab. 2.5). In

contradistinction, in the southern Ufipa terrane metapelites contain sillimanite, K-feldspar, cordierite and garnet (T22-1-06 and T132-2-04), indicating higher temperatures and lower pressures than in the north.

In the Mbozi terrane, the dated mylonitic garnet-sillimanite-gneiss (T1-1-06) crops out in association with abundant mafic granulites and quartzites near the Mbeya-Tunduma road. Here, similar P - T conditions as in the southern Ufipa terrane seem to have prevailed.

The Katuma terrane samples are a garnet-biotite-muscovite-plagioclase-quartz schist and a garnet-bearing mafic granulite (Tab. 2.5). Fine grained mafic granulites dominate in the area and metapelitic gneisses crop out only locally.

2.5.2 U-Pb SHRIMP zircon ages

Three of the four metapelite samples have zircons with oscillatory zoned cores which are overgrown by metamorphic rims (Fig. 2.13). Oscillatory growth zoning is normally interpreted as a magmatic texture (Corfu *et al.*, 2003). Zircon cores have Th/U ratios ranging between 0.32 and 2.01, which are higher than the Th/U ratios in the rims (0.01-0.06; Tab. 2.6). High Th/U ratios and growth zoning in zircon cores point to their inheritance from old magmatic zircons.

In the Ufipa terrane, the zircon of metapelite T108-11-04 is unusual as it contains no magmatic oscillatory zoned core. Rim and core show a weak luminescence in CL pictures (Fig. 2.13A) and yield a common concordant age at 1901 ± 37 Ma (Fig. 2.14A). Zircon of metapelite T132-1-04 gives a concordant metamorphic rim age at 1949 ± 16 while the cores are discordant with an upper intercept age at 2087 ± 13 Ma and a poorly defined lower intercept age at 465 ± 81 Ma (Fig. 2.14E). The two discordia intercept ages reflect a Neoproterozoic reworking of Paleoproterozoic detrital zircon cores.

In the Katuma terrane, metamorphic zircon rims of metapelite T89-1-04 give a concordant age at 1900 ± 14 Ma, whereas the oscillatory zoned cores point to detrital magmatic protolith ages of 2.4-2.2 Ga (Fig. 2.14B). Zircons of the mafic granulite (T73-1-04; Fig. 2.13D) differ in internal textures from the metapelitic zircons: the core shows a weak oscillatory zoning and is little luminescent. Core and rim analyses are slightly discordant and plot together near the upper discordia intercept at 1977 ± 40 . During the Kibaran (1206 ± 340 Ma, lower intercept) the isotopic system was disturbed (Fig. 2.14D).

In the Ubende terrane, zircon rims and cores of a mylonitic garnet-kyanite metapelite (T45-3-04) of the Ubende terrane yield slightly different ages from the Ufipa and Katuma terranes discussed above (Fig. 2.14C). Two analyses from the cores are concordant at 1817 ± 26 Ma, whereas other core analyses suffered Pb loss and plot discordantly with a big error at the lower intercept 1119 ± 80 Ma and upper intercept at 2151 ± 130 Ma (Fig. 2.14C). However, the zircon rims give a concordant well defined age at 1093 ± 10 Ma.

The data presented above allow to constrain the age of the Paleoproterozoic metamorphism in the Ubendian belt. The metamorphic zircon rims of the Ufipa and Katuma terrane metapelites give ages at 1900 ± 14 Ma, 1901 ± 37 Ma and 1949 ± 16 Ma. The last age is the best constrained one (10 points). The zircons of a meta-igneous rock (mafic granulite

T73-1-04) are slightly discordant indicating a magmatic crystallization age slightly older than the age of metamorphism in the Ufipa and Katuma terranes (1977 ± 40 Ma).

The few concordant data points at 1817 ± 26 Ma from a metamorphic zircon of a metapelite of the Ubende terrane seem to indicate that in this terrane the metamorphism might be younger than in the other terranes. This interpretation is supported by monazite ages that are discussed later.

Late-stage isotopic disturbance of Paleoproterozoic zircons during the Kibaran event is recorded in the mafic granulite of the Katuma terrane and metapelitic zircons of the Ubende terrane. The age of this overprint event has been dated at 1093 ± 10 Ma in the Ubende terrane (Fig. 2.14C) and corresponds to metamorphic ages found in the adjoining Wakole terrane (to be discussed in a separate paper). A second overprint recorded in the zircon data that occurred during the Pan-African time, has been found in the Ufipa terrane (poorly defined at 465 ± 81 Ma) and in the Ubende terrane at 596 ± 41 (T58-1-04, eclogite).

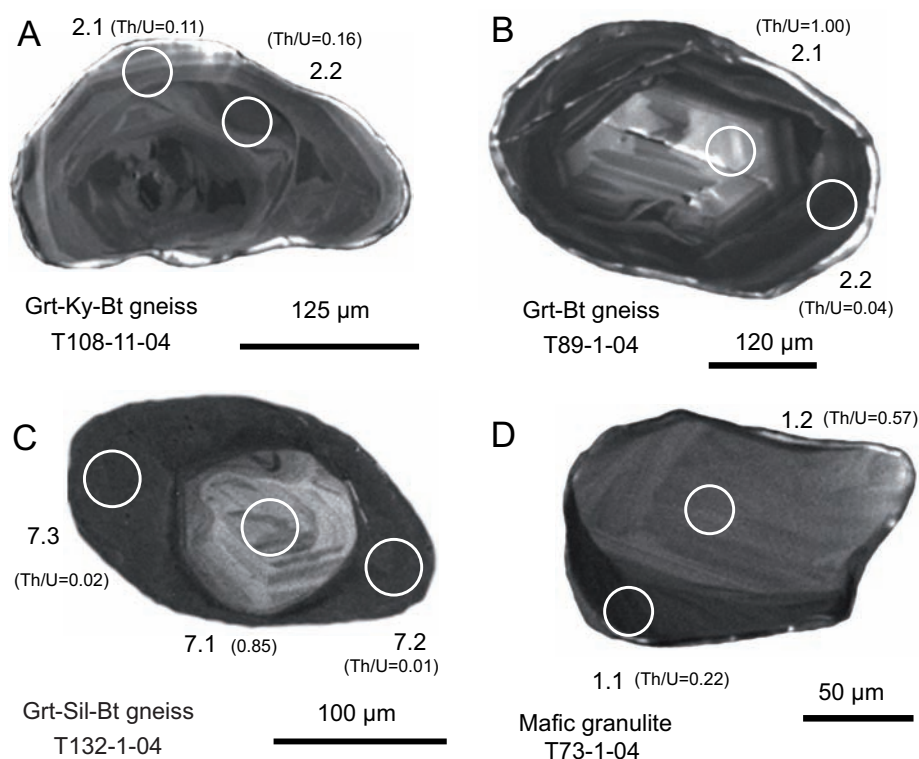


Figure 2.13: Representative textures and Th/U ratios of zircons from metapelites (Ufipa, Katuma terranes) and a mafic granulite (Katuma terrane). A: Metamorphic zircon with irregular domains and low Th/U ratios. B&C: Oscillatory zoned zircon core overgrown by dark luminescent rims which have lower Th/U ratios than the cores. D: Weakly zoned zircon core from a mafic granulite with overgrowth rim of indistinguishable age.

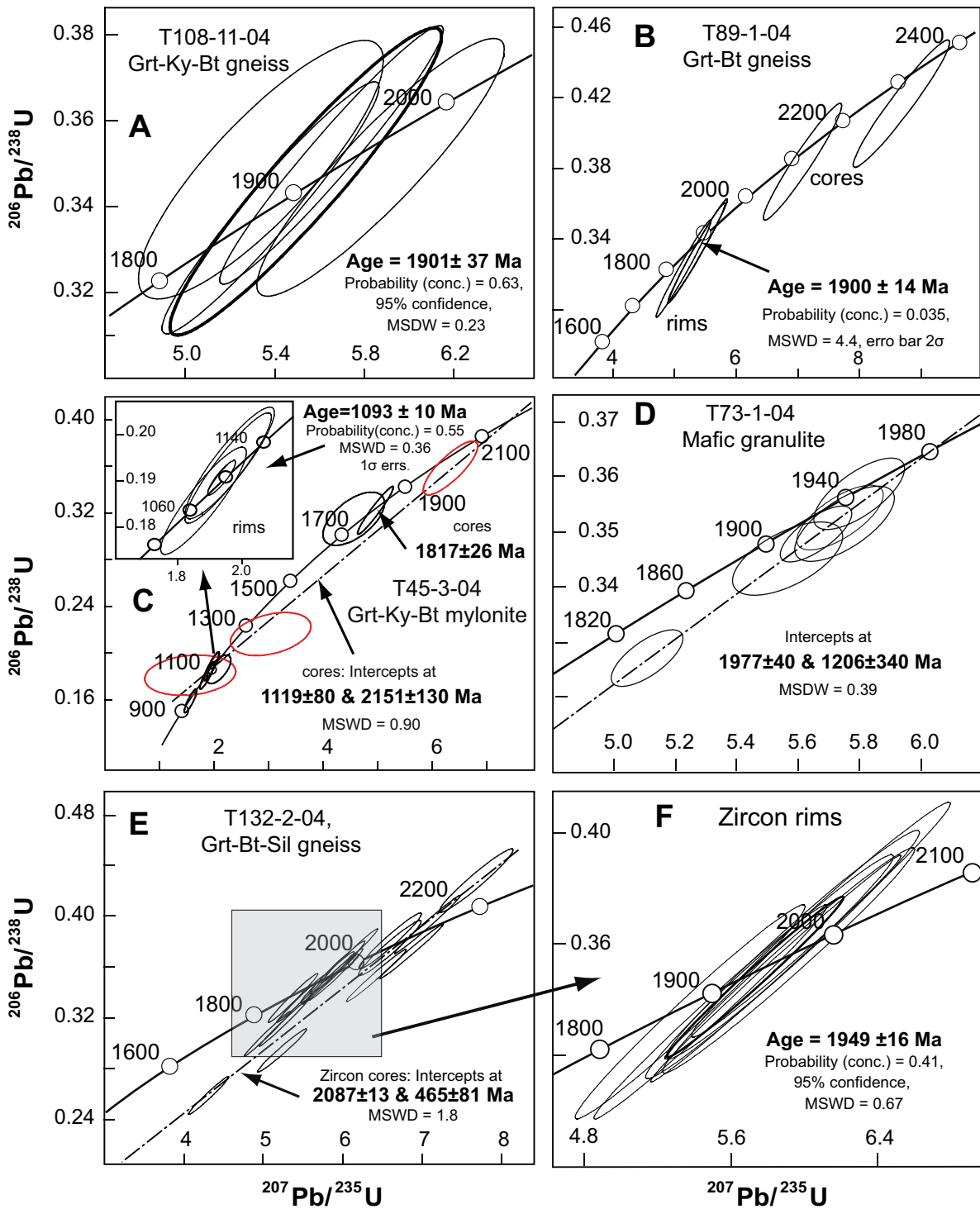


Figure 2.14: Concordia diagrams with U-Pb SHRIMP analyses of zircons from metapelites and one mafic granulite of the Ubendian belt.

Table 2.6: SHRIMP U-Pb zircon data of metapelites and a mafic granulite, Ubendian belt.

No.	U (ppm)	Th (ppm)	$\frac{\text{Th}}{\text{U}}$	$\frac{^{232}\text{Th}}{^{238}\text{U}}$	^{206}Pb (%) comm.	Apparent age (Ma)		$\frac{^{207}\text{Pb}^*}{^{206}\text{Pb}}$	error (%)	$\frac{^{206}\text{Pb}^*}{^{238}\text{U}}$	error (%)	$\frac{^{207}\text{Pb}^*}{^{235}\text{U}}$	error (%)	disc. (%)
						$\frac{^{207}\text{Pb}}{^{206}\text{Pb}}$	$\frac{^{206}\text{Pb}}{^{238}\text{U}}$							
T108-11-04														
1.1	174	37	0.21	0.22	0.06	1878±19	1885±58	0.115	1.1	0.34	3.5	5.38	3.7	0
1.2	158	44	0.28	0.29	–	1985±28	1931±59	0.122	1.6	0.349	3.5	5.87	3.8	3
2.1	181	20	0.11	0.12	0.98	1817±41	1928±59	0.111	2.3	0.349	3.5	5.34	4.2	-6
2.2	290	47	0.16	0.17	0.13	1903±16	1944±59	0.117	0.91	0.352	3.5	5.65	3.6	-2
T132-1-04														
rim														
1.1	433	7	0.02	0.02	0.01	1966±9	1940±80	0.121	0.48	0.351	4.8	5.84	4.8	1
3.1	475	10	0.02	0.02	0.10	1945±11	1728±71	0.119	0.64	0.307	4.7	5.05	4.7	13
3.2	379	7	0.02	0.02	0.20	1953±15	1943±79	0.120	0.82	0.352	4.7	5.81	4.8	1
4.2	469	7	0.01	0.01	0.03	1973±15	1954±79	0.121	0.82	0.354	4.7	5.91	4.8	1
4.3	490	8	0.02	0.02	–	1953±13	2023±81	0.120	0.72	0.369	4.7	6.09	4.7	-4
5.1	421	13	0.03	0.03	0.18	1935±12	1868±76	0.119	0.64	0.335	4.7	5.49	4.7	4
6.2	337	19	0.06	0.06	0.09	1899±15	1866±77	0.116	0.84	0.336	4.7	5.38	4.8	2
7.3	458	7	0.02	0.02	0.07	1951±16	1981±80	0.120	0.88	0.36	4.7	5.93	4.8	-1
7.2	544	5	0.01	0.01	0.11	1967±10	1770±73	0.121	0.58	0.316	4.7	5.25	4.7	11
core														
2.1	113	64	0.57	0.59	0.05	2086±17	1653±75	0.129	0.96	0.294	4.7	5.24	4.8	25
4.1	307	615	2.01	2.07	0.39	1968±17	1794±82	0.121	0.94	0.259	4.7	4.31	4.8	33
6.1	117	58	0.49	0.51	0.29	2066±23	2052±88	0.128	1.3	0.374	4.7	6.59	4.9	1
7.1	85	72	0.85	0.88	0.38	2101±23	2297±100	0.130	1.3	0.427	4.7	7.67	4.9	-8
8.1	446	258	0.58	0.60	0.02	3396±7	3025±120	0.286	0.45	0.598	4.7	23.6	4.7	12
9.1	513	166	0.32	0.33	0.42	2041±22	2084±87	0.126	1.2	0.38	4.7	6.59	4.9	-2
10.1	375	362	0.96	1.00	0.08	2149±11	2033±93	0.134	0.62	0.372	4.7	6.86	4.7	5
11.1	1230	687	0.56	0.58	0.04	2124±14	1953±85	0.132	0.77	0.353	4.7	6.42	4.8	9
12.1	338	417	1.23	1.28	0.07	2103±12	2129±100	0.130	0.67	0.393	4.7	7.07	4.7	-2
13.1	369	189	0.51	0.53	0.01	2586±7.7	2665±110	0.173	0.46	0.512	4.7	12.21	4.7	-3
T73-1-04														
rim														
1.1	822	185	0.22	0.23	0.17	1942±10	1909±10	0.119	0.55	0.345	0.62	5.657	0.83	2
3.1	407	124	0.30	0.31	0.03	1879±12	1800±10	0.115	0.66	0.322	0.65	5.105	0.93	4
4.1	357	88	0.25	0.26	0.12	1876±21	1883±11	0.115	1.20	0.339	0.69	5.368	1.4	0
core														
1.2	242	137	0.57	0.58	0.08	1962±15	1918±13	0.120	0.85	0.347	0.78	5.752	1.2	2
3.2	222	107	0.48	0.50	0.26	1936±19	1887±13	0.119	1.10	0.340	0.79	5.564	1.3	3
4.2	253	138	0.55	0.56	–	1948±13	1944±12	0.119	0.75	0.352	0.74	5.799	1.1	0
5.1	343	134	0.39	0.40	0.09	1952±13	1923±11	0.120	0.74	0.348	0.69	5.737	1	1
T89-1-04														
rim														
1.1	671	13	0.02	0.02	0.11	1911±11	1848±56	0.117	0.63	0.332	3.5	5.36	3.6	3
2.2	684	29	0.04	0.04	0.07	1911±11	1857±56	0.117	0.62	0.334	3.5	5.39	3.5	3
3.1	653	20	0.03	0.03	0.10	1888±12	1805±55	0.116	0.65	0.323	3.5	5.15	3.5	5
core														
1.2	169	139	0.82	0.85	0.09	2148±18	2094±63	0.134	1.00	0.384	3.5	7.08	3.7	3
2.1	122	122	1.00	1.03	–	2358±17	2245±67	0.151	1.00	0.417	3.5	8.68	3.7	5

*common Pb corrected by using measured ^{204}Pb

2.5.3 Th-U-total Pb CHIME monazite ages

In-situ monazite CHIME dating was performed on five metapelite samples of the Ufipa, Ubende and Mbozi terranes, parallel to zircon SHRIMP dating, to optimize the search for metamorphic overprints on the Paleoproterozoic Ubendian rocks. This technique has been successfully applied in assessing and dating the polyphase tectono-metamorphic evolution of rocks (e.g. Dahl *et al.*, 2005; Williams *et al.*, 2006; Braun & Appel, 2006; Jöns *et al.*, 2006).

Ufipa terrane

Three gneissic metapelites (T108-15-04, T22-1-06 and T28-4-06) of the Ufipa terrane were selected for monazite dating. Sample locations are given in Fig. 2.12 and mineral assemblages in Tab. 2.5. Monazites from these rocks occur as discrete matrix crystals with sizes up to 120 μm . Only in one metapelite (T28-4-06) monazite was also found as inclusion in garnet.

The BSE images show that monazites of the two metapelites T108-15-04 and T22-1-06 have cores overgrown by rims (Fig. 2.15A&C). Monazites of sample T108-15-04 have higher Y-HREE concentrations in the rims (dark) than in the cores (Fig. 2.16A). However an opposite distribution of Y-HREE exists in monazite of sample T22-1-06 (Fig. 2.16B) in which the monazite cores have higher Y-HREE concentrations than the (light) rims.

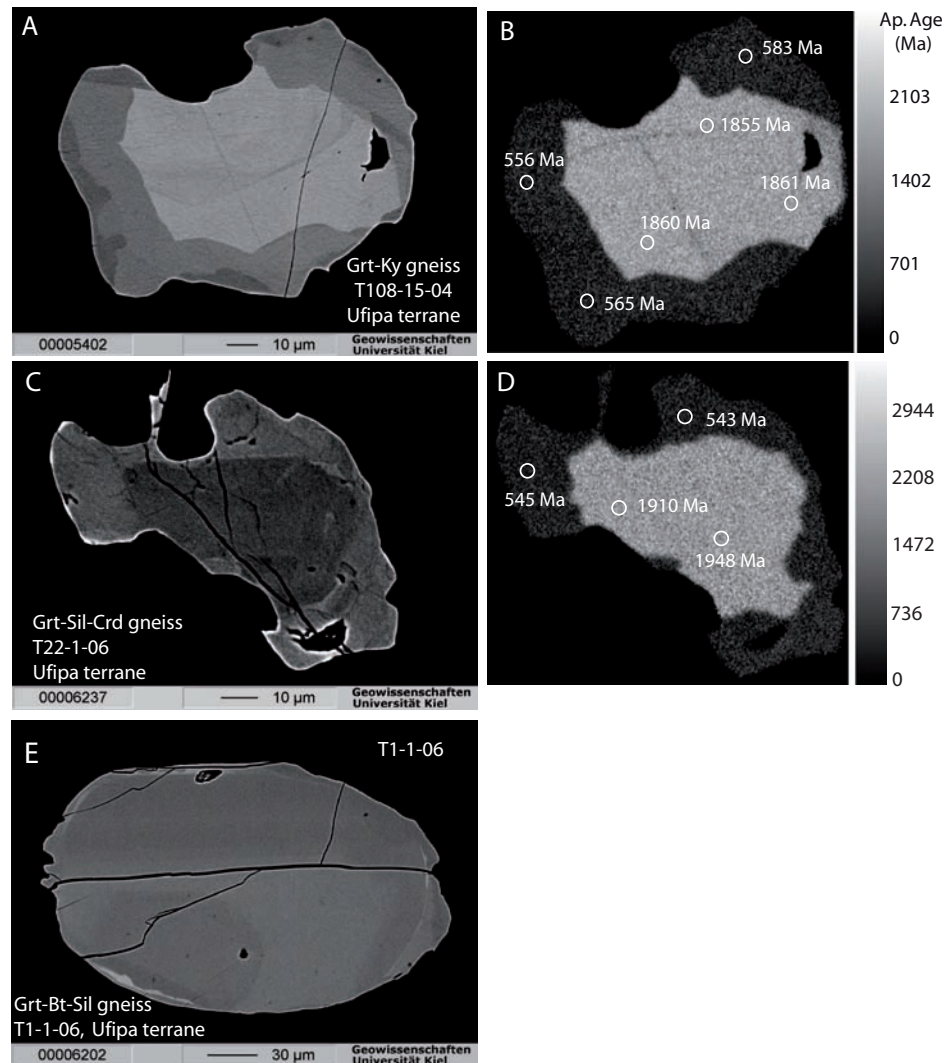


Figure 2.15:

Monazite zonation and corresponding apparent age maps. A&C: Monazite BSE image depicting cores and rims. B&D: Maps of apparent ages of the grains shown in A and C with old monazite cores (Paleoproterozoic) and young rims (Neoproterozoic). E: BSE image of uniformly dark luminescent monazite of the Mbozi terrane metapelite T1-1-06 of Paleoproterozoic age.

Among the minerals present in these metapelites, garnet takes a big budget of Y-HREE of the whole rock (Pyle *et al.*, 2001). Therefore differential depletion of Y-HREE in

monazite cores and rims reflect the garnet and monazite growth relations during metamorphism. Monazite cores of sample T108-15-04, with less Y-HREE than that of the overgrown rims (Fig. 2.15A&2.16A), might have grown together with garnet that took most of the Y-HREE. Later, garnet started to be consumed and released some Y-HREE, which therefore rise in the monazite rims (Fig. 2.16A). The opposite process seems to have operated in sample T22-1-06. In this case Y-HREE poor monazite rims grew together with the garnet (Fig. 2.15C). The brabantite substitution vector, $\text{Ca}+(\text{Th,U}) = 2\text{REE}$, was dominant in both, monazite cores and rims, whereas the huttonite substitution vector, $(\text{Th,U})+\text{Si} = \text{REE}+\text{P}$, was not important (Fig. 2.16B&D). However, some points show operations of huttonite and brabantite substitution in the monazite cores of sample T108-15-04 (Fig. 2.16B).

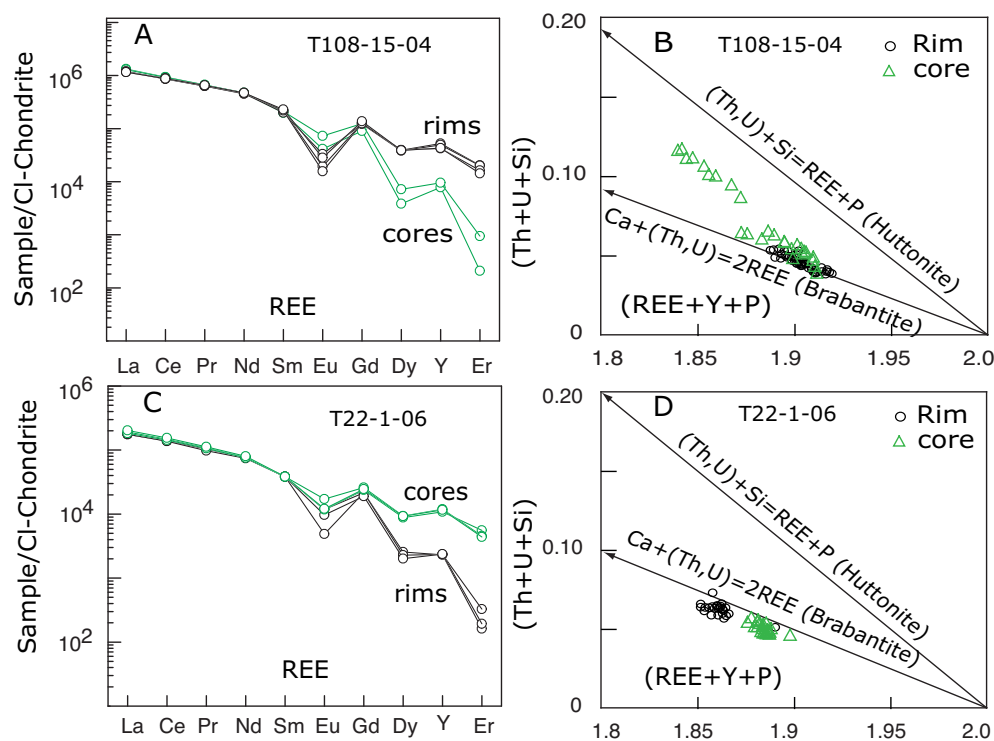


Figure 2.16: Composition of monazite of two metapelites of the Ufipa terrane. A&C: REE+Y patterns, normalizing values (McDonough & Sun, 1995). B&D: Plot of REE+Y+P vs. Th+U+Si showing brabantite and huttonite substitution vectors in monazite.

The distribution of apparent ages in monazite grains reveal Paleoproterozoic monazite cores overgrown by Neoproterozoic rims in both Ufipa samples (Fig. 2.15B&D). The calculated isochrons yield the ages of 1868 ± 55 Ma (cores) and 578 ± 66 Ma (rims) for sample T108-15-04 (Fig. 2.17A&B) and the ages of 1904 ± 52 Ma (cores) and 551 ± 63 Ma (rims) for sample T22-1-06 (Fig. 2.17C&D). The Paleoproterozoic monazite ages corroborate well with the SHRIMP zircon ages of metapelites T108-11-04, T89-1-04 and T132-2-04 with ages between ca. 1950 and 1900 Ma (Fig. 2.14A&F). However, the Neoproterozoic rim age was not recorded in zircon. This demonstrates that CHIME dating of monazite is a necessary tool to be applied when overprinting events have to be deciphered in polymetamorphic terranes.

Matrix grains and monazite inclusion in garnet of garnet-kyanite-biotite-muscovite schist T28-4-06 from the northern Ufipa terrane are not zoned and they give an isochron

age of 539 ± 56 Ma with a weighted mean age at 566 ± 8 Ma (Fig. 2.17E&F). In this case garnet grew during Pan-African time as it includes Pan-African monazite. Possible Eburnian parts of the monazite grains were completely erased.

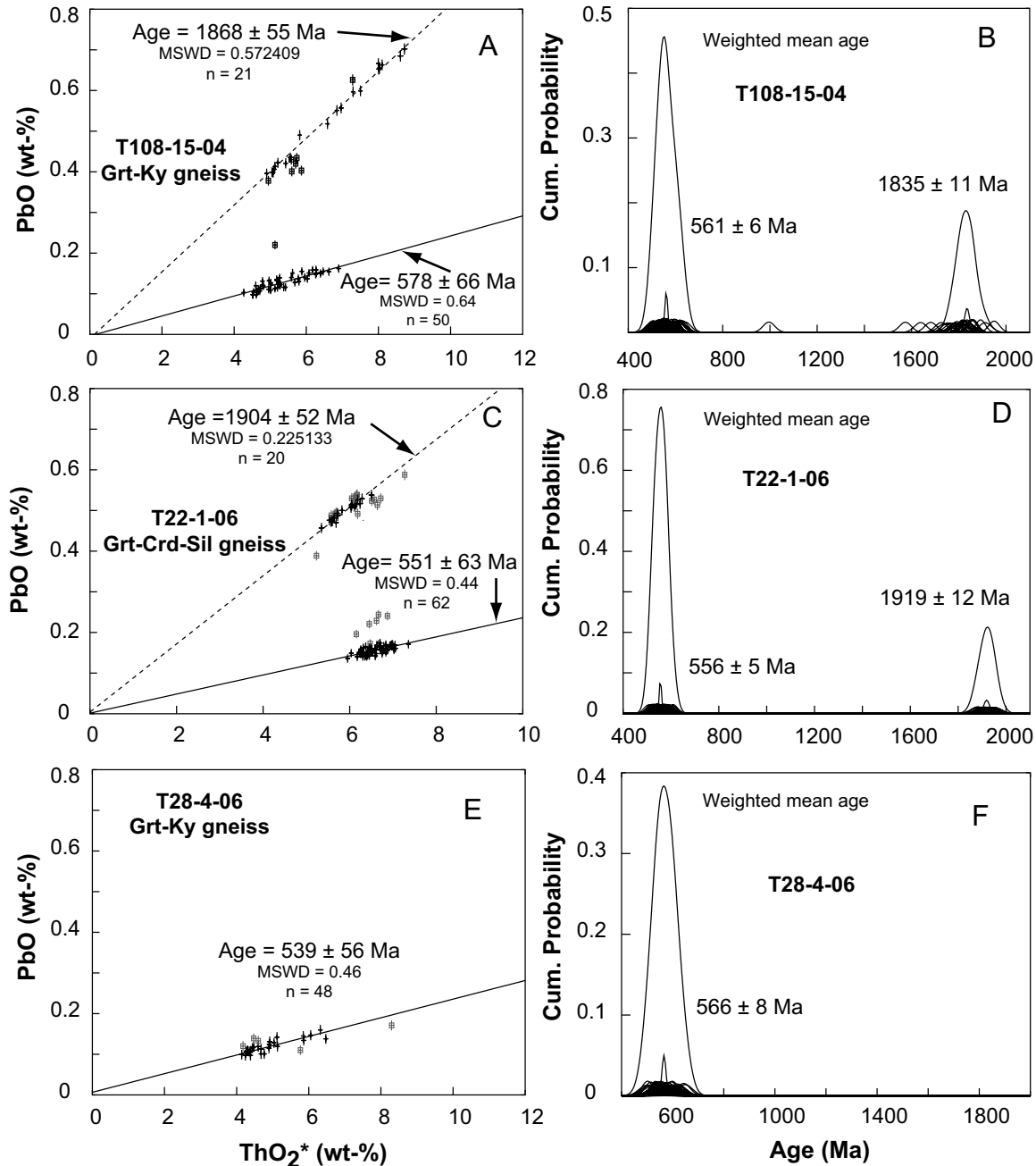


Figure 2.17: PbO vs ThO₂* monazite isochrons and the corresponding weighted mean ages of three Ufipa terrane metapelitic samples. Monazite cores have Paleoproterozoic ages that are overgrown by Neoproterozoic rims. Isochron error is at 2σ and the weighted mean age error is at 1σ .

Ubende terrane

Microprobe monazite dating was done on a mylonitic garnet-kyanite gneiss (sample T21-2-04) from the Ubende terrane (Karema area; Fig. 2.12). The mineral assemblage is given in Tab. 2.5. Monazite occurs in the rock matrix and as inclusion in garnet. The matrix monazite grains are composed of cores, inner rims (mantles) and outer rims (Fig. 2.18A). Monazite inclusions in garnet are composed of core and rims (Fig. 2.18C). The cores of monazite, both matrix and inclusions in garnet, have higher Y-HREE contents than their rims (Fig. 2.19A), which points to a synchronous growth of monazite rims and coexisting garnet and a growth of monazite cores in the absence of garnet. The brabantite substitution vector, characterizes the chemistry of monazite cores and rims, whereas the huttonite substitution vector, was not important (Fig. 2.19B). However, some analyses show intermediate operations of huttonite and brabantite cores and matrix.

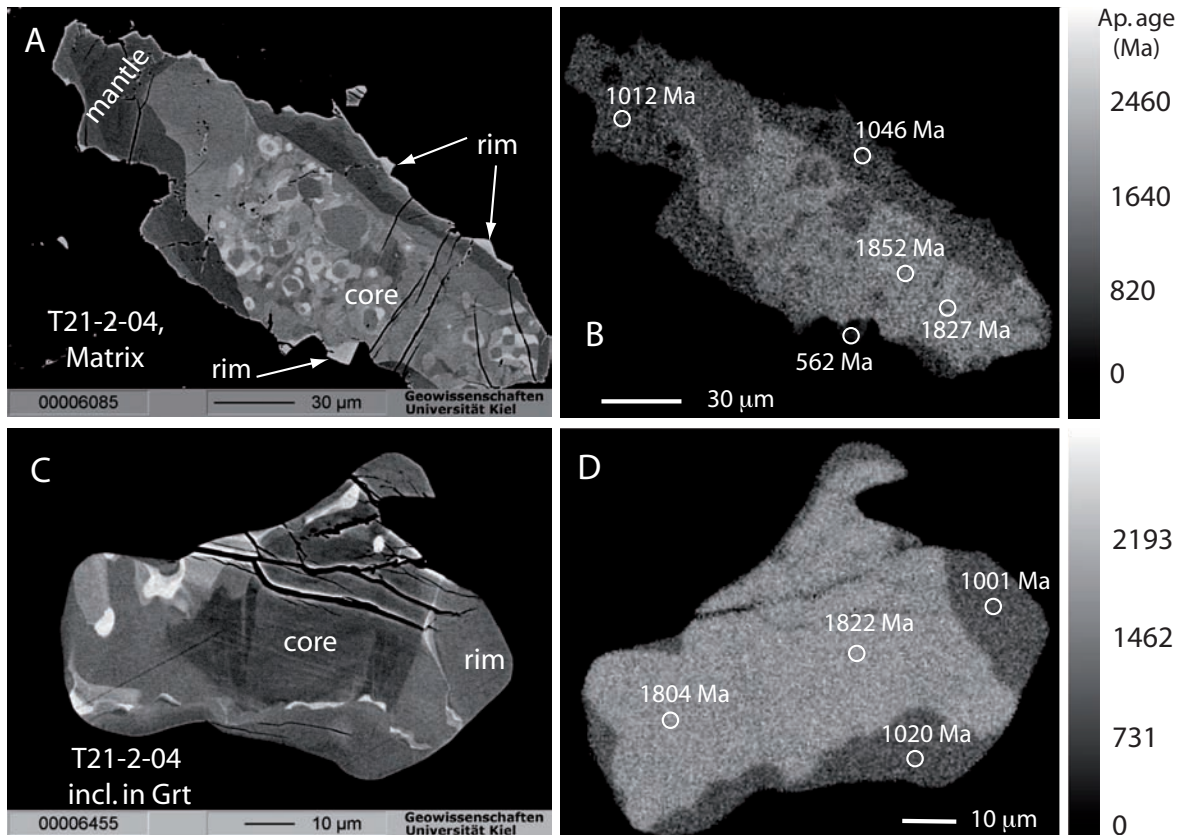


Figure 2.18: Monazite textures and maps of apparent ages of Ubende terrane metapelites. A: BSE image of matrix monazite of garnet-kyanite mylonite T21-2-04, Ubende terrane near Karema. A patchy textured core of Paleoproterozoic age is surrounded by a dark luminescent mantle (Mesoproterozoic and locally by a light luminescent outer overgrowth of Neoproterozoic age. B: Apparent age map for monazite A. C: BSE image of monazite inclusion in garnet indicating zones with Paleoproterozoic and Mesoproterozoic ages only. Neoproterozoic overgrowths like on matrix monazite grains, are missing. D: Apparent age map for monazite C.

The apparent age map of the matrix monazite shows three different ages from the core, mantle and a partial outer rim, whereas the monazite inclusion in garnet reveal only two ages from core and mantle (Fig. 2.18B&D). Consequently, three separate isochrons have been calculated for the different zones of the grains. The monazite core yields an age of 1807 ± 28 Ma (matrix and inclusions in garnet), the dark mantle around the core of matrix monazite and the rim around the core of monazite inclusions in garnet give together an age of 1177 ± 62 Ma. The outermost overgrown rim of the matrix monazites yield an age of 622 ± 79 Ma (Fig. 2.20A&B).

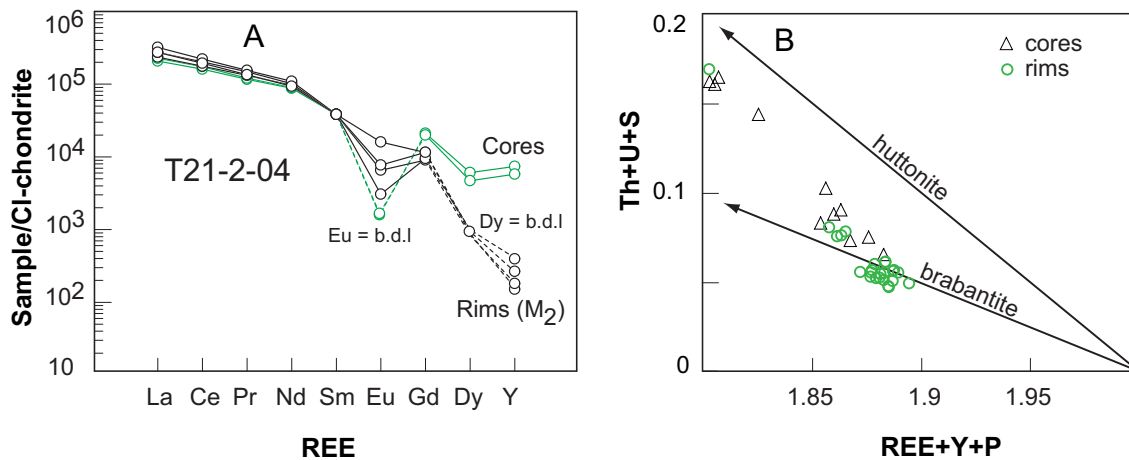


Figure 2.19: Composition of monazite. A: REE+Y patterns, normalizing values (McDonough & Sun, 1995). B: Plot of REE+Y+P vs. Th+U+Si showing brabantite and huttonite vectors.

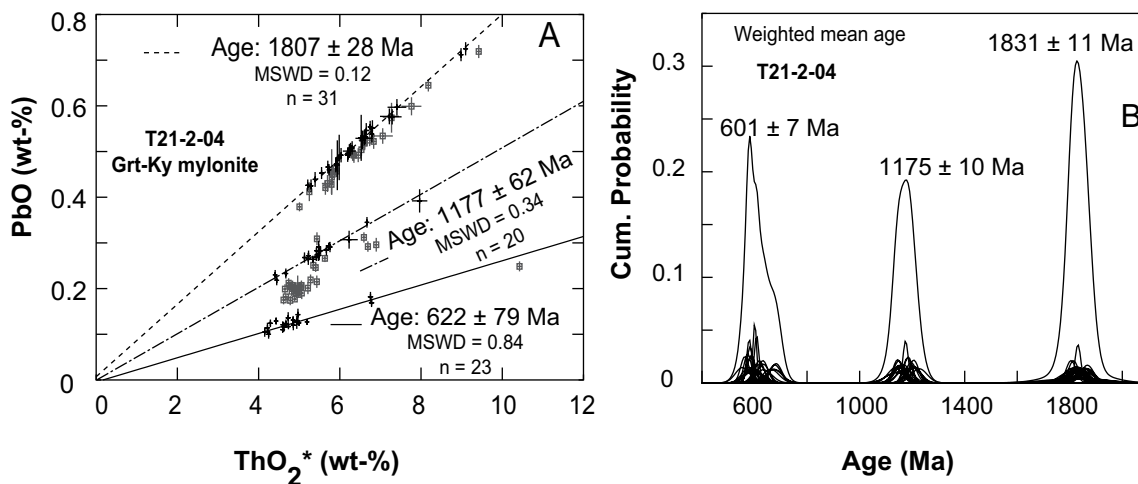


Figure 2.20: PbO vs. ThO₂* monazite isochrons and the corresponding weighted mean ages A: Three monazite ages in a mylonitic metapelite of the Ubende terrane near Karema. B: Weighted mean ages from A. Isochron error is at 2σ and the weighted mean age error is at 1σ .

Mbozi terrane

In contrast to the metapelitic monazites of the Ubende and Ufipa terranes, monazites from the Mbozi terrane (T1-1-06) do not have complex textures. The BSE images are uniformly dark luminescent (Fig. 2.15E). A single Paleoproterozoic age at 1806 ± 35 Ma was obtained, the corresponding weighted mean age is 1814 ± 7 Ma (Fig. 2.20A&B). This age is similar but somewhat younger than the Paleoproterozoic metamorphic ages obtained from zircons and monazites of the Ubende terrane.

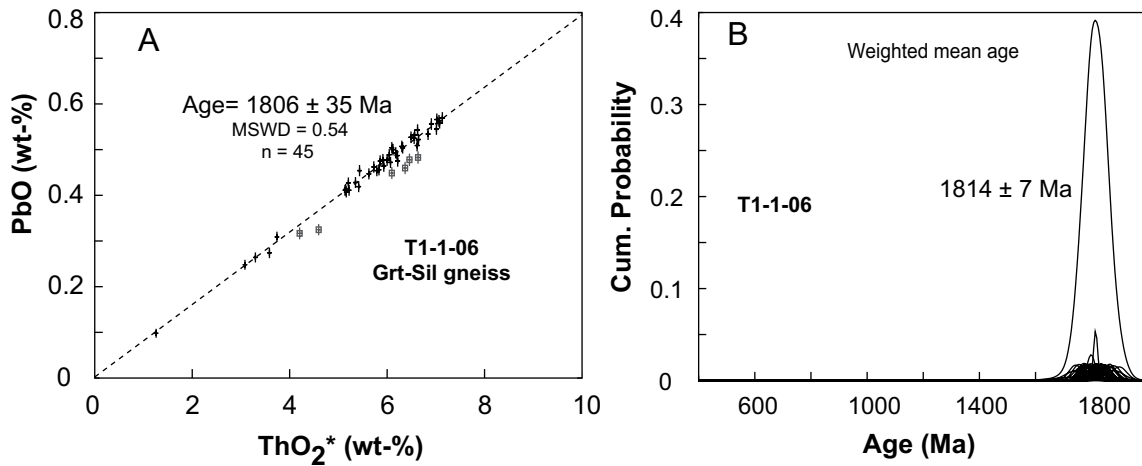


Figure 2.20: PbO vs ThO₂* monazite isochrons and the corresponding weighted mean ages. A: Isochron monazite age of the Mbozi terrane metapelite T1-1-06. B: Weighted mean ages from A. Isochron error is at 2σ and the weighted mean age error is at 1σ .

Table 2.7: Representative monazite compositions of the Ubendian belt metapelites.

Sample No.	T22-1-06 195 ^{core}	T22-1-06 193 ^{rim}	T21-2-04 35 ^{core}	T21-2-04 122 ^{rim}	T21-2-04 58 ^{rim}	T1-1-06 21
SiO ₂	0.19	0.31	2.05	0.33	0.67	0.24
P ₂ O ₅	30.39	30.27	27.72	29.83	30.75	29.76
Al ₂ O ₃	b.d.l	b.d.l	0.07	0.01	0.022	0.006
MgO	1.66	2.03	0.63	1.98	1.01	0.71
ThO ₂	5.24	5.54	8.94	4.42	4.70	3.27
UO ₂	0.28	0.21	0.01	0.08	0.08	0.01
PbO	0.53	0.15	0.71	0.21	0.14	0.26
La ₂ O ₃	13.18	13.84	12.85	17.26	16.68	14.39
Ce ₂ O ₃	25.88	27.72	28.51	29.96	29.61	31.52
Pr ₂ O ₃	3.02	3.15	3.30	2.89	3.16	3.43
Nd ₂ O ₃	10.86	11.87	13.50	10.92	11.45	13.52
Sm ₂ O ₃	1.75	1.96	1.40	1.08	1.75	1.62
Eu ₂ O ₃	0.35	0.15	b.d.l	b.d.l	0.19	b.d.l
Gd ₂ O ₃	1.67	1.42	0.51	0.42	1.01	0.94
Dy ₂ O ₃	0.88	0.21	b.d.l	b.d.l	b.d.l	b.d.l
Y ₂ O ₃	3.93	0.88	0.20	0.04	0.25	0.28
Er ₂ O ₃	0.28	0.04	0.04	b.d.l	0.03	0.03
<i>Total</i>	100.08	99.74	100.42	99.42	101.50	99.96
Si	0.007	0.012	0.081	0.013	0.025	0.009
P	0.992	0.994	0.932	0.988	0.993	0.991
Al	b.d.l	b.d.l	b.d.l	b.d.l	b.d.l	b.d.l
Ca	0.069	0.084	0.027	0.083	0.041	0.030
Th	0.046	0.049	0.081	0.039	0.041	0.029
U	0.002	0.002	0.000	0.001	0.001	0.000
Pb	0.006	0.002	0.008	0.002	0.002	0.003
La	0.188	0.198	0.188	0.249	0.235	0.209
Ce	0.366	0.394	0.414	0.429	0.414	0.454
Pr	0.042	0.045	0.048	0.041	0.044	0.049
Nd	0.150	0.164	0.191	0.153	0.156	0.190
Sm	0.023	0.026	0.019	0.015	0.023	0.022
Eu	b.d.l	b.d.l	b.d.l	b.d.l	b.d.l	b.d.l
Gd	0.021	0.018	0.007	0.006	0.013	0.012
Dy	b.d.l	b.d.l	b.d.l	b.d.l	b.d.l	b.d.l
Y	0.081	0.018	b.d.l	b.d.l	b.d.l	b.d.l
Er	b.d.l	b.d.l	b.d.l	b.d.l	b.d.l	b.d.l
<i>Total</i>	2.011	2.012	2.003	2.019	1.996	2.004
<i>X_{LREE}</i>	0.763	0.825	0.872	0.871	0.895	0.920
<i>X_{HREE}</i>	0.036	0.021	0.007	0.005	0.013	0.012
<i>X_{Hut}</i>	-0.015	-0.032	0.062	-0.040	0.002	0.002
<i>X_{Brb}</i>	0.136	0.168	0.054	0.163	0.085	0.059
<i>X_{YPO₄}</i>	0.080	0.018	0.004	0.001	0.005	0.006
<i>X_{GdPO₄}</i>	0.021	0.018	0.007	0.005		0.012
App. age	1910±26	566±18	1805±19	1155±28	674±30	1823±27

Cation calculations: oxygen=4 and b.d.l. = below detection limit.

2.6 Conclusions

2.6.1 Paleoproterozoic subduction of oceanic crust

Petrological, geochemical and geochronological data of the eclogites in the Ubende terrane of the northwestern part of the Ubendian belt indicate the closing of a Paleoproterozoic ocean along the SW margin of the Tanzania craton. The Ubende terrane eclogites have MORB-like chemistry and have been subducted between 1886 ± 16 Ma and 1866 ± 14 Ma. The subduction of oceanic crust during the Ubendian orogeny is about 120 Ma younger than the 2.0 Ga subduction in the Usagaran belt at the eastern margin of the Tanzania craton (Möller *et al.*, 1995). The oldest known MORB-like chemistry eclogites (2093 ± 45 Ma) occur at the western margins of the Congo craton in the Nyong complex of Cameroon (Loose, 2007).

The occurrence of MORB-like chemistry eclogites in the Ubendian-Usagaran belt and Nyong complex unequivocally advocate the idea that plate tectonics already operated on planet Earth in the Paleoproterozoic Era, apparently in a similar fashion as in the modern Earth.

Despite the intensive mylonitization of eclogites, garnet porphyroclasts preserved prograde inclusions of omphacitic pyroxene, sodic plagioclase and quartz, which give clues to the prograde part of the subduction. A subduction path with a geothermal gradient of less than $13^\circ\text{C}/\text{km}$ through amphibolite to eclogite facies was followed. A minimum peak pressure of 15 kbar was obtained from partially retrogressed eclogite-facies minerals.

The mylonitic overprint in the eclogites of the Ubende terrane occurred later at deep crustal levels under upper amphibolite- to granulite-facies conditions of about $680\text{-}750^\circ\text{C}/10\text{-}11$ kbar. Overgrown zircon rims dated at 596 ± 41 Ma are attributed to the mylonitisation stage of the eclogites. The mylonitic fabrics in the rocks of the Ubende terrane might have been attained during the Kibaran orogeny and reactivated during the Pan-African orogeny, because the mylonitic metapelites that are associated with eclogites record Kibaran and Pan-African overgrown rims in monazite and zircon.

2.6.2 Relationships between subduction and regional metamorphism

Metapelites of the terranes that are dominated by mafic metamorphic rocks, Ubende and Mbozi, yield metamorphic U-Pb zircon and monazite ages of ca. 1820 and 1810 Ma, which is the anticipated age of the crustal thickening as it postdates the subduction zone metamorphism in the Ubende terrane at ca. 1890-1860 Ma. However, metapelites and mafic granulites of the Ufipa and Katuma terranes yield U-Pb zircon SHRIMP and monazite ages at ca. 1980-1900 Ma, which is older than the subduction zone metamorphism. To explain this phenomenon, two models are suggested:

1. Metamorphism and accretion of the terranes in the Ubendian belt occurred at different periods. Structurally the Ubende and Mbozi terranes differ from the Ufipa terrane (Theunissen *et al.*, 1996; Boven *et al.*, 1999), which means they had different tectonic histories. The presence of a Pan-African suture between the Ubende and

the Ufipa terrane, which is marked by Neoproterozoic eclogites (chapter 1 and 4), and the distribution of Kibaran and Pan-African metamorphic ages suggests that the Ubende came in contact with the Ufipa terrane only Neoproterozoic time.

2. Crustal thickening metamorphism spanned a long period of time from about 1880 to 1810 Ma. Such a long period of time for an orogeny is assumed to be possible in accretionary orogens (Windley, 1998).

2.6.3 Kibaran and Pan-African orogenic impacts in the Ubendian belt

Kibaran (Mesoproterozoic) and Pan-African (Neoproterozoic) reworking processes of the Ubendian belt rocks were more intensive than previously thought. It was assumed that reworking occurred only locally and confined along sinistral transpressional shear zones (Theunissen *et al.*, 1992; Ring, 1993; Lenoir *et al.*, 1994; Theunissen *et al.*, 1996). The Kibaran orogenic event between 1180-1010 Ma overprinted only the terranes of Ubende, Katuma and Wakole in the northern Ubendian belt whereas, the Pan-African orogenic metamorphism (620-540 Ma) imprinted virtually all the terranes of the Ubendian belt.

The Pan-African and Kibaran imprints on the Ubendian belt completely erased the old monazite cores of some metapelites. The later events erased or masked the chemistry and textures of early grown of the Ubendian basement rocks, which complicate and hamper the calculation of metamorphic conditions during different metamorphic imprints.

2.7 Acknowledgment

DAAD and DFG (Sche 265/10) funded this research. The guidance of A. Mruma during a second field trip is highly valued. We greatly appreciate the guides on how to handle samples with acids and teflon bombs by T. John and thank the ICP-MS laboratory team under D. Garbe-Schönberg and his co-workers P. Fiedler and U. Westernströer for helping during sample preparation and analyses. We value the assistance provided by B. Mader with microprobe analyses and A. Fehler for producing thin sections. We thank A. Larionov, I. Paderin, S. Presniakov and N. Rodionov, a team of the SHRIMP laboratory at St. Petersburg, and lastly but not least thanks to Nambungu for driving us in the field.

References

- Armstrong, J. T., 1995. CITZAF: A package of correction programs for the quantitative electron microbeam X-ray analysis of thick polished materials, thin films and particles. *Microbeam Analysis*, **4**, 117–200.
- Black, L. P., Kamo, S. L., Allen, C. M., Aleinikoff, J. N., Davis, D. W., Korsch, R. J. & Foudoulis, C., 2003. TEMORA 1: a new zircon standard for Phanerozoic U-Pb geochronology. *Chemical Geology*, **200**, 155–170.

- Boven, A., Theunissen, K., Sklyarov, E., Klerkx, J., Melnikov, A., Mruma, A. & Punzalan, L., 1999. Timing of exhumation of a high-pressure mafic granulite terrane of the Paleoproterozoic Ubende Belt (West Tanzania). *Precambrian Research*, **93**, 119–137.
- Boynton, W. V., 1984. Cosmochemistry of the rare earth elements: meteorite studies. In: *Rare earth element geochemistry*, Elsevier Sci. Publ. 63–114.
- Braun, I. & Appel, P., 2006. U-Th-total Pb dating of monazite from orthogneisses and their ultra-high temperature metapelitic enclaves: implications for the multistage tectonic evolution of the Madurai Block, southern India. *European Journal of Mineralogy*, **18**, 415–427.
- Brock, P. W. G., 1963. *The Mbozi syenite-gabbro complex*. Unpublished Ph.D. thesis, University of Leeds.
- Carson, C. J., Ague, J. J. & Coath, C. D., 2002. U-Pb geochronology from Tonagh Island, East Antarctica: implications for the timing of ultra-high temperature metamorphism of the Napier Complex. *Precambrian Research*, **116**, 237–263.
- Cawood, P. A., Kroener, A. & Pisarevsky, S., 2006. Precambrian plate tectonics: criteria and evidence. *GSA Today*, **16**, 4–11.
- Collins, A. S., Reddy, S. M., Buchan, C. & Mruma, A., 2004. Temporal constraints on Palaeoproterozoic eclogite formation and exhumation (Usagaran Orogen, Tanzania). *Earth and Planetary Science Letters*, **224**, 175–192.
- Corfu, F., Hanchar, J. M., Hoskin, P. W. O. & Kinny, P. D., 2003. Atlas of zircon textures. In: *Zircon*, Mineralogical Society of America and Geochemical Society, Washington, DC, United States. 469–500.
- Dahl, P. S., Terry, M. P., Jercinovic, M. J., Williams, M. L., Hamilton, M. A., Foland, K. A., Clement, S. M. & Friberg, L. M., 2005. Electron probe (Ultrachron) microchronometry of metamorphic monazite: Unraveling the timing of polyphase thermotectonism in the easternmost Wyoming Craton (Black Hills, South Dakota). *American Mineralogist*, **90**, 1712–1728.
- Daly, M. C., 1988. Crustal shear zones in Central Africa: a kinematic approach to Proterozoic tectonics. *Episodes*, **11**, 5–11.
- Daly, M. C., Klerkx, J. & Nanyaro, J. T., 1985. Early Proterozoic terranes and strike-slip accretion in the Ubendian belt of southwest Tanzania. *Terra Cognita (Abstract)*, **5**, 257.
- Ellis, D. J. & Green, D. H., 1979. An experimental study of the effect of Ca upon garnet-clinopyroxene Fe-Mg exchange equilibria. *Contributions to Mineralogy and Petrology*, **71**, 13–22.

- Ferry, J. M. & Watson, E. B., 2007. New thermodynamic models and revised calibrations for the Ti-in-zircon and Zr-in-rutile thermometers. *Contributions to Mineralogy and Petrology*, **154**, 429–437.
- Gabe-Schönberg, C. D., 1993. Simultaneous determination of thirty seven trace elements in twenty-eight international rock standards by ICP-MS. *Geostandards Newsletter*, **17**, 81–97.
- Gill, J. B., 1987. Early geochemical evolution of an oceanic island-arc and back-arc: Fiji and the South Fiji Basin. *Journal of Geology*, **95**, 589–615.
- Goodwin, A. M., 1996. *Principles of Precambrian Geology*. London, Academic Press.
- Hamilton, W. B., 1998. Archean tectonics and magmatism. *International Geology Review*, **40**, 1–39.
- Hanson, R. E., 2003. Proterozoic geochronology and tectonic evolution of southern Africa. In: *Proterozoic East Gondwana: supercontinent assembly and breakup*, Geological Society of London. Special volume, 427–463.
- Harley, L. S., Kelly, M. N. & Möller, A., 2007. Zircon Behaviour and the Thermal Histories of Mountain Chains. *Elements: An international Magazine of Mineralogy, Geochemistry, and Petrology*, **3**, 25–30.
- Hawkins, J. W. & Melchior, J. T., 1985. Petrology of Mariana Trough and Lau Basin basalts. *Journal of Geophysical Research. B. 90*, **13**, 11431–11468.
- Hofmann, A. W., 1988. Chemical differentiation of the Earth: the relationship between mantle, continental crust, and oceanic crust. In: *Isotope geochemistry: the Crafoord symposium*, Elsevier, Amsterdam, Netherlands. 297–314.
- Holland, T. J. B., 1980. The reaction albite = jadeite + quartz determined experimentally in the range 600–1200 °C. *American Mineralogist*, **65**, 129–134.
- Jarosewich, E. & Boatner, L. A., 1991. Rare-earth element reference samples for electron microprobe analysis. *Geostandards Newsletter*, **15**, 397–399.
- John, T., Klemd, R., Gao, J. & Garbe-Schoenberg, D., 2008. Trace element mobilization in slabs due to non steady fluid-rock interaction: Constraints from an eclogite-facies transport vein in blueschist (Tianshang, China). *Lithos*, **103**, 1–24.
- John, T., Schenk, V., Haase, K., Scherer, E. & Tembo, F., 2003. Evidence for a Neoproterozoic ocean in south-central Africa from mid-oceanic-ridge-type geochemical signatures and pressure-temperature estimates of Zambian eclogites. *Geology*, **31**, 243–246.
- Jöns, N., Schenk, V., Appel, P. & Razakamanana, T., 2006. Two-stage metamorphic evolution of the Bemarivo Belt of northern Madagascar: constraints from reaction textures and in situ monazite dating. *Journal of Metamorphic Geology*, **24**, 329–347.

- Kato, T., Suzuki, K. & Adachi, M., 1999. Computer program for the CHIME age calculation. *Journal of Earth Science, Nagoya University*, **46**, 49–56.
- Kelly, N. M. & Harley, S. L., 2005. An integrated microtextural and chemical approach to zircon geochronology: refining the Archaean history of the Napier Complex, East Antarctica. *Contributions to Mineralogy and Petrology*, **149**, 57–84.
- Kretz, R., 1983. Symbols for rock-forming minerals. *American Mineralogist*, **68**, 277–279.
- Lenoir, J. L., Liegeois, J. P., Theunissen, K. & Klerkx, J., 1994. The Palaeoproterozoic Ubendian shear belt in Tanzania: geochronology and structure. *Journal of African Earth Sciences*, **19**, 169–184.
- Loose, D., 2007. *Metamorphe Entwicklung des nördlichen und östlichen Randes des Kongo-Kratons in paläoproterozoischer und panafrikanischer Zeit*. Ph.D. thesis, Universität zur Kiel.
- Ludwig, K., 2001. SQUID 1.02. A Users Manual. *Berkeley Geochronology Center Special Publication*, **2**, 19.
- McConnell, R., 1950. Outline of the Geology of Ufipa and Ubende. Bulletin 19, Geological Survey of Tanganyika.
- McDonough, W. F. & Sun, S. S., 1995. The composition of the Earth. In: *Chemical evolution of the mantle*, Elsevier, Amsterdam, Netherlands. 223–253.
- Morimoto, N., Fabries, J., Ferguson, A. K., Ginzburg, I. V., Ross, M., Seifert, F. A., Zussman, J., Aoki, K. & Gottardi, G., 1988. Nomenclature of pyroxenes. *American Mineralogist*, **73**, 1123–1133.
- Muhongo, S., Tuisiku, P., Mnali, S., Temu, E., Appel, P. & Stendal, H., 2002. High-pressure granulite-facies metagabbros in the Ubendian Belt of SW Tanzania: preliminary petrography and P-T estimates. In: *18th colloquium of African Geology*, Pergamon, Oxford, United Kingdom. 279–285.
- Möller, A., Appel, P., Mezger, K. & Schenk, V., 1995. Evidence for a 2 Ga subduction zone: eclogites in the Usagaran Belt of Tanzania. *Geology*, **23**, 1067–1070.
- Möller, A., O' Brien, P. J., Kennedy, A. & Kröner, A., 2003. Linking growth episodes of zircon and metamorphic textures to zircon chemistry: an example from the ultrahigh-temperature granulites of Rogaland, SW Norway. In: *Geochronology: linking the isotopic record with petrology and textures*, Geological Society of London, London. Special volume, 65–81.
- Nanyaro, J. T., Basu, N. K., Muhongo, S. M., Mruma, A. H., Djare, S. A., Mduma, I., Mudiguza, K. M., Van, S. P. & Klerkx, J., 1983. Structural evolution of the Ubendian Belt: preliminary results of a traverse between Karema and Mpanda (Tanzania). *Rapport Annuel - Musee Royal de l'Afrique Centrale*.

- Newton, R. C. & Perkins, I., D., 1982. Thermodynamic calibration of geobarometers based on the assemblages garnet-plagioclase-orthopyroxene (clinopyroxene)-quartz. *American Mineralogist*, **67**, 203–222.
- Paquette, J. L., Nedelec, A., Moine, B. & Rakotondrazafy, M., 1994. U–Pb, single zircon Pb-evaporation and Sm–Nd isotopic study of a granulitic domain in SE Madagascar. *The Journal of Geology*, **102**, 523–538.
- Pearce, J. A., 1996. A user's guide to basalt discrimination diagrams. In: *Trace element geochemistry of volcanic rocks: applications for massive sulphide exploration*, Geological Association of Canada, John's, NF, Canada. 79–113.
- Pearce, J. A. & Cann, J. R., 1973. Tectonic setting of basic volcanic rocks determined using trace element analyses. *Earth and Planetary Science Letters*, **19**, 290–300.
- Powell, R., 1985. Regression diagnostics and robust regression in geothermometer/ geobarometer calibration: the garnet-clinopyroxene geothermometer revisited. *Journal of Metamorphic Geology*, **3**, 231–243.
- Powell, R. & Holland, T. J. B., 1988. An internally consistent dataset with uncertainties and correlations: 3, Applications to geobarometry, worked examples and a computer program. *Journal of Metamorphic Geology*, **6**, 173–204.
- Pyle, J. M., Spear, F. S., Rudnick, R. L. & McDonough, W. F., 2001. Monazite-xenotime-garnet equilibrium in metapelites and a new monazite-garnet thermometer. *Journal of Petrology*, **42**, 2083–2107.
- Pyle, J. M., Spear, F. S., Wark, D. A., Daniel, C. G. & Storm, L. C., 2005. Contributions to precision and accuracy of monazite microprobe ages. *American Mineralogist*, **90**, 547–577.
- Ray, G. E., 1974. The structural and metamorphic geology of northern Malawi. *Journal of Geological Society of London*, **130**, 427–440.
- Ring, U., 1993. Aspects of the Kinematic History and Mechanisms of Superposition of the Proterozoic Mobile Belts of Eastern Central-Africa (Northern Malawi and Southern Tanzania). *Precambrian Research*, **62**, 207–226.
- Ring, U., Kroener, A. & Toulkeridis, T., 1997. Palaeoproterozoic granulite-facies metamorphism and granitoid intrusions in the Ubendian-Usagaran Orogen of northern Malawi, east-central Africa. *Precambrian Research*, **85**, 27–51.
- Rubatto, D., 2002. Zircon trace element geochemistry: partitioning with garnet and the link between U-Pb ages and metamorphism. *Chemical Geology*, **184**, 123–138.

- Schilling, J. G., Zajac, M., Evans, R., Johnston, T., White, W., Devine, J. D. & Kingsley, R., 1983. Petrologic and geochemical variations along the Mid-Atlantic Ridge from 29 degrees N to 73 degrees N. *American Journal of Science*, **238**, 510–586.
- Sklyarov, E. V., Theunissen, K., Melnikov, A. I., Klerkx, J., Gladkochub, D. P. & Mruma, A., 1998. Paleoproterozoic eclogites and garnet pyroxenites of the Ubende Belt (Tanzania). *Schweiz. Mineral. Petrogr. Mitt.*, **78**, 257–271.
- Smirnov, V., Pentelkov, V., Tolochko, V., Trifan, M. & Zhukov, S., 1973. Geology and minerals of the central part of the western rift. Technical report, Mineral and Resource Division, Dodoma, Tanzania. Unpublished report of the geological mapping.
- Spear, F. S., Wark, D. A., Cheney, J. T., Schumacher, J. C. & Watson, E. B., 2006. Zr-in-rutile thermometry in blueschists from Sifnos, Greece. *Contributions to Mineralogy and Petrology*, **152**, 375–385.
- Sutton, J., Watson, J. & James, T., 1954. A Study of the Metamorphic Rocks of Karema and Kungwe Bay, Western Tanganyika. Bulletin 22, Geological Survey of Tanganyika.
- Suzuki, K. & Adachi, M., 1991. The chemical Th-U-total Pb isochron ages of zircon and monazite from the Gray Granite of the Hida terrane, Japan. *Journal of Earth Science, Nagoya University*, **38**, 11–37.
- Tatsumi, Y., Hamilton, D. L. & Nesbitt, R. W., 1986. Chemical characteristics of fluid phase released from a subducted lithosphere and origin of arc magmas: evidence from high-pressure experiments and natural rocks. In: *M. Sakuyama and H. Fukuyama memorial volume*, Elsevier, Amsterdam, Netherlands. 293–309.
- Theunissen, K., Klerkx, J., Melnikov, A. & Mruma, A., 1996. Mechanisms of inheritance of rift faulting in the western branch of the East African Rift, Tanzania. *Tectonics*, **15**, 776–790.
- Theunissen, K., Lenoir, J. L., Liegeois, J. P., Delvaux, D. & Mruma, A., 1992. Major Pan-African imprint in the Ubendian belt of SW Tanzania: U-Pb zircon geochronology and structural context. *C. R. Acad. Sci. Paris*, **314**, 1355–1362.
- Tomkins, H. S., Powell, R. & Ellis, D. J., 2007. The pressure dependence of the zirconium-in-rutile thermometer. *Journal of Metamorphic Geology*, **25**, 703–713.
- Volodichev, O. I., Slabunov, A. I., Bibikova, E. V., Konilov, A. N. & Kuzenko, T. I., 2004. Archean Eclogites in the Belomorian Mobile Belt, Baltic Shield. *Petrology*, **12**, 609–631.
- Watson, E. B., Wark, D. A. & Thomas, J. B., 2006. Crystallization thermometers for zircon and rutile. *Contributions to Mineralogy and Petrology*, **151**, 413–433.

- Williams, I., 1998. U-Th-Pb Geochronology by Ion Microprobe. In: *Application of microanalytical techniques to understanding mineralizing processes* (eds. McKibben, M., Shanks III, W. & Ridley, W.), Reviews in Economic Geology. 1–35.
- Williams, M. L., Jercinovic, M. J., Goncalves, P. & Mahan, K., 2006. Format and philosophy for collecting, compiling, and reporting microprobe monazite ages. *Chemical Geology*, **225**, 1–15.
- Windley, B. F., 1998. Tectonic development of early Precambrian orogens. In: *Origin and evolution of continents: proceedings of the International symposium*, National Institute of Polar Research, Tokyo, Japan. 8–28.
- Zhao, G., Cawood, P. A., Wilde, S. A. & Sun, M., 2002. Review of global 2.1-1.8 Ga orogens: implications for a pre-Rodinia supercontinent. *Earth-Science Reviews*, **59**, 125–162.

Chapter 3

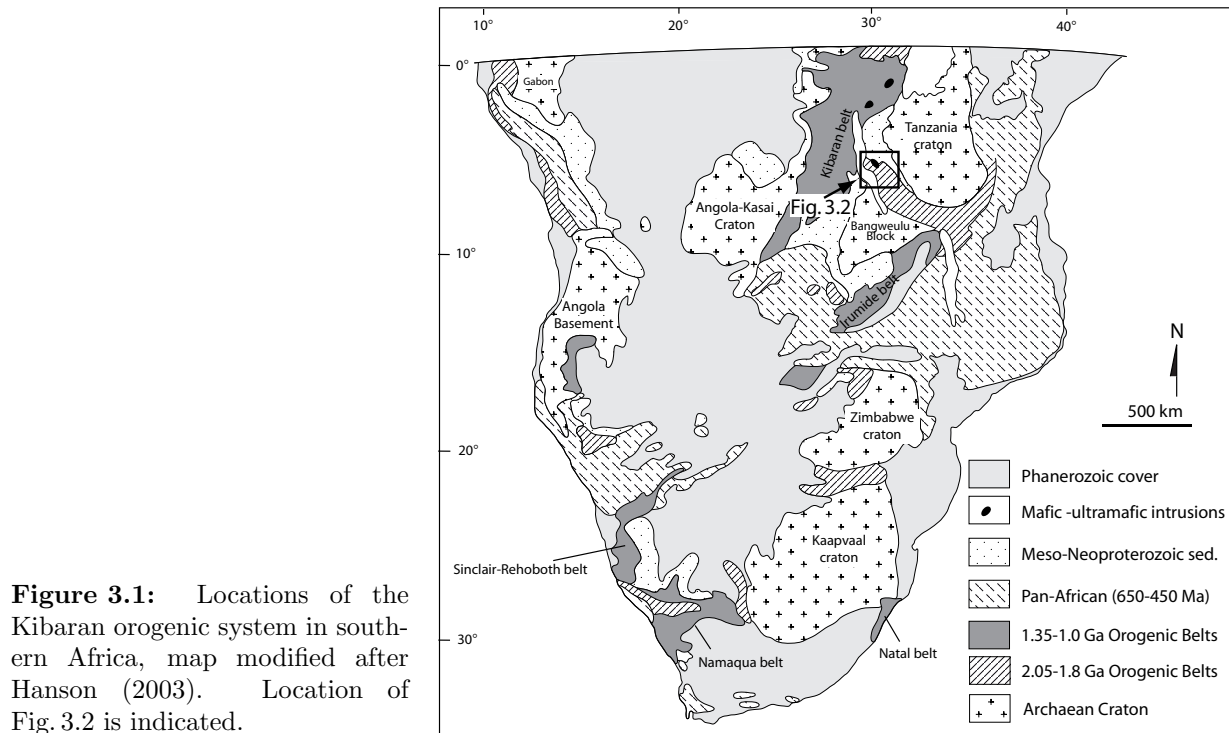
High-grade metamorphism of Kibaran age in the northwestern Ubendian belt of Tanzania

Abstract

Paleoproterozoic basement rocks are thought to form the northwestern end of the Ubendian belt in Tanzania that disappears towards the north below a Mesoproterozoic sedimentary cover. However, in three litho-tectonic terranes of that NW part of the belt, the Wakole, the Ubende and the Katuma terranes, covering an area of 150x75 km, high-grade metamorphic rocks of Kibaran age, have been detected by U-Pb SHRIMP dating of zircons and CHIME dating of monazites. Two phases of Kibaran reworking, separated in time by about 160 Ma (dated at about 1170 and 1010 Ma), have been recognized by distinct growth zones in monazite and zircon. In the Wakole terrane, which is dominated by metasediments, only Kibaran metamorphic ages have been found, but no older or younger metamorphic imprint. Mineral assemblages and reaction textures in Grt-Ky±St-Bt-Ms gneisses (peak at 670-680 °C/8.5-8.9 kbar) point to a clockwise *P-T* path attributed to Kibaran crustal thickening. In contrast, in the adjoining Ubende and Katuma terranes, the Kibaran metamorphism affected high-grade basement rocks (eclogites and granulites) of Paleoproterozoic age that have been overprinted a second time (at least in the Ubende terrane) during the Pan-African orogeny. The Kibaran overprinting in the Ubende terrane is due to mylonitization at deep crustal levels (10 kbar 700-750 °C). It seems to terminate at the southern end of the Ubende and Wakole terranes, where Pan-African eclogites are outcropping. This terrane boundary is interpreted as a Neoproterozoic suture.

3.1 Introduction

The Kibaran orogenic system of Africa, refers to the Mesoproterozoic orogenic belts ascribed to the sutures of the Mesoproterozoic Rodinia supercontinent. The Kibaran orogenic system includes several orogenic belts of Africa: Kibarides, Irumides, Namaqua-Natal, Namaqua-Sinclair-Rehoboth (Fig. 3.1). The NNE-SSE oriented Kibaran belt cutting the NW end of the Paleoproterozoic Ubendian belt formed as the result of the collision be-



tween the Tanzania craton/Bangweulu block and the Congo-Kasai craton at ca. 1.4-1.1 Ga (Cahen *et al.*, 1984).

The Kibaran belt in western Tanzania and Burundi, locally known also as Karagwe-Ankolean and Burundian belts, hosts rift related mafic-ultramafic magmatic rocks, which are famous for their potential of hosting Ni and PGE ore deposits (Wadsworth *et al.*, 1982). Recently the Kabanga layered intrusion and the Kapalagulu igneous complex (in the northern Ubendian belt) in Tanzania have been dated by Maier *et al.* (2007) at 1403 ± 14 Ma and 1392 ± 26 Ma.

In the course of dating metamorphic rocks of the Ubendian belt, Kibaran metamorphic ages were detected in the terranes of the northeastern part of the Ubendian belt (Wakole, Ubende and Katuma terranes). Monazite and zircon of the Wakole terrane metapelitic gneisses show no relicts of Paleoproterozoic metamorphic ages, whereas in the Ubende and Katuma terranes, the Kibaran event overprinted Paleoproterozoic basement rocks of the Ubendian belt. It is the aim of the present study to present petrological informations, U-Pb zircon and monazite data of the newly discovered Kibaran event in the NW part of the Ubendian belt.

3.2 Geological settings

The Wakole terrane is one of the eight lithotectonic terranes in which the Paleoproterozoic Ubendian belt has been subdivided by Daly *et al.* (1985). The Wakole terrane trends NW-SE between the Ubende and Katuma terranes of the Ubendian belt (Fig. 3.2). Biotite-

garnet-kyanite-schist forms the largest part and is the most characteristic rock of the Wakole terrane; metaquartzites and garnetiferous hornblende-gneisses are also common (McConnell, 1950). In the north, lenses of garnet metabasite, amphibolite and amphibole schist intercalated with kyanite-garnet mica schist and biotite-gneiss occur. In the southern part of the terrane kyanite-garnet mica schists and gneisses dominate and are interlayered with amphibolite and quartzite (Smirnov *et al.*, 1970, 1971; Makyao *et al.*, 1997).

The Ubende terrane is dominated by hornblende-rich mafic gneisses that host mylonitic eclogites, rare mylonitic garnet-kyanite gneisses and high-pressure felsic garnet-clinopyroxene granulites. The detailed geology of the Ubende terrane has been described by McConnell (1950), Sutton *et al.* (1954) and Nanyaro *et al.* (1983).

Migmatitic biotite-plagioclase gneisses are common in the Katuma terrane (Smirnov *et al.*, 1973). Fine grained mafic granulites and hornblende gneisses crop out in addition. The 1.4-1.39 Ga Kapalagulu igneous complex (Maier *et al.*, 2007) cuts the Itiaso Mesoproterozoic sedimentary rocks (Wadsworth *et al.*, 1982) overlaying the basement at the northern end of the Ubendian belt (Katuma terrane) (Fig. 3.2).

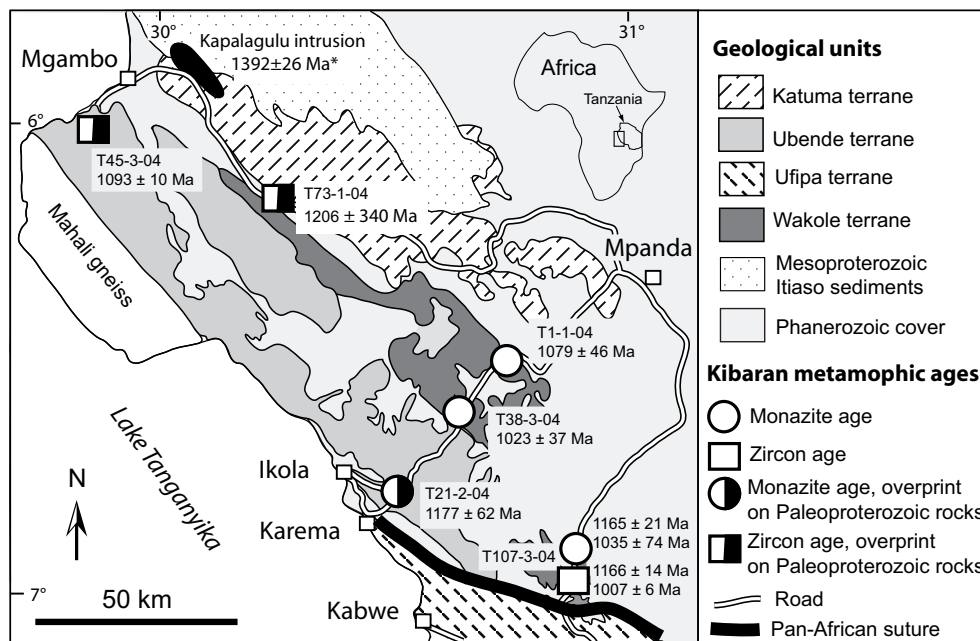


Figure 3.2: Geological map depicting Kibaran metamorphic events in the terranes of Wakole, Ubende and Katuma in the northern Ubendian belt. * Age of Kapalagulu intrusion (Maier *et al.*, 2007).

The Kibaran belt (termed as Kibaran “Supergroup” by Cahen *et al.*, 1984) is dominated by supracrustal rock assemblages (arenaceous and pelitic metasedimentary rocks). However, granites of A- and S-type (1330-1260 Ma) and mafic-ultramafic layered intrusions are present as well (Tack *et al.*, 1994). Metapelites are represented by chlorite schists, muscovite schists, garnet-biotite-sillimanite gneisses, garnet-biotite-sillimanite-kyanite gneisses and chloritoid schists. In southeastern Congo, orthogneisses associated with these metapelites yield a U-Pb zircon age at 1079 ± 14 Ma (Kokonyangi *et al.*, 2006).

The Mesoproterozoic Irumide belt to the southeast of the Bangweulu block experienced a regional metamorphism ranging from greenschist to granulite facies, ultrahigh-temperature metamorphism (UHT) and migmatization (Ridgway & Ramsay, 1986; Schenk & Appel, 2001; De Waele *et al.*, 2006a). U-Th-total Pb dating of monazite gave an age for the UHT event at 1046 ± 3 Ma (Schenk & Appel, 2001), which is consistent with the zircon SHRIMP data at 1021 ± 16 Ma, 1018 ± 5 Ma (southwestern Irumide) and 1004 ± 16 Ma (northeastern Irumide) for lower grade rocks (De Waele *et al.*, 2003, 2006b).

3.3 Analytical techniques

In-situ U-Th-total Pb dating of monazite was performed by using an electron microprobe 'JEOL Superprobe JXA-8900R' at the University of Kiel, Germany. The Jeol H-Type spectrometer with reduced Rowland circle for high count rates was used for measurements of lead, thorium and uranium. Background offsets were selected after long time fine WD scans of natural monazite. The interference of Th $M\gamma$ on U $M\beta$ was corrected with an experimentally determined correction factor.

As standard materials synthetic REE orthophosphates (Jarosewich & Boatner, 1991) were used for P, REE and Y, synthetic U-bearing glass for U, natural wollastonite for Ca and Si, natural thorianite for Th, crocoite for Pb and corundum for Al. Matrix correction for the analyses was performed by the JEOL ZAF program. Counting times for Pb and U were adapted to net intensities to achieve the desired objective of a low error for counting statistics at reasonable counting times. To control the quality of the data an internal laboratory standard from SE Madagascar (kindly provided by Michael Raith, Bonn), was repetitively analysed during the measurements. This monazite is homogeneous in composition and was dated with the U-Pb method of cogenetic zircon and by a Sm-Nd monazite-biotite-garnet-zircon isochron at 545 ± 2 and 542 ± 11 Ma, respectively (Paquette *et al.*, 1994), and recently by A. Möller (pers. comm.) with TIMS at an age of 560 ± 1 Ma. Data with significant Al contents were rejected to eliminate analyses with secondary fluorescence artefacts that may occur if analytical points are close to grain boundaries.

Two methods were used to calculate ages for a set of data: (1) the widely used chemical isochron method (Suzuki & Adachi, 1991) and (2) the calculation of a weighted average, which is frequently used in more recent studies on chemical dating of monazite (e.g. Pyle *et al.*, 2005). Isochron calculations were performed with the CHIME-program of (Kato *et al.*, 1999). The isochron plot has the advantage that it easily enables the identification of data sets with distinct ages and provides information about the chemical variation of the analysed monazite in terms of ThO_2^* and PbO. Also, the intercept of the isochron with the axis yields information about the quality of the analytical data. A drawback of this method is that it can suffer from high errors. This may especially occur when the variation of ThO_2^* is small, thus leading to a poorly defined regression line. In contrast to this, the error of the weighted mean does not depend on the chemical variation of the data. Errors that are calculated for the weighted mean tend to decrease with the number

of points and typically are significantly lower than the error calculated from the isochrone method.

Age maps were calculated from raw elemental x-ray maps of U, Th and Pb. X-ray maps were measured with 12 kV accelerating potential and a probe current of 200 or 250 nA. Counting times per pixel vary between 0,5 and 0.8 s. The Jeol H-Type spectrometer with reduced Rowland circle was used for Pb. The conversion from count rate maps to concentration maps was performed with the in-house-written software MacAgeMap¹. This software applies a simple calibration line method using monazite as standard material (ZAF=1) to perform a background correction and then convert net intensities to concentration data. Afterwards the program converts each image pixel to an apparent age by solving the age equation iteratively for each pixel and archives the data to an image file.

Zircons were separated from the crushed rocks by using the conventional magnetic and heavy liquid methods at the University of Kiel. Isotopic *U-Pb* dating of zircon was done on a SHRIMP-II at the Center of Isotopic Research of VSEGEI in Saint Petersburg, Russia. Handpicked round and prismatic zircons were mounted on epoxy resin discs and polished to expose their cores, whose transmitted light and cathodoluminescence (CL) images were prepared. The diameter of the analyzing ion beam was approximately 20 μm and the primary beam intensity was about 4 nA. Data reduction was done in the manner described by Williams (1998), using the SQUID Excel Makro by Ludwig (2001). The Pb/U ratios have been normalized relative to a value of 0.0668 for the $^{206}\text{Pb}/^{238}\text{U}$ ratio of the TEMORA-1 internal standard reference zircon, equivalent to an age of 416.75 Ma (Black *et al.*, 2003).

3.4 Petrography and mineral chemistry

3.4.1 Wakole terrane

Garnet-kyanite-biotite is the key mineral assemblage for the Wakole terrane metapelites. The mineral assemblages of the four dated samples are listed in Tab. 3.1 and sample locations are indicated on the geological map (Fig. 3.2).

Some of the rock samples equilibrated in the muscovite-quartz (T1-1-04) and others in the kyanite-K-feldspar (T37-2-04 and T38-3-04) stability fields. Only in the lower grade, muscovite-bearing samples, staurolite occurs besides garnet as relict grains included in kyanite, indicating the high temperature breakdown of the staurolite-muscovite-quartz assemblage. In the higher grade samples, kyanite is partially replaced by sillimanite that is locally intergrown with the abundant, coarse-grained K-feldspar of the matrix. This high-grade assemblage is partially replaced and overgrown by late-stage muscovite (Fig. 3.3C) due to retrogression.

Garnet of the Wakole metapelites forms coarse grained (up to 2 cm in diameter) ellipsoidal porphyroblasts containing abundant quartz, plagioclase, biotite and kyanite as prograde inclusions. Kyanite of the high-grade assemblages is very coarse grained con-

¹Software available from PA on request

Table 3.1: Metamorphic mineral assemblages of the metapelites of the Wakole and Ubende terranes.

Sample	Mineral assemblage							Comments		
Wakole terrane										
T1-1-04	Grt	Ky		Bt	Ms	Pl	Qtz	(St)	Ilm	St incl. in Ky
T37-2-04	Grt	Ky	[Sil]	Bt	[Ms]	Pl	Kfs	Qtz	Ilm	Sil in shear zones
T38-3-04	Grt	Ky	[Sil]	Bt	[Ms]	Pl	Kfs	Qtz	Ilm	Sil & Kfs replace Ms
T107-3-04	Grt	Ky		Bt		Pl	[Cld]	Qtz		
Ubende Terrane										
T21-2-04	Grt	Ky		Bt	[Ms]	Pl	Qtz			
T45-3-04	Grt	Ky		Bt		Pl	Qtz	Hbl	Scp	

(St) early-stage mineral; [Sil], [Cld] and [Ms] late-stage minerals

taining biotite quartz and sometimes garnet inclusions. Due to late-stage deformation kink-bending of kyanite and biotite is very common.

The chemical compositions of garnet, plagioclase, staurolite, biotite and muscovite are given in Tab. 3.2 and Tab. 3.3. Garnet is Fe rich ($X_{Fe} \approx 0.84$) and has low X_{Grs} and X_{Sps} . It is not zoned except at the margins where a slight rise of X_{Alm} and a drop of X_{Prp} due to retrograde Fe-Mg exchange occurs (Fig. 3.4A). A representative composition of a garnet core from the staurolite bearing sample T1-1-04 is $X_{Alm} = 0.78$, $X_{Prp} = 0.15$, $X_{Grs} = 0.03$ and $X_{Sps} = 0.03$. Garnet of the high grade rock samples is similar in composition.

Staurolite is Fe rich with $X_{Fe} \approx 0.85$. It was found in one sample only (T1-1-04). Plagioclase is not zoned with X_{Ab} between 0.85 and 0.74. This compositional range is for both, matrix plagioclase and those included in garnet. Biotite is Fe rich ($X_{Fe} = 0.60-0.57$), and its Ti content varies between 0.21 and 0.14 (p.f.u, 11 oxygens). The biotite Ti values of the staurolite-kyanite schist (T1-1-04) correspond to those found in biotite of the sillimanite-staurolite zone of New England, whereas the higher values of the higher-grade kyanite-K-feldspar samples (T37-1-04 and T38-3-04) correspond to those of the sillimanite-K-feldspar zone of New England (Fig. 3.4B; Robinson *et al.*, 1982). Muscovite has a low phengite component, with Si (p.f.u, 11 oxygens) ranging from 3.08 to 3.10 Fig. 3.4C.

3.4.2 Ubende terrane

Metapelites are very rare in the Ubende terrane and have been found at two locations only (Fig. 3.2). The garnet-kyanite metapelites of the Ubende terrane are mylonitic and contain garnet, kyanite, plagioclase and \pm scapolite porphyroclasts in a matrix of recrystallized biotite, quartz and \pm hornblende (Fig. 3.3D and Tab. 3.1). Chemical data of garnet, plagioclase and biotite used to calculate pressure and temperature conditions are given in Tab. 3.2 and Tab. 3.3.

The core of garnet porphyroclasts is Fe rich with X_{Fe} between 0.7 and 0.6. Retrograde diffusional zoning is seen at the garnet rims by the rising of Fe and dropping of Mg contents. The molar proportions of the garnet end member constituents of samples T45-3-04 are $X_{Alm} = 0.52$, $X_{Prp} = 0.36$, $X_{Grs} = 0.04$ and $X_{Sps} = 0.08$ (Fig. 3.4E) and of sample T21-2-04

are $X_{Alm}=0.62$, $X_{Prp}=0.27$, $X_{Grs}=0.09$ and $X_{Sprs}=0.02$). Plagioclase porphyroclasts which occur in aggregates are zoned with Ca richer cores ($X_{An} = 0.39$) than rims ($X_{An} = 0.29$) (Fig. 3.4F).

3.5 Mineral reactions

A prograde dehydration reaction, in which staurolite+muscovite breaks down to form kyanite, biotite and garnet is manifested by relicts of staurolite inclusions in kyanite (Fig. 3.3A). The corresponding mineral reaction $St + Ms + Qtz = Ky + Grt + Bt + H_2O$ is illustrated in an AFM diagram (Fig. 3.4D).

In the higher-grade rocks with K-feldspar-kyanite garnet assemblages, kyanite inclusions in garnet are evident that the prograde garnet growth occurred in the stability field of kyanite. However, the occurrence of sillimanite-K-feldspar intergrowths in the rock matrix is evidence for the late-stage evolution within the sillimanite stability field. Retrograde rehydration led to a partial back-reaction and to the formation of muscovite overgrowing sillimanite-K-feldspar.

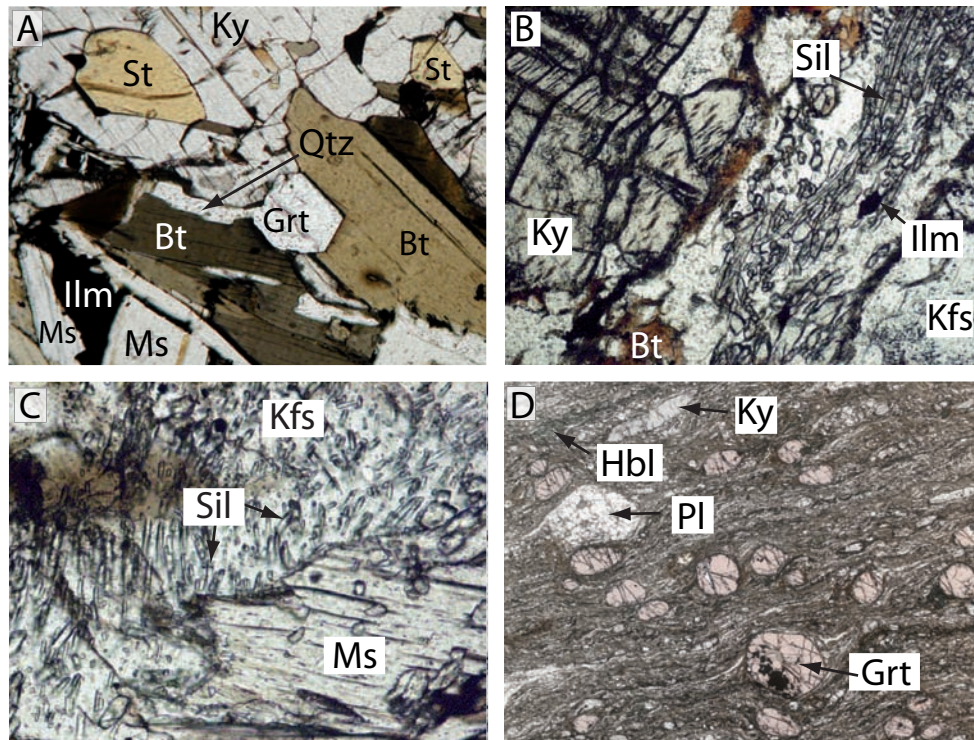


Figure 3.3: The textures of Grt-Bt-Ky-bearing metapelites of the Wakole terrane. A: Prograde St included in Ky (sample T1-1-04, Wakole terrane). B: Kink banded Ky and the growth of late-stage Sil in shear zone (sample T38-3-04 Wakole terrane). C: Late-stage muscovite overgrowing highgrade Kfs-Sil intergrowths (sample T37-1-04 Wakole terrane). D: Mylonitic metapelite of the Ubende terrane (T45-3-04), which has been overprinted in Kibaran time.

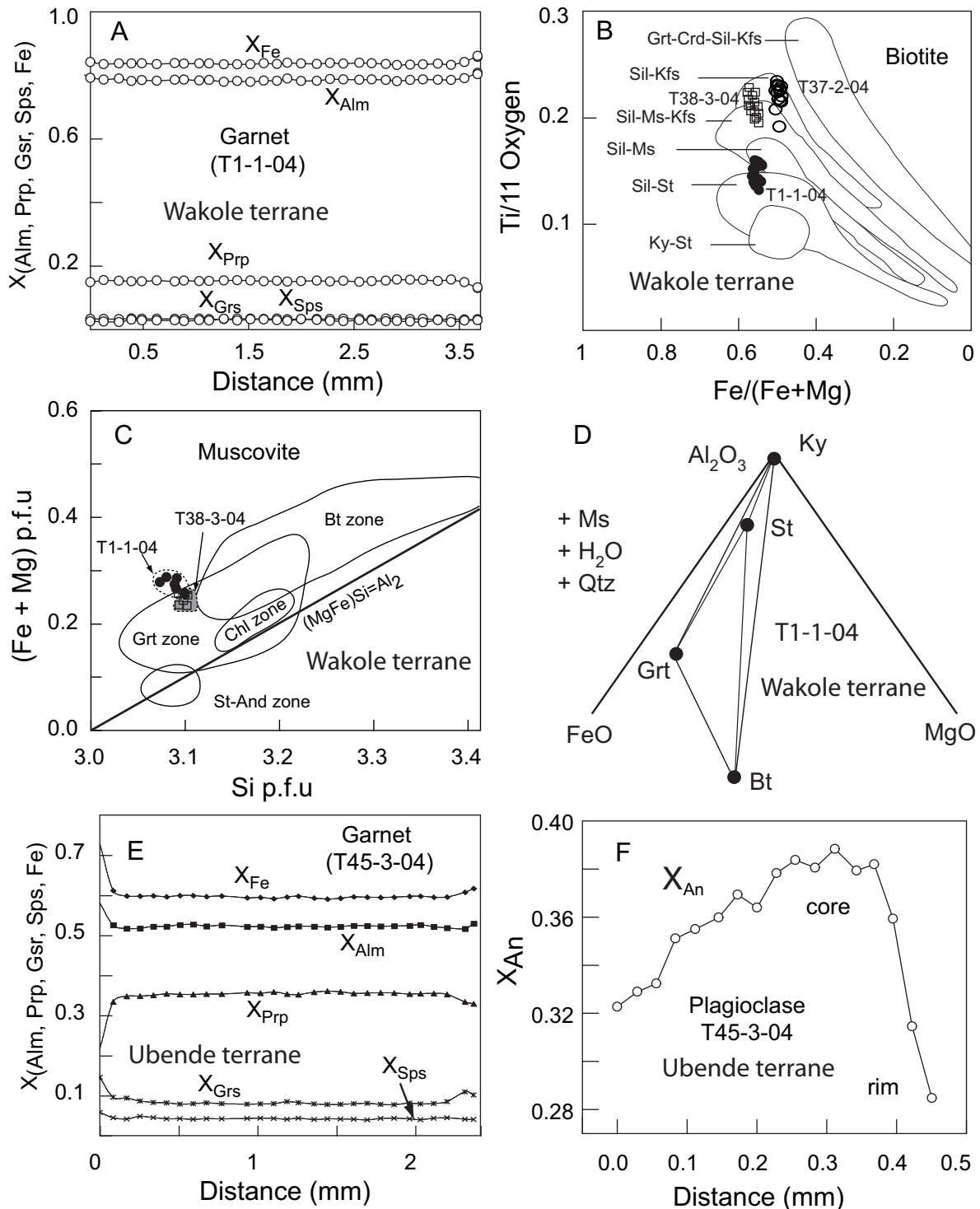


Figure 3.4: A: Garnet profile of metapelite T1-1-04. B: Biotite of Kibaran Grt-Ky-Ms and Grt-Ky-Kfs gneisses are compared with biotite from metamorphic zones of New England; Ti vs X_{Fe} diagram after Robinson *et al.* (1982). C: $(\text{Fe}+\text{Mg})$ vs Si diagram showing the phengite component in Ms, diagram after Graessner & Schenk (1999). D: Phase relations in an AFM projection from muscovite for sample T1-1-04 showing the breakdown of staurolite to form garnet-biotite-kyanite. E: Garnet profile of mylonitic metapelite (T45-3-04) of the Ubende terrane. F: Plagioclase profile of the mylonitic metapelite T45-3-04.

Table 3.2: Representative electron microprobe analyses of garnet and plagioclase of the Wakole and Ubende terrane metapelites

Sample No.	T1-1 87 ^{core}	T1-1 88 ^{core}	T37-2 119 ^{core}	T37-2 121 ^{core}	T38-3 158 ^{core}	T38-3 156 ^{core}	T21-1 118 ^{core}	T45-3 40 ^{core}	T45-3 29 ^{rim}	Sample No.	T1-1 80	T1-1 83	T1-1 84	T38-3 25 ^{incl.}	T38-3 26 ^{incl.}	T38-3 147	T38-3 153	T21-1 82	T45-3 22 ^{core}	T45-3 28 ^{rim}
Garnet																				
SiO ₂	36.71	36.70	37.52	37.39	36.71	36.79	38.16	39.30	38.50	SiO ₂	65.44	64.99	65.08	60.97	61.34	62.26	61.72	61.41	58.40	61.41
Al ₂ O ₃	20.72	20.86	21.35	21.23	20.85	20.75	21.58	22.28	21.62	Al ₂ O ₃	21.97	21.96	21.91	24.67	24.66	23.82	23.57	24.23	25.82	24.44
FeO	36.08	36.00	35.05	34.47	35.27	35.94	29.25	24.52	26.56	CaO	3.25	3.31	3.34	5.50	5.43	5.65	5.60	5.28	8.14	5.96
MgO	3.97	3.98	3.61	3.58	3.36	3.08	6.96	9.41	5.55	Na ₂ O	9.52	9.45	9.50	8.49	8.56	8.11	8.29	8.40	7.24	8.19
MnO	1.31	1.33	0.58	0.51	1.31	1.28	0.72	2.00	2.62	K ₂ O	0.10	0.09	0.08	0.15	0.16	0.29	0.31	0.05	0.12	0.13
CaO	1.20	1.19	2.28	2.35	2.12	2.20	3.34	2.89	5.19	BaO	0.00	0.00	0.00	0.00	0.00	0.00	0.00	0.00	0.00	0.00
Total	99.99	100.06	100.39	99.53	99.62	100.04	100.01	100.40	100.04	Total	100.31	99.80	99.91	99.78	100.15	100.16	99.49	99.37	99.72	100.13
Plagioclase																				
Si	2.97	2.96	2.99	3.00	2.97	2.98	2.98	3.00	3.01	Si	2.87	2.86	2.86	2.70	2.71	2.75	2.75	2.74	2.62	2.72
Al	1.97	1.98	2.01	2.01	1.99	1.98	1.99	2.00	1.99	Al	1.13	1.14	1.14	1.29	1.28	1.24	1.24	1.27	1.36	1.28
Fe	2.44	2.43	2.34	2.31	2.39	2.43	1.91	1.56	1.74	Ca	0.15	0.16	0.16	0.26	0.26	0.27	0.27	0.25	0.39	0.28
Mg	0.48	0.48	0.43	0.43	0.41	0.37	0.81	1.07	0.65	Na	0.81	0.81	0.81	0.73	0.73	0.70	0.72	0.73	0.63	0.70
Mn	0.09	0.09	0.04	0.03	0.09	0.09	0.05	0.13	0.17	K	0.01	0.01	0.00	0.01	0.01	0.02	0.02	0.00	0.01	0.01
Ca	0.10	0.10	0.20	0.20	0.18	0.19	0.28	0.24	0.44	Ba	0.00	0.00	0.00	0.00	0.00	0.00	0.00	0.00	0.00	0.00
Total	8.05	8.05	8.00	7.99	8.03	8.03	8.02	8.00	8.00	Total	4.97	4.97	4.97	4.99	4.99	4.98	4.99	4.99	5.01	4.99
X _{Fe}	0.84	0.84	0.84	0.84	0.86	0.87	0.70	0.59	0.73	X _{An}	15.78	16.13	16.20	26.12	25.75	27.33	26.70	0.26	0.38	0.28
X _{Alm}	0.78	0.78	0.78	0.78	0.78	0.79	0.63	0.52	0.58	X _{Ab}	83.63	83.34	83.37	73.05	73.35	70.98	71.55	0.74	0.61	0.71
X _{Prp}	0.15	0.15	0.14	0.14	0.13	0.12	0.27	0.36	0.22	X _{Or}	0.59	0.53	0.43	0.83	0.90	1.69	1.75	0.00	0.01	0.01
X _{Grs}	0.03	0.03	0.06	0.07	0.06	0.06	0.09	0.04	0.06											
X _{Sps}	0.03	0.03	0.01	0.01	0.03	0.03	0.02	0.08	0.15											

Cations calculated on the basis of 12 oxygens for Grt, 8 oxygens for Pl; incl. = inclusions in Grt

Table 3.3: Representative electron microprobe analyses of biotite, muscovite and staurolite of metapelite of the Wakole and Ubende terranes.

Sample No.	T1-1 12	T1-1 63	T1-1 64	T37-2 347	T37-2 348	T38-3 18	T38-3 185	T45-3 136	T1-1 13	T1-1 14	T38-3 44	T38-3 45	Sample No.	T1-1 52	T1-1 53	T1-1 54
Biotite									Muscovite				Staurolite			
SiO ₂	34.54	35.39	35.38	36.26	35.93	34.69	35.49	44.39	37.60	44.33	45.33	45.06	SiO ₂	27.51	27.52	27.61
TiO ₂	2.19	2.54	2.42	4.08	4.14	3.76	3.98	0.96	1.81	1.09	1.06	1.09	TiO ₂	0.63	0.75	0.706
Al ₂ O ₃	17.84	17.93	18.02	17.65	17.54	17.28	17.13	32.11	17.80	32.17	32.55	32.27	Al ₂ O ₃	53.90	53.71	53.78
FeO	19.87	20.32	20.83	17.70	18.01	21.16	21.26	3.24	11.60	3.21	2.75	2.92	Cr ₂ O ₃	0.17	0.19	0.162
MgO	9.32	8.24	8.33	10.19	9.94	8.52	7.83	0.87	14.01	0.81	0.80	0.88	FeO	13.05	13.27	13.30
MnO	0.01	0.04	0.06	0.02	0.08	0.01	0.00	0.05	0.08	0.03	0.00	0.02	MgO	1.38	1.37	1.29
Na ₂ O	0.24	0.21	0.16	0.09	0.04	0.09	0.11	0.98	0.16	0.97	0.35	0.28	MnO	0.06	0.07	0.10
K ₂ O	9.72	9.63	9.55	10.29	10.27	10.26	10.03	10.41	10.26	10.50	11.48	11.63	ZnO	1.65	1.65	1.72
Total	93.73	94.37	94.79	96.36	96.04	95.77	95.31	93.01	93.39	93.11	94.32	94.15	Total	98.19	98.34	98.51
Si	5.39	5.48	5.46	5.44	5.42	5.35	5.45	6.16	6.16	6.14	6.20	6.19	Si	7.97	7.97	7.99
Ti	0.26	0.30	0.28	0.46	0.47	0.44	0.46	0.10	0.10	0.11	0.11	0.11	Ti	0.14	0.16	0.1535
Al	3.28	3.27	3.28	3.12	3.12	3.14	3.10	5.24	5.25	5.26	5.24	5.22	Al	18.40	18.33	18.33
Fe	2.60	2.63	2.69	2.22	2.27	2.73	2.73	0.38	0.38	0.37	0.31	0.34	Cr	0.04	0.04	0.04
Mg	2.17	1.90	1.92	2.28	2.24	1.96	1.79	0.18	0.18	0.17	0.16	0.18	Fe	3.16	3.21	3.22
Mn	0.00	0.01	0.01	0.00	0.01	0.00	0.00	0.00	0.01	0.00	0.00	0.00	Mg	0.60	0.59	0.56
Na	0.07	0.06	0.05	0.03	0.01	0.03	0.03	0.26	0.26	0.26	0.09	0.07	Mn	0.02	0.02	0.02
K	1.94	1.90	1.88	1.97	1.98	2.02	1.97	1.84	1.84	1.86	2.00	2.04	Zn	0.35	0.35	0.37
Total	15.71	15.57	15.58	15.53	15.54	15.66	15.66	14.18	14.17	14.17	14.12	14.15	Total	30.64	30.64	30.64
X _{Fe}	0.54	0.58	0.58	0.49	0.50	0.58	0.60	0.68	0.32	0.69	0.66	0.65	X _{Fe}	0.84	0.84	0.85

Cations calculated on the basis of 22 oxygens for Bt and Ms, 48 oxygens for St

3.6 Geothermobarometry

Pressure-temperature conditions during metamorphism have been calculated for one Ms-Qtz, two Kfs-Ky bearing metapelites of the Wakole terrane and one biotite-garnet-kyanite porphyroclastic mylonite of the Ubende terrane. We applied the THERMOCALC program of Holland & Powell (1998) and conventional geothermobarometers: GASP geobarometer calibrated by Koziol (1989), the Fe-Mg exchange between garnet and biotite calibrated by Ferry & Spear (1978), Hodges & Spear (1982) and Gessmann *et al.* (1997). The *P-T* results of the four samples (T 1-1-04, T37-2-04, T38-3-04 and T45-3-04) are given in Tab. 3.4.

The Ms-Qtz bearing metapelite (T1-1-04) gives average *P-T* values at 672±52 °C/ 9.2±1.9 kbar calculated by using the THERMOCALC program (Holland & Powell, 1998), the mineral activities were calculated by using the AX-program (version 0.1, 2004) of T.J.B Holland. Similar temperatures and pressures to those of the THERMOCALC at 670-680 °C/8.8-8.9 kbar were obtained by applying the Fe-Mg exchange between garnet and biotite (Ferry & Spear, 1978; Hodges & Spear, 1982; Gessmann *et al.*, 1997) and the GASP geobarometer (Koziol, 1989).

The Ky-Kfs-bearing metapelite (T38-3-04) yields an average *P-T* at 747±42 °C/ 9.1±1.3 kbar, which corroborate with conventional geothermobarometry that gives a result of 710-740 °C/ 9-9.5 kbar. Pressures could not be estimated with the GASP equilibrium from

sample T37-2-04, because plagioclase is absent in that rock. However, average P - T values at $771\pm 30^\circ\text{C}/12\pm 3$ were estimated by using the THERMOCALC program (Holland & Powell, 1998).

Table 3.4: Results of pressure and temperature estimates for Wakole terrane metapelites. The Fe-Mg exchange thermometer (garnet-biotite) FS = Ferry & Spear (1978), HS = Hodges & Spear (1982) and G = Gessmann *et al.* (1997), GASP geobarometer K = Koziol (1989).

Sample No.	Used minerals	T ($^\circ\text{C}$)	P (kbar)	σ fit	
THERMOCALC program (Holland & Powell, 1998)					
T1-1-04	Grt-Bt-Ky-Ms-Pl-St-Qtz	672 ± 52	9.2 ± 1.9	2.23	
T37-1-04	Grt-Bt-Ky-Kfs-Qtz	771 ± 30	12.0 ± 3.0	1.48	
T38-3-04	Grt-Bt-Ky-Pl-Kfs-Qtz	747 ± 42	9.1 ± 1.3	0.63	
Conventional geothermobarometry					
	Mineral & analysis No.	HS	FS	G	K
T1-1-04	Grt ₈₇ -Bt ₁₂ -Pl ₈₀	670	680	680	8.5-8.9
T38-3-04	Grt ₁₅₈ -Bt ₁₈₅ -Pl ₂₂	730	710	740	9-9.5

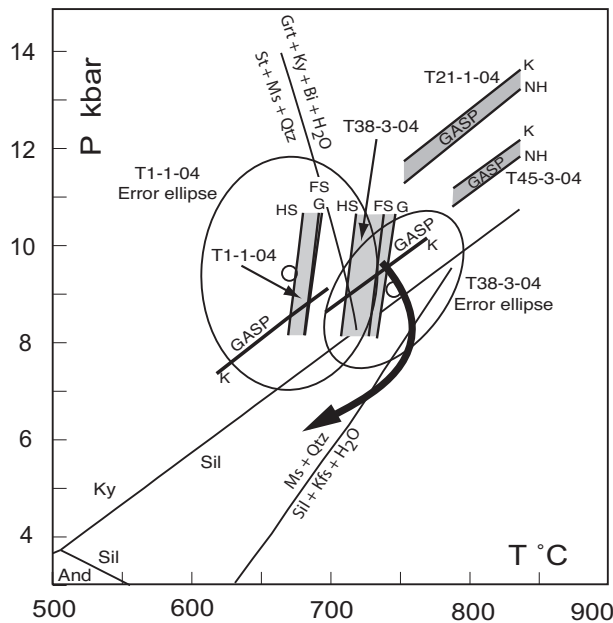


Figure 3.5: P - T diagram depicting metamorphic conditions for the Kibaran metapelites of the Wakole and Ubende terranes. Muscovite and staurolite breakdown reactions were taken from the petrogenetic grid of Spear & Cheney (1989). Fe-Mg exchange thermometers (garnet-biotite) and GASP geobarometers are given in abbreviations: FS = Ferry & Spear (1978), HS = Hodges & Spear (1982), G = Gessmann *et al.* (1997), K = Koziol (1989) and NH = Newton & Haselton (1981).

The results of the thermobarometric calculations are in agreement with the petrographical observations. The calculated peak conditions of all samples fall into the kyanite stability field. The muscovite + quartz-bearing samples containing staurolite relicts experienced temperatures slightly below the maximum thermal stability of the St-Ms-Qtz assemblage (Fig. 3.5) and the higher grade Kfs-Ky bearing assemblage experienced conditions of slightly higher temperatures than the staurolite-out reaction, near the kyanite to sillimanite boundary (Fig. 3.5). Since muscovite was not stable in the later rocks but

kyanite + K-feldspar, a slightly reduced water activity has to be assumed to match the petrographic observations (Fig. 3.5). A possible metamorphic evolution path of the Wakole terrane metapelites is illustrated in Fig. 3.5.

In the Ubende terrane, peak pressure conditions estimated from the composition of garnet core and unzoned matrix plagioclase by GASP equilibrium (Koziol, 1989; Newton & Haselton, 1981) from two mylonites (T21-1-04 and T45-3-04) fall in the kyanite stability field (Fig. 3.5). Peak temperatures could not be estimated due to strong recrystallization of matrix biotite.

3.7 U-Pb SHRIMP zircon dating

3.7.1 Zircon textures and U-Th contents

Prismatic and round zircons were separated from two metapelites: sample T107-3-04 of the southern part of the Wakole terrane and sample T45-3-04 of the northwestern Ubende terrane (Fig. 3.2). The CL images of zircons of sample T107-03-04 reveal relicts of magmatic cores, which are surrounded by inner rims (mantles) and outer rims (Fig. 3.6A). The Th/U ratios range between 0.73 and 0.38 in the cores, decrease to a range of 0.14 and 0.03 in the inner rims and become lowest in the outer rims (0.02 and 0.004) (Tab. 3.5). The CL images of zircons of sample T45-3-04 reveal relicts of magmatic cores with Th/U ratios at 4.47-0.93 surrounded by metamorphic rims with lower Th/U ratios of 0.02-0.17 than in the cores (Fig. 3.6E; Tab. 3.5). The low Th/U ratios in the zircon rims suggest their growth in a metamorphic environment (Rubatto, 2002). However, it has to be kept in mind that higher Th/U ratios than those observed in magmatic zircons are known from zircons of the granulite facies (Möller *et al.*, 2003).

3.7.2 Zircon ages

U-Pb dating of zircon was performed on the Wakole metapelite T107-3-04, whose zoned zircons have cores, inner rims (mantles) and outer rims (Fig. 3.6A). The zircon cores are older, yielding a $^{207}\text{Pb}/^{206}\text{Pb}$ apparent age of ≈ 1.4 Ga whereas inner rims and outer rims give two different Kibaran ages. The outer rims yield a concordant age at 1007 ± 6 Ma (Fig. 3.7B). The inner rims are discordant, yielding an upper intercept age at 1166 ± 14 Ma and a lower intercept age at 177 ± 63 Ma (an age without geological significance) (Fig. 3.6D). Thus, the metapelitic zircons of the Wakole terrane show two periods of growth during the Kibaran orogenic cycle that are separated by about 160 Ma.

Zircons of a mylonitic garnet-kyanite metapelite (T45-3-04) of the northern Ubende terrane have Paleoproterozoic cores that are overgrown by Mesoproterozoic rims. Two analyses from the cores are concordant at 1817 ± 26 Ma, whereas other core analyses suffered Pb loss and plot discordantly with a big error at the lower (1119 ± 80 Ma) and upper intercept (2151 ± 130 Ma) (Fig. 3.7D). However, the zircon rims give a concordant well defined Kibaran age at 1093 ± 10 Ma.

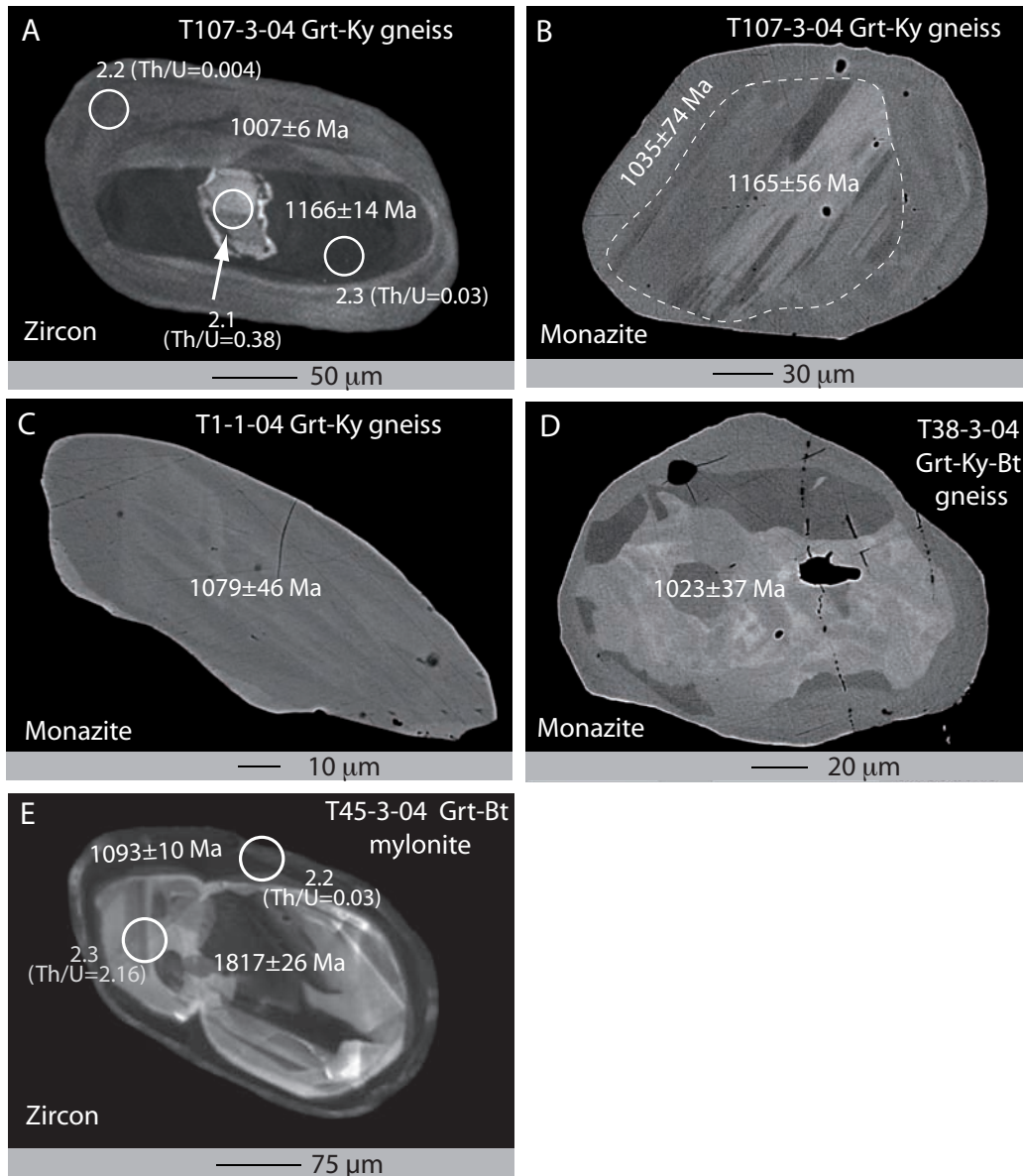


Figure 3.6: CL and BSE images showing zircon and monazite textures. A: CL image of zircon from metapelite T107-3-04 showing relict magmatic core and two consecutive metamorphic growth rims of Kibaran age. B: BSE image showing monazite with a core, which corresponds in age to the outer rim of the zircon in A. The monazite and zircon outer rims correspond in age to each other (ca 1040-1000 Ma). Zircon in image A and monazite in B are from the same Grt-Ky gneiss T107-3-04. C: BSE image of monazite from Wakole sample T1-1-04 shows monophase growth history. D: BSE image of monazite from sample T38-3-04, shows domains, which differ only in Y-HREE concentrations, but not in age (ca. 1020 Ma). E: CL image showing zircon of the sample T45-3-04 with a Paleoproterozoic core overgrown by a Mesoproterozoic rim.

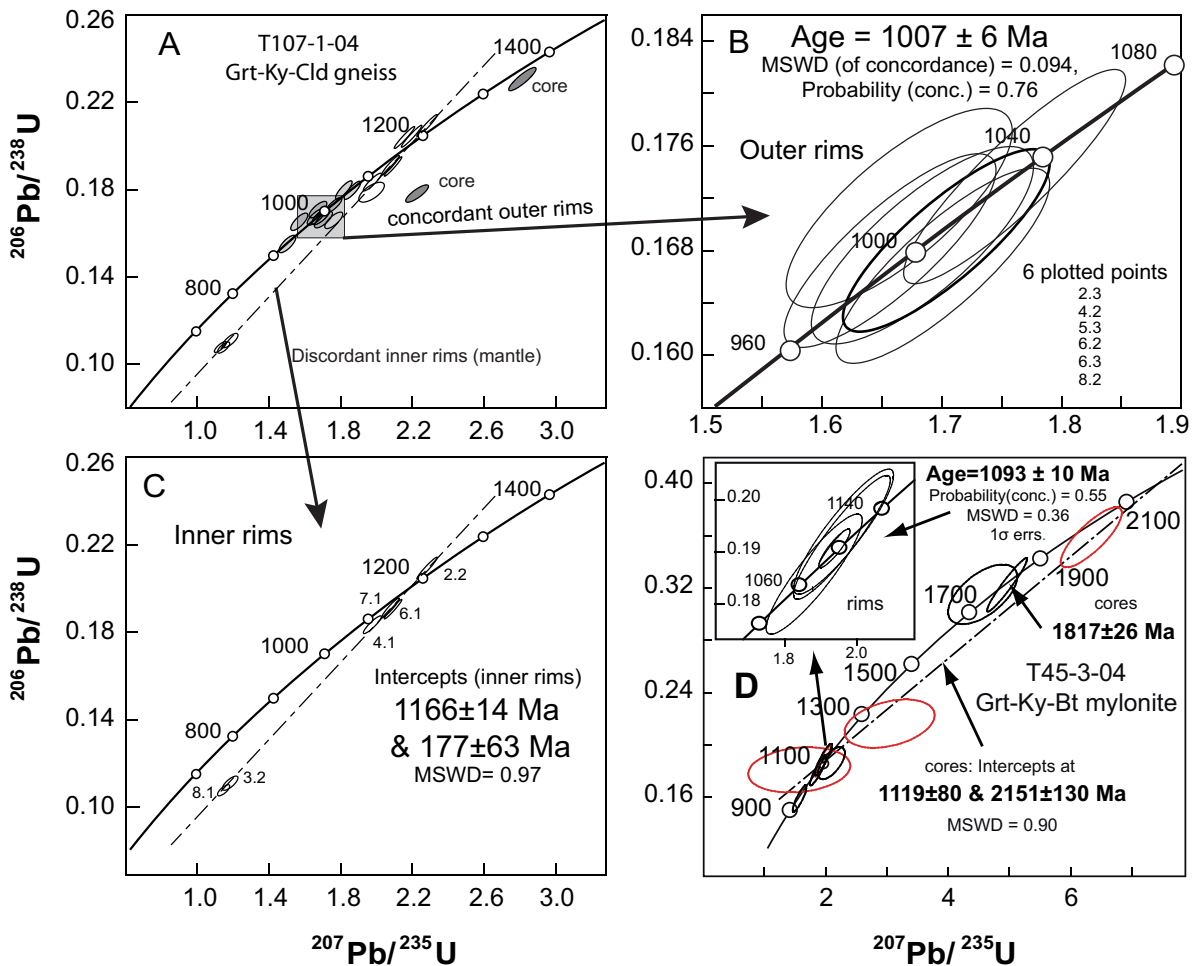


Figure 3.7: A : Concordia diagrams with core, inner rims and outer rim data points used to calculate U-Pb zircon ages of the metapelite sample T107-3-04 of the Wakole terranem. B: Concordant ages from the outer rim of the zircon. C: Discordant data obtained from the inner rims of zircon. D: U-Pb zircon ages obtained from zircon core and rim of the metapelite sample T45-3-04 of the Ubende terrane. Errors at 1σ , decay constant errors included.

3.8 Th-U-total Pb monazite dating

3.8.1 Monazite composition and textures

Three metapelite samples (T1-1-04, T38-3-04, T107-3-04) were selected for *in-situ* monazite CHIME dating. The BSE images reveal monazites with domains, which slightly differ in concentrations of REE, but are uniform in U-Th-Pb concentrations (Fig. 3.6B-D). Some of the monazites occur as inclusions in garnet, but the majority occur in the matrix. Both groups show similarities in terms of REE and U-Th-Pb composition. The molar proportions of the monazite end members brabantite and huttonite (Pyle *et al.*, 2001) are plotted

in Fig. 3.8B&D. In all samples, brabantite $\text{Ca}+(\text{Th,U}) = 2\text{REE}$ was the dominant substitution vector. The huttonite $(\text{Th,U})+\text{Si} = \text{REE}+\text{P}$ vector was not important. There is a uniformity in the REE patterns of monazites of all samples in the Cl-Chondrite normalized REE diagrams, in which Y-HREE are strongly depleted and a negative Eu anomaly is unequivocal (Fig. 3.8A&C). The budget of Y-HREE in rocks is immensely influenced by the presence of garnet, which is the major phase hosting Y-HREE (Pyle *et al.*, 2001). Therefore, the depletion of Y-HREE in monazite is attributed to the synchronous growth of garnet and monazite. The negative Eu anomaly is known to be due to the presence of plagioclase, which takes most of the Eu of a rock. We can conclude that the monazite in the Wakole terrane metapelites were growing together with metamorphic garnet.

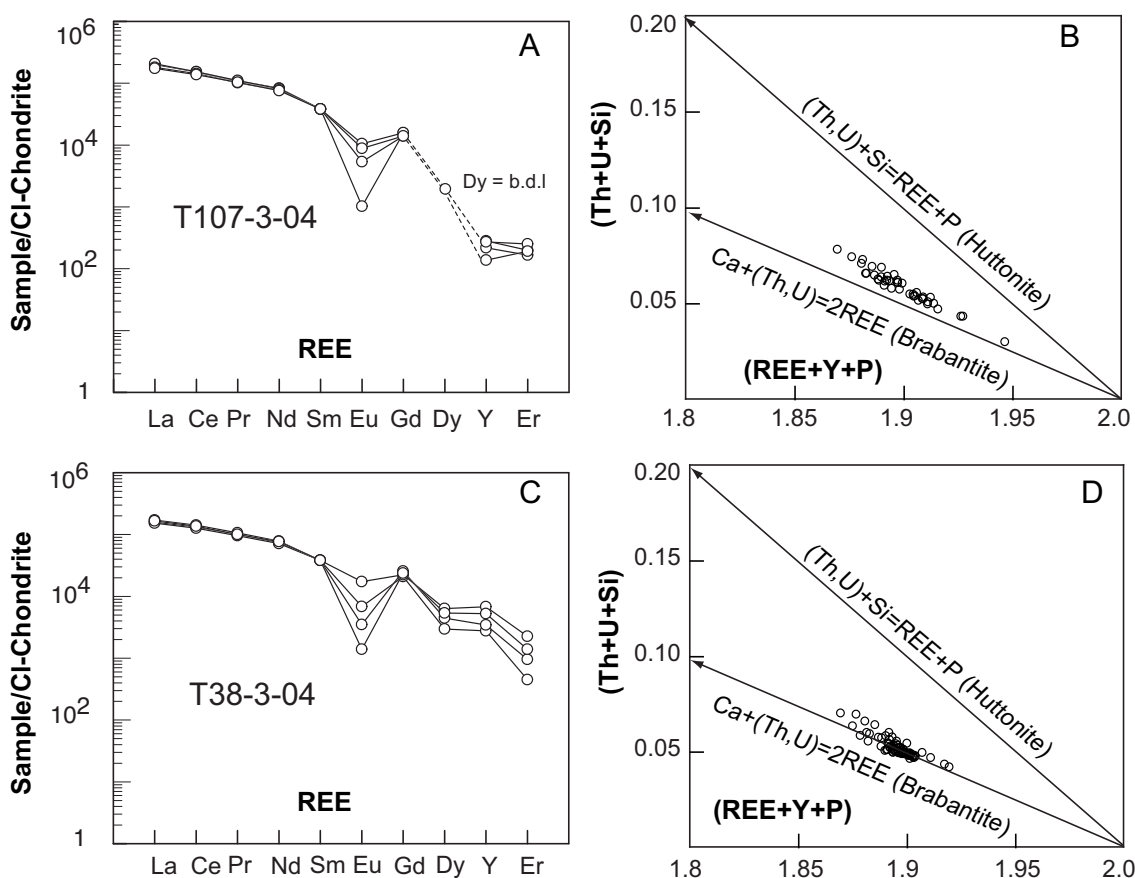


Figure 3.8: REE composition of monazite of the Wakole terrane metapelite. A&C: Plots of REE+Y pattern, normalized to Cl-chondrite (McDonough & Sun, 1995). Similar patterns with Y-HREE depletion and Eu negative anomaly are revealed for both samples. B&D: Plots of (REE+Y+P) vs. (Th+U+Si) showing brabantite and huttonite vectors of monazites in A and C.

3.8.2 Monazite isochron ages

Similar isochron ages were obtained from two of the three analyzed metapelitic monazite samples of the Wakole terrane (T1-1-04 and T38-3-04), giving an age of 1079 ± 46 Ma (weighted mean age 1114 ± 7 Ma) and in 1023 ± 37 (weighted mean age 1022 ± 5 Ma) (Fig. 3.9A-D). The later age corresponds to the U-Pb zircon SHRIMP age obtained for the inner (mantle) metamorphic growth rim of metapelite T107-3-04.

Monazite rims of the third sample (T107-3-04), from which also zircon has been dated, give an isochron age of 1035 ± 74 Ma (weighted mean age = 1016 ± 10 Ma) and the cores an isochron of 1165 ± 21 Ma (weighted mean age = 1170 ± 10 Ma) (Fig. 3.9 E&F). Like zircon of the same sample, also the monazite reflects two metamorphic growth periods that are separated by about 160 Ma.

Table 3.5: SHRIMP U-Pb zircon analyses of metapelite T107-3-04 of the Wakole terrane

No.	U (ppm)	Th (ppm)	$\frac{^{232}\text{Th}}{^{238}\text{U}}$	^{206}Pb (%) comm.	Apparent age (Ma)		$\frac{^{207}\text{Pb}^*}{^{206}\text{Pb}}$	error (%)	$\frac{^{206}\text{Pb}^*}{^{238}\text{U}}$	error (%)	$\frac{^{207}\text{Pb}^*}{^{235}\text{U}}$	error (%)	disc. (%)
T107-304													
Cores													
2.1	355	132	0.38	0.27	1425 ± 27	1061 ± 18	0.090	1.4	0.1789	1.8	2.219	2.3	34
3.1	386	175	0.47	0.08	1390 ± 20	1337 ± 22	0.088	1.1	0.2304	1.8	2.806	2.1	4
5.1	175	124	0.73	0.38	1188 ± 46	1063 ± 19	0.080	2.3	0.1793	1.9	1.969	3	12
Inner rims (mantles)													
2.3	414	12	0.03	–	1039 ± 24	995 ± 17	0.074	1.2	0.1669	1.8	1.701	2.2	4
4.2	482	13	0.03	0.19	942 ± 30	1019 ± 17	0.071	1.5	0.1713	1.8	1.664	2.3	-8
5.2	482	25	0.05	0.01	877 ± 34	990 ± 17	0.068	1.6	0.166	1.9	1.563	2.5	-11
5.4	610	83	0.14	0.21	1082 ± 39	670 ± 12	0.076	1.9	0.1094	1.8	1.139	2.7	62
6.2	478	33	0.07	0.15	1000 ± 28	1003 ± 17	0.073	1.4	0.1684	1.8	1.683	2.3	0
6.3	513	20	0.04	0.08	1108 ± 25	993 ± 17	0.077	1.3	0.1665	1.8	1.756	2.2	12
8.2	462	15	0.03	0.06	972 ± 25	1001 ± 17	0.072	1.2	0.168	1.8	1.657	2.2	-3
8.3	407	16	0.04	0.22	915 ± 32	935 ± 16	0.070	1.6	0.1561	1.8	1.496	2.4	-2
9.2	790	23	0.03	0.08	1068 ± 18	1067 ± 17	0.075	0.89	0.1801	1.8	1.862	2	0
9.3	748	21	0.03	0.16	1010 ± 20	1068 ± 17	0.073	0.97	0.1803	1.8	1.811	2	-5
Outer rims													
1.1	1549	6	0.00	–	1136 ± 12	1201 ± 19	0.078	0.58	0.2047	1.7	2.19	1.8	-5
2.2	2177	8	0.00	0.03	1167 ± 10	1227 ± 22	0.079	0.49	0.2096	1.9	2.277	2	-5
3.2	1675	7	0.00	1.28	1096 ± 38	687 ± 15	0.076	1.9	0.1124	2.2	1.179	2.9	60
4.1	1743	8	0.00	0.11	1139 ± 17	1089 ± 17	0.078	0.87	0.184	1.7	1.971	2	5
5.3	1109	15	0.01	0.10	1028 ± 18	1032 ± 19	0.074	0.89	0.1737	1.9	1.761	2.1	0
6.1	1835	8	0.00	0.06	1177 ± 11	112 ± 19	0.079	0.53	0.1913	1.8	2.089	1.9	4
7.1	2014	7	0.00	–	1167 ± 19	1129 ± 19	0.079	0.98	0.1913	1.8	2.079	2.1	3
8.1	1632	35	0.02	0.52	1054 ± 26	670 ± 11	0.074	1.3	0.1095	1.8	1.124	2.2	57
9.1	3164	18	0.01	0.07	1105 ± 11	1197 ± 22	0.076	0.57	0.2041	2	2.149	2.1	-8
T45-3-04													
Cores													
1.2	18	78	4.47	0.78	1662 ± 170	1253 ± 48	0.102	9.2	0.2145	4.2	3.02	10	33
2.1	281	253	0.93	–	1827 ± 14	1790 ± 55	0.112	0.76	0.32	3.5	4.93	3.6	2
2.3	25	52	2.16	0.59	1715 ± 75	1753 ± 58	0.105	4.1	0.312	3.8	4.53	5.5	-2
5.1	192	188	1.01	0.30	2073 ± 33	1962 ± 59	0.128	1.9	0.356	3.5	6.29	4	6
Rims													
1.1	98	5	0.05	–	1234 ± 64	1094 ± 36	0.082	3.3	0.185	3.6	2.08	4.9	13
2.2	505	17	0.03	0.11	981 ± 29	945 ± 31	0.072	1.4	0.1579	3.5	1.563	3.8	4
3.1	413	16	0.04	0.07	1080 ± 25	1064 ± 34	0.075	1.3	0.1795	3.5	1.867	3.7	2
3.2	11	2	0.17	2.53	705 ± 450	1064 ± 45	0.063	21	0.1795	4.5	1.56	22	-34
4.1	317	8	0.02	–	1077 ± 25	1108 ± 36	0.075	1.3	0.1876	3.5	1.948	3.7	-3
4.2	416	13	0.03	0.03	1084 ± 22	1102 ± 35	0.076	1.1	0.1865	3.5	1.943	3.7	-2

*common Pb corrected by using measured ^{204}Pb

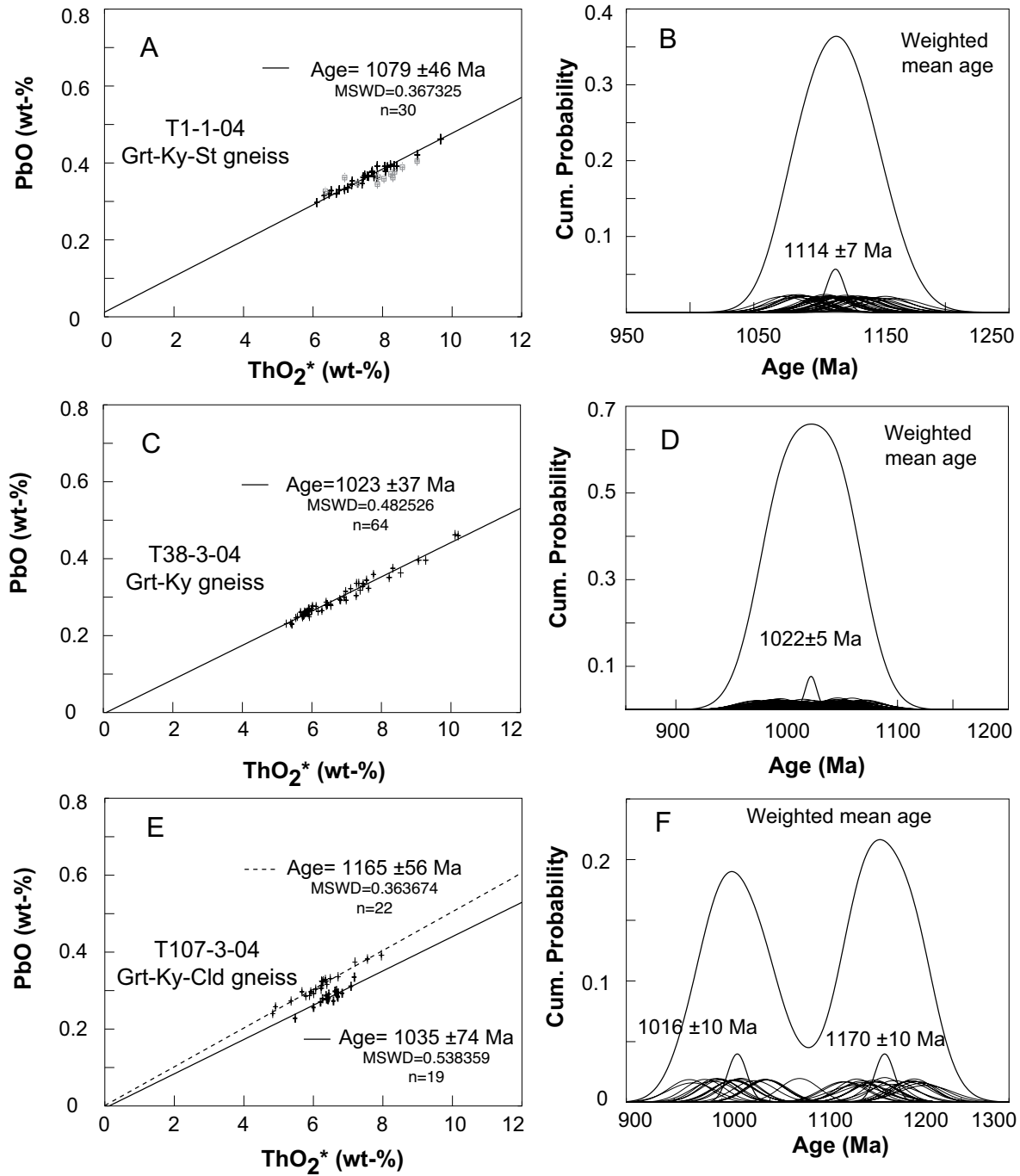


Figure 3.9: PbO vs ThO₂* monazite isochrons and the corresponding weighted mean ages of the Wakole terrane metapelites. A&C: Monazite isochron ages of samples T1-1-04 and T38-3-04 and their respective weighted mean ages in B&D. E: Isochron ages from cores and rims of monazite of sample T107-3-04 and their respective weighted mean ages in F. Isochron error is at 2σ and the weighted mean age error is at 1σ .

Table 3.6: Representative monazite compositions of the Wakole terrane metapelites.

Sample No.	T107-3-04 161 ^{rim}	T107-3-04 162 ^{core}	T38-3-04 150	T1-1-04 212
SiO ₂	0.44	0.23	0.16	0.38
P ₂ O ₅	29.77	30.04	31.12	30.02
Al ₂ O ₃	b.d.l	0.01	0.00	b.d.l
MgO	1.18	0.83	1.04	1.35
ThO ₂	6.42	3.89	4.61	6.43
UO ₂	0.44	0.42	0.31	0.74
PbO	0.39	0.27	0.26	0.41
La ₂ O ₃	14.48	15.93	13.27	12.90
Ce ₂ O ₃	28.72	30.02	27.72	27.29
Pr ₂ O ₃	3.11	3.23	3.01	2.91
Nd ₂ O ₃	12.44	12.43	12.01	11.31
Sm ₂ O ₃	2.07	1.96	2.24	1.95
Eu ₂ O ₃	0.16	0.12	0.13	0.07
Gd ₂ O ₃	1.17	1.00	1.61	1.61
Dy ₂ O ₃	b.d.l	b.d.l	0.54	0.54
Y ₂ O ₃	0.01	0.10	2.26	2.12
Er ₂ O ₃	0.00	0.01	0.12	0.11
Total	100.81	100.50	100.40	100.13
Si	0.017	0.009	0.006	0.015
P	0.986	0.994	1.010	0.990
Al	b.d.l	0.000	0.000	b.d.l
Ca	0.050	0.035	0.043	0.056
Th	0.057	0.035	0.040	0.057
U	0.004	0.004	0.003	0.006
Pb	0.004	0.003	0.003	0.004
La	0.209	0.230	0.188	0.185
Ce	0.411	0.430	0.389	0.389
Pr	0.044	0.046	0.042	0.041
Nd	0.174	0.173	0.164	0.157
Sm	0.028	0.026	0.030	0.026
Eu	0.002	0.002	0.002	0.001
Gd	0.015	0.013	0.020	0.021
Dy	b.d.l	b.d.l	0.007	0.007
Y	0.000	0.002	0.046	0.044
Er	0.000	0.000	0.001	0.001
Total	2.002	2.001	1.993	2.001
X_{LREE}	0.869	0.909	0.833	0.802
X_{HREE}	0.015	0.013	0.029	0.029
X_{Hut}	0.016	0.006	0.003	0.011
X_{Brb}	0.100	0.070	0.088	0.113
X_{YPO_4}	0.000	0.002	0.047	0.044
X_{GdPO_4}	0.015	0.013	0.021	0.021

Cations calculations: oxygen=4 and b.d.l= below detection limit.

3.9 Discussion and conclusions

SHRIMP U-Pb zircon and U-Th-total Pb monazite ages presented in this study indicate that a crustal block consisting of three lithotectonic terranes at the northwestern end of the Paleoproterozoic Ubendian belt (Ubende, Wakole and Katuma terranes, as defined by Daly *et al.*, 1985) have been affected by high-grade metamorphism during the Kibaran orogeny. The Mesoproterozoic N-S striking Kibaran orogen that formed during the assembly of Rodinia is known to occur on the western side of the Tanzania craton, with outcrops only at the western side of Lake Tanganyika. To the south of the Ubende-Wakole-Katuma crustal block that was affected by the Kibaran orogeny no Mesoproterozoic metamorphic ages do occur, but Neoproterozoic eclogites. This indicates a Neoproterozoic suture to the south of the “Kibaran block” in the Ubendian belt.

Our petrological and geochronological data allow to constrain the ages and P - T conditions during the Kibaran event in the Ubende and Wakole terranes. In contrast, our data of the Katuma terrane are not sufficient to characterize the degree of metamorphism and its age. However, the SHRIMP zircon data of a Katuma mafic granulite clearly reflect a disturbance of the isotopic system during the Kibaran event (1206 ± 340 Ma).

Zircons and monazites of three metapelitic samples of the Wakole terrane have been dated, in addition to those of two mylonitic metapelites of the Ubende terrane and of one mafic granulite of the Katuma terrane. The two samples from the southern border of the Kibaran crustal block (T21-2-04 of the Ubende terrane and T107-3-04 of the Wakole terrane; Fig. 3.2) give evidence of two metamorphic growth episodes during the Kibaran orogeny that are separated by about 160 Ma. The two ages, at about 1170 Ma and 1010 Ma, were found in zircon and monazite. These minerals were dated with different methods, which underscores the validity of the two distinct Kibaran ages. However, the two additional monazite samples of the Wakole terrane show only one, the younger, metamorphic age. The Kibaran monazite of the Wakole terrane metapelites is depleted in Y-HREE indicating that it grew in equilibrium with garnet. No older (Paleoproterozoic) or younger (Neoproterozoic) ages were found so far. In contrast, zircon and monazite of the Ubende terrane gave besides Kibaran also Paleoproterozoic and Neoproterozoic ages.

Since monazite of the mylonitic metapelite of the Ubende terrane (T21-2-04) is included in garnet and the growth zone of Kibaran age is depleted in Y-HREE, it grew in equilibrium with garnet. P - T estimates during the mylonitic overprint of the Paleoproterozoic Ubende terrane rocks indicate 10 kbar at 700-750 °C for the Kibaran reworking, which is high-grade and at deep crustal levels (chapter 2). These P - T values of metamorphism are similar to those obtained from the Wakole terrane metasediments that experienced only the Kibaran orogenic metamorphism (8.5-12 kbar and 670-770 °C). Such P - T values in combination with the clockwise P - T path of the Wakole terrane indicate that both terranes, thought to be only part of the Paleoproterozoic Ubendian belt, were buried during the Kibaran orogeny deep in a tectonically thickened crust.

3.10 Acknowledgment

DAAD and DFG (Sche 265/10) funded this research. We value the assistance provided by B. Mader with microprobe analyses and A. Fehler for producing thin sections. We thank A. Larionov, I. Paderin, S. Presniakov and N. Rodionov a team of SHRIMP laboratory at St. Petersburg.

References

- Black, L. P., Kamo, S. L., Allen, C. M., Aleinikoff, J. N., Davis, D. W., Korsch, R. J. & Foudoulis, C., 2003. TEMORA 1: a new zircon standard for Phanerozoic U-Pb geochronology. *Chemical Geology*, **200**, 155–170.
- Cahen, L., Snelling, N. J., Delhal, J. & Vail, J., 1984. *The geochronology and evolution of Africa*. Clarendon Press, Oxford.
- Daly, M. C., Klerkx, J. & Nanyaro, J. T., 1985. Early Proterozoic terranes and strike-slip accretion in the Ubendian belt of southwest Tanzania. *Terra Cognita (Abstract)*, **5**, 257.
- De Waele, B., Kampunzu, A. B., Mapani, B. S. E. & Tembo, F., 2006a. The Mesoproterozoic Irumide belt of Zambia. *Journal of African Earth Sciences*, **46**, 36–70.
- De Waele, B., Liegeois, J. P., Nemchin, A. A. & Tembo, F., 2006b. Isotopic and geochemical evidence of proterozoic episodic crustal reworking within the Irumide belt of south-central Africa, the southern metacratonic boundary of an Archaean Bangweulu Craton. *Precambrian Research*, **148**, 225–256.
- De Waele, B., Wingate, M. T. D., Fitzsimons, I. C. W. & Mapani, B. S. E., 2003. Untying the Kibaran knot: A reassessment of Mesoproterozoic correlations in southern Africa based on SHRIMP U-Pb data from the Irumide belt. *Geology*, **31**, 509–512.
- Ferry, J. M. & Spear, F. S., 1978. Experimental calibration of the partitioning of Fe and Mg between biotite and garnet. *Contributions to Mineralogy and Petrology*, **66**, 113–117.
- Gessmann, C. K., Spiering, B. & Raith, M., 1997. Experimental study of the Fe-Mg exchange between garnet and biotite: constraints on the mixing behavior and analysis of the cation-exchange mechanisms. *American Mineralogist*, **82**, 1225–1240.
- Graessner, T. & Schenk, V., 1999. Low-pressure metamorphism of Palaeozoic pelites in the Aspromonte, southern Calabria: constraints for the thermal evolution in the Calabrian crustal cross-section during the Hercynian Orogeny. *Journal of Metamorphic Geology*, **17**, 157–172.
- Hanson, R. E., 2003. Proterozoic geochronology and tectonic evolution of southern Africa. In: *Proterozoic East Gondwana: supercontinent assembly and breakup*, Geological Society of London. Special volume, 427–463.

- Hodges, K. V. & Spear, F. S., 1982. Geothermometry, geobarometry and the Al_2SiO_5 triple point at Mt. Moosilauke, New Hampshire. *American Mineralogist*, **67**, 1118–1134.
- Holland, T. J. B. & Powell, R., 1998. An internally consistent thermodynamic data set for phases of petrological interest. *Journal of Metamorphic Geology*, **16**, 309–343.
- Jarosewich, E. & Boatner, L. A., 1991. Rare-earth element reference samples for electron microprobe analysis. *Geostandards Newsletter*, **15**, 397–399.
- Kato, T., Suzuki, K. & Adachi, M., 1999. Computer program for the CHIME age calculation. *Journal of Earth Science, Nagoya University*, **46**, 49–56.
- Kokonyangi, J. W., Kampunzu, A. B., Armstrong, R., Yoshida, M., Okudaira, T., Arima, M. & Ngulube, D. A., 2006. The Mesoproterozoic Kibaride belt (Katanga, SE D.R. Congo). *Journal of African Earth Sciences*, **46**, 1–35.
- Koziol, A. M., 1989. Recalibration of the garnet - plagioclase - Al_2SiO_5 - quartz (GASP) geobarometer and applications to natural parageneses. *EOS Transactions*, **70**, 493.
- Ludwig, K., 2001. SQUID 1.02. A Users Manual. *Berkeley Geochronology Center Special Publication*, **2**, 19.
- Maier, W. D., Peltonen, P. & Livesey, T., 2007. The ages of the Kabanga north and Kapalagulu intrusions, western Tanzania: A reconnaissance study. *Economic Geology*, **102**, 147–154.
- Makyao, F., Kanza, E., Troöng, B., Eriksson, B. & Temu, E., 1997. Nkamba Geological Map, Quarter Degree Sheet 169: Based on Geological mapping by B. L. Iskahakov, S. Y., W. W. Stefanovsky, E.G. Kostunin, W. and L. Mahanga: 1970.
- McConnell, R., 1950. Outline of the Geology of Ufipa and Ubende. Bulletin 19, Geological Survey of Tanganyika.
- McDonough, W. F. & Sun, S. S., 1995. The composition of the Earth. In: *Chemical evolution of the mantle*, Elsevier, Amsterdam, Netherlands. 223–253.
- Möller, A., O' Brien, P. J., Kennedy, A. & Kröner, A., 2003. Linking growth episodes of zircon and metamorphic textures to zircon chemistry: an example from the ultrahigh-temperature granulites of Rogaland, SW Norway. In: *Geochronology: linking the isotopic record with petrology and textures*, Geological Society of London, London. Special volume, 65–81.
- Nanyaro, J. T., Basu, N. K., Muhongo, S. M., Mruma, A. H., Djare, S. A., Mduma, I., Mudiguza, K. M., Van, S. P. & Klerkx, J., 1983. Structural evolution of the Ubendian Belt: preliminary results of a traverse between Karema and Mpanda (Tanzania). *Rapport Annuel - Musee Royal de l'Afrique Centrale*.

- Newton, R. C. & Haselton, H. T., 1981. Thermodynamics of the garnet- plagioclase- Al_2SiO_5 -quartz geobarometer. In: *Thermodynamics of Minerals and Melts*, Springer-Verlag, New York. 131–147.
- Paquette, J. L., Nedelec, A., Moine, B. & Rakotondrazafy, M., 1994. U–Pb, single zircon Pb-evaporation and Sm–Nd isotopic study of a granulitic domain in SE Madagascar. *The Journal of Geology*, **102**, 523–538.
- Pyle, J. M., Spear, F. S., Rudnick, R. L. & McDonough, W. F., 2001. Monazite-xenotime-garnet equilibrium in metapelites and a new monazite-garnet thermometer. *Journal of Petrology*, **42**, 2083–2107.
- Pyle, J. M., Spear, F. S., Wark, D. A., Daniel, C. G. & Storm, L. C., 2005. Contributions to precision and accuracy of monazite microprobe ages. *American Mineralogist*, **90**, 547–577.
- Ridgway, J. & Ramsay, C. R., 1986. A provisional metamorphic map of Zambia: explanator notes. *Journal of African Earth Sciences*, **5**, 441–446.
- Robinson, P., Hollocher, K. T., Tracy, R. J. & Dietsch, C. W., 1982. High grade Acadian regional metamorphism in South-central Massachusetts. In: *Guidebook for fieldtrips in Connecticut and South central Massachusetts*, State Geological and Natural History Survey of Connecticut, Storrs. 289–339.
- Rubatto, D., 2002. Zircon trace element geochemistry: partitioning with garnet and the link between U-Pb ages and metamorphism. *Chemical Geology*, **184**, 123–138.
- Schenk, V. & Appel, P., 2001. Anti-clockwise P-T path during ultrahigh-temperature (UHT) metamorphism at ca.1050 Ma in the Irumide belt of eastern Zambia. *Berichte der Deutschen Mineralogischen Gesellschaft, Beihefte zum European Journal of Mineralogy*, **13**, 161.
- Smirnov, V., Pentelkov, V., Tolochko, V., Trifan, M. & Zhukov, S., 1973. Geology and minerals of the central part of the western rift. Technical report, Mineral and Resource Division, Dodoma, Tanzania. Unpublished report of the geological mapping.
- Smirnov, V., Shulyatin, O., Tolochko, V., Zhukov, S. & Mwakisunga, M., 1970. Katuma Geological Map, Quarter Degree Sheet 152.
- Smirnov, V., Shulyatin, O., Tolochko, V., Zhukov, S. & Mwakisunga, M., 1971. Mwese Geological Map, Quarter Degree Sheet 151.
- Spear, F. S. & Cheney, J. T., 1989. A petrogenetic grid for pelitic schists in the system SiO_2 - Al_2O_3 - FeO - MgO - K_2O - H_2O . *Contributions to Mineralogy and Petrology*, **101**, 149–164.

- Sutton, J., Watson, J. & James, T., 1954. A Study of the Metamorphic Rocks of Karema and Kungwe Bay, Western Tanganyika. Bulletin 22, Geological Survey of Tanganyika.
- Suzuki, K. & Adachi, M., 1991. The chemical Th-U-total Pb isochron ages of zircon and monazite from the Gray Granite of the Hida terrane, Japan. *Journal of Earth Science, Nagoya University*, **38**, 11–37.
- Tack, L., Liegeois, J. P., Deblond, A. & Duchesne, J. C., 1994. Kibaran A-type granitoids and mafic rocks generated by two mantle sources in a late orogenic setting (Burundi). *Precambrian Research*, **68**, 323–356.
- Wadsworth, W. J., Dunham, A. C. & Almohandis, A. A., 1982. Cryptic variation in the Kapalagulu layered intrusion, western Tanzania. *Mineralogical Magazine*, **45**, 227–236.
- Williams, I., 1998. U-Th-Pb Geochronology by Ion Microprobe. In: *Application of microanalytical techniques to understanding mineralizing processes* (eds. McKibben, M., Shanks III, W. & Ridley, W.), Reviews in Economic Geology. 1–35.

Chapter 4

Neoproterozoic eclogites in the Paleoproterozoic Ubendian belt of Tanzania: evidence for a Pan-African suture between the Bangweulu block and the Tanzania craton

Abstract

Kyanite-bearing and kyanite-free eclogites of the Ufipa terrane in the Paleoproterozoic Ubendian belt of Tanzania have U-Pb zircon ages of 590-520 Ma and are evidence of a Pan-African suture that separated the Archean Tanzania craton from the Paleoproterozoic Bangweulu block prior to the Pan-African orogeny. So far, these eclogites were assumed to be Paleoproterozoic in age like those of the adjoining Ubende terrane of the Ubendian belt. The trace element patterns and ratios of the kyanite-free eclogites strikingly resemble those of modern back-arc (group I eclogites) or island-arc (group II eclogites) tholeiite basalts. The group I eclogites have LREE 10-30 times chondritic values and their Th/Yb and Ta/Yb ratios suggest a depleted mantle source for the precursor melts of the eclogites similar to that of mid oceanic ridge basalts. The group II eclogites display the characteristic HFSE (Na, Ta, Zr and Hf) depletion relative to LILE and LREE.

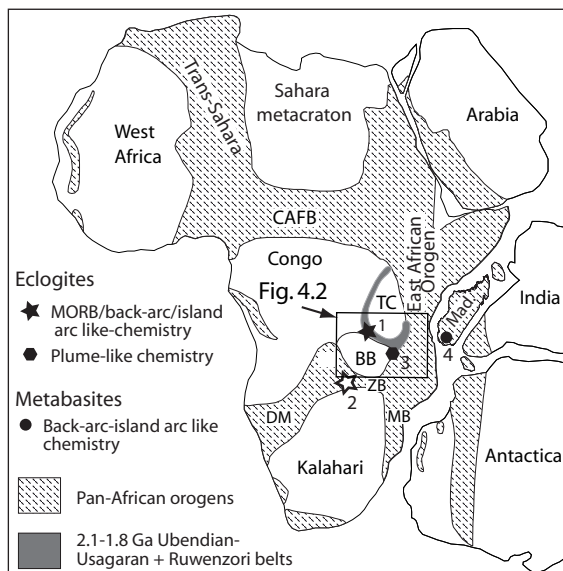
Concordant U-Pb SHRIMP zircon ages at 593 ± 20 Ma and 524 ± 6 Ma were obtained from the kyanite-free eclogites containing metamorphic zircon. Discordant U-Pb ages were obtained from magmatic zircon cores of a kyanite-bearing eclogite, for which the discordia lower intercept age at 548 ± 39 Ma is interpreted as the age of the eclogite-facies metamorphism. The upper intercept age of 1832 ± 20 Ma and a concordant age at 1877 ± 20 Ma found in an overgrown inner zircon mantle are attributed to xenocrysts which formed during a Paleoproterozoic magmatic event.

The occurrences of Neoproterozoic eclogites in the Ubendian belt suggests the existence of a Neoproterozoic convergent plate boundary between the Tanzania craton and the Bangweulu block. The linear zone of Neoproterozoic high-grade reworking associated with eclogite formation between Lake Tanganyika and Lake Malawi is interpreted as the result of the collision (at ca. 560 Ma) between the Bangweulu block and the Tanzania craton (we suggest the name "Tanganyika orogeny" for this event). The occurrences of Neoproterozoic eclogites to the north (Tanganyika orogenic belt), the east (Malawi) and the south (Zambezi belt) of the Bangweulu block suggest that this continental block formed a microplate during the Neoproterozoic Era.

4.1 Introduction

Only few eclogites are known to crop out in the Neoproterozoic orogenic belts of southern Africa (Fig. 4.1). This limits the knowledge about metamorphic subduction processes and the distribution of ocean basins during the formation of Gondwana. However, petrology, geochemistry and geochronology data of a few Pan-African eclogites have been established: The Zambezi belt eclogites in Zambia have a MORB-like chemistry and experienced their subduction metamorphism at 650-610 Ma (John *et al.*, 2003); the eclogites of northern Malawi, thought to belong to the Mozambique belt, have the composition of plume related basalts and and were subducted ca. 530-500 Ma ago (Ring *et al.*, 2002). In addition, the ≈ 850 -700 Ma back-arc/island-arc and continental arc related metabasites of the Vohibory block in southwestern Madagascar experienced collisional metamorphism at 612 ± 5 Ma (Jöns & Schenk, 2008).

Figure 4.1: Pan-African sutures in the central part of Gondwana. 1 = Back-arc/island-arc related eclogites in the Paleoproterozoic Ubendian belt, this study. 2 = MORB-like chemistry eclogites in the Pan-African Zambezi belt (John *et al.*, 2003). 3 = Plume-like chemistry eclogites in northern Malawi (Ring *et al.*, 2002). 4 = Back-arc/island-arc related metabasites in the Vohibory block of Madagascar (Jöns & Schenk, 2008). DM = Damara belt, ZB = Zambezi belt, MB = Mozambique belt, BB = Bangweulu block, TC = Tanzania craton, CAFB = Central African Fold Belt, Mad = Madagascar; map modified after Kusky *et al.* (2003).



The discovery of Pan-African eclogites (Boniface & Schenk, 2007) in the Ubendian belt, which separates the Archean Tanzania craton from the Paleoproterozoic Bangweulu block, provides a new perspective on the spatial and temporal distribution of Pan-African suture zones. Former simplifying models of Gondwana formation had assumed that West Gondwana (Congo-Kalahari-Southern America) formed one continental block when Indo-Antarctica and later Antarctica-Australia (East Gondwana) amalgamated (Boger & Miller, 2004) or that the Congo-Tanzania-Bangweulu block formed one continental block throughout the Neoproterozoic (Collins & Pisarevsky, 2005). In this paper we demonstrate that the Bangweulu block was separated by a Neoproterozoic suture from the Tanzania craton in the north and that it formed most likely a microplate, because also at its southern border the eclogites of the Zambezi belt were formed from a subducted oceanic floor (John *et al.*, 2003). The aim of this study is to present petrological, geochemical and geochronological data of the Ufipa terrane eclogites for the purpose of deducing the tectonic setting

of the formation of the eclogite's precursor melts, determining their formation ages and establishing the P - T path during the subduction process.

4.2 Analytical techniques

Minerals were analysed by using a "JEOL Superprobe JXA-8900R" electron microprobe at the University of Kiel. The acceleration potential used for analyses was 15 to 20 kV for a beam current of 20 nA. The raw data were corrected by using the CITZAF method (Armstrong, 1995).

Major and trace element concentrations of whole rocks were analyzed at the University of Kiel. The Philips PW 1400 X-ray fluorescence analyzer was used to acquire the major element data. The elements were determined on fused glass discs, which were prepared by mixing in a platinum crucible 0.6g of sample powder with 3.6g of $\text{Li}_2\text{B}_4\text{O}_7$, and then the mixture was subjected to the OXIFLUX 5-stage burner. Trace elements were measured by using the Agilent 75000C ICP-MS machine, the sample preparation procedure was that as described by Gabe-Schönberg (1993) and John *et al.* (2008). The data quality, precision and accuracy were ensured by using international reference standards, blanks and some sample duplicates.

Zircons were separated from the crashed rocks by using the conventional magnetic and heavy liquid methods at the University of Kiel. Isotopic U - Pb dating of zircon was done on a SHRIMP-II at the Center of Isotopic Research of VSEGEI in St. Petersburg, Russia. Handpicked round and prismatic zircons were mounted on epoxy resin discs and polished to expose their cores, whose transmitted light and cathodoluminescence (CL) images were prepared. The diameter of the analyzing ion beam was approximately 20 μm and the primary beam intensity was about 4 nA. Data reduction was done in the manner described by Williams (1998), using the SQUID Excel Makro by Ludwig (2001). The Pb/U ratios have been normalized relative to a value of 0.0668 for the $^{206}\text{Pb}/^{238}\text{U}$ ratio of the TEMORA-1 internal standard reference zircon, equivalent to an age of 416.75 Ma (Black *et al.*, 2003).

4.3 Geological setting

The NW-SE elongated Ubendian belt (ca. 500 km long and 150 km wide) is bordered by the Archean Tanzania craton to the northeast and the Paleoproterozoic Bangweulu block to the southwest. The N-S trending Mesoproterozoic Kibaran orogen borders the Ubendian belt towards the northwest and in the SE lie the Paleoproterozoic Usagaran belt and the N-S oriented Neoproterozoic East African Orogen (Fig. 4.2).

The Ubendian belt has been divided into eight lithotectonic terranes namely Ubende, Wakole, Katuma, Ufipa, Mbozi, Lupa, Upagwa and Nyika (Daly *et al.*, 1985; Daly, 1988, Fig. 4.2). Paleoproterozoic eclogites crop out as mylonitic pods within felsic garnet-clinopyroxene gneisses and hornblende-rich mafic gneisses of the Ubende terrane, whereas the Pan-African eclogites described here crop out in the Ufipa terrane as massive lense-shaped

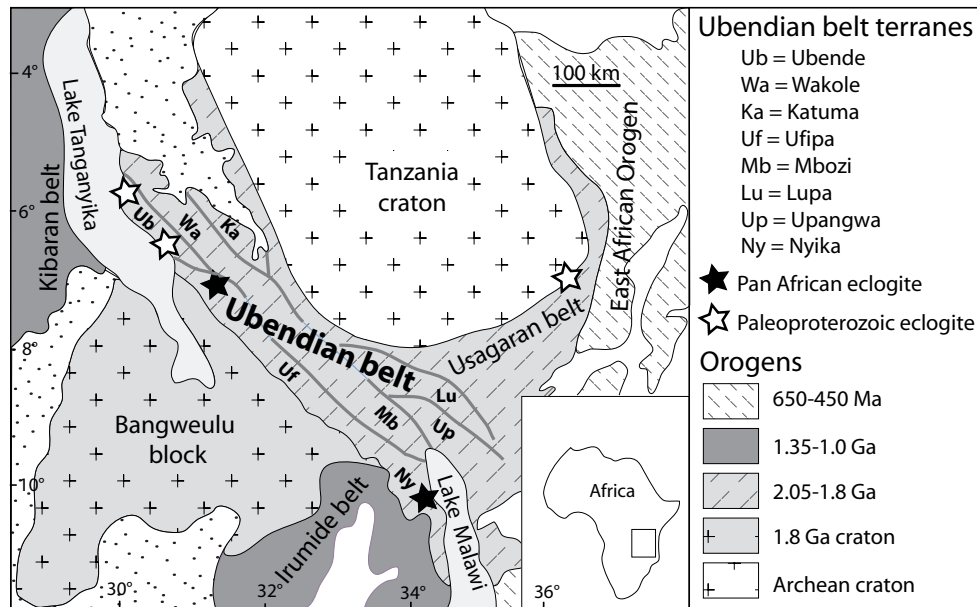


Figure 4.2: Geological map of south-eastern Africa indicating the location of the Ubendian belt. Subdivision in litho-tectonic terranes by Daly *et al.* (1985) and Daly (1988).

bodies (10-100 m scale) enclosed in garnet-kyanite mica schists and gneisses. The Pan-African eclogites of the Ufipa terrane are coarse grained and were not deformed after peak metamorphism (Fig. 4.3). This feature distinguishes them from the Paleoproterozoic eclogites of the Ubende terrane, which are fine grained and mylonitized eclogites. The occurrence of eclogites in the Ubendian belt is known since the reports of Smirnov *et al.* (1973). Sklyarov *et al.* (1998) did a petrological study and determined a *P-T* evolution for the eclogites of the Ubendian belt. However, in the absence of geochronological data these authors mixed together petrological data from Paleoproterozoic and Pan-African eclogites to deduce a single *P-T* evolution for these Ubendian rocks of different ages. It was assumed that the eclogites are Paleoproterozoic in age, in analogy to the 2.0 Ga eclogites found in the Usagaran belt at the SE side of the Tanzania craton (Fig. 4.2; Möller *et al.*, 1995).

The Ufipa terrane, which hosts the Pan-African eclogites, is dominated by Bt-gneiss of granitic composition (McConnell, 1950; Sutton *et al.*, 1954). However, other lithological units like metapelites are present: Grt-Bt-Ky-Ms gneisses and schists that are interlayered with eclogites crop out in the north of the Ufipa terrane near Chisi and Tambaruka villages, whereas Grt-Bt-Sil±Crđ gneisses and schists are found in the southern part of the Ufipa terrane (Fig. 4.4). The transition from muscovite-quartz to higher grade sillimanite(kyanite)-K-feldspar gneisses is near the town of Sumbawanga. Monazites and zircons of these schists and gneisses show evidence that the Ufipa terrane was affected by two orogenic events, the Paleoproterozoic Ubendian and the Neoproterozoic Pan-African (chapter 2). In one sample (garnet-kyanite-muscovite-biotite schist from Tambaruka) relicts of Paleoproterozoic monazites could not be detected.

The Pan-African orogenic cycle in the Ubendian belt was associated with the intrusion of alkali-granitoids dated at 842 ± 80 Ma (Lenoir *et al.*, 1994) and at 724 ± 6 Ma (Theunissen *et al.*, 1992) in the Upangwa terrane, and with syenites in the Mbozi terrane dated at 743 ± 30 (Brock, 1963) and 685 ± 62 Ma (Ray, 1974) (Fig. 4.4). These early Pan-African ages may reflect a time of extension preceding the collision event.

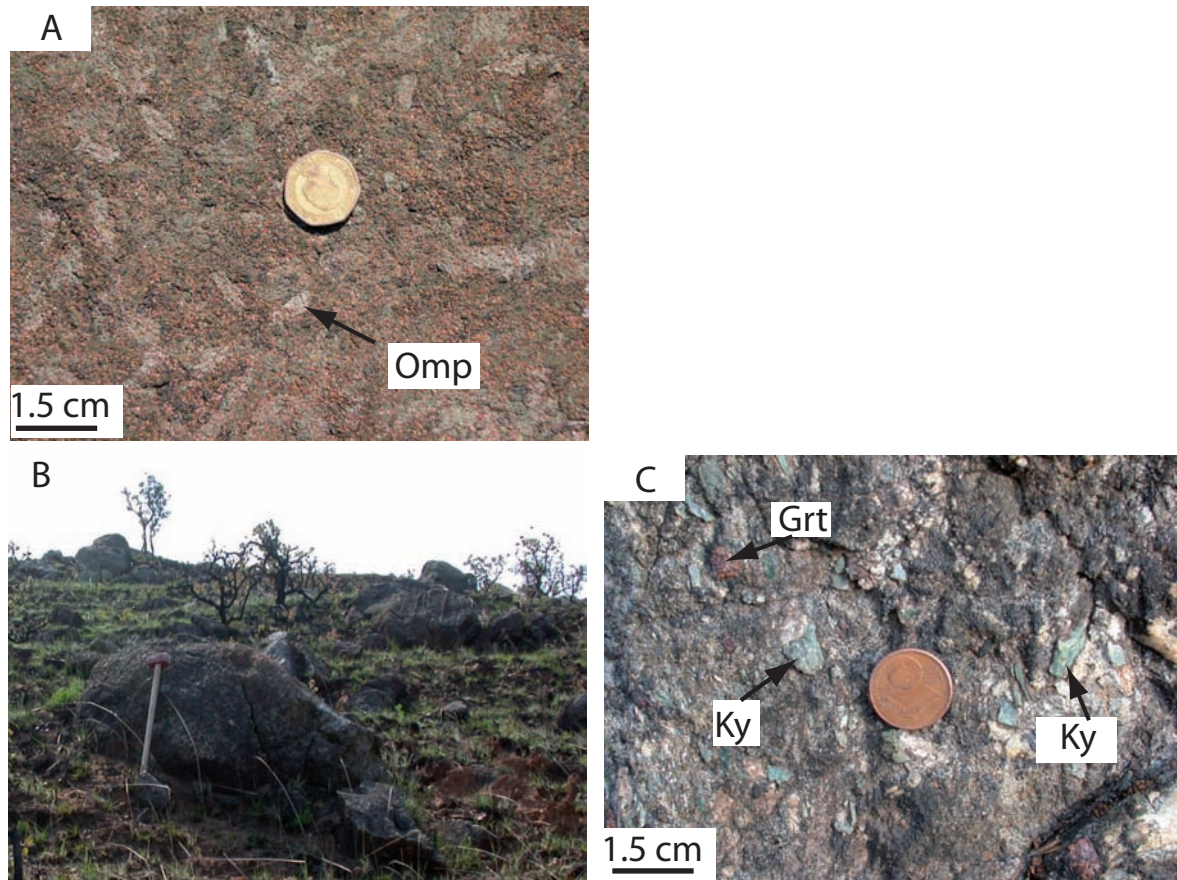


Figure 4.3: Field photos of the Pan-African eclogites in the Ufipa terrane. A: A photo of a kyanite-free eclogite T108-7-04 from Chizi village. Omphacite porphyroblasts are poikilitic including numerous garnet grains. B: Outcrops of a kyanite-bearing eclogite at Tambaruka village. C: Photo of a kyanite-bearing eclogite, outcrop at Tambaruka village. Kyanite is surrounded by garnet rims.

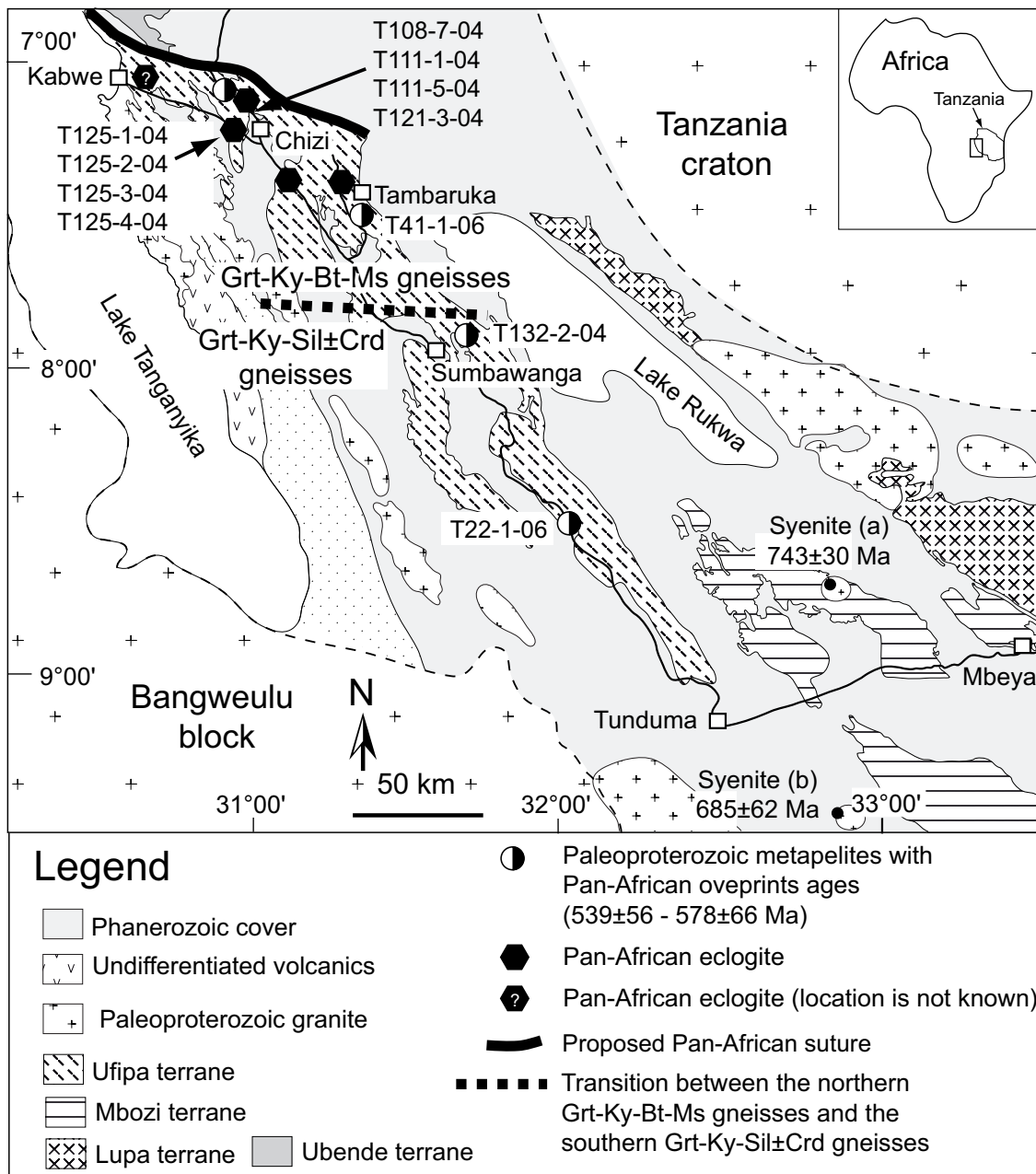


Figure 4.4: Locations of Pan-African eclogites in the Ubendian belt. Ages of Pan-African syenites in the Mbozi terrane are from (a) Brock (1963) and (b) Ray (1974). The zircons and/or monazites of four metapelites of the Ufipa terrane show a strong Neoproterozoic overprint.

4.4 Petrography and mineral chemistry

4.4.1 Kyanite-free eclogites

The kyanite-free eclogites are commonly composed of Omp-Grt-Rt-Ap-Qtz-Zrn (mineral abbreviations after Kretz, 1983), as the peak mineral assemblage in which omphacite and garnet may occupy up to 90 % by volume. Rutile reaching up to 0.5 mm is a common matrix mineral and occurs also as inclusion in garnet and clinopyroxene. Garnet contains prograde inclusions of plagioclase, rutile, quartz and omphacite (Fig. 4.5A). Abundant plagioclase-diopside symplectites replace omphacite, whereas hornblende coronas sometimes occur between garnet and omphacite (Fig. 4.5B). The abundance of retrograde minerals, diopside-plagioclase and hornblende, differs from sample to sample, in which the least retrogressed rocks may contain less than 5 % by volume of the late-stage minerals.

The chemical composition of garnet, omphacite, plagioclase and hornblende is given in Tab. 4.1, Tab. 4.2, and Tab. 4.3. Garnet core is chemically not zoned, however, a retrograde zone at the rims is displayed, in which X_{Prp} drops and X_{Alm} rises (Fig. 4.6A). The garnet cores are pyrope rich with a representative composition of $X_{Prp}=0.48$, $X_{Alm}=0.39$, $X_{Grs}=0.12$ and $X_{Sps}=0.01$. However, one sample (T121-3-04) is almandine rich with a composition of $X_{Alm}=0.47$, $X_{Prp}=0.33$, $X_{Grs}=0.19$ and $X_{Sps}=0.01$ (Tab. 4.1). Clinopyroxene porphyroblast cores and the inclusions in garnet are rich in Na with Jd values reaching up to 40 mol% whereas clinopyroxene in the symplectites is poor in Na with Jd reaching up to 18 mol% (Fig. 4.6C). The X_{Mg} is high in all clinopyroxenes ranging between 0.70 and 0.87 (Tab. 4.2). Plagioclase in symplectites is richer in Na ($X_{Ab} = 0.75-0.80$) than the plagioclase inclusion in garnet ($X_{Ab} = 0.63-0.68$; Tab. 4.3). Rutile coexisting with zircon and quartz has average Zr contents between 207 ± 8 ppm and 316 ± 24 ppm (Tab. 4.7).

4.4.2 Kyanite-bearing eclogites

Kyanite-bearing eclogites are composed of Ky-Grt-Omp-Rt-Zo-Qtz-Pl-Zrn forming the peak mineral assemblage. Kyanite is blue and coarse grained reaching up to ≈ 2 cm grain size. It contains inclusions of rutile, quartz, omphacite, garnet, plagioclase, zoisite and in one sample also of staurolite (Fig. 4.5C&D). Garnet coronas, up to ≈ 3 mm wide, commonly enclose kyanite (Fig. 4.5C&D). However, garnet porphyroblasts with inclusions of omphacite, rutile, plagioclase and quartz are abundant in the matrix. Plagioclase in the matrix is regarded as a peak mineral, however, secondary plagioclase replacing omphacite, garnet and kyanite is also abundant. Abundant symplectites of plagioclase, hornblende and ilmenite commonly replace omphacite and garnet (Fig. 4.5E), whereas silica poor domains, characterized by symplectites of staurolite, spinel, plagioclase and corundum commonly occur between kyanite and garnet (Fig. 4.5F). Clinopyroxene is partly replaced by plagioclase-diopside \pm hornblende in the form of symplectites or sieve textures (Fig. 4.5B). Sanders *et al.* (1987) regarded the sieve textures to be equivalent to symplectites. They are interpreted to be formed during decompression under high temperatures and/or during long periods of retrogression.

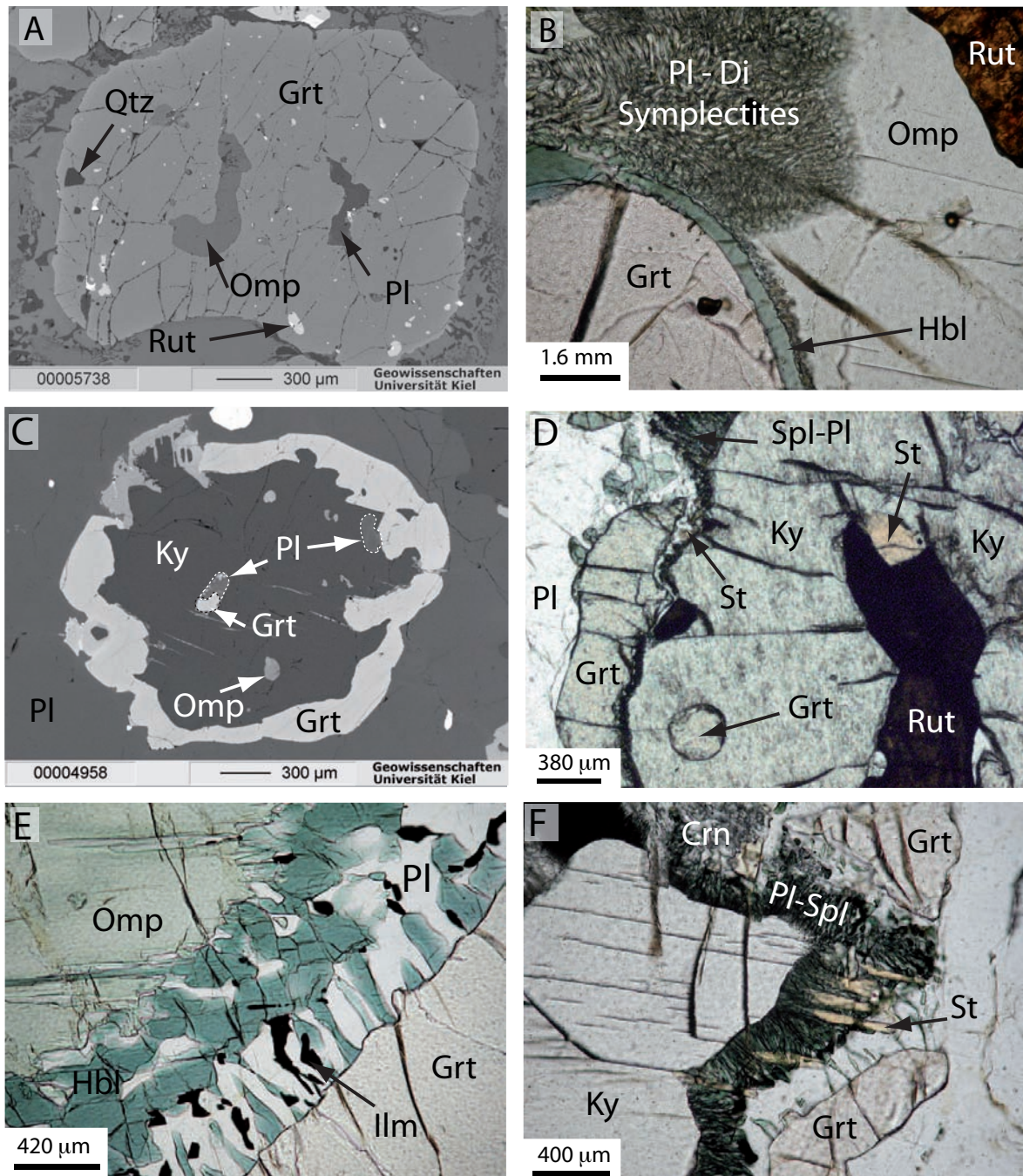


Figure 4.5: Microphotographs showing reaction textures in eclogites; plane polarized light images (B, D, E and F) and backscattered images (A and C). A: Omp, Pl and Rt inclusions in Grt (T111-1-04). B: Pl-Di symplectites and Hbl corona replacing Omp (T111-5-04). C: Grt corona around Ky; Omp, Pl and Grt inclusions in Ky (T125-4B-04). D: St and Grt inclusion in Ky; Grt corona around Ky (T125-3-4). E: Pl-Hbl-Ilm symplectites between Grt and Omp (T125-1-04). F: Spl-St-Pl-Crn symplectites between Ky and Grt corona (T125-1-04).

The compositions of garnet, clinopyroxene, plagioclase, spinel, staurolite and zoisite are given in Tab. 4.4, Tab. 4.5 and Tab. 4.6. Garnet is Fe and Ca rich with homogeneous core compositions of $X_{Alm}=0.44$, $X_{Grs}=0.33$, $X_{Prp}=0.21$ and $X_{Sps}=0.02$ (Fig. 4.6B). The X_{Prp} and the X_{Mg} show a slight increase and an abrupt drop near the margins whereas X_{Grs} decreases towards the rims (Fig. 4.6B). The garnet corona around kyanite has X_{Grs} of about 0.24, which is lower than that of cores of garnet porphyroblasts. Other contents are similar to the rims of garnet porphyroblasts (Tab. 4.6).

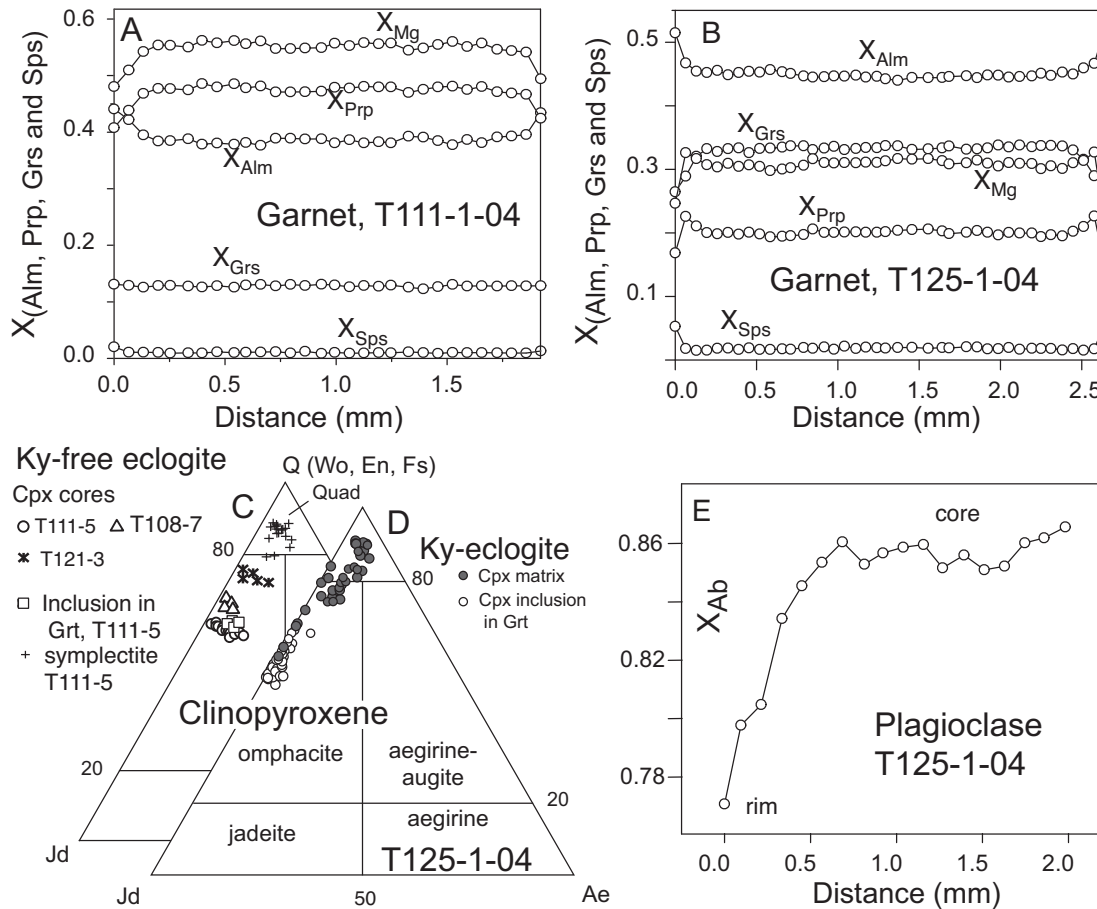


Figure 4.6: Mineral compositions of the Neoproterozoic eclogites. A: Garnet profile of a kyanite-free eclogite. B: Grt profile of a kyanite-bearing eclogite. C: Cpx composition in kyanite-free eclogites; classification after Morimoto *et al.* (1988). D: Cpx composition of the kyanite-bearing eclogites. E: Pl profile of the Ky eclogite.

Clinopyroxene porphyroblasts are zoned: the jadeite content drops from about 37 mol% in the core to about 7 mol% at the rims. Clinopyroxene inclusion in garnet are Na rich with jadeite contents of up to 44.4 mol% (Fig. 4.6D, Tab. 4.4). The X_{Mg} is similar in all analyzed clinopyroxene grains ranging between 0.63 and 0.70 (Tab. 4.1). Matrix plagioclase is zoned, its core has $X_{Ab}=0.87$ which drops to 0.77 in the rims (Fig. 4.6E). Plagioclase inclusions in garnet are also Na rich with X_{Ab} between 0.78 and 0.83. Plagioclase in the

plagioclase-diopside symplectites replacing omphacite and in the plagioclase-hornblende-ilmenite-symplectites between garnet and omphacite have lower contents of Na, with X_{Ab} ranging between 0.24 and 0.46 (Tab. 4.6). Staurolite in symplectites have little ZnO, which ranges between 0.02 to 0.04 wt%; it has more Mg than most amphibolite-facies staurolites ($X_{Fe} = 0.65$ to 0.69). Spinel in symplectites between garnet coronas and kyanite have X_{Fe} ratios that range between 0.65 and 0.69.

4.5 Mineral reaction history

4.5.1 Kyanite-free eclogites

In the kyanite-free eclogites mainly retrograde reactions are preserved. The prograde history is reflected by the preserved inclusions of omphacite, plagioclase and quartz in garnet porphyroblast.

The hornblende coronas (Fig. 4.5B) formed by replacements of omphacite and garnet. The addition of fluids (H_2O) to the dry garnet-omphacite assemblage during uplift was necessary for the formation of these coronas. Plagioclase-diopside symplectites were formed by replacing omphacite.

4.5.2 Kyanite-bearing eclogites

Garnet coronas around kyanite and staurolite inclusions in kyanite (Fig. 4.5C&D) seem to represent the relicts of prograde reactions during subduction. The garnet-kyanite assemblage may partly have formed at the expense of staurolite and quartz that is included in kyanite. The garnet corona may also form as a reaction product between omphacite and kyanite, as described for similar textures in ultra high-pressure granulites and eclogites of Poland (Klemd & Bröcker, 1999).

During uplift garnet of the coronas reacted with the enclosed kyanite and water to form corundum-spinel-plagioclase symplectites (Fig. 4.5F).

Simultaneously during uplift garnet and omphacite reacted to form the symplectites of hornblende, plagioclase and ilmenite (Fig. 4.5E). Water addition was necessary to produce hornblende ($Grt + Omp + H_2O = Hbl + Pl + Ilm$).

Table 4.1: Representative electron microprobe analyses of garnet of the kyanite-free eclogites

Sample No.	T108-7 90 ^{core}	T108-7 91 ^{core}	T108-7 92 ^{core}	T108-7 93 ^{core}	T111-5 28 ^{rim}	T111-5 40 ^{core}	T111-5 41 ^{core}	T111-1 202 ^{core}	T111-5 48 ^{rim}	T121-3 56 ^{core}	T121-3 59 ^{core}	T121-3 60 ^{core}	T121-3 73 ^{rim}
Garnet													
SiO ₂	40.18	40.19	39.72	40.31	39.77	39.99	40.28	40.10	39.72	39.66	39.61	39.81	39.71
Al ₂ O ₃	22.96	22.76	22.44	22.64	22.11	22.50	22.57	22.45	22.13	21.97	21.93	21.88	22.07
FeO _{tot}	18.91	19.12	18.99	19.01	21.43	19.14	19.16	18.73	22.35	21.93	22.22	22.09	23.15
MgO	12.25	12.09	12.07	12.12	11.30	13.24	13.33	13.22	10.83	9.18	8.81	9.01	8.64
MnO	0.50	0.40	0.38	0.38	0.66	0.39	0.58	0.50	0.65	0.42	0.35	0.48	0.40
CaO	5.84	5.91	5.97	5.89	4.74	4.73	4.87	4.98	4.71	7.24	7.20	7.23	6.63
Total	100.64	100.49	99.59	100.37	100.01	99.99	100.79	99.98	100.39	100.46	100.18	100.60	100.67
Si	2.98	2.99	2.98	3.00	3.00	2.98	2.98	2.99	3.00	3.01	3.01	3.01	3.01
Al	2.01	2.00	1.99	1.99	1.97	1.98	1.97	1.97	1.97	1.96	1.97	1.95	1.97
Fe	1.17	1.19	1.19	1.18	1.35	1.19	1.19	1.17	1.41	1.39	1.41	1.40	1.47
Mg	1.36	1.34	1.35	1.34	1.27	1.47	1.47	1.47	1.22	1.04	1.00	1.02	0.98
Mn	0.03	0.03	0.02	0.02	0.04	0.02	0.04	0.03	0.04	0.03	0.02	0.03	0.03
Ca	0.46	0.47	0.48	0.47	0.38	0.38	0.39	0.40	0.38	0.59	0.59	0.59	0.54
Total	8.01	8.01	8.02	8.01	8.01	8.02	8.03	8.02	8.02	8.01	8.00	8.00	8.00
X _{Mg}	0.54	0.53	0.53	0.53	0.48	0.55	0.55	0.44	0.46	0.43	0.41	0.42	0.40
X _{Alm}	0.39	0.39	0.39	0.39	0.44	0.39	0.39	0.38	0.46	0.46	0.47	0.46	0.49
X _{Prp}	0.45	0.44	0.44	0.44	0.41	0.48	0.48	0.48	0.40	0.34	0.33	0.34	0.32
X _{Grs}	0.15	0.16	0.16	0.16	0.12	0.12	0.13	0.13	0.12	0.19	0.19	0.19	0.18
X _{Sps}	0.01	0.01	0.01	0.01	0.01	0.01	0.01	0.01	0.01	0.01	0.01	0.01	0.01

Cations calculated on the basis of 6 oxygen for Cpx and 12

4. Neoproterozoic eclogites in the Ubendian belt

Table 4.2: Representative electron microprobe analyses of clinopyroxene of the kyanite-free eclogites

Clinopyroxene																					
Sample No.	91 _{core}	T108-7 79 _{core}	T108-7 93 _{core}	T108-7 94 _{core}	T111-5 176 _{incl.}	T111-5 177 _{incl.}	T111-5 200 _{core}	T111-5 203 _{core}	T111-5 72 _{symp.}	T111-5 77 _{symp.}	T121-3 15 _{core}	T121-3 42 _{core}	T121-3 44 _{core}								
SiO ₂	54.89	54.03	54.79	54.96	54.23	54.57	55.44	54.55	52.23	52.43	53.15	53.72	53.84								
TiO ₂	0.15	0.13	0.30	0.26	0.00	0.00	0.00	0.00	0.49	0.38	0.34	0.28	0.34								
Al ₂ O ₃	10.01	9.61	10.13	10.12	9.92	10.50	9.85	9.91	6.71	3.84	7.17	6.87	6.83								
Cr ₂ O ₃	0.07	0.06	0.05	0.13	0.05	0.07	0.01	0.09	0.00	0.11	0.08	0.06	0.04								
FeO	3.50	2.52	4.15	4.30	5.28	5.29	6.40	5.57	5.43	5.07	4.47	5.38	5.36								
Fe ₂ O ₃	2.39	3.95	1.85	1.88	2.45	1.95	0.97	1.98	2.53	1.87	3.09	2.40	2.07								
MgO	9.17	9.33	9.24	9.22	8.45	8.69	8.44	8.48	11.23	13.22	10.70	10.63	10.76								
MnO	0.07	0.10	0.05	0.03	0.01	0.09	0.06	0.08	0.07	0.09	0.04	0.01	0.08								
CaO	14.04	15.12	13.82	14.00	13.41	14.05	13.39	13.60	19.00	20.70	16.89	16.97	17.01								
Na ₂ O	5.99	5.63	5.91	5.87	5.89	5.69	5.96	5.83	2.81	1.68	4.02	3.97	3.94								
K ₂ O	0.03	0.00	0.00	0.01	0.00	0.00	0.00	0.00	0.00	0.00	0.00	0.00	0.00								
Total	100.31	100.47	100.30	100.78	99.70	100.90	100.52	100.10	100.50	99.39	99.95	100.29	100.27								
Si	1.96	1.94	1.96	1.96	1.96	1.95	1.99	1.97	1.91	1.94	1.94	1.95	1.95								
Ti	0.00	0.00	0.01	0.01	0.00	0.00	0.00	0.00	0.01	0.01	0.01	0.01	0.01								
Al	0.42	0.41	0.43	0.42	0.42	0.44	0.42	0.42	0.29	0.17	0.31	0.29	0.29								
Cr	0.00	0.00	0.00	0.00	0.00	0.00	0.00	0.00	0.00	0.00	0.00	0.00	0.00								
Fe ²⁺	0.10	0.08	0.12	0.13	0.16	0.16	0.19	0.17	0.17	0.16	0.14	0.16	0.16								
Fe ³⁺	0.06	0.11	0.05	0.05	0.07	0.05	0.03	0.05	0.07	0.05	0.08	0.07	0.06								
Mg	0.49	0.50	0.49	0.49	0.46	0.46	0.45	0.46	0.61	0.73	0.58	0.58	0.58								
Mn	0.00	0.00	0.00	0.00	0.00	0.00	0.00	0.00	0.00	0.00	0.00	0.00	0.00								
Ca	0.54	0.58	0.53	0.53	0.52	0.54	0.51	0.52	0.74	0.82	0.66	0.66	0.66								
Na	0.41	0.39	0.41	0.41	0.41	0.39	0.41	0.41	0.20	0.12	0.28	0.28	0.28								
K	0.00	0.00	0.00	0.00	0.00	0.00	0.00	0.00	0.00	0.00	0.00	0.00	0.00								
Total	4.00	4.00	4.00	4.00	4.00	4.00	4.00	4.00	4.00	4.00	4.00	4.00	4.00								
X _{Mg}	0.82	0.87	0.80	0.79	0.74	0.75	0.70	0.73	0.79	0.82	0.81	0.78	0.78								
Ac%	3.5	4.9	2.5	2.4	2.9	0.3	1.2	2.1	2.1	1.5	4.0	3.4	2.3								
Jd%	38	34	38	38	38	39	40	38	18	11	24	25	26								

Cations calculated on the basis of 6 oxygen; incl. = Cpx inclusion in Grt, symp. = symplectites

Table 4-3: Representative electron microprobe analyses of plagioclase and hornblende of the kyanite-free eclogites.

Sample No.	T111-5 6 ^{corona}	T111-5 7 ^{corona}	T111-5 8 ^{corona}	T111-5 13 ^{corona}	Sample No.	T111-1 140 ^{incl.}	T111-1 157 ^{incl.}	T111-1 158 ^{incl.}	T111-1 159 ^{incl.}	T111-5 50 ^{symp.}	T111-5 53 ^{symp.}	T111-5 55 ^{symp.}
Hornblende					Plagioclase							
SiO ₂	42.30	41.66	41.91	42.03	SiO ₂	58.69	60.05	58.69	59.03	63.34	63.99	63.66
TiO ₂	0.27	0.26	0.21	0.24	Al ₂ O ₃	26.46	26.08	26.10	25.98	22.70	22.11	20.73
Al ₂ O ₃	15.27	16.67	16.23	15.65	Fe ₂ O ₃	0.39	0.32	0.28	0.22	0.30	0.26	0.72
Cr ₂ O ₃	0.05	0.04	0.06	0.02	CaO	7.52	6.28	6.70	6.45	4.10	3.62	5.36
Fe ₂ O ₃	10.32	10.51	10.76	11.01	Na ₂ O	7.05	7.50	7.20	7.35	8.90	9.17	8.84
MgO	13.85	13.45	13.63	13.46	K ₂ O	0.03	0.05	0.04	0.04	0.03	0.00	0.00
MnO	0.07	0.11	0.13	0.10	Total	100.15	100.28	99.01	99.07	99.42	99.15	99.34
CaO	10.37	9.90	9.62	10.11								
Na ₂ O	3.48	3.74	3.85	3.44								
Total	95.98	96.33	96.39	96.07								
Si	6.24	6.13	6.16	6.211	Si	2.62	2.66	2.64	2.65	2.81	2.84	2.84
Ti	0.03	0.03	0.02	0.027	Al	1.39	1.36	1.38	1.37	1.19	1.16	1.09
Al	2.66	2.89	2.81	2.726	Fe ³⁺	0.01	0.01	0.01	0.01	0.01	0.01	0.02
Cr	0.01	0.00	0.01	0.003	Ca	0.36	0.30	0.32	0.31	0.20	0.17	0.26
Fe ³⁺	1.27	1.29	1.32	1.361	Na	0.61	0.64	0.63	0.64	0.77	0.79	0.77
Mg	3.05	2.95	2.99	2.965	K	0.00	0.00	0.00	0.00	0.00	0.00	0.00
Mn	0.01	0.01	0.02	0.013	Total	4.99	4.98	4.98	4.98	4.97	4.97	4.98
Ca	1.64	1.56	1.52	1.601								
Na	1.00	1.07	1.10	0.986								
Total	15.90	15.93	15.95	15.891								
X _{Mg}	0.71	0.70	0.69	0.69	X _{Ab}	0.63	0.68	0.66	0.67	0.80	0.82	0.75
					X _{An}	0.37	0.32	0.34	0.33	0.20	0.18	0.25
					X _{Or}	0.00	0.00	0.00	0.00	0.00	0.00	0.00

Cations calculated on the basis of 8 oxygen for Pl and 23 for Hbl ; incl. = inclusion in Grt, symp. = symplectites

Table 4.4: Representative electron microprobe analyses of garnet and clinopyroxene of the kyanite-bearing eclogites

Sample No.	T125-2 289 ^{core}	T125-2 290 ^{core}	T125-1 523 ^{core}	T125-2 265 ^{rim}	T125-1 298 ^{corona}	T125-4 98 ^{in.}	T125-4 119 ^{in.}	Sample No.	T125-4 80 ^{in.}	T125-4 126 ^{in.}	T125-2 160 ^{in.}
Garnet								Clinopyroxene			
SiO ₂	38.92	38.86	38.72	38.54	39.12	39.29	39.43	SiO ₂	51.81	52.23	53.77
TiO ₂	0.11	0.12	0.00	0.05	0.00	0.10	0.06	TiO ₂	0.15	0.44	0.35
Al ₂ O ₃	22.02	21.89	21.67	21.39	21.97	21.90	21.83	Al ₂ O ₃	11.09	12.96	14.13
FeO	19.94	19.51	20.69	23.12	22.71	21.99	22.30	Cr ₂ O ₃	0.02	0.00	0.00
MgO	5.59	5.50	4.86	4.10	6.91	6.77	6.47	FeO	5.66	6.74	5.84
MnO	0.65	0.73	0.81	2.18	0.62	0.49	0.54	Fe ₂ O ₃	2.05	0.00	0.00
CaO	12.80	13.15	13.31	10.64	8.93	9.21	9.39	MgO	7.91	6.81	6.40
Total	100.03	99.75	100.06	100.02	100.26	99.75	100.02	MnO	0.04	5.79	0.02
								CaO	16.57	14.27	13.43
								Na ₂ O	4.53	0.08	6.27
								K ₂ O	0.01	0.02	0.03
								Total	99.85	99.33	100.24
Si	2.990	2.993	2.993	3.010	3.000	3.018	3.024	Si	1.890	1.910	1.921
Ti	0.006	0.007	0.000	0.003	0.000	0.006	0.003	Ti	0.004	0.012	0.009
Al	1.994	1.987	1.975	1.969	1.986	1.983	1.973	Al	0.477	0.558	0.595
Fe	1.281	1.257	1.337	1.510	1.457	1.413	1.430	Cr	0.001	0.000	0.000
Mg	0.640	0.632	0.560	0.477	0.790	0.775	0.740	Fe ²⁺	0.173	0.206	0.174
Mn	0.042	0.047	0.053	0.144	0.040	0.032	0.035	Fe ³⁺	0.056	0.000	0.000
Ca	1.054	1.085	1.102	0.890	0.733	0.758	0.772	Mg	0.430	0.371	0.341
Total	8.008	8.008	8.020	8.003	8.006	7.984	7.978	Mn	0.001	0.179	0.001
								Ca	0.648	0.559	0.514
								Na	0.320	0.006	0.434
								K	0.001	0.001	0.002
								Total	4.000	3.802	3.990
X_{Mg}	0.333	0.335	0.295	0.240	0.352	0.354	0.341	XMg	0.714	0.643	0.661
X_{Alm}	0.425	0.416	0.438	0.500	0.482	0.474	0.480	Jd%	32	41	44
X_{Prp}	0.212	0.209	0.183	0.158	0.262	0.260	0.248	Ac%	0.000	0.000	0.000
X_{Grs}	0.349	0.359	0.361	0.295	0.243	0.255	0.259				
X_{Sps}	0.014	0.016	0.017	0.048	0.013	0.011	0.012				

Cations calculated on the basis of 12 oxygen for Grt and 6 for Cpx; in. = inclusions in Grt or Ky

Table 4.5: Representative electron microprobe analyses of staurolite and spinel of retrograde symplectites, zoisite and hornblende of the kyanite-bearing eclogites

Sample No.	T125-1 19 ^{sy.}	T125-1 20 ^{sy.}	T125-1 21 ^{sy.}	T125-1 377 ^{sy.}	T125-1 378 ^{sy.}	T125-1 381 ^{sy.}	T125-2 206 ^{rim}	T125-2 209 ^{core}	T125-2 212 ^{core}	T125-2 16 ^{sy.}	T125-2 104 ^{sy.}	T125-2 227 ^{mt.}	T125-2 228 ^{mt.}	T125-2 229 ^{mt.}
Staurolite			Spinel			Zoisite			Hornblende					
SiO ₂	25.21	25.16	25.13	0.07	0.09	0.12	38.95	39.79	39.73	40.28	39.57	40.37	40.41	40.80
TiO ₂	0.24	0.12	0.13	0.00	0.01	0.00	0.29	0.13	0.17	0.74	0.69	0.40	0.43	0.50
Al ₂ O ₃	56.98	57.01	57.08	58.94	59.24	61.17	26.36	30.86	30.76	16.20	16.54	15.13	15.34	14.86
Cr ₂ O ₃	0.00	0.00	0.00	0.00	0.03	0.01	0.13	0.01	0.04	0.04	0.00	0.00	0.03	0.02
FeO	13.05	13.04	13.03	26.22	26.21	26.05	6.65	0.86	0.50	14.78	16.47	15.40	15.28	15.31
Fe ₂ O ₃	0.00	0.00	0.00	3.80	3.01	0.00	1.85	2.31	2.32	0.00	0.00	0.00	0.00	0.00
MgO	3.27	3.27	3.29	9.48	9.42	8.25	0.26	0.12	0.11	10.21	9.31	10.32	10.08	10.22
MnO	0.00	0.02	0.01	0.17	0.24	0.17	0.07	0.04	0.03	0.19	0.18	0.25	0.37	0.38
CaO	0.29	0.28	0.36	0.09	0.08	0.06	22.74	22.83	22.97	11.42	11.36	11.71	11.56	11.38
Na ₂ O	0.00	0.00	0.00	0.00	0.00	0.00	0.02	0.07	0.05	2.91	2.86	2.86	2.83	2.81
K ₂ O	0.00	0.00	0.00	0.00	0.00	0.00	0.00	0.02	0.00	0.16	0.47	0.15	0.15	0.16
ZnO	0.04	0.07	0.08	-	-	-	-	-	-	-	-	-	-	-
Total	99.08	98.95	99.10	98.77	98.33	95.84	97.31	97.05	96.67	96.93	97.45	96.59	96.47	96.43
Si	7.220	7.210	7.200	0.020	0.020	0.030	3.060	3.070	3.080	6.045	5.969	6.109	6.116	6.173
Ti	0.050	0.030	0.030	0.000	0.000	0.000	0.020	0.010	0.010	0.084	0.078	0.046	0.049	0.057
Al	19.240	19.270	19.280	15.340	15.450	16.170	2.440	2.810	2.810	2.865	2.941	2.699	2.736	2.650
Cr	0.000	0.000	0.000	0.000	0.000	0.000	0.010	0.000	0.000	0.005	0.000	0.000	0.003	0.002
Fe ²⁺	3.130	3.130	3.120	4.840	4.850	4.890	0.120	0.150	0.150	1.855	2.078	1.949	1.934	1.937
Fe ³⁺	0.000	0.000	0.000	0.630	0.500	0.000	0.390	0.050	0.030	0.000	0.000	0.000	0.000	0.000
Mg	1.400	1.400	1.400	3.120	3.110	2.760	0.030	0.010	0.010	2.284	2.094	2.328	2.274	2.305
Mn	0.070	0.070	0.090	0.030	0.040	0.030	0.000	0.000	0.000	0.024	0.022	0.032	0.048	0.048
Ca	0.000	0.000	0.000	0.020	0.020	0.010	1.920	1.890	1.910	1.836	1.836	1.899	1.875	1.845
Na	0.000	0.000	0.000	0.000	0.000	0.000	0.000	0.010	0.010	0.847	0.837	0.839	0.830	0.824
K	0.000	0.000	0.000	0.000	0.000	0.000	0.000	0.000	0.000	0.031	0.091	0.029	0.029	0.030
Zn	0.010	0.010	0.020	-	-	-	-	-	-	-	-	-	-	-
Total	31.110	31.120	31.130	24.000	24.000	23.890	8.000	8.000	8.000	15.875	15.946	15.930	15.895	15.872
X_{Mg}	0.31	0.31	0.31	0.39	0.39	0.36				0.56	0.55	0.50	0.54	0.54

Cations calculated on the basis of 48 oxygen for St, 12.5 for Zo, 23 for Hbl and 32 for Spl; sy.= symplectite; mt.=matrix

Table 4.6: Representative electron microprobe analyses of plagioclase of the kyanite-bearing eclogites

Sample No.	T125-1 273 ^{rim}	T125-3 274 ^{rim}	T125-1 290 ^{core}	T125-2 31 ^{core}	T125-2 26 ^{core}	T125-2 260 ^{sy.1}	T125-2 264 ^{sy.1}	T125-2 19 ^{sy.2}	T125-2 26 ^{sy.2}	T125-1 395 ^{in.}	T125-1 443 ^{in.}	T125-2 109 ^{in.}
Plagioclase												
SiO ₂	62.33	63.07	65.31	64.44	64.23	52.32	50.53	50.02	54.76	59.59	63.08	63.97
Al ₂ O ₃	23.07	22.87	21.53	21.53	21.46	30.70	31.16	32.15	28.89	25.54	23.18	22.35
Fe ₂ O ₃	0.05	0.00	0.14	0.12	0.12	0.67	0.84	0.45	0.32	0.24	0.12	0.29
CaO	4.75	4.13	2.77	3.49	3.44	13.27	14.10	14.99	11.06	7.22	4.45	3.95
Na ₂ O	8.86	9.05	10.01	9.59	9.76	3.72	2.58	2.92	5.28	7.41	9.10	9.21
K ₂ O	0.03	0.03	0.04	0.09	0.10	0.05	0.13	0.04	0.02	0.03	0.07	0.04
BaO	0.00	0.00	0.00	0.03	0.05	0.07	0.06	0.05	0.03	0.00	0.00	0.00
Total	99.09	99.15	99.80	99.29	99.16	100.80	99.40	100.61	100.36	100.02	100.00	99.91
Si	2.78	2.81	2.88	2.861	2.858	2.358	2.312	2.269	2.462	2.66	2.790	2.828
Al	1.21	1.20	1.12	1.127	1.126	1.630	1.681	1.719	1.531	1.34	1.210	1.165
Fe ³⁺	0.00	0.00	0.00	0.004	0.004	0.023	0.029	0.015	0.011	0.01	0.000	0.011
Ca	0.23	0.20	0.13	0.166	0.164	0.640	0.692	0.729	0.533	0.35	0.210	0.187
Na	0.77	0.78	0.86	0.825	0.842	0.325	0.229	0.257	0.460	0.64	0.780	0.789
K	0.00	0.00	0.00	0.005	0.006	0.003	0.007	0.002	0.001	0.00	0.000	0.002
Ba	0.00	0.00	0.00	0.001	0.001	0.001	0.001	0.001	0.001	0.00	0.000	0.000
Total	4.99	4.98	4.99	4.989	5.001	4.980	4.951	4.993	4.998	4.99	5.000	4.986
X _{Ab}	0.77	0.80	0.87	0.828	0.832	0.336	0.247	0.260	0.463	0.65	0.788	0.807
X _{An}	0.23	0.20	0.13	0.167	0.162	0.661	0.745	0.738	0.536	0.35	0.212	0.191
X _{Or}	0.00	0.00	0.00	0.005	0.006	0.003	0.008	0.002	0.001	0.00	0.000	0.002

Cations calculated on the basis of 8 oxygen; in. = inclusions in Grt and cor.=corona

sy.1= symplectite between Grt and Ky; sy.2=symplectite between Grt and Omp

4.6 Geothermobarometry

A summary of the estimates of the prograde (subduction), peak and retrograde (uplift) pressure and temperature conditions that are recorded in the eclogites is given in Tab. 4.7. The mineral assemblages and textures of the kyanite-bearing eclogites provide a possibility to calculate a P - T path and to estimate the P - T conditions at different stages during subduction and uplift. The peak mineral assemblage Grt-Pl-Ky-Zo-Qtz-Rt yield a peak pressure of 20.1 ± 3.4 kbar and a temperature of 785 ± 81 °C as calculated by the average P - T method with the THERMOCALC program of Holland & Powell (1998). Mineral core compositions were used for the calculations. The activities of components were calculated by using the AX-program of Holland (version 0.1, 2004). A pressure of ca. 20 kbar is obtained on the GASP equilibrium (Koziol, 1989), calculated by using unzoned cores of garnet and plagioclase at the inferred temperature of 785 °C calculated by using THERMOCALC (Fig. 4.7A and Tab. 4.7).

The prograde P - T conditions of the Grt-Omp-Pl-Qtz mineral assemblage enclosed in kyanite porphyroblast were constrained by using different geothermobarometers. The THERMOCALC program gives an average pressure of 15.5 ± 3.0 kbar and a temperature of 715 ± 108 °C. The GASP (Koziol, 1989) and the Ab=Jd+Qtz (Holland, 1980) geobarometers give similar pressures of 16 kbar at the inferred temperature of 715 °C, which is consistent to the calculated average P - T above.

Different geothermobarometers give similar P - T conditions for the retrograde formation of the Spl-St-Pl-Crn symplectites between garnet corona and kyanite and the hornblende-plagioclase symplectites between garnet and clinopyroxene (Fig. 4.5 E&F). The THERMOCALC program yields an average pressure of 11.0 ± 3.5 kbar and a temperature of 700 ± 131 °C for the spinel-staurolite-plagioclase-corundum symplectites coupled with kyanite and garnet corona composition. The Grt+Ky=An+Crn equilibrium, which is equivalent to GASP in the absence of Qtz (Indares & Rivers, 1995), result in a pressure estimate of 12 kbar at a reference temperature of 700 °C, when using garnet corona composition and plagioclase symplectites. The Grt-Hbl Fe-Mg exchange thermometry (Graham & Powell, 1984) combined with Grt-Pl-Hbl geobarometry (Kohn & Spear, 1990) yield temperature of 740 °C and a pressure of ca. 10 kbar, when using the composition of symplectitic Hbl and Pl coupled with Grt rims. These data could lead to the conclusion that the symplectites formed when the pressure dropped nearly isothermally from peak eclogite-facies conditions at about 20 kbar ($T=760$ - 790 °C) to amphibolite-facies conditions of about 10-12 kbar and 700-740 °C (Fig. 4.7A).

Like the kyanite-bearing eclogite, also garnet porphyroblasts of kyanite-free eclogites contain inclusions of the prograde assemblage Pl-Omp-Qtz that allow to estimate pressure and temperature conditions during prograde subduction (Fig. 4.5B). The chemistry of the mineral inclusions (Ab₈₅-Jd₁₀-Qtz) results in prograde pressures that are very similar to those obtained with the inclusions found in kyanite of the kyanite-bearing eclogites (Fig. 4.7). However, temperature estimates using the Fe-Mg exchange between garnet and the included omphacite result in very high temperatures of 930-940 °C, which is not regarded as realistic. Two additional samples gave slightly lower temperatures of 760-790 °C

Table 4.7: A summary of pressure and temperature estimates of the kyanite-bearing and kyanite-free eclogites. For thermobarometry Fe³⁺ of pyroxene has been calculated assuming stoichiometry.

Sample	Mineral & analysis No.	Calibration	T (°C)	P (kbar)	Remarks
Fe-Mg exchange in Grt-Cpx and Grt-Hbl geothermometers					
T108-7-04	Grt ₉₁ -Cpx ₇₉	Ellis & Green (1979)	850	17*	Grt-Cpx cores
		Powell (1985)	890	17*	Grt-Cpx cores
T121-3-04	Grt ₅₉ -Cpx ₁₅	Ellis & Green (1979)	760	17*	Grt-Cpx cores
		Powell (1985)	790	17*	Grt-Cpx cores
T111-5-04	Grt ₂₀₂ -Cpx ₁₇₆	Ellis & Green (1979)	930	17*	Grt-Cpx cores
		Powell (1985)	940	17*	Grt-Cpx cores
T111-5-04	Grt ₂₈ -Hbl ₁₃	Graham & Powell (1984)	710	12 ^J	Hbl corona & Grt rim
T125-2-04	Grt ₂₆₅ -Hbl ₁₆	Graham & Powell (1984)	740	10 ^H	Hbl symp. & Grt rim
Ab = Jd + Qtz and GASP geobarometers					
T111-1-04	Cpx ₁₇₆ -Pl ₁₅₇	Holland (1980)	700*	17	Inclusion in Grt
T111-5-04	Cpx ₉₅ -Pl ₅₃	Holland (1980)	710 ⁺	12	Symplectites
T125-4-04	Cpx ₈₀ -Pl ₈₄	Holland (1980)	715 ^t	16	Pl inclusion in ky
T125-4-04	Grt ₉₈ -Pl ₉₀	Koziol (1989)	715 ^t	16	Inclusion in Ky
T125-1-04	Grt ₅₂₃ -Pl ₂₉₀	Koziol (1989)	785 ^t	20	Grt-Pl cores
T125-2-04	Grt ₂₆₅ -Hbl ₁₆ -Pl ₂₆	Kohn & Spear (1990)	740 ⁺	10	Hbl-Pl symp.
Thermocalc					
T125-2-04	Grt ₂₉₀ -Cpx ₁₆₀ -Pl ₃₁ -Zo ₂₁₂	Holland & Powell (1998)	785±81	20.1±3.4	Peak P-T
	Grt ₁₉ -Cpx ₈₀ -Pl ₁₀₉	Holland & Powell (1998)	715±108	15.5±3.0	Inclusion in Ky
	Grt ₂₉₈ -St ₂₀ -Spl ₃₇₇ -Pl ₃₉₅	Holland & Powell (1998)	700±131	11.0±3.5	Symp. & Grt corona
* = inferred temperature or pressure; ⁺ = Grt-Hbl thermometry (Graham & Powell, 1984); ^t = thermocalc (Holland & Powell, 1998); ^H = Grt-Pl-Hbl geobarometry Kohn & Spear (1990); ^J = Cpx-Pl-Qtz geobarometry; symp. = symplectite					

Zr-in-rutile thermometry of Ky-free eclogites

Thermometers: W=Watson *et al.* (2006), T= Tomkins *et al.* (2007) and FW = Ferry & Watson (2007)For the calibration of Tomkins *et al.* (2007) temperatures were calculated at a reference peak pressure of 17 kbar

Sample	Grain	No. of spots	Mean Zr (ppm) error at 1σ	Mean T (°C) error at 1σ		
				W	T	FW
T108-7-04	Rt-1 inclusion in Omp	30	312±15	646±4	683±4	641±4
	Rt-2 matrix	25	299±21	642±8	679±8	637±7
	Rt-3 inclusion in Grt	20	312±6	646±4	683±4	641±4
T111-5-04	Rt-1 inclusion in Omp	30	300±17	642±5	680±5	638±5
	Rt-2 matrix	20	316±24	647±7	684±7	642±6
	Rt-3 inclusion in Grt	20	282±12	637±4	675±4	633±3
T121-3-04	Rt-1 matrix	30	227±14	620±5	657±5	616±4
	Rt-2 inclusion in Grt	20	207±8	613±4	650±4	609±3

and 850-890 °C depending on the applied calibration (Tab. 4.7; T108-7-04 and T121-3-04). As we do not consider these temperature as realistic we applied also the Zr-in-rutile thermometry. The temperature dependence of Zr substitution in rutile has a great potential in geothermometry for metabasites (e.g. Spear *et al.*, 2006). The Zr-in-rutile thermometer calibrations of Watson *et al.* (2006), Tomkins *et al.* (2007) and Ferry & Watson (2007) were applied. Matrix rutile and rutile included in garnet and omphacite of the three studied samples have uniform Zr contents and are unzoned. This results in similar temperatures for these kyanite-free eclogite samples (Tab. 4.7 and Fig. 4.8). The calibration of Watson *et al.* (2006) and Ferry & Watson (2007) yield similar average temperatures, which

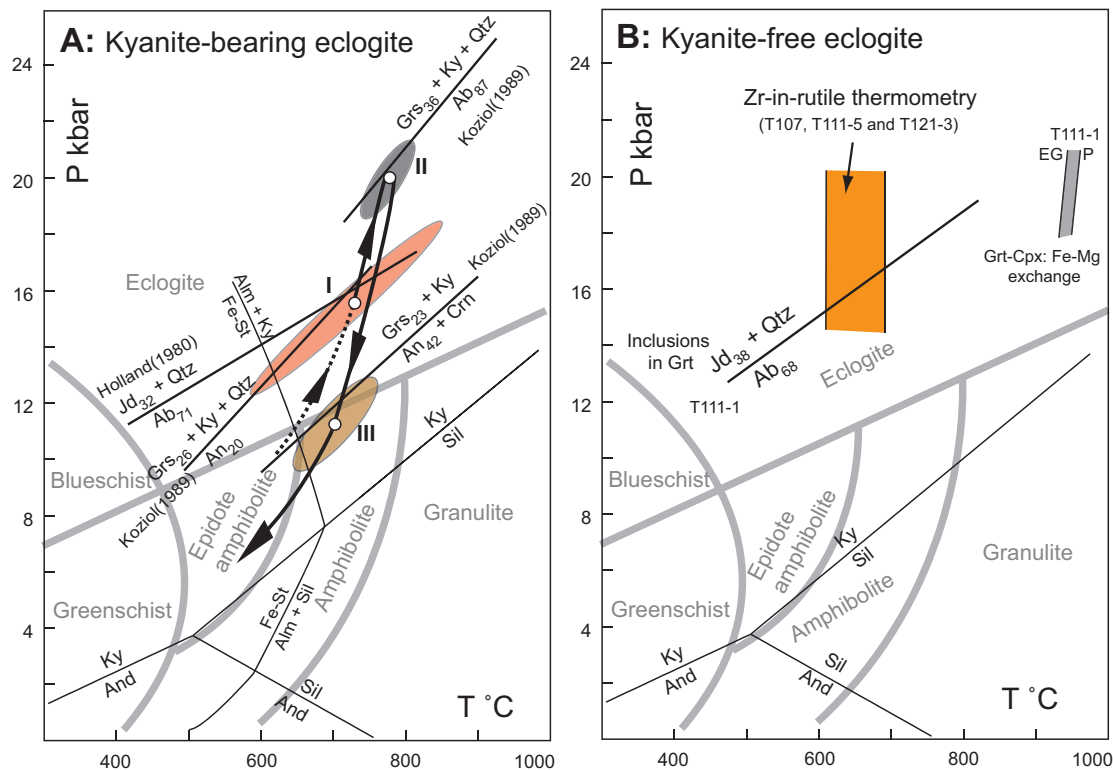


Figure 4.7: (A) The subduction P - T path of the Ky-bearing eclogites of the Ufipa terrane. The circles in the error ellipses labeled I, II and III mark the average P - T values calculated by using the THERMOCALC program (Holland & Powell, 1998). Ellipse I indicates the prograde average $P=15.5$ kbar and $T=715$ °C constrained by using the Grt-Omp-Pl-Qtz inclusions in Ky. Ellipse II shows the peak average P - T values of $P=20$ kbar and $T=785$ °C calculated by using the peak mineral assemblage Grt-Ky-Zo-Pl-Qtz. Ellipse III shows the retrograde average P - T values $P=11$ kbar and $T=700$ °C calculated by using the Crn-Pl-Spl-St symplectites and the rim of Grt corona. Other geothermobarometers give similar P - T conditions as the average P - T estimates: the GASP and $Ab=Jd+Qtz$ equilibria. The Fe-St out reaction is from Spear & Cheney (1989). (B) P - T estimates for the kyanite-free eclogites. Zr-in-rutile thermometers (Watson *et al.*, 2006; Tomkins *et al.*, 2007; Ferry & Watson, 2007) give temperatures of 610-690 °C, which correspond to peak pressures at 15-17 kbar estimated by using the $Ab = Jd + Qtz$ equilibrium of Holland (1980). Fe-Mg exchange (garnet-clinopyroxene) thermometers EG = Ellis & Green (1979) and P = Powell (1985) give higher temperatures than Zr-in-rutile thermometers.

range between 610 °C and 650 °C. However, the calibration of Tomkins *et al.* (2007) gives slightly higher average temperatures between 650 °C and 690 °C (Tab. 4.7), which is still about 200 °C lower than the results garnet-clinopyroxene Fe-Mg exchange thermometry on the same samples (Tab. 4.7; Fig. 4.7). If we combine the Zr-in-rutile temperatures of 610-690 °C with pressure calculations from inclusions (Ab-Jd-Qtz) we obtain 16-17 kbar during prograde burial (Fig. 4.7B). A further temperature increase to possible higher peak temperatures seems not to be recorded in rutile grains of the matrix, as matrix rutile has similar Zr contents as rutile inclusions. This may indicate that rutile became included near the peak temperature, when burial by subduction was still going on. Peak pressures can not be calculated for the kyanite-free eclogites as plagioclase was not stable in the matrix, but was only found as relict grains of inclusions in garnet. If we take the values of 20 kbar/785 °C (THERMOCALC) and 20 kbar/690 °C (rutile thermometry) as the peak metamorphic conditions of the eclogites, we obtain geothermal gradients in the corresponding subduction zone in the range of 10-11 °C/km. This indicates a relatively warm subduction.

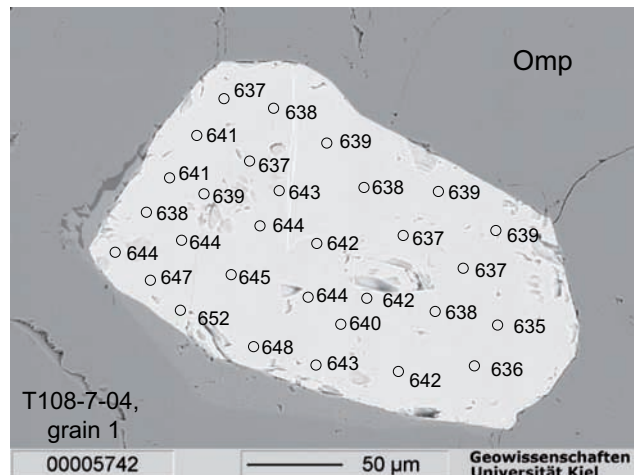


Figure 4.8: Backscattered electron image of rutile crystal from sample T108-7-04. Circles show location of analysis points. Numbers are temperatures in °C calculated from rutile thermometer (calibration of Ferry & Watson, 2007).

4.7 Geochemistry of kyanite-free eclogites

A total of 12 samples of the kyanite-free eclogites from the Chisi area were selected for major and trace element analyses, whose results are given in Tab. 4.8. SiO₂-contents range between 45.8-51.9 wt.% and the ratios Nb/Y (0.07-0.95) and Zr/Ti (0.01-0.07) are similar to those of tholeiitic basalts (Fig. 4.9). The FeO-TiO₂ enrichment is displayed in the AFM diagram (Fig. 4.9B) a characteristic that is also observed in MORB tholeiite glass. This observation suggests that the precursors of the eclogites were tholeiite basalts. Tholeiitic magmas are known to erupt in different tectonic settings such as MOR (mid oceanic ridges), island-arcs, oceanic islands and in continental rifts (Pearce & Cann, 1973). Elements such as Na₂O and K₂O are easily mobilized during metamorphism (e.g., Tatsumi *et al.*, 1986). Therefore, to establish the original geochemical character of the metamorphosed

igneous rocks trace elements, which are least mobilized and fractionated during diagenesis and metamorphism, need to be considered.

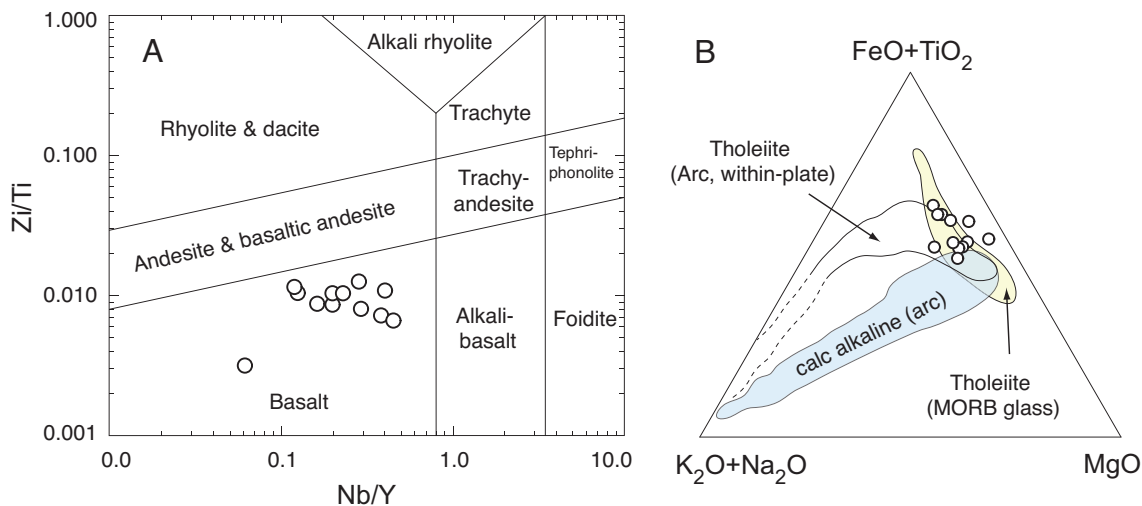


Figure 4.9: A: Magma series discrimination diagram after Pearce (1996): the kyanite-free eclogites plot in the basalt field. B: The eclogites show the MORB Fe-enrichment trend in the AFM diagram.

The chondrite normalized REE (rare earth elements) patterns reveal two geochemical groups of eclogites labeled group I with LREE (light rare earth elements) 10-30 times chondritic values, and group II eclogites, which has LREE contents 30-80 times chondritic values (Fig. 4.10 A&C). The chondrite normalized REE pattern of group I is generally similar to the average MORB (mid oceanic basalts). However, the HREE (heavy rare earth elements), Dy, Ho, Er, Tm, Yb and Lu lie below the average MORB pattern, which is true for group II as well.

The MORB normalized REE and HFSE (high field strength elements) concentrations of group I eclogites plot parallel to MORB values with minor deviations. However, the easily mobilized elements like U, Ba and sometimes Rb are strongly enriched or depleted, up to about ten folds of the MORB values (Fig. 4.10B). These observations imply that the group I eclogites have a strong affinity to melts from a MORB source. This interpretation is supported by the Th/Yb vs Ta/Yb diagram and the Th-Hf-Ta diagram, in which a depleted mantle source as MORB is suggested for the melt precursors of group I eclogites (Fig. 4.11A&B).

The MORB-normalized trace element patterns of group II eclogites are strikingly similar to the MORB normalized island-arc basalt pattern (Fig. 4.10D). The Nb-Ta depletion relative to LREE and LILE, which is a typical arc signature, is evident in all group II eclogite samples. The elements Zr-Hf are depleted relative to Nd and Sm; Ti is depleted relative to Eu and Gd. Mismatch of the patterns is only seen at the easily mobilized Cs and Rb. The affinity of group II eclogites to island-arc basalts is also seen in the Th/Yb vs Ta/Yb diagram and the Th-Hf-Ta diagram, in which group II eclogites plot in the island-arc fields (Fig. 4.11A&B).

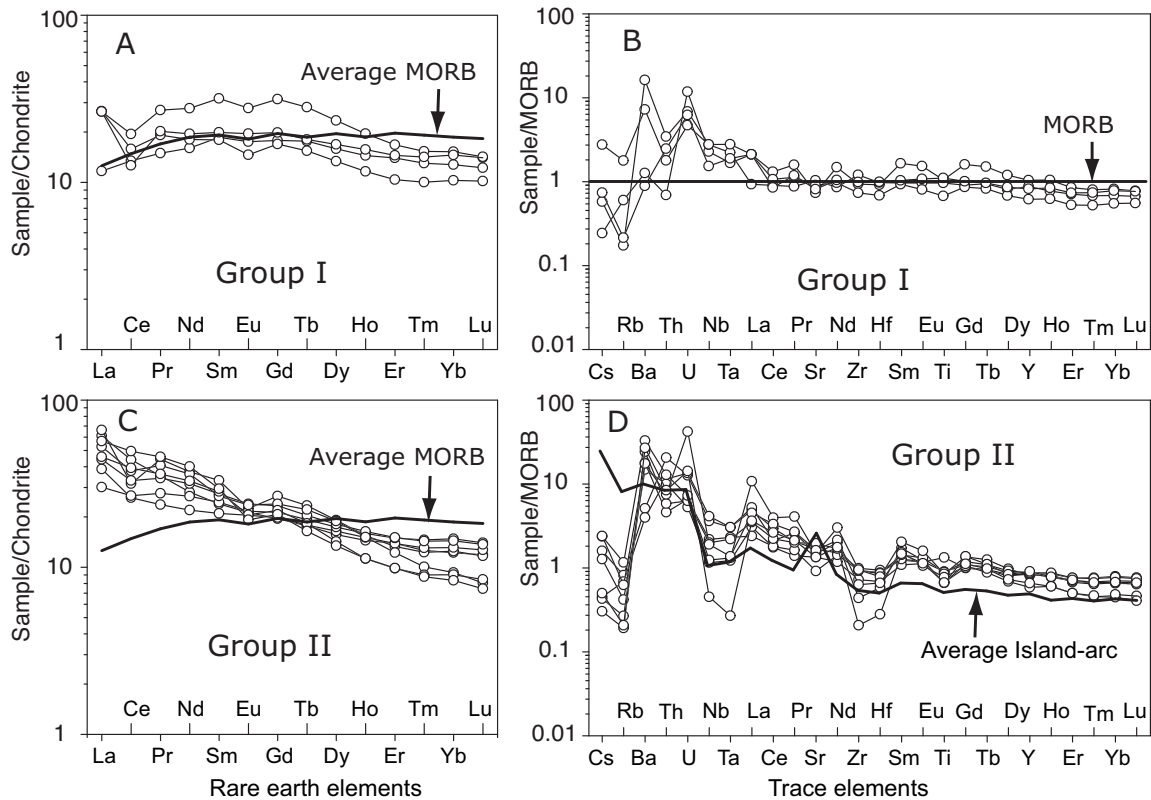


Figure 4.10: Trace element patterns of the kyanite-free eclogites. A: Chondrite normalized REE patterns of the group I eclogites; the chondrite values are from (Boynnton, 1984). B: MORB normalized trace element patterns of the group I eclogites; the MORB normalizing value is according to (Hofmann, 1988). C: Chondrite normalized REE patterns of the group II eclogites. D: MORB normalized trace element patterns of the group II eclogites. The average trace element concentrations of the island-arc basalts is according to Kelemen *et al.* (2003).

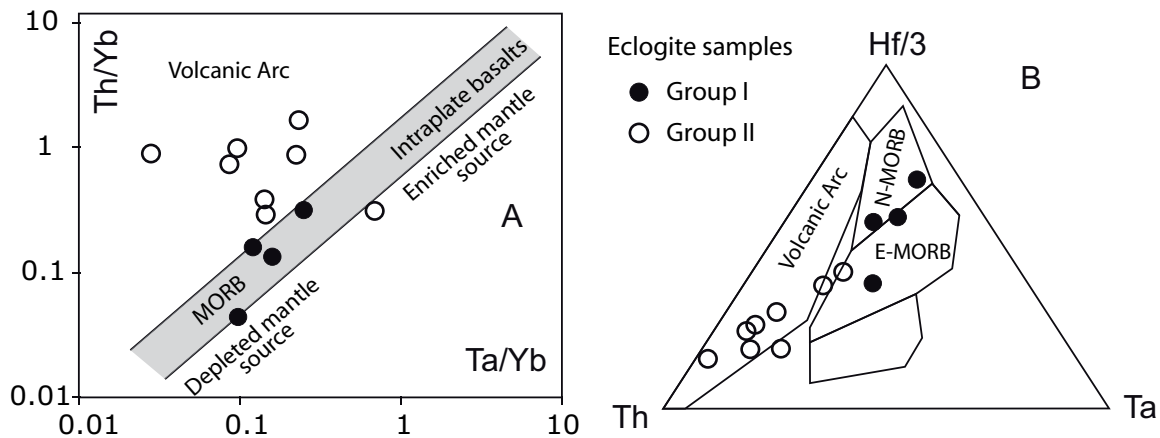


Figure 4.11: Basalt discrimination diagrams. A: Diagram of trace element ratios Th/Yb vs Ta/Yb after Pearce (1982); B: Hf/3-Th-Ta diagram after Wood (1980). In both plots the group I eclogites plot in the field of MORB and group II in the field of island-arcs.

Table 4.8: Major and trace element composition of the kyanite-free eclogites of the Ufpa terrane.

Sample	T111-5	T109-2	T123-2	T124-2	T108-4	T110-1	T110-2	T112-4	T121-1	T121-3	T123-1	T129-1
Group I					Group II							
Major elements in wt%												
SiO ₂	45.96	46.87	48.65	51.27	47.32	47.41	46.88	45.81	51.34	45.96	51.86	48.60
TiO ₂	1.56	1.70	1.09	1.79	1.09	1.46	1.44	5.22	2.15	1.08	1.07	1.25
Al ₂ O ₃	15.67	16.13	14.37	13.48	15.84	14.64	14.84	10.79	14.16	13.68	14.80	7.15
FeO	13.93	14.56	12.04	13.23	13.01	12.99	13.06	11.27	13.33	15.55	11.40	17.64
MnO	0.24	0.24	0.29	0.21	0.24	0.22	0.22	0.20	0.21	0.23	0.16	0.25
MgO	10.58	7.04	9.80	6.33	8.74	9.85	10.10	8.19	5.88	9.51	6.46	14.38
CaO	9.16	9.88	10.05	10.39	9.44	9.21	9.47	13.85	9.55	12.07	9.51	9.40
Na ₂ O	2.73	3.27	3.86	3.27	3.59	3.70	3.43	3.03	3.22	2.00	4.88	1.51
K ₂ O	0.06	0.05	0.01	0.01	0.02	0.01	0.01	0.03	0.04	0.01	0.07	0.03
P ₂ O ₅	0.19	0.17	0.16	0.18	0.05	0.19	0.27	0.58	0.03	0.02	0.02	0.18
LOI	0.00	0.00	0.00	0.00	0.00	0.00	0.00	0.00	0.00	0.00	0.00	0.00
Total	100.08	99.98	100.48	100.28	99.46	99.82	99.89	99.19	99.91	100.27	100.23	100.39
Trace elements in ppm												
Zr	126	117	92	134	91	124	121	296	139	39	63	74
Li	8.50	14.7	14.0	19.0	17.4	9.83	8.48	9.90	13.2	11.1	8.08	8.25
Sc	42.7	38.8	32.8	46.3	35.1	38.4	37.5	36.0	52.0	49.7	37.1	67.1
V	257	305	252	342	249	257	248	354	330	465	319	338
Co	68.6	46.3	51.7	46.1	56.5	57.4	57.8	43.4	49.6	64.0	40.7	92.3
Ni	275	91.7	278	61.2	207	257	244	128	68.2	140	112	219
Cu	38.5	46.4	21.8	43.4	207	23.5	27.8	111	388	777	108	114
Zn	147	140	110	129	157	141	141	147	141	102	118	148
Ga	16.0	19.6	17.3	19.4	17.6	16.8	16.2	20.9	20.8	18.7	20.0	10.0
Rb	2.25	0.758	0.220	0.271	0.530	0.338	0.243	1.66	1.03	0.261	0.87	0.791
Sr	117	83.3	103	92	152	104	222	318	190	153	168	184
Y	31.4	37.2	22.2	29.4	29.7	30.4	31.4	27.5	30.6	23.6	29.1	21.0
Zr	126	97.4	76.7	103	75.5	97.6	96.6	244	103	21.6	45.7	65.9
Nb	9.70	8.01	9.74	5.39	4.06	7.70	7.00	132	12.7	1.58	14.5	6.66
Cs	0.039	0.003	0.008	0.010	0.018	0.006	0.004	0.025	0.023	0.007	0.006	0.034
Ba	101	17.6	226	12.3	206	246	336	314	71.2	374	55.2	243
La	3.63	8.23	8.26	8.22	12.0	9.34	13.7	16.3	18.9	14.2	20.5	17.6
Ce	10.9	15.7	12.8	10.2	21.1	21.6	26.7	30.4	35.5	31.7	25.5	39.9
Pr	1.82	3.30	2.34	2.47	2.89	3.37	4.16	4.96	4.30	4.41	5.41	5.59
Nd	9.62	16.6	10.8	11.7	13.2	16.0	19.0	21.7	16.9	19.7	22.3	24.0
Sm	3.63	6.19	3.51	3.88	4.09	4.77	5.36	5.20	4.67	5.53	6.45	5.74
Eu	1.29	2.05	1.07	1.44	1.51	1.59	1.76	1.73	1.56	1.51	1.65	1.41
Gd	4.61	8.15	4.39	5.14	5.14	5.52	6.04	6.20	5.05	5.68	6.91	5.37
Tb	0.836	1.33	0.732	0.856	0.847	0.914	0.967	1.05	0.838	0.867	1.11	0.78
Dy	5.11	7.55	4.31	5.43	5.29	5.59	5.82	6.08	5.05	4.59	6.15	4.34
Ho	1.04	1.40	0.83	1.13	1.08	1.14	1.17	1.09	1.04	0.81	1.11	0.81
Er	2.94	3.52	2.18	3.05	2.91	3.14	3.16	2.57	2.92	2.07	2.79	2.07
Tm	0.422	0.497	0.325	0.459	0.423	0.473	0.464	0.325	0.408	0.291	0.398	0.284
Yb	2.67	3.19	2.15	3.05	2.74	3.10	3.01	1.94	2.56	1.89	2.61	1.75
Lu	0.394	0.457	0.327	0.452	0.409	0.451	0.441	0.259	0.382	0.272	0.376	0.239
Hf	2.90	2.73	2.04	2.96	2.05	2.61	2.55	6.74	2.81	0.84	1.74	1.97
Ta	0.427	0.320	0.535	0.363	0.235	0.445	0.423	6.80	0.585	0.052	0.585	0.263
Pb	6.89	3.75	3.83	5.15	22.8	8.51	14.4	13.7	22.2	21.0	14.7	115
Th	0.335	0.130	0.644	0.463	1.87	0.86	1.09	0.677	3.86	1.58	2.14	1.41
U	0.334	0.841	0.488	0.443	0.377	0.469	0.447	0.949	0.902	1.02	0.964	3.002

4.8 Geochronology

4.8.1 Textures and U-Th-Pb compositions of zircons

Rounded and subrounded zircons were selected from two kyanite-free eclogite samples (T111-5 and T108-7) and one kyanite-bearing eclogite sample (T125-3) for geochronology (Fig. 4.12). The analytical results are presented in Tab. 4.9 and Fig. 4.13. The CL (cathodoluminescence) images reveal zoned zircons from all samples (Fig. 4.12). Kyanite-free eclogites contain zircons with uniform composition that are interpreted as metamorphic in origin (Fig. 4.12A), and those with cores overgrown by rims (Fig. 4.12B). The cores might be of magmatic origin and are overgrown by metamorphic rims. Zircons of the kyanite-bearing eclogite have a metamorphic rim, which surrounds a core and a mantle that are characterized by magmatic growth zoning (Fig. 4.12C).

The cores and rims of zircons of the kyanite-free eclogite have similar low Th/U ratios in the range of 0.09-0.38 (Tab. 4.9). The absence of a concentric growth zoning in these zircons and the low Th/U ratios may be an indication for a growth during metamorphism of both, cores and rims (Rubatto, 2002; Corfu *et al.*, 2003).

Th/U ratios of the zircon cores of the kyanite-bearing eclogite overlap with those of the mantles in a range 0.25-1.71, the outer most rims have lower Th/U ratios ranging between 0.03 and 0.13 (Tab. 4.9; Fig. 4.12B).

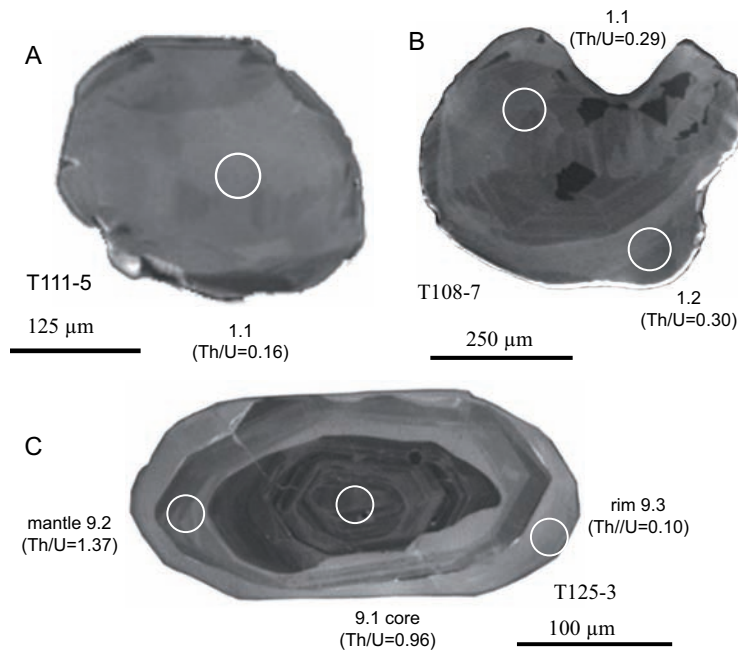


Figure 4.12: Textures and the Th/U ratios of the zircons of Pan-African eclogites of the Ubendian belt. A: Metamorphic zircon of a kyanite-free eclogite without magmatic cores. B: Zircon of a kyanite-free eclogite with cores and rims that have similar Th/U ratios. C: Zircon of a kyanite-bearing eclogite whose core and mantle with magmatic growth zones are surrounded by a rim.

4.8.2 Results of the U-Pb dating

The core and rim analyses of zircons of the kyanite-free eclogites plot together on the U-Pb concordia, for which a concordant age at 593 ± 20 Ma for sample T111-5 was calculated (Fig. 4.13A). A concordant age of 524 ± 6 Ma was obtained for core and rim analyses of sample T108-7 (Fig. 4.13B). If a magmatic event is recorded in the zircon cores, the obtained results imply that magmatic formation and subduction took place in a narrow time interval.

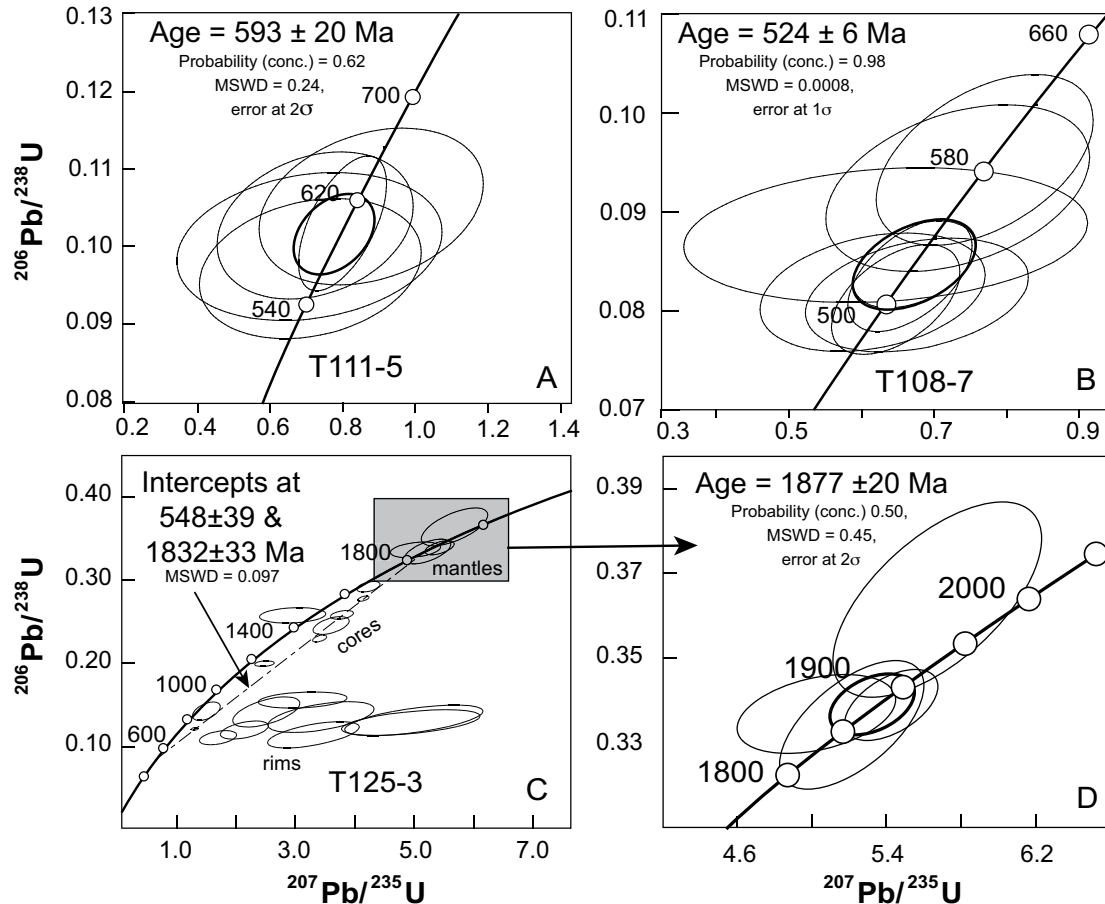


Figure 4.13: Concordia diagrams of Ufipa terrane eclogites. A & B: Two samples of the kyanite-free eclogites. Zircon cores and rims give concordant Pan-African ages. C: Zircons of the kyanite-eclogite have cores, mantle and rims of different ages: cores plot along a discordia intersecting at 548 ± 39 Ma and 1832 ± 33 Ma. The mantles are concordant at 1877 ± 20 Ma and the rims scatter discordantly giving no age.

The magmatic zircon cores of the kyanite-bearing eclogite plot discordantly. The discordia has an upper intercept at 1832 ± 33 Ma and a lower intercept at 548 ± 39 Ma (Fig. 4.13C). The analyses from the zircon mantles yield a magmatic concordant age at 1877 ± 20 Ma, whereas the outer rim analyses plot randomly, giving no meaningful age (Fig. 4.13C). The lower intercept age of the discordia discussed above points to a metamorphic event which is coeval with the concordant Pan-African ages of the kyanite-free eclogites.

4. Neoproterozoic eclogites in the Ubendian belt

Table 4.9: U-Pb isotopic zircon composition for the kyanite-free and kyanite-bearing eclogites of the Ubendian belt.

No.	U (ppm)	Th (ppm)	$\frac{^{232}\text{Th}}{^{238}\text{U}}$	^{206}Pb (%) comm.	Apparent ^{207}Pb ^{206}Pb	age (Ma) ^{206}Pb ^{238}U	$^{207}\text{Pb}^*$ ^{206}Pb	error (%)	$^{206}\text{Pb}^*$ ^{238}U	error (%)	$^{207}\text{Pb}^*$ ^{235}U	error (%)	disc. (%)
T111-5													
1.1 core	34	5	0.16	0.97	729 ± 290	615 ± 24	0.064	14	0.88	14	0.100	4.1	19
1.2 rim	130	23	0.19	0.59	573 ± 110	602 ± 21	0.059	5	0.80	6.2	0.098	3.6	-5
2.1 rim	34	3	0.10	1.56	360 ± 330	601 ± 23	0.054	15	0.72	15	0.098	4.0	-40
3.1 rim	37	9	0.26	2.39	450 ± 380	568 ± 22	0.056	17	0.71	18	0.092	4.0	-21
3.2 core	35	3	0.09	1.62	374 ± 470	585 ± 23	0.054	21	0.71	21	0.095	4.1	-36
T108-7													
1.1 core	78	22	0.29	0.93	514 ± 210	570 ± 20	0.058	9.4	0.73	10	0.092	3.7	-10
1.2 rim	75	22	0.30	0.54	556 ± 150	586 ± 21	0.059	7	0.77	7.9	0.095	3.7	-5
2.1 rim	137	48	0.36	1.14	307 ± 400	541 ± 17	0.053	18	0.63	18	0.088	3.2	-43
2.2 core	130	37	0.30	0.00	308 ± 160	427 ± 13	0.053	7.2	0.50	7.8	0.068	3.1	-28
3.1 rim	98	36	0.38	0.85	396 ± 220	507 ± 15	0.055	9.8	0.62	10	0.082	3.0	-22
4.1 rim	77	23	0.30	1.12	612 ± 190	505 ± 14	0.060	8.8	0.66	9.3	0.082	2.9	21
4.2 core	161	59	0.38	0.28	528 ± 97	517 ± 14	0.058	4.4	0.67	5.2	0.084	2.8	2
4.3 core	99	30	0.31	0.56	528 ± 110	503 ± 14	0.058	4.8	0.65	5.6	0.081	2.8	5
T125-3													
1.1 core	216	214	1.02	2.19	1108 ± 220	859 ± 51	0.077	11	0.143	6.4	1.50	13	29
1.2 mnt.	48	80	1.71	0.00	1739 ± 110	1415 ± 46	0.106	5.9	0.245	3.6	3.60	6.9	23
1.3 rim	5	0	0.06	0.00	2904 ± 250	697 ± 75	0.210	15	0.114	11.0	3.30	19	317
2.1 core	170	218	1.32	0.38	1715 ± 61	1651 ± 26	0.105	3.3	0.292	1.8	4.23	3.8	4
2.2 mnt.	90	120	1.38	2.71	1273 ± 300	1478 ± 39	0.083	15	0.258	2.9	2.95	15	-14
2.3 rim	9	0	0.02	0.00	2094 ± 240	730 ± 51	0.130	14	0.120	7.4	2.14	15	187
3.1 rim	13	1	0.04	0.00	1821 ± 250	677 ± 40	0.111	14	0.111	6.2	1.70	15	169
4.1 core	212	140	0.68	0.00	1758 ± 55	1333 ± 18	0.108	2.5	0.230	1.5	3.41	2.9	32
4.2 mnt	131	151	1.19	0.36	1897 ± 46	1881 ± 34	0.116	3.1	0.339	2.1	5.42	3.7	1
5.1 rim	3	0	0.03	0.00	3337 ± 240	796 ± 86	0.275	15	0.131	11.0	4.99	19	319
6.1 mnt	32	36	1.18	—	2290 ± 330	934 ± 44	0.145	19	0.156	5.1	3.12	20	145
7.1 mnt	348	254	0.75	0.12	1770 ± 29	1580 ± 13	0.108	1.6	0.278	0.94	4.15	1.9	12
7.2 rim	3	0	0.03	0.00	2078 ± 270	854 ± 84	0.129	15	0.142	10.0	2.51	18	143
8.1 core	295	72	0.25	0.27	1152 ± 72	738 ± 7.6	0.078	3.6	0.121	1.1	1.31	3.8	56
8.2 mnt	50	87	1.78	1.17	1770 ± 120	1869 ± 37	0.108	6.5	0.336	2.3	5.02	6.9	-5
8.3 rim	2	0	0.06	0.00	3930 ± 210	1519 ± 200	0.406	14	0.266	15.0	14.9	20	159
9.1 core	137	126	0.96	0.65	1736 ± 71	1481 ± 22	0.106	3.8	0.258	1.7	3.78	4.2	17
9.2 mnt	34	45	1.37	—	1853 ± 90	1859 ± 59	0.113	5	0.334	3.6	5.22	6.2	0
9.3 rim	4	0	0.10	0.00	2686 ± 300	819 ± 86	0.184	18	0.135	11.0	3.43	21	228
10.1 core	329	309	0.97	0.81	1427 ± 100	1173 ± 15	0.090	5.3	0.200	1.4	2.48	5.5	22
10.2 mnt	41	65	1.64	1.16	1850 ± 110	2000 ± 88	0.113	6.2	0.364	5.1	5.67	8.1	-8
10.3 rim	3	0	0.13	0.00	3352 ± 260	781 ± 72	0.278	17	0.129	9.7	4.94	19	329

*common Pb corrected by using measured ^{204}Pb , mnt. = mantle

4.9 Discussion

4.9.1 Geochronological and geochemical results

The Pan-African U-Pb SHRIMP zircon ages at 593 ± 20 , 548 ± 39 Ma and 524 ± 6 Ma, obtained from the Ufipa terrane eclogites is a surprising result. These eclogites were assumed by previous authors to represent relicts of a Paleoproterozoic Ubendian suture (Sklyarov *et al.*, 1998). The trace element compositions of the two recognized geochemical groups of kyanite-free eclogites (group I and group II eclogites) indicate that they are relicts of a subducted marginal ocean basin in which oceanic island-arc volcanics were associated with back-arc rocks during Pan-African time.

The striking similarities between group II eclogites and oceanic island-arc lavas, which are characterized by the depletion of the HFSE (Zr, Nb, Hf, Zr and Ti) relative to LILE and LREE (Perfit *et al.*, 1980; Kelemen *et al.*, 2003), and the presence of group I eclogites with MORB-like geochemistry imply that during Pan-African time an ocean basin and a magmatic-arc separated the Tanzania craton from the Bangweulu block along the Ubendian belt. The closure of this marginal ocean basin occurred between 590-520 Ma by the process of subduction of oceanic lithosphere.

The Pan-African age of 548 ± 39 Ma (lower intercept age of a discordia) of Paleoproterozoic zircon cores (1832 ± 33 Ma) is interpreted as the metamorphic age of the kyanite-bearing eclogites. It is similar to the age found in kyanite-free eclogites and in monazites of metapelites that host the eclogites of the Ufipa terrane. Therefore it can be concluded that the precursors of the kyanite-bearing eclogite were either aluminous metabasites of the Paleoproterozoic Ubendian crust which were subducted during Pan-African time, or, alternatively, the zircon cores may represent xenocrysts in Neoproterozoic mafic rocks that became subsequently eclogites.

4.9.2 Neoproterozoic eclogite formation in the Ubendian belt and geodynamic consequences

The subduction of Neoproterozoic island-arc and back-arc basalts in the Ubendian belt took a clockwise *PT* path and climaxed at pressures of 15-20 kbar and temperatures of 610-790 °C which indicates a geothermal gradient of about 10-11 °C/km. This subduction is slightly warmer than that of the Pan-African Zambezi belt subduction (≈ 8 °C/km; John *et al.*, 2003).

Rapid uplift resulted in a nearly isothermal decompression to amphibolite-facies conditions (about 10-12 kbar/ 700-740 °C), when abundant symplectites, coronas and sieve textured omphacites developed to replace eclogite peak mineral assemblages. Limited rehydration favored the growth of hornblende and staurolite-bearing late-stage symplectites.

Several mechanisms and geological processes have been proposed to explain rapid uplift and exhumation of deep seated high-pressure rocks: (1) erosion process (e.g. Hsue, 1991; Nie *et al.*, 1994), (2) large scale extensional collapse of a tectonically thickened continental crust (e.g. Burchfiel & Royden, 1985; Burchfiel *et al.*, 1989), (3) arrival of a continent at the subduction zone, which produces stress that promote the rise of the deeper parts of the

subduction zone against the flow of subduction (Hynes *et al.*, 1996), (4) subduction channel processes, in which eclogites are exposed by bouyocuy forces of the partially hydrated mantle wedge above a subducting slab (Gerya *et al.*, 2002). One or the combination of these mechanisms might have been responsible for the uplift and exposure of the Pan-African eclogites in the Ubendian belt.

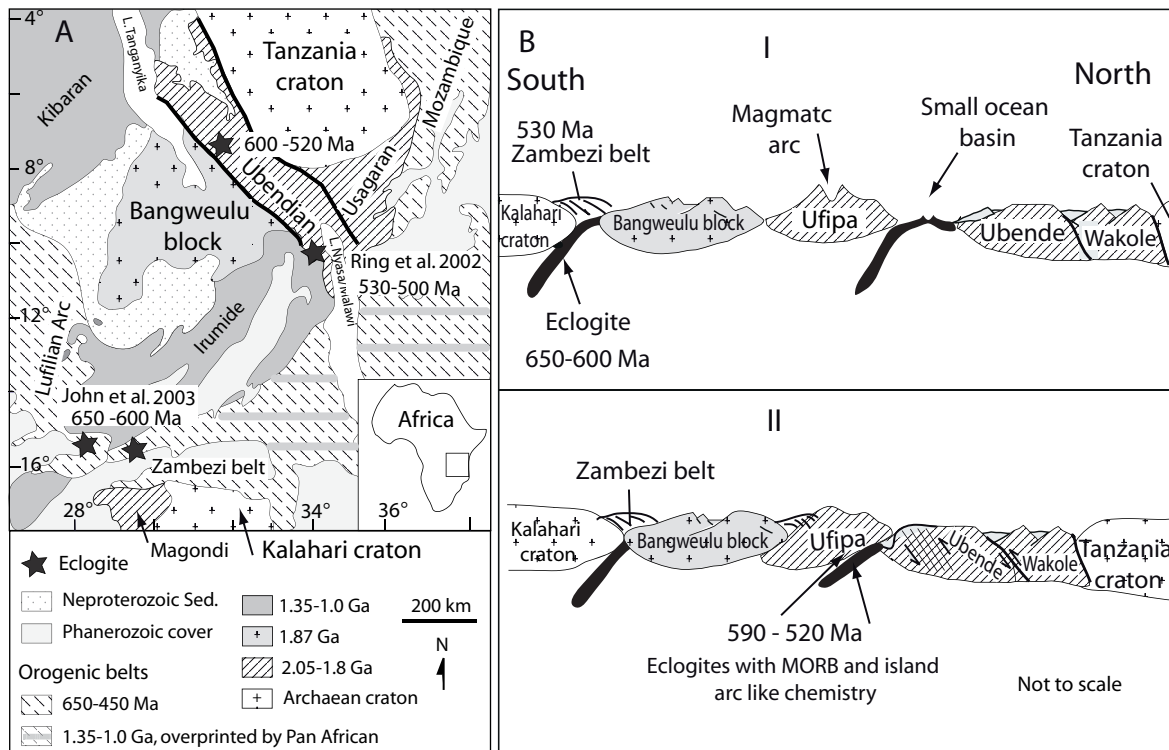


Figure 4.14: A: A geological map of southern central Africa indicating the location of Pan-African back-arc and island-arc like chemistry eclogites between the Bangweulu block and the Tanzania craton, the MORB-like chemistry eclogites of the Zambezi belt (John *et al.*, 2003) and the plume related Mozambique belt eclogites in northern Malawi (Ring *et al.*, 2002), a geological map was modified after from Hanson (2003). B: A cartoon depicting a possible scenario of tectonic plates between the cratons of Congo and Kalahari during Pan-African time.

In the search of possible information about the direction of subduction dip, we looked at the distribution of Neoproterozoic mineral assemblage in the metapelitic country rocks of the eclogites. The high-temperature mineral assemblages cordierite-garnet-sillimanite in the southeastern part of the Ufipa terrane are in contrast to the kyanite-muscovite assemblages found along the northwestern border in the Ufipa terrane, where the eclogites are exposed. This contrast in the Pan-African assemblages along the Ufipa terrane may point to a southward directed subduction zone, above which a high heat flow may have caused the high-temperature metamorphism in the upper plate.

The Pan-African suture between the Tanzania craton and the Bangweulu block is coeval with eclogite formation at ca. 530-500 Ma in northern Malawi (Fig. 4.14A; Ring *et al.*, 2002) and the crustal thickening at ca. 530 Ma in the Zambezi belt (Fig. 4.14B; John *et al.*, 2003),

which followed the subduction of oceanic crust between 659 ± 14 Ma and 607 ± 14 Ma (John *et al.*, 2003, 2004).

The presence of Pan-African eclogites in the Ubendian belt in combination with a high-grade metamorphic reworking of their country rocks (chapter 2) suggests the existence of a Neoproterozoic collision zone in the Ubendian belt, for which the name Tanganyika orogeny has been proposed (chapter 1). In combination with the known eclogite occurrences in the Zambezi belt (John *et al.*, 2003) at the southern border of the Bangweulu block and those to the east in northern Malawi (Ring *et al.*, 2002), the newly discovered Neoproterozoic eclogites in the Ubendian belt suggest that the Bangweulu block formed a microplate during Neoproterozoic Gondwana formation. This has to be considered by future models of Gondwana assembly.

4.10 Conclusions

1. The magmatic precursors of kyanite-free eclogites of the Ufipa terrane in the Ubendian belt are island-arc and back-arc tholeiitic basalts, which became subducted at the end of the Gondwana assembly between 590 Ma and 520 Ma. Core and rim of eclogite zircons give indistinguishable U-Pb ages indicating a short time interval between magmatic formation and subduction of the precursor basalts.
2. Zircons of a kyanite-bearing eclogite of the Ufipa terrane have magmatic cores and overgrown mantles that are Paleoproterozoic in age. These are overgrown by metamorphic Neoproterozoic rims. The cores can be interpreted either as Paleoproterozoic xenocrysts in Neoproterozoic mafic rocks that became subsequently subducted, or as Paleoproterozoic aluminous mafic rocks of the Ufipa crust that became subducted during the Pan-African orogeny in the Ubendian belt.
3. Some kyanite-free eclogites of the Ufipa terrane (geochemical group I eclogites) resemble melts from a depleted mantle source. Because of their affinity to E-MORB chemistry, they may be derived from a not well developed ocean basin or a back-arc basin.
4. The subduction of the island-arc and back-arc basalts in the Ubendian belt followed a clockwise P - T path with a geothermal gradient of about 10 - 11 °C/km and culminated at pressures of about 15 - 20 kbar/ 610 - 790 °C which is equivalent to a depth of approximately 50 - 70 km.
5. The presence of eclogites at three localities at the margins of the Bangweulu block (Ufipa terrane in the Ubendian belt, Zambezi belt and in northern Malawi) suggests that the Bangweulu block formed a microplate during Neoproterozoic Gondwana formation. This plate collided with the Tanzania craton about 560 Ma ago forming the Tanganyika orogenic belt within the Paleoproterozoic Ubendian belt.

4.11 Acknowledgment

DAAD and DFG (Sche 265/10) funded this research. N. Boniface is grateful for the field guidance during the second trip by A. Mruma and appreciates the guides from T. John on how to handle samples with acids and teflon bombs. We wish to thank the ICP-MS laboratory team of D. Garbe-Schönberg and his co-workers P. Fiedler and U. Westernströer for helping during sample preparation and analyses. We value the assistance provided by P. Appel and B. Mader with microprobe analyses and A. Fehler for producing thin sections. We thank A. Larionov, I. Paderin, S. Presniakov and N. Rodionov a team of the SHRIMP laboratory at St. Petersburg and last but not least thanks to Nambungu for driving us during the first field trip.

References

- Armstrong, J. T., 1995. CITZAF: A package of correction programs for the quantitative electron microbeam X-ray analysis of thick polished materials, thin films and particles. *Microbeam Analysis*, **4**, 117–200.
- Black, L. P., Kamo, S. L., Allen, C. M., Aleinikoff, J. N., Davis, D. W., Korsch, R. J. & Foudoulis, C., 2003. TEMORA 1: a new zircon standard for Phanerozoic U-Pb geochronology. *Chemical Geology*, **200**, 155–170.
- Boger, S. D. & Miller, J. M., 2004. Terminal suturing of Gondwana and the onset of the Ross-Delamerian Orogeny: the cause and effect of an Early Cambrian reconfiguration of plate motions. *Earth and Planetary Science Letters*, **219**, 35–48.
- Boniface, N. & Schenk, V., 2007. Polymetamorphism in the Paleoproterozoic Ubendian Belt, Tanzania. *Geochimica et Cosmochimica Acta*, **71**, A107.
- Boynton, W. V., 1984. Cosmochemistry of the rare earth elements: meteorite studies. In: *Rare earth element geochemistry*, Elsevier Sci. Publ. 63–114.
- Brock, P. W. G., 1963. *The Mbozi syenite-gabbro complex*. Unpublished Ph.D. thesis, University of Leeds.
- Burchfiel, B. C., Deng, Q., Molnar, P., Royden, L., Wang, Y., Zhang, P. & Zhang, W., 1989. Intracrustal detachment within zones of continental deformation. *Geology (Boulder)*, **17**, 748–752.
- Burchfiel, B. C. & Royden, L. H., 1985. North-south extension within the convergent Himalayan region. *Geology (Boulder)*, **13**, 679–682.
- Collins, A. S. & Pisarevsky, S. A., 2005. Amalgamating eastern Gondwana: the evolution of the circum-Indian orogens. *Earth-Science Reviews*, **71**, 229–270.

- Corfu, F., Hanchar, J. M., Hoskin, P. W. O. & Kinny, P. D., 2003. Atlas of zircon textures. In: *Zircon*, Mineralogical Society of America and Geochemical Society, Washington, DC, United States. 469–500.
- Daly, M. C., 1988. Crustal shear zones in Central Africa: a kinematic approach to Proterozoic tectonics. *Episodes*, **11**, 5–11.
- Daly, M. C., Klerkx, J. & Nanyaro, J. T., 1985. Early Proterozoic terranes and strike-slip accretion in the Ubendian belt of southwest Tanzania. *Terra Cognita (Abstract)*, **5**, 257.
- Ellis, D. J. & Green, D. H., 1979. An experimental study of the effect of Ca upon garnet-clinopyroxene Fe-Mg exchange equilibria. *Contributions to Mineralogy and Petrology*, **71**, 13–22.
- Ferry, J. M. & Watson, E. B., 2007. New thermodynamic models and revised calibrations for the Ti-in-zircon and Zr-in-rutile thermometers. *Contributions to Mineralogy and Petrology*, **154**, 429–437.
- Gabe-Schönberg, C. D., 1993. Simultaneous determination of thirty seven trace elements in twenty-eight international rock standards by ICP-MS. *Geostandards Newsletter*, **17**, 81–97.
- Gerya, T. V., Stockhert, B. & Perchuk, A. L., 2002. Exhumation of high-pressure metamorphic rocks in a subduction channel: A numerical simulation. *Tectonics*, **21**.
- Graham, C. M. & Powell, R., 1984. A garnet-hornblende geothermometer: calibration, testing, and application to the Pelona Schist, Southern California. *Journal of Metamorphic Geology*, **2**, 13–21.
- Hanson, R. E., 2003. Proterozoic geochronology and tectonic evolution of southern Africa. In: *Proterozoic East Gondwana: supercontinent assembly and breakup*, Geological Society of London. Special volume, 427–463.
- Hofmann, A. W., 1988. Chemical differentiation of the Earth: the relationship between mantle, continental crust, and oceanic crust. In: *Isotope geochemistry: the Crafoord symposium*, Elsevier, Amsterdam, Netherlands. 297–314.
- Holland, T. J. B., 1980. The reaction albite = jadeite + quartz determined experimentally in the range 600–1200 °C. *American Mineralogist*, **65**, 129–134.
- Holland, T. J. B. & Powell, R., 1998. An internally consistent thermodynamic data set for phases of petrological interest. *Journal of Metamorphic Geology*, **16**, 309–343.
- Hsue, K. J., 1991. Exhumation of high-pressure metamorphic rocks. *Geology (Boulder)*, **19**, 107–110.

- Hynes, A., Arkani, H. J. & Greiling, R., 1996. Subduction of continental margins and the uplift of high-pressure metamorphic rocks. *Earth and Planetary Science Letters*, **140**, 13–25.
- Indares, A. & Rivers, T., 1995. Textures, metamorphic reactions and thermobarometry of eclogitized metagabbros: a Proterozoic example. In: *Fourth international eclogite conference*, Schweizerbart'sche Verlagsbuchhandlung (Naegle u. Obermiller), Stuttgart, Federal Republic of Germany. 43–56.
- John, T., Klemd, R., Gao, J. & Garbe-Schoenberg, D., 2008. Trace element mobilization in slabs due to non steady fluid-rock interaction: Constraints from an eclogite-facies transport vein in blueschist (Tianshang, China). *Lithos*, **103**, 1–24.
- John, T., Schenk, V., Haase, K., Scherer, E. & Tembo, F., 2003. Evidence for a Neoproterozoic ocean in south-central Africa from mid-oceanic-ridge-type geochemical signatures and pressure-temperature estimates of Zambian eclogites. *Geology*, **31**, 243–246.
- John, T., Scherer, E. E., Haase, K. & Schenk, V., 2004. Trace element fractionation during fluid-induced eclogitization in a subducting slab: trace element and Lu-Hf-Sm-Nd isotope systematics. *Earth and Planetary Science Letters*, **227**, 441–456.
- Jöns, N. & Schenk, V., 2008. Relics of the Mozambique Ocean in the central East African Orogen: Evidence from the Vohibory Block of southern Madagascar. *Journal of Metamorphic Geology*, **26**, 17–28.
- Kelemen, P. B., Hanghøj, K. & Greene, A. R., 2003. One view of the geochemistry of subduction-related magmatic arcs, with emphasis on primitive andesite and lower crust. In: *The Crust* (ed. Rudnick, R.), Treatise on Geochemistry (eds. H.D. Holland and K.K. Turekian), Elsevier-Pergamon, Oxford. 593–659.
- Klemd, R. & Bröcker, M., 1999. Fluid influence on mineral reactions in ultrahigh-pressure granulites: a case study in the Snieznik Mts. (West Sudetes, Poland). *Contributions to Mineralogy and Petrology*, **136**, 358–373.
- Kohn, M. J. & Spear, F. S., 1990. Two new geobarometers for garnet amphibolites, with applications to southeastern Vermont. *American Mineralogist*, **75**, 89–96.
- Koziol, A. M., 1989. Recalibration of the garnet - plagioclase - Al_2SiO_5 - quartz (GASP) geobarometer and applications to natural parageneses. *EOS Transactions*, **70**, 493.
- Kretz, R., 1983. Symbols for rock-forming minerals. *American Mineralogist*, **68**, 277–279.
- Kusky, T. M., Abdelsalam, M., Tucker, R. D. & Stern, R. J., 2003. Evolution of the East African and related orogens, and the assembly of Gondwana. *Precambrian Research*, **123**, 81–85.

- Lenoir, J. L., Liegeois, J. P., Theunissen, K. & Klerkx, J., 1994. The Palaeoproterozoic Ubendian shear belt in Tanzania: geochronology and structure. *Journal of African Earth Sciences*, **19**, 169–184.
- Ludwig, K., 2001. SQUID 1.02. A Users Manual. *Berkeley Geochronology Center Special Publication*, **2**, 19.
- McConnell, R., 1950. Outline of the Geology of Ufipa and Ubende. Bulletin 19, Geological Survey of Tanganyika.
- Morimoto, N., Fabries, J., Ferguson, A. K., Ginzburg, I. V., Ross, M., Seifert, F. A., Zussman, J., Aoki, K. & Gottardi, G., 1988. Nomenclature of pyroxenes. *American Mineralogist*, **73**, 1123–1133.
- Möller, A., Appel, P., Mezger, K. & Schenk, V., 1995. Evidence for a 2 Ga subduction zone: eclogites in the Usagaran Belt of Tanzania. *Geology*, **23**, 1067–1070.
- Nie, S., Yin, A., Rowley, D. B. & Jin, Y., 1994. Exhumation of the Dabie Shan ultra-high-pressure rocks and accumulation of the Songpan-Ganzi flysch sequence, central China. *Geology (Boulder)*, **22**, 999–1002.
- Pearce, J. A., 1982. Trace element characteristics of lavas from destructive plate boundaries. In: *Andesites: orogenic andesites and related rocks*, John Wiley and Sons, Chichester, United Kingdom. 525–548.
- Pearce, J. A., 1996. A user's guide to basalt discrimination diagrams. In: *Trace element geochemistry of volcanic rocks: applications for massive sulphide exploration*, Geological Association of Canada, John's, NF, Canada. 79–113.
- Pearce, J. A. & Cann, J. R., 1973. Tectonic setting of basic volcanic rocks determined using trace element analyses. *Earth and Planetary Science Letters*, **19**, 290–300.
- Perfit, M. R., Gust, D. A., Bence, A. E., Arculus, R. J. & Taylor, S. R., 1980. Chemical characteristics of island-arc basalts: implications for mantle sources. In: *Chemical characterization of tectonic provinces*, Elsevier, Amsterdam, Netherlands. 227–256.
- Powell, R., 1985. Regression diagnostics and robust regression in geothermometer/ geobarometer calibration: the garnet-clinopyroxene geothermometer revisited. *Journal of Metamorphic Geology*, **3**, 231–243.
- Ray, G. E., 1974. The structural and metamorphic geology of northern Malawi. *Journal of Geological Society of London*, **130**, 427–440.
- Ring, U., Kroener, A., Buchwaldt, R., Toulkeridis, T. & Layer, P. W., 2002. Shear-zone patterns and eclogite-facies metamorphism in the Mozambique Belt of northern Malawi, east-central Africa: implications for the assembly of Gondwana. *Precambrian Research*, **116**, 19–56.

- Rubatto, D., 2002. Zircon trace element geochemistry: partitioning with garnet and the link between U-Pb ages and metamorphism. *Chemical Geology*, **184**, 123–138.
- Sanders, I. S., Daley, J. S. & Davies, G. R., 1987. Late Proterozoic high-pressure granulite facies metamorphism in the North-east Ox Inlier, North-west Ireland. *Journal of Metamorphic Geology*, **5**, 69–85.
- Sklyarov, E. V., Theunissen, K., Melnikov, A. I., Klerkx, J., Gladkochub, D. P. & Mruma, A., 1998. Paleoproterozoic eclogites and garnet pyroxenites of the Ubende Belt (Tanzania). *Schweiz. Mineral. Petrogr. Mitt.*, **78**, 257–271.
- Smirnov, V., Pentelkov, V., Tolochko, V., Trifan, M. & Zhukov, S., 1973. Geology and minerals of the central part of the western rift. Technical report, Mineral and Resource Division, Dodoma, Tanzania. Unpublished report of the geological mapping.
- Spear, F. S. & Cheney, J. T., 1989. A petrogenetic grid for pelitic schists in the system $\text{SiO}_2\text{-Al}_2\text{O}_3\text{-FeO-MgO-K}_2\text{O-H}_2\text{O}$. *Contributions to Mineralogy and Petrology*, **101**, 149–164.
- Spear, F. S., Wark, D. A., Cheney, J. T., Schumacher, J. C. & Watson, E. B., 2006. Zr-in-rutile thermometry in blueschists from Sifnos, Greece. *Contributions to Mineralogy and Petrology*, **152**, 375–385.
- Sutton, J., Watson, J. & James, T., 1954. A Study of the Metamorphic Rocks of Karema and Kungwe Bay, Western Tanganyika. Bulletin 22, Geological Survey of Tanganyika.
- Tatsumi, Y., Hamilton, D. L. & Nesbitt, R. W., 1986. Chemical characteristics of fluid phase released from a subducted lithosphere and origin of arc magmas: evidence from high-pressure experiments and natural rocks. In: *M. Sakuyama and H. Fukuyama memorial volume*, Elsevier, Amsterdam, Netherlands. 293–309.
- Theunissen, K., Lenoir, J. L., Liegeois, J. P., Delvaux, D. & Mruma, A., 1992. Major Pan-African imprint in the Ubendian belt of SW Tanzania: U-Pb zircon geochronology and structural context. *C. R. Acad. Sci. Paris*, **314**, 1355–1362.
- Tomkins, H. S., Powell, R. & Ellis, D. J., 2007. The pressure dependence of the zirconium-in-rutile thermometer. *Journal of Metamorphic Geology*, **25**, 703–713.
- Watson, E. B., Wark, D. A. & Thomas, J. B., 2006. Crystallization thermometers for zircon and rutile. *Contributions to Mineralogy and Petrology*, **151**, 413–433.
- Williams, I., 1998. U-Th-Pb Geochronology by Ion Microprobe. In: *Application of microanalytical techniques to understanding mineralizing processes* (eds. McKibben, M., Shanks III, W. & Ridley, W.), Reviews in Economic Geology. 1–35.
- Wood, D. A., 1980. The application of a Th-Hf-Ta diagram to problems of tectonomagmatic classification and to establishing the nature of crustal contamination of basaltic lavas of the British Tertiary volcanic province. *Earth and Planetary Science Letters*, **50**, 11–30.

Curriculum vitae

Personal particulars

Name	Nelson Boniface
Address	Ludewig Meyn Straße 10 24118 Kiel Or Box 35052 Dar es Salaam Tanzania
E-mail	nb@min.uni-kiel.de
Date of birth	20. January 1974
Nationality	Tanzanian

Education profile

Tabora Boys high school 1995 - 1997	Advanced certificate (secondary education)
University of Dar es Salaam 1998 - 2001	Bachelor of Science (Geology)
2002 - 2004	Master of Science (Geology)
University of Kiel 2005 - 2009	Ph.D. research (Mineralogy)

Kiel, July 1, 2009